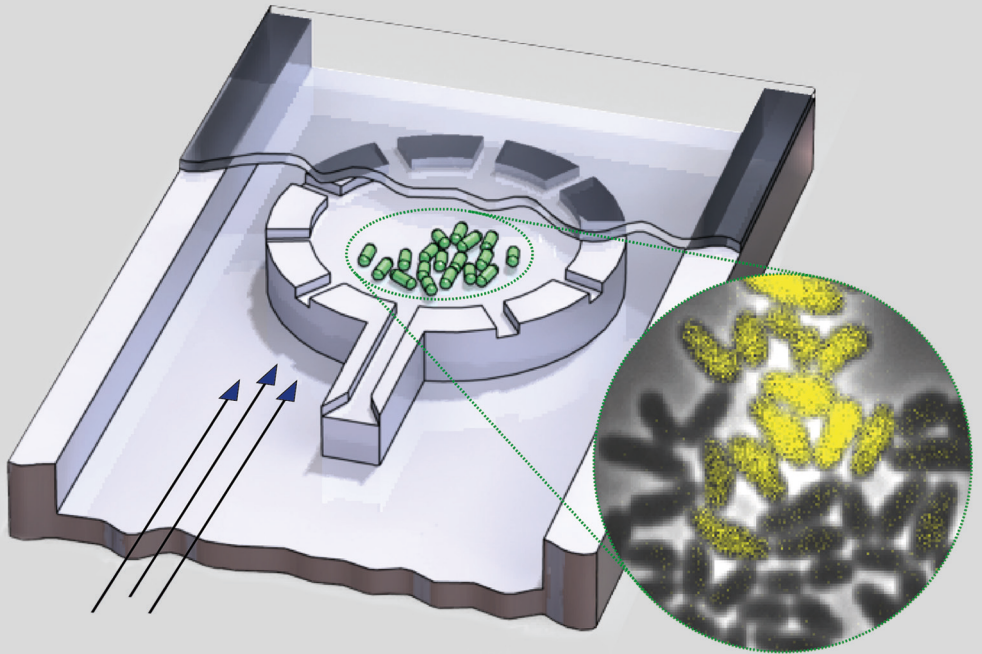


Single-Cell Analysis of Microbial Production Strains in Microfluidic Bioreactors

Alexander Manuel Grünberger



Forschungszentrum Jülich GmbH
Institute of Bio- and Geosciences
Biotechnology (IBG-1)

Single-Cell Analysis of Microbial Production Strains in Microfluidic Bioreactors

Alexander Manuel Grünberger

Schriften des Forschungszentrums Jülich
Reihe Schlüsseltechnologien / Key Technologies

Band / Volume 114

ISSN 1866-1807

ISBN 978-3-95806-092-0

Bibliographic information published by the Deutsche Nationalbibliothek.
The Deutsche Nationalbibliothek lists this publication in the Deutsche
Nationalbibliografie; detailed bibliographic data are available in the
Internet at <http://dnb.d-nb.de>.

Publisher and
Distributor: Forschungszentrum Jülich GmbH
Zentralbibliothek
52425 Jülich
Tel: +49 2461 61-5368
Fax: +49 2461 61-6103
Email: zb-publikation@fz-juelich.de
www.fz-juelich.de/zb

Cover Design: Grafische Medien, Forschungszentrum Jülich GmbH

Printer: Grafische Medien, Forschungszentrum Jülich GmbH

Copyright: Forschungszentrum Jülich 2015

Schriften des Forschungszentrums Jülich
Reihe Schlüsseltechnologien / Key Technologies, Band / Volume 114

D 82 (Diss. RWTH Aachen University, 2014)

ISSN 1866-1807

ISBN 978-3-95806-092-0

The complete volume is freely available on the Internet on the Jülicher Open Access Server (JuSER)
at www.fz-juelich.de/zb/openaccess.

Neither this book nor any part of it may be reproduced or transmitted in any form or by any
means, electronic or mechanical, including photocopying, microfilming, and recording, or by any
information storage and retrieval system, without permission in writing from the publisher.

Engineering or Technology is the making of things that did not previously exist, whereas science is the discovering of things that have long existed.

(David Billington)

Measurement has too often been the leitmotif of many investigations rather than the experimental examination of hypotheses. Mounds of data are collected, which are statistically decorous and methodologically unimpeachable, but conclusions are often trivial and rarely useful in decision making. This results from an overly rigorous control of an insignificant variable and a widespread deficiency in the framing of pertinent questions. Investigators seem to have settled for what is measurable instead of measuring what they would really like to know.

(Edmund D. Pellegrino)

Vorwort und Danksagung

Die vorliegende Arbeit entstand während meiner Tätigkeit als wissenschaftlicher Mitarbeiter im Forschungszentrum Jülich GmbH. Die Forschungsarbeit wurde am Institut für Bio- und Geowissenschaften 1: Biotechnologie in der Arbeitsgruppe Microscale Bioengineering durchgeführt. Das Forschungsprojekt war als „Machbarkeitsstudie“ angelegt und diente der Etablierung der Einzelzell-Mikrofluidik als Werkzeug für die Beantwortung biotechnologischer und bioprozesstechnologischer Fragestellungen.

Ohne die Mithilfe vieler Menschen wäre diese Arbeit nicht in der jetzigen Form zustande gekommen. Für diese Unterstützung bedanke ich mich insbesondere bei den folgenden Personen:

Mein besonderer Dank gilt meinem Doktorvater Herrn Prof. Dr. Wolfgang Wiechert, Leiter der Systembiotechnologie am Institut für Bio- und Geowissenschaften und Inhaber des Lehrstuhls für „Computational Systems Biotechnology“ der Aachener Verfahrenstechnik, für die Möglichkeit dieses Promotionsthema zu bearbeiten und für die kontinuierlichen guten Arbeitsbedingungen. Insbesondere möchte ich mich für den Freiraum bedanken, eigene Ideen und Konzepte verfolgen zu dürfen. Ich möchte mich bei Professor Jochen Büchs für die Übernahme der Zweitkorrektur bedanken. Mein Dank gilt vor allem dem Interesse für die Thematik und den nützlichen Anregungen während der vergangenen Jahre.

Als direkter Betreuer meiner Arbeit und Arbeitsgruppenleiter der „Microscale Bioengineering Gruppe“ möchte ich mich bei Dr. Dietrich Kohlheyer bedanken, sowohl für die zahlreichen Hilfestellungen und Diskussionen zum Thema Mikrofluidik, als auch die zahlreichen Anmerkungen, Hinweise und kritischen Fragen, die alle dazu beigetragen haben den roten Faden während der letzten drei Jahre nicht zu verlieren. Des Weiteren danke ich für die kontinuierliche Hilfe beim Schreiben und Illustrieren von Veröffentlichungen, Vorträgen und Postern.

Besonderer Dank gebührt darüber hinaus Dr. Stephan Noack, Dr. Julia Frunzke und Dr. Katharina Nöh. Ihre Unterstützung, Anregungen und ihre Offenheit gegenüber neuen Ideen waren Voraussetzung für das Gelingen dieser Arbeit. Jede der zahlreichen Diskussionen zum Thema Metabolismus, Heterogenität und Modellierung haben auf ihre Art und Weise dazu beigetragen, die Einzelzellkultivierung am Institut zu etablieren.

Von unverzichtbarer Bedeutung für die Bearbeitung des stark interdisziplinären Themas war die enge Zusammenarbeit innerhalb der Arbeitsgruppe, des Institutes, als auch der Mitarbeiter des Reinraumteams. Herausheben möchte ich dabei meine direkten Kollegen Christopher Probst und Agnes Müller-Schröer, die meinen Weg vom ersten Moment an mitbeschritten haben. Christophers geniales technisches Verständnis und die Gabe, zu handeln statt zu reden, als auch Agnes mikrobiologische Fachkenntnisse und organisatorisches Talent sind eng mit dem Erfolg dieser Arbeit verbunden.

Großer Dank gilt auch den von mir betreuten Studenten Mengmeng Wang (Master), Johanna Heinrich (Master), Christian Sachs (Praktikum und Master) und Sophie Weber (Praktikum und Bachelor) für das Interesse an der Thematik, die zahlreichen Diskussionen, die harte Arbeit und auch lustigen Momente während ihrer Praktika und Abschlussarbeiten.

Bedanken möchte ich mich darüber hinaus bei zahlreichen Arbeitskollegen für das Interesse an der Mikrofluidik und für den Tatendrang, diese am Institut zu etablieren. Dieser Dank gilt insbesondere Nadja Braun, Christina Krämer, Nuriye Mustafi, Stephan Binder, Georg Schendzielorz, Regina Mahr, Dennis Binder, Anita Loeschke, Roland Moussa, Nicole Paczia, Simon Unthan, Stefan Helfrich, Kathrin Scholz, Peter Kusen, Martin Diener, Daniel Minör, Andrea Michel, Elisabeth Zelle, Sebastian Niedenführ, Peter Rohe, Steffen Ostermann, Arun Nanda, Daniel Jussen, Jan van Ooyen, Katja Schmitz, Birgit Stute, Jochem, Gätgens, Jan Marienhagen, Lothar Eggeling und allen, die ich hier aus Platzgründen nicht mehr aufzählen konnte. Ihnen danke ich auch für die angenehme Arbeitsatmosphäre und für die freundschaftliche Verbundenheit auch außerhalb des Lehrstuhls. Insbesondere die Abende im Pub werden mir noch länger in Erinnerung bleiben.

Die exzellenten Rahmenbedingungen für das Gelingen der vorliegenden Arbeit verdanke ich der technischen und administrativen Infrastruktur des IBG-1. Bedanken möchte ich mich deshalb bei Marianne Hess, Dr. Iris Eggeling und allen Mitarbeitern der Infrastruktur für die ununterbrochene Unterstützung bei diversen technischen und administrativen Angelegenheiten. Besonderer Dank gilt Hubert Ruhrig und Mario Fricke für die Planung und Erstellung mechanischer Versuchsaufbauten aller Art. Außerdem möchte ich mich bei Frau Bräker für die „Fotosessions“ unserer mikrofluidischen Chips bedanken.

Nicht zu vergessen sind einige externe „Mitleidende“ der gleichen Thematik, deren reger Austausch von Erfahrungen die unzähligen Rückschläge erträglicher machten. Namentlich nennen möchte ich hierbei Christian Dusny und Frederik Fritsch, Doktoranden der Einzelzellanalytik der TU Dortmund.

Danken möchte ich schließlich meinen Eltern und Brüdern für die Unterstützung während meines Studiums, der Auslandsaufenthalte und der vorliegenden Promotionsarbeit.

Jülich, im März 2014

Alexander Grünberger

Abstract

Industrial biotechnology is concerned with the sustainable production of, for example, fine and bulk chemicals, pharmaceuticals and proteins by utilizing microorganisms for the conversion of renewable carbon sources. Well known examples include the production of amino acids by *Corynebacterium glutamicum* at a million ton scale per year worldwide, or the recombinant production of insulin by *Escherichia coli*.

Growth and productivity of the underlying host microorganisms are two key performance indicators in biotechnological production processes. Assuming isogenic starting populations, optimal reactor control and mixing, a uniform cell behavior during growth might be expected. However, as confirmed in recent years, isogenic bacterial populations can be physiologically heterogeneous. Obviously, there is a strong demand to unravel microbial population heterogeneity, understand its origin and gain knowledge on its impact on large scale biotechnological production. Therefore, new analytical techniques addressing single-cell behavior are the key for further optimization.

In particular, state-of-the-art microfluidic cultivation systems facilitating single-cell resolution and accurate environmental control over long time periods at the same time, offer completely new experimental assays on microbial populations. In contrast to conventional systems, for example, fluorescence activated cell sorting, microfluidic cultivations enable the analysis of cell dynamics by automated time-lapse microscopy with full spatio-temporal resolution.

The aim of the present thesis was to develop and establish a new microfluidic platform technology for microbial single-cell analysis in order to address key concerns on population heterogeneity and reactor inhomogeneity in industrial biotechnology. Several unique single-cell cultivation chips were successfully fabricated and validated with a variety of industrially applied microorganisms. Each device contained up to several thousand micrometer sized cultivation structures in parallel intended for high-throughput analysis of single cells and isogenic microcolonies

In the present research two major single-cell investigations were performed demonstrating the universal applicability and potential of the microfluidic single-cell cultivation technology:

(i) Growth analysis of industrially relevant bacteria (in particular *E. coli* and *C. glutamicum*) with single-cell resolution was performed. Therefore, isogenic microcolonies were grown in monolayers up to several hundred cells in each growth chamber and imaging was performed by time-lapse microscopy. Compared to a typical 1 liter lab-scale batch cultivation, interestingly a 1.5-fold enhanced growth rate of *C. glutamicum* wild type cells under constant microfluidic cultivation conditions was found.

(ii) Morphological characterization: The cellular response of several *C. glutamicum* strains under various environmental conditions was investigated in more detail. Studies included artificially induced starvation, occurrence of spontaneously induced stress response of single cells, as well as morphological characterization during growth on different carbon sources.

In a multi-scale approach, the elevated single-cell growth rates were investigated in more detail. Therefore, various lab-scale cultivations were performed and results compared with our microfluidic single-cell analysis. This systematic study revealed a maximum growth rate of $\mu_{\max} = 0.6 \text{ h}^{-1}$ during microfluidic cultivation compared to $\mu_{\max} = 0.4 \text{ h}^{-1}$ during bioreactor, flask and microtiter cultivation. Further single-cell analysis exposed that solely the medium composition was the growth enhancing factor, rather than the continuous perfusion during single-cell cultivation or the analytical method itself.

It turned out that the medium compound protocatechuate (PCA), initially added as iron chelator, serves as an additional carbon source and is co-metabolized by *C. glutamicum*, resulting in higher growth rates when PCA is continuously supplied during microfluidic cultivation. In contrast, the limited amount of PCA is fully consumed during the early process of a typical batch process. Follow-up studies proved that even in conventional batch cultivation systems, the improved growth rates can be realized if PCA is made accessible for a longer time.

Short innovation times allowed the fabrication of tailor made systems depending on microbial species and application. In an overview, it is shown, how these systems can be used to cultivate other industrial important organisms such as fungi and yeast. Furthermore, examples are given how the developed system in combination with genetically modified fluorescence sensors can be used to investigate heterogeneity of growth coupled production processes at the single-cell level. The results confirm that cell-to-cell heterogeneity can have significant impact on production processes and need to be further investigated in future.

In the present project, novel single-use microfluidic cultivation devices with structures in the sub-micrometer range for trapping and cultivation of individual bacteria were developed and successfully validated. Automated live-cell imaging in combination with accurate environmental control facilitates spatio-temporal analysis of single bacteria with respect to, for example, growth, morphology and single-cell productivity. In a highly interdisciplinary approach, the microfluidic single-cell technology was efficiently utilized to derive cellular information which was not accessible before. The presented findings clearly demonstrate the high potential of microbial single-cell analysis for biotechnological strain and process optimization. The present work established the foundation for further progress in the field.

Zusammenfassung

Seit Jahrzehnten werden mikrobielle Produktionsprozesse für die Umsetzung nachwachsender Rohstoffe zu industriell genutzten Grund- und Feinchemikalien verwendet. Das Auftreten von unterschiedlichen Subpopulationen (z.B. in Wachstum und Produktion) in mikrobiellen Produktionsprozessen kann einen signifikanten Einfluss auf Ertrag und Stabilität haben. Im Allgemeinen werden biologische Prozesse basierend auf Durchschnittswerten analysiert und optimiert. Hierbei bleibt jedoch das Verhalten einzelner Zellen unbeachtet, mit oftmals nicht abschätzbaren Folgen. Essentiell für die Wirtschaftlichkeit von etablierten als auch neuen Bioprozessen sind deshalb fundierte Kenntnisse bezüglich der Ursache und Ausmaßes von Populationsheterogenität, sowie den zugrunde liegenden molekularen Vorgängen.

Die Forschung und Entwicklung im Bereich der mikrofluidischen Einzelzellanalysen hat in den letzten Jahren einen Aufschwung erlebt. Fortschritte in den Fabrikationsmethoden ermöglichen die Herstellung immer kleinerer Strukturen, selbst im Submikrometer-Bereich. Die Verwendung von mikrofluidischen Analysetechniken wie zum Beispiel mikrofluidischen Einzelzell-Bioreaktoren, ermöglicht die Untersuchung biologischer Prozesse auf Einzelzellebene. Im Gegensatz zu konventionellen Systemen, wie zum Beispiel der fluoreszenz-markierten Durchflusszytometrie, ermöglichen mikrofluidische Kultivierungssysteme die Analyse zellulärer Prozesse mit voller räumlicher und zeitlicher Auflösung. Die Kultivierung von Zellen in mikrofluidischen Bioreaktoren bietet zahlreiche Vorteile: Durch einen kontinuierlichen Medienfluss können die Kultivierungsbedingungen wie zum Beispiel Nährstoff- und Sauerstoffversorgung optimal eingestellt werden. Für die Charakterisierung und ein besseres Verständnis von mikrobiologischen Produktionsprozessen wurden diese Systeme bisher allerdings kaum herangezogen.

In dieser Arbeit wurde die Herstellung, der Aufbau und die Verwendung von Einzelzell-Bioreaktoren für die Kultivierung von Bakterien untersucht. Um dieses Ziel zu erreichen wurden folgende Arbeitspakete durchgeführt: (i) Entwicklung von Einzelzell-Bioreaktoren für die Fixierung und die Kultivierung von Mikroorganismen; (ii) Etablierung eines Fertigungsprozesses für die Herstellung einer Abgussform; (iii) Abguss und Herstellung eines Polymer-Glas Chips; (iv) Aufbau der mikroskopischen Versuchseinheit für die Echtzeit-Beobachtung industriell genutzter Bakterienstämme.

Die Einzelzell-Bioreaktoren wurden für erste Wachstums- und Metabolismusstudien der industriell genutzten Bakterien *Corynebacterium glutamicum* und *Escherichia coli* genutzt. In diesem Kultivierungssystem wurden für *C. glutamicum* höhere Wachstumsraten im Vergleich zu konventionellen Kultivierungen gemessen. Weitere systematische Analysen beinhalteten sowohl Untersuchung von Wachstum und Morphologie einzelner Kolonien und Zellen bei verschiedenen Medienbedingungen, als

auch die Untersuchung seltener zellulärer Ereignisse, wie dem Auftreten von spontan induzierter SOS Antwort von *C. glutamicum*.

In einer Vergleichsstudie mit alternativ entwickelten Einzelzellkultivierungssystemen (Agarose Pads und Dielektrophorese-Reaktoren) wurde der Einfluss der verschiedenen Kultivierungssysteme auf die Physiologie von *C. glutamicum* näher untersucht. Es konnten signifikanten Unterschiede bezüglich des Wachstumsverhaltens von *C. glutamicum* in den verschiedenen Systemen festgestellt werden.

Im zweiten Teil der Arbeit wurden die unter mikrofluidischen Bedingungen erzielten höheren Wachstumsraten von *C. glutamicum* näher untersucht. Systematische Untersuchungen in verschiedenen Kultivierungsmaßstäben (Pikoliter bis Liter) bestätigten die höheren Wachstumsraten im Pikoliter-Kultivierungsmaßstab. Durch detailliertere Studien in verschiedenen Kultivierungsmaßstäben sowie diverser gerichteter und ungerichteter Analyseverfahren konnte der Faktor gefunden werden, der für die höheren Wachstumsraten verantwortlich ist. Protocatechusäure, ursprünglich als Eisenchelator dem Medium zugesetzt, wird parallel zu Glukose als zusätzliche Kohlenstoffquelle verstoffwechselt. Erste Studien zeigen, dass auch in traditionellen Kultivierungssystemen eine höhere Wachstumsrate erreicht werden kann, solange dem Organismus Protocatechusäure in ausreichender Menge zur Verfügung steht.

Zuletzt wird ein Ausblick über weitere Anwendungsmöglichkeiten der entwickelten Einzelzellsysteme gegeben. Die Flexibilität im Herstellungsprozess kann genutzt werden, um die vorgestellten mikrofluidischen Systeme der jeweiligen biologischen Fragestellung anzupassen. Dies erhöht nicht nur das Spektrum an Anwendungsmöglichkeiten, wie z.B. Langzeit-Wachstumsuntersuchungen, sondern ermöglicht auch die Untersuchung anderer biotechnologisch wichtiger Organismen wie z.B. Pilze und Hefen.

Die Beispiele zeigen, dass mikrofluidische Einzelzell-Bioreaktoren nicht nur Einblicke in zelluläre Vorgänge ermöglichen, sondern auch das Potential bieten Bioprozesse nachhaltig zu verstehen und zu verbessern. In den folgenden Jahren gilt es nun die Systeme zu optimieren, zu charakterisieren, aber auch die Grenzen derartiger Systeme eingehend zu bewerten.

Table of content

Vorwort und Danksagung	V
Abstract	VII
Zusammenfassung	IX
Table of content	XI
Abbreviations and symbols	XV
1 Motivation and background	1
1.1 Industrial biotechnology	2
1.2 Bioprocess development	2
1.2.1 Reactor inhomogeneity	2
1.2.2 Population heterogeneity.....	3
1.3 Microfluidic single-cell analysis	4
1.4 Project objectives	5
1.5 Workflow	6
1.6 Thesis outline	7
2 Technology overview	11
2.1 Microbial single-cell analysis	12
2.1.1 Abstract	12
2.1.2 Introduction	12
2.1.3 Single-cell analysis: snapshot vs. dynamic	13
2.1.4 Microfluidic single-cell cultivation - Physics and fabrication	16
2.1.5 Microfluidic single-cell cultivation systems - Overview and examples	19
2.1.6 Challenges and future directions.....	32
2.1.7 Conclusions.....	33
2.2 Single-cell microfluidics for bioprocess development	34
2.2.1 Abstract	34
2.2.2 Introduction.....	34
2.2.3 Application fields.....	38
2.2.4 Conclusion	43
3 Single-cell microfluidics: Development and validation	45
3.1 Microfabrication	46
3.1.1 Abstract	46
3.1.2 Introduction.....	46

3.1.3	Protocol	48
3.1.4	Representative results	52
3.1.5	Discussion	58
3.2	Picoliter bioreactors	61
3.2.1	Abstract	61
3.2.2	Introduction	61
3.2.3	Device principle and design	64
3.2.4	Material and methods	66
3.2.5	Results and discussion	68
3.2.6	Conclusions	74
3.3	High-throughput single-cell cultivation.....	76
3.3.1	Abstract	76
3.3.2	Introduction	76
3.3.3	Materials and methods.....	78
3.3.4	Results	80
3.3.5	Discussion	89
3.3.6	Conclusion.....	91
3.4	Systematic comparison of single-cell cultivation technologies.....	92
3.4.1	Abstract	92
3.4.2	Introduction	93
3.4.3	Materials and methods.....	94
3.4.4	Results	97
3.4.5	Discussion	106
4	Single-cell analysis in bioprocess development.....	111
4.1	Growth rate investigation I: Cultivation at different scales	112
4.1.1	Abstract	112
4.1.2	Introduction	112
4.1.3	Material and methods	116
4.1.4	Results and discussion.....	119
4.1.5	Conclusions and outlook	125
4.2	Growth rate investigation II: What triggers faster growth ?	126
4.2.1	Abstract	126
4.2.2	Introduction	126
4.2.3	Materials and methods.....	128
4.2.4	Results and discussion.....	131
4.2.5	Conclusions	143
4.3	Carbon source dependent cell size and growth of <i>C. glutamicum</i>	145
4.3.1	Abstract	145

4.3.2	Introduction	145
4.3.3	Materials and methods	148
4.3.4	Results	150
4.3.5	Discussion	154
4.3.6	Conclusion	156
5	Future application	157
5.1	Optimization of single-cell designs.....	158
5.1.1	Continuous colony reactor	158
5.1.2	Single-cell growth channels	159
5.1.3	Single-cell traps.....	160
5.2	Further fields of application.....	160
5.2.1	Optimization for industrial platform organisms.....	160
5.2.2	Fluorescence coupled growth and production studies.....	164
5.2.3	Co-cultivation.....	166
6	Final conclusion	167
6.1	Summary and conclusions.....	168
6.2	Recommendations	169
6.2.1	Platform optimization and characterization	169
6.2.2	Cultivation parameter and analysis	171
6.2.3	Single-cell manipulation	172
6.2.4	Automated image analysis and visualization	172
6.2.5	Data management.....	173
Appendix	175
Appendix A	175
Appendix B	178
Appendix C	181
Appendix D	193
Appendix E	194
Appendix F	202
Appendix G	207
References	208
Publications	224

Abbreviations and symbols

Table I: General abbreviations

Abbreviation	Explanation
AC	Acetate
AcCOA	Acetyl-CoA
Arg	Arginine
AR	Advanced research
ATCC	American Type Culture Collection
ATP	Adenosine triphosphate
a.u/AU	Arbitrary unit
BS	Back scatter
BSA	Bovine serum albumin
BHI	Brain heart infusion
CAD	Computer-aided design
CC	Coulter counter
CCD (camera)	Charge-coupled device (camera)
CCR	Continuous colony reactor
cf.	Compared to
CFD	Computational fluid dynamics
cDNA	Copy deoxyribonucleic acid
CDW	Cell dry weight
DFA	Deferoxamine
DI water	Deionized water
DIC	Differential interference contrast
DNA	Deoxyribonucleic acid
DO	Dissoved oxygen
E-beam	Electron- beam
e.g.	Exempli gratia
Eq	Equation
et al.	et alii
FACS	Fluorescence activated cell sorting

FC	Flow cytometry
FRU	Fructose
FSC	Forward scatter
FVA	Flux variance analysis
Gal	Galactose
GC	Gas chromatography
GFP	Green fluorescent protein
GB	Giga byte
GLC	Glucose
GNT	Gluconate
HPLC	High-performance liquid chromatography
HR	High-resolution
HT	High-throughput
HTC	High-throughput cultivation
IB	Inclusion body
ID	Inner diameter
i.e.	id est
IPTG	Isopropyl-β-D-thiogalactopyranosid
LAC	Lactate
LB	Lysogeny broth
LC	Liquid chromatography
LOC	Lab on a chip
LOQ	Limit of quantification
Lys	Lysine
MFA	Metabolic flux analysis
MGC	Monolayer growth chamber
MI	Microscopy image
MOPS	3-(N-morpholino)propanesulfonic acid
MF	Microfluidic
MSCC	Microfluidic single-cell cultivation
MS	Mass spectroscopy
MTP	Microtiterplate
n.d.	Not determined

nDEP	N egativ d ielectrophorese
NA	N ot available
NADPH	Oxidized form of n icotinamide a dentine d inucleotide p hosphate
OD₆₀₀	O ptical d ensity
OD	O uter d iameter
PC	P olycarbonate
PCA	P rotocatechuic a cid
PDMS	P oly d imethylsiloxane
PLBR	P icoliter b ioreactor
PMMA	P oly(m ethyl m ethacrylate)
PI	P ropidium i odide
RecA	R ecombinase A
RNA	R ibonucleic a cid
ROI	R egion of i nterest
RPM	R otation p er m inute
SEM	S canning electron m icroscopy
SCA	S ingle-cell a nalysis
SCC	S ingle-cell c ultivation
SCCM	S tandard cubic centimeters per m inute
SOS response	global response to DNA damage
SS	single-stranded
SSC	S ide s catter
SucCOA	S uccinyl- C o A
TB	T era b yte
TCA cycle	C itric a cid c ycle
TOF	T ime-of-flight
YFP	Y ellow f luorescent p rotein
EYFP	E nhanced yellow f luorescent p rotein
VS	V is s pectrometry
WT	W ild t ype
μBR	M icro b ioreactor
μTAS	M icro t otal a nalysis s ystem

Table II: Symbols

Symbol	Term	Unit
C	Concentration	g L^{-1}
C_v	Coefficient of variation	---
D	Diffusion coefficient	$\text{m}^2 \text{s}^{-1}$
D_h	Hydraulic diameter	m
h	Height	m
K	Half-saturation constant in Monod kinetics	---
k	Inhibition constant	---
L	Length	m
M	Mass	kg
O_ur	Oxygen uptake rate	$\text{Mol L}^{-1} \text{h}^{-1}$
pH	Concentration of dissolved hydrogen ions (H^+)	---
P	Promoter	---
P₀	Product concentration at $t = 0$	g L^{-1}
p_{CO2}	Dissolved carbon dioxide concentrations	bar
r	Rate (of growth, product formation etc.)	h^{-1}
r	Radii of cell poles	m
R²	Coefficient of determination	---
S₀	Substrate concentration at $t = 0$	g L^{-1}
SU-8	Name of photoresist	---
t	Time	h
upt_i	Uptake rate of i	$\text{g}^{-1} \text{h}^{-1}$
V	Volume	L
v/v	Volume concentration	---
w/v	Mass concentration	---
X	Biomass	g
Y	Yield coefficient	---
α	Division angle of cells	°
η	Fluid viscosity	$\text{kg m}^{-1} \text{s}^{-1}$
ρ	Fluid density	kg m^{-3}
ρ_{Cell}	Cell density	kg m^{-3}
v	Fluid velocity	s
v_i	Dilution factor	---
μ	Specific growth rate	h^{-1}

Δ	Difference of two states	----
----------	--------------------------	------

Table III: Superscripts and Subscripts

Abbreviation	Explanation
Av	average
d	doubling
Max	Maximum
S	Substrate
P	Product

1 Motivation and background

This introduction chapter gives a general overview about the aspects of this thesis. The reader is provided with the motivation for this work and the development process leading to the presented results of this study. Furthermore, the aim and specific objectives of this work are presented. Finally, the outline of this thesis is given.

1.1 Industrial biotechnology

Fermentation processes have been in use for thousands of years, for example, for the production of beer, wine and cheese [1]. The modern science in the 19th and 20th century investigated biobased transformation processes in more detail. Novel products became available, such as insulin extracted from animal pancreas. Since the advent of genetic engineering techniques, organisms were genetically modified to produce pharmaceuticals such as insulin [2], food and laundry detergent additives [3]. Progress in the field of genetic engineering, protein engineering, metabolic engineering as well as synthetic biology enabled a deeper understanding of biobased production processes and led to the improvement and redesign of microbial cell factories. As a result various industrially viable strains of bacteria, yeast, and fungi are currently used for the production of natural and non-natural value-added products [4]. According to Festel *et al.* [5] the global industrial biotechnology sector is expected to grow from 48 billion € in 2008, to 348 billion € in 2017, and even further.

Today, several national and international initiatives (for example the National Research Strategy BioEconomy 2030 – Federal Ministry of Education and Research) are concerned with the establishment of a sustainable biobased economy. Among other efforts, industrially applied microbial cell factories, converting renewable carbon sources into valuable products, will play a major role in this challenging development process [6-9]. Therefore, the continuous improvement of biobased production processes [3] and the complete understanding of the underlying microbial cell factories is essential for further improvement of existing as well as the development of novel bioprocesses.

1.2 Bioprocess development

The development of novel bioprocesses includes four steps. In the first step, the production strain is identified and selected. In the second step, the production of the desired compound is enhanced using different microbial and molecular biological techniques [10]. This is followed by step three, the optimization of the cultivation parameters and medium compositions. In the last stage (step four), the process is transferred from laboratory scale to production scale [11].

1.2.1 Reactor inhomogeneity

Small scale reactors [μL – mL] are used in high-throughput manner for screening of production strains and process parameters [12] before the process is transferred to laboratory scale [L] and industrial scale [m^3] (Figure 1.1A). The scale-up is still one of the major hurdles in bioprocess development. During process scale-up, monitoring and control becomes increasingly challenging. In contrast to laboratory scales in which equilibrium conditions are accomplished within seconds, mixing times at industrial scale

may easily exceed several minutes [13]. As expected, this results in undesired environmental heterogeneity and microgradients, for example, of medium composition and oxygen availability. A process which can be efficiently operated at laboratory scale, may be inefficient at industrial scale, since cells are exposed to significant environmental fluctuations as illustrated in Figure 1.1B, resulting in reduced biomass formation and productivity [13-15]. Thus, a better understanding of scale-up mechanisms is one major goal for future bioprocess development [16].

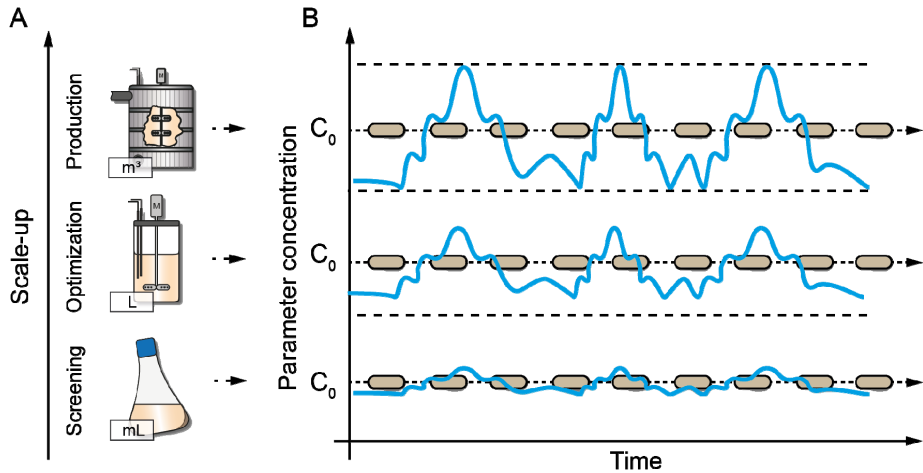


Figure 1.1: Environmental fluctuations in different cultivation scales. (A) Scale-up scheme from mL to m³ scale. (B) Concentration profile (e.g., oxygen, pH, chemical compound) an average cell experiences in the different cultivation scales over time.

1.2.2 Population heterogeneity

Conventionally, isogenic bacteria cultures are considered to be uniform in their local environment. Cell-to-cell heterogeneity has been observed in large-scale bioprocesses [17, 18] often exhibiting severe differences (Figure 1.2B). The occurrence of cell-to-cell heterogeneity in bioprocesses has been recognized during the last years. However, single-cell properties are rarely measured in biotechnological production processes. Typically, bulk measurements are performed, delivering average values of process parameters such as growth and production of billions of cells (Figure 1.2C) neglecting single-cell behavior. Misleadingly, the average response of cells was, and still is, interpreted as the response of each single cell within a sample. The cell-to-cell heterogeneity of microbial population remains hidden inside the obtained average.

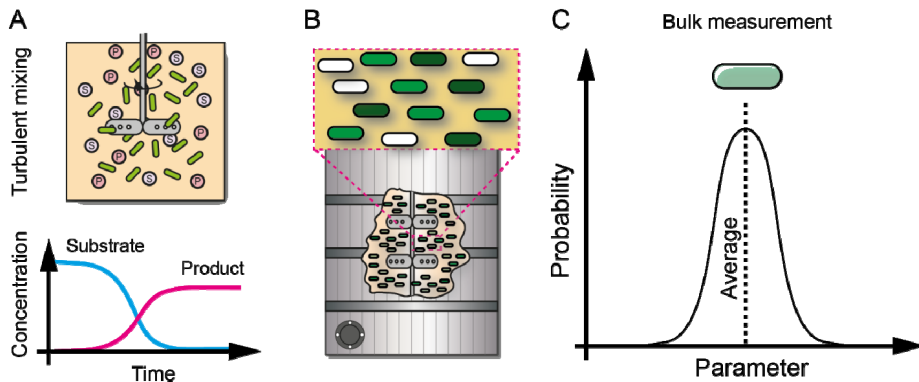


Figure 1.2: Cell-to-cell heterogeneity within large-scale production processes. (A) Turbulent mixing leads to environmental heterogeneity, for example, within the substrate and product concentration. (B) Due to environmental heterogeneity in large-scale cultivation, cells are in different states. (C) “Average cell” behavior is obtained by bulk measurements, masking the true behavior of single cells.

The knowledge of population heterogeneity has improved during the last years. Cell-to-cell heterogeneity may be induced by intrinsic (*e.g.*, genetic variation, stochastic variation) as well as extrinsic factors (*e.g.*, nutrient fluctuations, microgradients, mixing time) [19]. It is known that during reactor scale-up environmental inhomogeneity increases, which may lead to enhanced population heterogeneity at the same time. Currently, flow cytometrical methods such as FACS and Coulter counter are used to identify cell-to-cell heterogeneity (Chapter 2.1). However, the underlying reasons leading to cell-to-cell heterogeneity can hardly be investigated using such tools. Furthermore, the inability for continuous monitoring results in snapshot analysis of population behavior at selected time-points. As a consequence, the complex interplay between environmental inhomogeneity and cellular response is hardly understood to date. Both, organism and environment are highly dynamic and continuously influence each other, making it difficult to understand the underlying molecular mechanisms. Therefore, novel methods are necessary to address investigations on single-cell level under constant conditions.

1.3 Microfluidic single-cell analysis

Novel Lab-on-a-chip devices, capable of handling liquid in nanoliter to picoliter scale, offer promising approaches to perform unique single-cell analysis (SCA). In microfluidic cultivation systems well defined environmental conditions can be realized and maintained by continuous perfusion of medium (Chapter 2.1). Products and by-product are continuously removed (Figure 1.3A), whereas in conventional cultivation devices microgradients and the accumulation of products and by-products are likely (Figure 1.2A). This allows the investigation of a more specific biological behavior related to defined and constant environmental parameters.

Over the last years, many systems were developed, predominantly for the investigation of eukaryotic cells [20, 21]. The major hurdles to apply microfluidic single-cell cultivation to bacteria include the challenge to fabricate suitable systems to isolate single bacteria cells as well as to maintain constant cultivation conditions over time. Especially, the small size of bacteria ($< 1 \mu\text{m}$ in diameter), fast division rates ($< \text{hours}$), as well as a rod-shaped morphology, make the establishment of reliable single-cell systems a challenging task. However, research on bacterial single-cell level is recently gaining more interest [22]. Therefore, microfluidic systems especially fabricated by soft lithography can be used as single-use and easy-to-handle single-cell analysis systems. In combination with automated live-cell imaging, time resolved single-cell studies are possible, allowing to investigate cell-to-cell heterogeneity with spatio-temporal resolution (Figure 1.3C). Yet, these systems have been rarely applied to industrially relevant organisms (see Chapter 2.2).

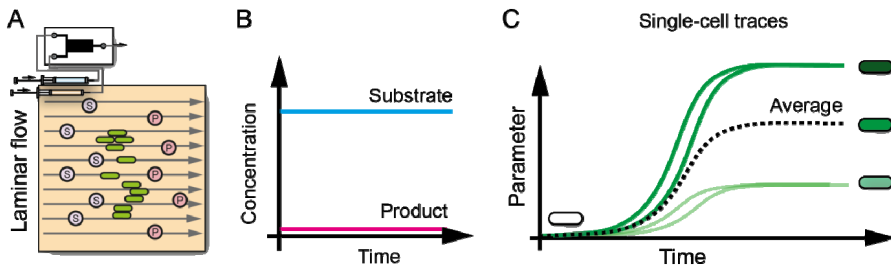


Figure 1.3: Microfluidic single-cell analysis. (A) Microfluidic systems offer constant environmental conditions by laminar flow. (B) Concentration profile of substrate and product of a microfluidic single-cell cultivation. Substrate is continuously provided and product removed. (C) Live-cell imaging allows for dynamic analysis of single cells with spatio-temporal resolution.

1.4 Project objectives

As described in the previous sections, profound knowledge on single-cell behavior is essential for understanding and optimizing bioprocesses. The primary objective of the present research project is the development of single-cell cultivation systems for bacteria and its application to industrially applied organisms such as *Corynebacterium glutamicum* and *Escherichia coli*.

Cell growth is one of the most important performance indicators of industrial production processes utilizing microorganisms such as bacteria or yeast. It is directly related to all growth coupled processes, e.g., the production of amino acids [23] and recombinant proteins [24, 25]. Optimizing growth conditions is a major goal during bioprocess development and has to be investigated in more detail. Limited knowledge is available about growth performance of industrially applied bacteria strains and the gradually engineered production strains at the single-cell level. The secondary objective is to investigate important bioprocess parameters such as growth, morphology and production using the new developed single-cell systems.

This work is performed in close cooperation with many groups within our institute, which develop novel microbial cell factories that need to be understood in more detail. Their questions and strains are used as key motivation for the development and optimization of novel single-cell systems that are addressed within this work.

1.5 Workflow

In the present project, a new workflow was established as illustrated in Figure 1.4. Major tasks including the design, fabrication, assembly and application of our microfluidic single-cell systems for the investigation of bioprocess relevant questions were addressed:

- Design of novel single-cell cultivation systems (Figure 1.4B)
- Fabrication of microfluidic devices (Figure 1.4C)
- Assembly of microfluidic chips (Figure 1.4D)
- Automated time-lapse experiments (Figure 1.4E)
- Image analysis (Figure 1.4F)

The obtained results were used to improve the microfluidic single-cell analysis pipeline as well as to gather new information about bacterial behavior. This information is finally used to further understand and optimize bioprocesses.

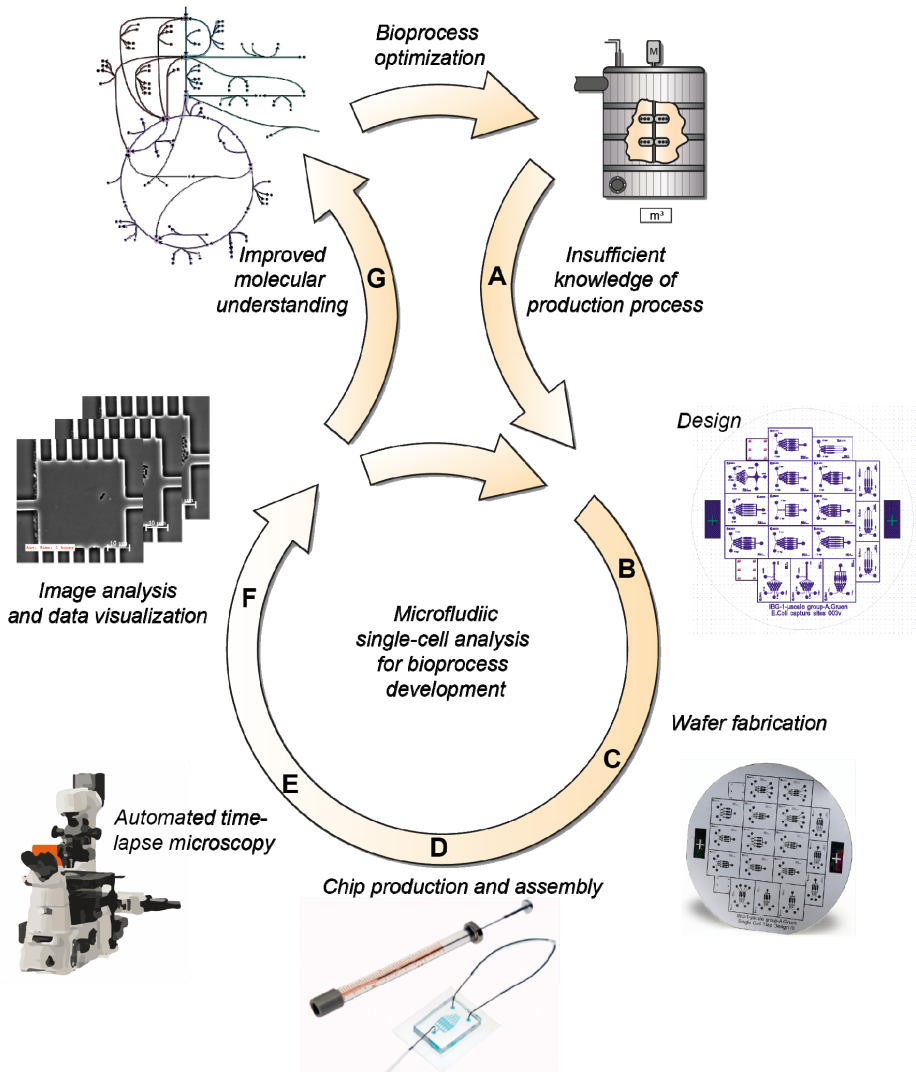


Figure 1.4: Microfluidic single-cell analysis workflow established within the present work. (A) The bioprocess/organism as well as established microfluidic knowledge were used to design new single-cell cultivation systems (B), which are used to fabricate a silicon wafer (C). (D) Using soft lithography disposable PDMS chips were assembled. (E) The chips, combined with automated live-cell imaging, are used for dynamic single-cell studies. (F) The obtained image-based data are analyzed and visualized. (G) Potentially, new insights into the metabolism of cells are acquired, which can be used to improve bioprocesses. The metabolic network was kindly provided by Elisabeth Zelle.

1.6 Thesis outline

Figure 1.5 displays a graphical outline of this thesis. In Chapter 2, conventional single-cell technologies are compared with novel microfluidic single-cell systems. Furthermore, a survey of existing microfluidic single-cell cultivation systems is presented

and discussed critically. Additionally, the application of the developed systems in the field of bioprocess development is discussed.

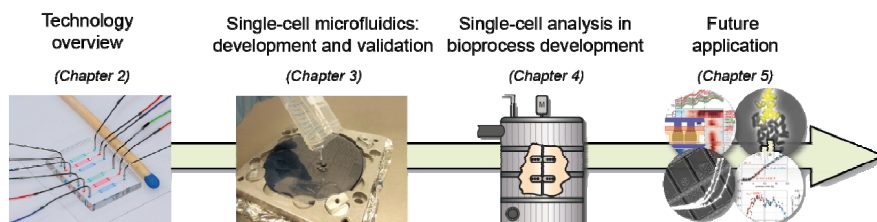


Figure 1.5: Thesis overview. The different work packages were chronologically ordered in subsequent chapters, ranging from technology overview (Chapter 2), development and validation of single-cell microfluidic systems (Chapter 3). In Chapter 4, single-cell growth studies as an example for single-cell analysis in bioprocess development is given. Finally, further examples of applications are presented in the “Future application” chapter (Chapter 5).

In the first year of my thesis, the single-cell cultivation system was established. Chapter 3 deals with the design, fabrication, setup and operation of novel single-cell cultivation systems. The fabrication, design and principle of picoliter bioreactors (PLBR) are discussed. Furthermore, the design and development of a highly parallelized cultivation platform is described. This platform enables the high-throughput growth analysis of various bacteria strains in monolayer growth chambers (MGC). The system was benchmarked with two competitive systems used for single-cell investigations, namely agarose pad and negative dielectrophoretic systems (nDEP). For the first time, a systematic comparison of different systems was performed, investigating the impact of the cultivation principle onto cellular physiology of *Corynebacterium glutamicum*.

Chapter 4 has a highly interdisciplinary character, and contains the experiments and results performed in the second year. The developed PLBR and MGC were used to investigate single-cell growth of *C. glutamicum* in detail. Interestingly, significant higher growth rates were obtained compared to growth rates obtained in different large-scale cultivation systems. In the following sub-chapter, potential factors responsible for the higher growth rates were investigated. Single-cell cultivation in combination with conventional cultivation systems and analytical methods such as transcriptomics and metabolomics identified the factor leading to higher growth rate. This chapter describes one example demonstrating single-cell cultivation in combination with conventional cultivation systems to further understand large-scale cultivation processes. Finally, latest developments and results for an improved understanding of the higher growth rates as well as first trials to transfer higher growth rates to large-scale are given.

In Chapter 5, an outlook is given into several application fields that were investigated in the third year of my thesis. First, an overview of additionally developed single-cell designs is given. The chapter describes the ongoing miniaturization of single-cell design for the analysis of small sub-colonies as well as for single bacteria cells. Furthermore, the potential of microfluidic system for the investigation of other industrial

important organisms is shown. This includes bacteria as well as industrially important organisms such as fungi.

In Chapter 6, overall conclusions are drawn. Necessary improvements and future challenges which are indispensable for the successful establishment of single-cell cultivation devices into daily lab routines are critically discussed.

Since most of the different chapters are based on published articles, some information is redundant. This allows to read the chapters independently.

2 Technology overview

2.1 Microbial single-cell analysis

This overview chapter gives a general summary of the existing single-cell cultivation systems. The reader is provided with an overview and critical assessment of existing technologies.

2.1.1 Abstract

Single-cell studies are of interest in many disciplines. Traditionally, flow cytometry and agarose pad based image analyses are used to study single-cell behavior. Microfluidics provides novel technologies, especially for single-cell analysis (SCA) at well controllable environmental conditions. Thus far, microfluidic single-cell growth studies were not pursued systematically, since many systems operated only on the level of proof of principle and methods were difficult to apply for systematic studies. This has drastically changed during the last three years and especially disposable microfluidic PDMS-glass systems are of increased popularity. This review critically discusses existing microfluidic single-cell cultivation systems, ranging from systems for population growth studies to systems intended for single cells. Focus is put on systems with full single-cell resolution for quantitative growth and metabolic studies of yeast and bacteria.

2.1.2 Introduction

A detailed understanding of the growth and metabolism of single cells, is of interest in many disciplines, ranging from molecular biology [26], food engineering [27], systems and synthetic biology [28, 29] to bioprocess engineering [22].

New insights into microbiological systems have been achieved by population based analysis of billions of cells masking individual cell behavior. However, it has become clear that isogenic populations can be quite heterogeneous, comprising cells in various different state and phenotypes.

Reasons for cell-to-cell heterogeneity are manifold and can range from cellular factors to environmental factors [30]. Cellular factors include genetic variations and/or stochastic variations within transcription and translation machinery and regulatory effects [19]. Environmental factors mainly include changes in the medium composition during cultivation as well as microgradients caused by inefficient mixing [13]. Both phenomena appear simultaneously, making a detailed understanding about cell-to-cell heterogeneity a difficult task.

The incomplete understanding of this complex interplay makes a prediction and modeling of cellular processes not feasible or may lead to the misinterpretation of the obtained data. This holds true for all fields within biotechnology and is thus of major interest for future microbial research. Thus, quantifying and understanding micro- and macro heterogeneities is one of the most challenging problems facing single-cell research.

A variety of analytical tools have been applied to obtain detailed information about single cells physiological status in their environment. These technologies are discussed in the following sub-chapters.

2.1.3 Single-cell analysis: snapshot vs. dynamic

Flow cytometry

One of the most frequently used methods to detect cell-to-cell differences in cellular population is flow cytometry (FC). Single cells pass through a laser beam or electric detection unit in a hydrodynamically focused fluid stream. The interaction of the cells with the laser beam, absorption scattering or fluorescence excitation, can be monitored for each individual cell. These data can then be correlated with different cell characteristics and resulting distributions can give an insight into a cell population [31].

Most flow cytometers are based on fluorescence monitoring, allowing for the characterization of intrinsic fluorescence signal. Whereas no pretreatment is necessary for the intrinsic fluorescence, extrinsic fluorescence requires a sample preparation with fluorescence dyes and staining procedure prior to analysis [32]. One advantage of FC is the simultaneous measurement of multiple fluorescence signals/spectra, as well as forward and side scatter. In addition, flow cytometers can be combined with sorting units that offer the possibility of isolating selected subpopulations [33, 34].

Electronic measurements (Coulter counter principle) can be used to determine parameters such as cell volume [35]. In contrast to laser based FC which only indirectly measures the cell volume [36], the Coulter counter allows for direct and precise cell volume measurements. Within Coulter counters, the passage of a cell through a buffer-filled orifice will transiently increase the electrical impedance of the orifice, which is displaced proportional to the buffer volume. The Coulter volume measurement is thus relatively independent of the shape of the cell [35].

Using these technologies, it is possible to detect up to 80,000 cells/s, deciphering cell-to-cell differences, and thereby elucidating the heterogeneity of the population. Figure 2.1A illustrates a small cell population, which was sampled at two distinct time points. Although the change of an intrinsic fluorescence signal can be followed and quantified from time point to time point for a culture, neither the history nor the temporal development of an individual cell is traceable. However, this is prerequisite to understand the reason, for example, when cells spontaneously change the state or if a subpopulation of cells belong to a common ancestor.

Many studies have worked on the evaluation of growth processes. This includes studies on parameters such as the cell size, granularity or DNA content revealing valuable insights into the metabolic status and the fitness of the whole population [37, 38]. Bromodeoxyuridine in combination with propidium iodide (PI) staining allows to derive respective doubling times [39]. Neumeyer *et al.* [40] investigated the population dynamics of *C. glutamicum*. Using fluorescent dyes Syto 9, PI, and DiOC₂(3) (3,3'-

Diethyloxycarbocyanine iodide) they identified subpopulations with reduced viability and membrane potential inside early log and stationary phase populations. They revealed first insights into population processes and cellular dynamics within large populations, but a deeper understanding remains hidden.

During the last years automated FC systems have been developed, which reduce the extensive workload for sample handling. These systems significantly expand the utility of FC by eliminating cumbersome and time-consuming steps. These improvements have led to higher sampling frequencies and reduced influence on sample degradation. This allows the construction of detailed pictures of cellular changes of a population as a function of the cultivation time [41, 42]. Despite all those advantages, FC-based applications remain snapshot analyses, reflecting the state of a cell at a certain moment in time and still lack the problem, that individual cells cannot be traced in a spatio-temporal manner.

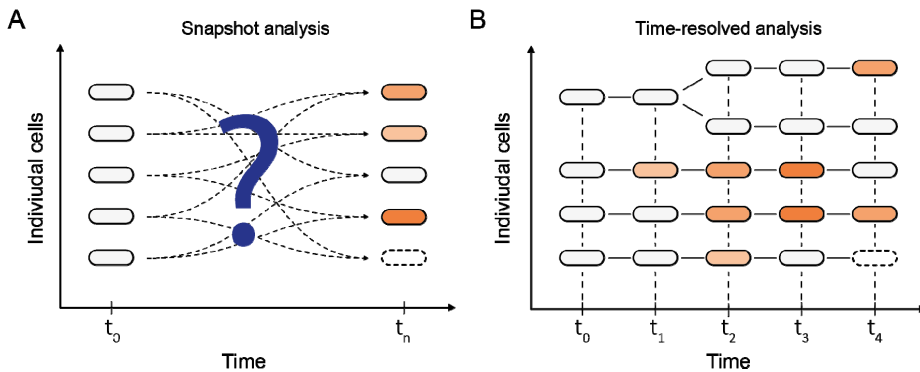


Figure 2.1: Comparison of flow cytometric methods and time-resolved analysis. (A) Using flow cytometry (FC), single-cell behavior can be analyzed in high throughput. Single cells cannot be tracked and the dynamic development of single cells remains hidden. (B) Using live-cell imaging, cells can be tracked, revealing the dynamics of individual cells within populations.

Live-cell imaging

Live-cell imaging is performed to provide insight into the fundamental nature of cellular processes with spatio-temporal resolution [43]. In comparison to FC methods, live-cell imaging allows for time resolved analysis of single cells (Figure 2.1 B). During the last years, continuous progress was made in the field of live-cell imaging. For the current trends and progress of different novel microscopical setups and analysis the reader is referred to [44, 45]. For advances in novel fluorescence proteins and their application in live-cell imaging the reader is referred to [46].

Especially the development of motorized microscope components and accessories enable the investigator to automate live-cell image acquisition and are particularly useful for time-lapse experiments that range in timescale intervals from milliseconds to tens or hundreds of minutes (Figure 2.2). This allows the investigation of dynamic processes, ranging from fast cell movement to slow metabolic processes.

If fast cellular events such as single molecule tracking are under investigation [47-49], the number of spots is restricted to one region of interest (ROI) (Figure 2.2 A). This also holds true if bacterial movement such as chemotaxis and motility are studied. Typically frame rates are in seconds or sub-second range. For different events such as single-cell division or morphological development, frame rates are in the order of several minutes. This allows the investigation of more ROIs in sequence. For colony-based investigation such as growth rate, or comparison of different microcolony behavior, sampling can be done in the range of hours and several hundred positions can be investigated in sequence.

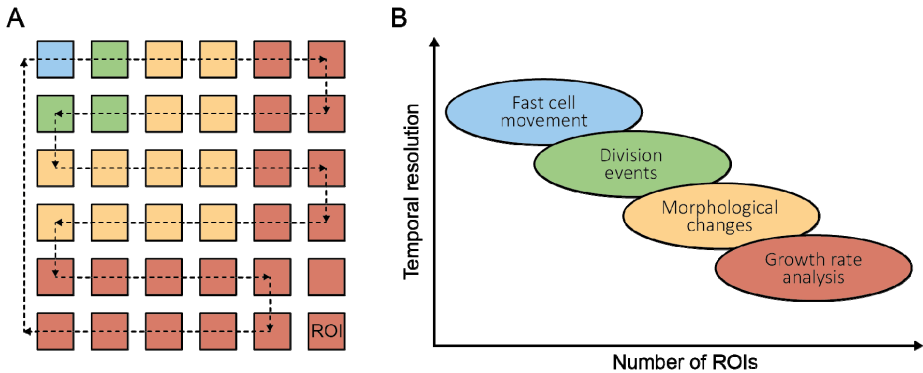


Figure 2.2: Overview of the spectrum of live-cell imaging microscopy. Using automated microscopy setups, both real-time microscopy as well as time-lapse experiments are possible. (A) The number of positions that can be investigated, correlates directly with the frame-rate necessary to investigate the biological phenomena. (B) For fast cell movement studies as well as intracellular investigations, only a low number of ROIs are possible. For colony based analysis, such as growth rate, many ROI can be investigated in parallel.

Crucial for time-lapse imaging is the control of the cultivation conditions. In the last three years, especially the field of maintaining cultivation conditions through novel microfluidic cultivation chambers was revolutionized. The systems that were developed, range from simple colony based cultivation chambers to cultivation system for one single cell. In the next section, the development of cultivation setups for live-cell imaging with a special focus on yeast and bacteria will be summarized. Finally, current progress in single-cell cultivation systems is discussed.

Agarose pad cultivation

Dynamic single-cell cultivations have attracted scientist for a long time. First efforts to isolate single cells ranging back for more than 100 years [50, 51] and lead to the first dynamic single-cell studies on agarose-glass slides [52, 53]. Single cells were placed between a glass plate and a mixture of molten agarose dissolved in growth medium. Agarose is soft, porous and transparent and holds the cells in place for imaging. Although being simple this method was still subject to uncertainties. For this reason, it was subsequently improved during the following decades [54] and is still undergoing improvements [55]. Today agarose pads are used to investigate growth of various

organisms, ranging from bacteria to yeast [56, 57] and has proven to be a versatile tool for many biologist. Despite these efforts, agar pads still have their limitations. The main drawback is the very limited control of cultivation conditions of the setup, making investigations at controlled defined environments difficult [58]. Potential risks are evaporation and nutrient consumption during cultivation and slow replenishment through diffusion, leading to an in space-time inhomogeneous environment.

2.1.4 Microfluidic single-cell cultivation - Physics and fabrication

Physical laws in microfluidic environments

At the microscale different phenomena become dominant over those in the macroscopic world. These phenomena include laminar flow, diffusion, heat transfer, surface area to volume ratio, and surface tension [59]. Here the most important topics for the present review are shortly explained.

Flow regime

The flow regime is determined through the Reynolds number (Eq. 2.1).

$$\text{Re} = \frac{\rho \cdot v \cdot D_h}{\eta} \quad (2.1)$$

Equation 2.1 describes the Reynolds number with the fluid density ρ , the characteristic velocity of the fluid v , the hydraulic diameter D_h and the fluid viscosity η . The hydraulic diameter depends on the channels' cross sectional geometry. In micro channels the flow is normally laminar, in comparison to macroscale with turbulent flow, and has a small $\text{Re} < 1$. Due to the laminar flow, two adjacent streams in a micro channel are only mixed by diffusion [60].

Diffusion

In a diffusion process a concentrated group of molecules will spread out over time until an equilibrium in concentration is reached [59]. Equation 2.2 is a model for the diffusion in one dimension where a particle with the diffusion coefficient D moves a distance d in the time t .

$$d^2 = 2 \cdot D \cdot t \quad (2.2)$$

Diffusion becomes the dominating factor of mass transport in microchannels. Taking the diffusion of glucose at room temperature, with a diffusion coefficient $D = 7 \cdot 10^{-10} \frac{\text{m}^2}{\text{s}}$ less than two seconds are necessary to cover a distance of 50 μm (neglecting diffusion in z direction).

Trapping and cultivation principles

Cells need to be isolated and trapped by appropriate mechanisms to perform live-cell imaging of single cells. Figure 2.3 illustrates different cell trapping principles that were developed over the years. This includes for example laser trapping [61, 62], acoustic trapping [63], magnetic trapping [64], nDEP trapping [65, 66] and hydrodynamic trapping [67]. All principles shown in Figure 2.3 have their special advantages and disadvantages but are not further discussed within this work. For a detailed comparison, the reader is referred to [68, 69]. Whether cells get stressed during trapping and cultivation remains an ongoing debate [70].

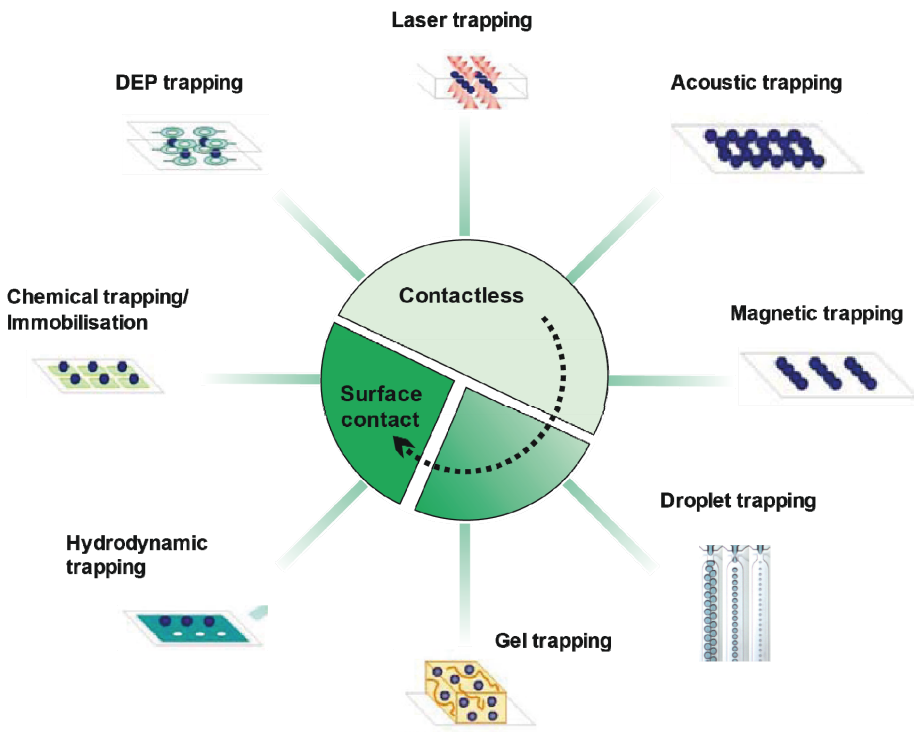


Figure 2.3: Overview of single-cell trapping principles. Existing trapping principles are: hydrodynamic trapping, chemical trapping, DEP trapping, laser trapping, acoustic trapping, magnetic trapping, droplet trapping and gel trapping. Adapted and modified from [68].

NDEP trapping, laser trapping, hydrodynamic trapping, gel trapping and droplet trapping led to the development of systems that were applied for proof of principle growth studies of bacteria and yeast [29]. For quantitative microfluidic single-cell studies only hydrodynamic systems, droplets [71, 72] and nDEP were used. Figure 2.4A illustrates the nDEP setup and exemplary yeast and bacteria cultivated in the so called “Envirostat” [73]. Figure 2.4B shows the cultivation principle of droplet systems. In both systems cells are not in one focal plane but immobilized at one distinct position.

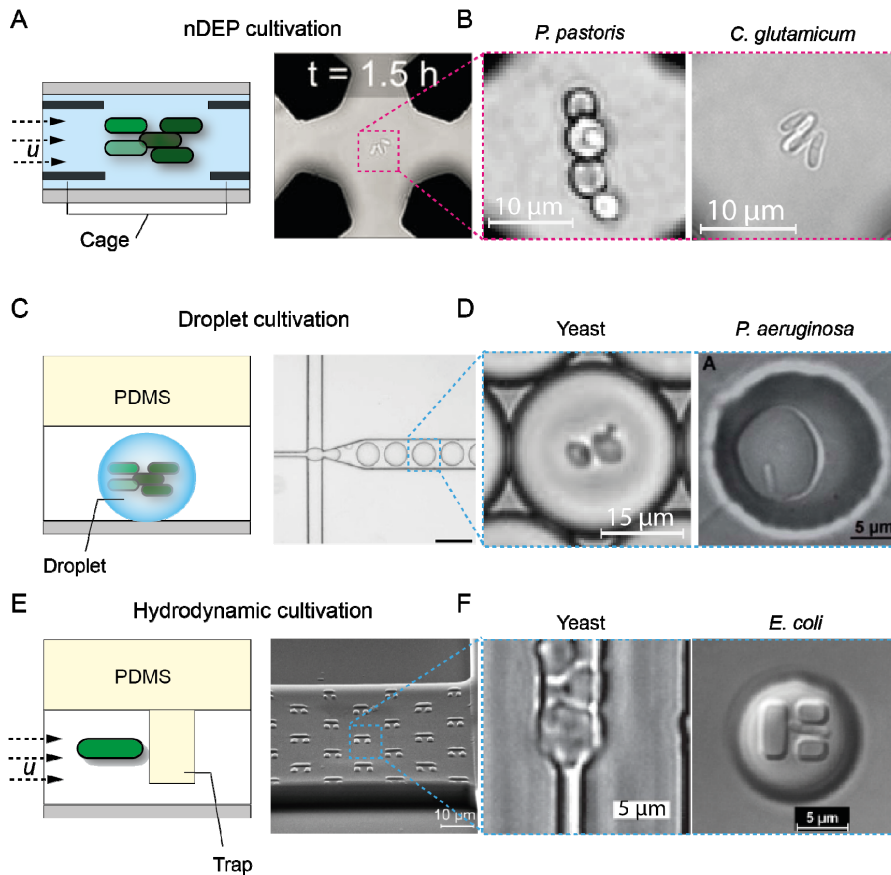


Figure 2.4: Droplet, nDEP and hydrodynamic cultivation systems. (A) Schematic drawing of cells trapped within nDEP cage. (B) Example for yeast and bacteria cultivation in an nDEP system. (C) Schematic drawing of cells in a microdroplet. (D) Example of yeast and bacteria trapped and growing within microdroplet. (E) Schematic drawing of cells trapped within hydrodynamic barrier structure. (F) Example for yeast and bacteria cultivation in a hydrodynamic trapping system. Figures adapted and modified from [73-77].

In recent years especially hydrodynamic cell trapping and cultivation in PDMS – glass systems are increasingly used (Figure 2.4E) [22, 78]. Easy fabricate procedures, short innovation cycles as well as the ability to observe cells in one focal plane are the main reasons.

Fabrication methods

Various manufacturing techniques have been developed to fabricate microfluidic cultivation systems. Amongst others, silicon and glass systems were developed with the disadvantage of being costly and the necessary for highly specialized skills. Polymers such as poly(methylmethacrylate) (PMMA) and polycarbonate (PC) have outstanding material properties, however, require substantial investment. At large device numbers, PMMA and PC remain the optimal materials. With the advent of soft lithography,

revolutionized by the research of the Whitesides group [79], polydimethylsiloxane (PDMS)-glass systems became the method of choice for constructing low microfluidic device numbers applied in live-cell imaging or for rapid prototyping. PDMS-glass systems can be manufactured easily and at relatively low cost. Furthermore, PDMS is transparent and gas permeable, ideally for live-cell imaging and cultivation of various biological cell systems.

Advances in softlithographic methods have evolved during the last years, finally allowing the fabrication of structures in the sub-micrometer scale [80]. Figure 2.5 displays a typical scheme for the fabrication of PDMS chips. Silicon wafers are structured by photolithography (Figure 2.5B and C) in a cleanroom, leading to a structured wafer containing the positive design microstructure. These wafers are repetitively used to mold PDMS chips that are further processed.

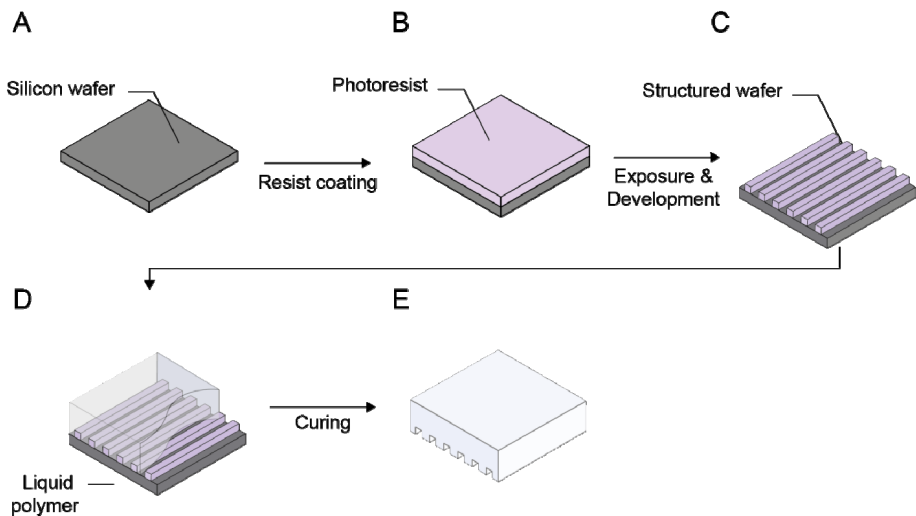


Figure 2.5: PDMS chip fabrication. (A-C) Silicon wafers are structured with photoresist containing the positive chip design information. (D-E) The structured wafer can be repetitively used to mold PDMS chips. Figure obtained and modified from Christopher Probst (Microscale bioengineering group; IBG-1: Biotechnology)

2.1.5 Microfluidic single-cell cultivation systems - Overview and examples

Classification

In the last ten years many different microfluidic single-cell cultivation systems have been developed. Therefore, a simple classification into subcategories is difficult. Different classification criteria have been proposed [20, 81, 82]. PDMS systems can be classified regarding the trapping design/principle as well as regarding the mode of operation (batch, fed-batch, perfusion, etc.). In this review systems are classified regarding to the number of cells that can be investigated and the possibility to maintain cultivation within single-cell resolution.

Droplet microfluidic systems are not discussed any further, due to the inability to track cells and because environmental control is limited. Furthermore we will not discuss simple flow channels where cells adhere randomly to channel systems (*e.g.*, [83]) making quantitative and reproducible growth analysis impossible.

Overview

In general the published PDMS based systems allowing single-cell cultivation can be classified with respect to four main principles, namely “single-cell traps”, “single-cell growth channels”, “single-cell growth chambers” and 3D cultivation chambers with single-cell resolution (Figure 2.6). Each of the four designs has unique advantages and disadvantages, but all of them have obvious benefits over the cultivation systems presented in the previous chapters and can be used to investigate problems that have not been possible to investigate before. General advantages are the possibility of high-parallelization, reduced gradients and the ability to investigate single-cell behavior in detail.

3D single-cell growth chambers allow for the cultivation of densely packed cultures, starting from one single cell (Figure 2.6A). Although single-cell resolution is reached, the growing cells prevent a long-term investigation and tracking of single cells.

Tracking and analyzing single cells over generations requires the cell colony to be in a monolayer. The advantage of the monolayer is that large numbers of cells can be captured in a single frame without interfering signal from overlapping cells. In the last years various systems were reported.

Monolayer growth chambers (Figure 2.6B) allow the investigation of complete isogenic microcolonies, similar to agar-pad methods. Complete colony profiles can be generated. Tracking is difficult and the growing microcolonies might be affected by potential gradients, when metabolites are not removed fast enough.

Using growth channels (Figure 2.6C), long-term investigations can be done, allowing not only for a high degree of parallelization but also for easy tracking since cells are restricted to grow in a narrow channel. The disadvantages are incomplete lineages and the current lack of a reliable seeding procedure for most of the reported systems.

Single-cell traps (Figure 2.6D) allowing for “real” SCA, without potential effects of neighboring cells. These designs are difficult to fabricate for bacteria and yeast and have to date not revealed their full potential.

Each of these designs will be explained and critically evaluated on selected examples, with the focus of the potential for future use of systematic single-cell cultivation. In comparison to the growth chambers presented in Chapter 2.2.5, all presented systems are operated in continuous cultivation mode.

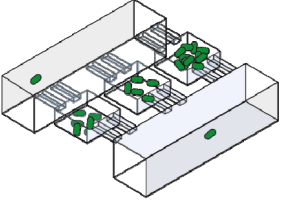
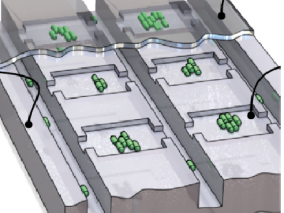
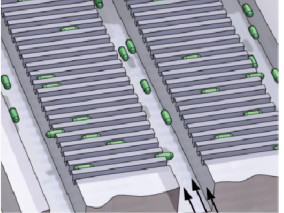
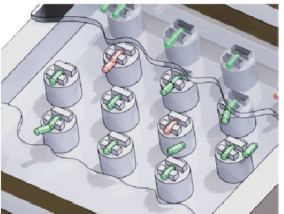
<p>A 3D growth chambers</p> 	<p>Advantages</p> <ul style="list-style-type: none"> ▶ Easy seeding procedure ▶ Easy to fabricate ▶ High degree of parallelization ▶ Continuous and batch operation 	<p>Disadvantages</p> <ul style="list-style-type: none"> ▶ Tracking not possible ▶ Potential gradients ▶ Cell-to-cell communication
<p>B Monolayer growth chambers</p> 	<p>Advantages</p> <ul style="list-style-type: none"> ▶ Complete lineage information ▶ Easy seeding procedure ▶ Easy to fabricate ▶ High degree of parallelization 	<p>Disadvantages</p> <ul style="list-style-type: none"> ▶ Tracking difficult ▶ Potential gradients ▶ Cell-to-cell communication ▶ < 9 generations ▶ Potential loss of cells
<p>C Single-cell growth channels</p> 	<p>Advantages</p> <ul style="list-style-type: none"> ▶ Long-term investigations ▶ Easy tracking of cells ▶ High degree of parallelization ▶ Aging studies possible 	<p>Disadvantages</p> <ul style="list-style-type: none"> ▶ Fraction of lineage tree ▶ Morphological investigations limited ▶ Cells could be squeezed ▶ Loading procedure still difficult
<p>D Single-cell traps</p> 	<p>Advantages</p> <ul style="list-style-type: none"> ▶ True single-cell investigations ▶ No communication ▶ No environmental gradients ▶ High degree of parallelization 	<p>Disadvantages</p> <ul style="list-style-type: none"> ▶ Sub-μm fabrication difficult ▶ No representative trapping guaranteed ▶ Morphological investigations limited

Figure 2.6: Overview of the four different single-cell cultivation concepts. (A) 3D cultivation chambers with single-cell resolution. (B) Monolayer growth chambers with for short-term and long-term investigation of microcolonies. (C) Single-cell growth channels with for controlled long-term cultivation of small subpopulations. (D) Single-cell trap for the investigation of exactly one cell.

Growth chambers (3D)

One of the first devices with single-cell resolution was developed by Groisman *et al.* [84], allowing to start a bacteria cultivation with one single cell. Only overall colony growth was analyzed within the 3D culture chamber, because cells are not immobilized or trapped. Groisman *et al.* [84], Balaggade *et al.* [85] and Luo *et al.* [86] were the first using imaging as a new way to quantify growth within microfluidic cultivation devices, instead of measuring absorbance based OD_{600} . Most of the growth chamber systems developed in the last years (see Table 2.1) have chamber heights between 10 - 35 μm . Dai *et al.* [87] all published the first proof of principle of a batch cultivation device with single-cell resolution. Sun *et al.* [88] and Mohan *et al.* [89] used a 3D microfluidic system for growth behavior and antibiotic screening.

Although growth can be observed with single-cell resolution, individual cells are not possible to trace. Furthermore, morphological characteristics are difficult to quantify and inner parts of the colony might be affected by gradients. To perform real single-cell cultivation at constant environment, chambers need to be miniaturized further.

Colony growth chambers

Similar to agarose pad cultivation systems (Chapter 2.1.3), one of the most straight forward methods are monolayer chambers, that restrict cellular growth into one focal plane. This enables the growth of micro-populations up to several hundred cells. Typically single cells are trapped, and growth and metabolism can be followed over time.

Two kinds of growth chambers were developed. Category A (“Closed design”) represent chambers that allow for a limited time of investigation until the chambers are filled (Figure 2.7A). The systems of category B (“Continuous design”) allow for long-term cultivation through continuous removal of growing cells (Figure 2.7B).

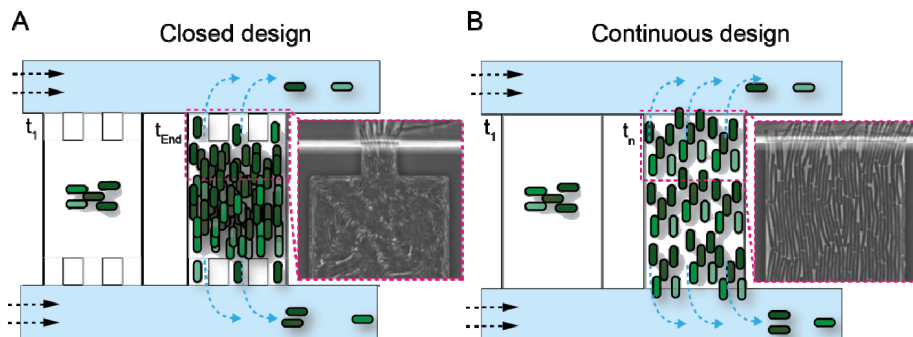


Figure 2.7: Schematic drawing of colony designs. (A) Closed designs allow for the investigation until the chambers are filled. Afterwards cells cannot be analyzed anymore. (B) Continuous designs allow long-term investigation. Excess cells are pushed out of the chamber, allowing for continuous cultivation and observation on single-cell level.

Table 2.1: Overview of miniaturized growth chambers within single-cell resolution. The heights of the 3D growth chambers allow to investigate cells with single-cell resolution, but detailed morphological investigation are not possible.

Name	Organism	Dimension (h x w x l) μm Volume [nl]	Application	System specific characteristics	Year	Reference
Circular micro-channel	<i>E. coli</i>	10 x 140 x 11.5 mm in circumference 16 nl	Population dynamics	Batch as well as perfusion	2005	Balagadde <i>et al.</i> [85]
Microfluidic chemostat	<i>E. coli</i> <i>S. cerevisiae</i>	6 x 100 x (70-200) 50 nl	Proof of principle	Perfusion	2005	Groisman <i>et al.</i> [84]
Micro turbidostat	<i>E. coli</i>	200 x 200 x NA 1 nl	Proof of principle		2010	Luo <i>et al.</i> [86]
Microfluidic system in zero flow environment	<i>E. coli</i>	35 x 300 x 300 ~3 nl	Antibiotic testing	Single-cell resolution	2013	Sun <i>et al.</i> [88]
Multiplex microfluidic platform	<i>E. coli</i>	15 x 400 x 1000 ~6 nl	Antibiotic screening	Single-cell resolution	2013	Mohan <i>et al.</i> [89]
Nanoliter batch bioreactor	<i>E. coli</i>	10 x 100 x 500 ~0.5 nl	Proof of principle	Batch cultivation on single-cell level	2013	Dai <i>et al.</i> [87]
Microchemostat	<i>S. cerevisiae</i>	(20-100) x NA x NA 250 nl	Proof of principle	Small-volume fraction replenishment for steady-state microbial culture	2013	Park <i>et al.</i> [90]

One of the first closed monolayer concepts for the cultivation of yeast (see Table 2.2) was published by Taylor *et al.* [91]. They trapped yeast between partially closing “sieve” valves thereby allowing for media exchange around the trapped yeast cells. They successfully investigated the dynamics in MAPK signaling of single yeast cells. The disadvantage of the design was a partial loss or migration of cells within the chambers, making tracking of cells difficult or impossible. Furthermore the colony size was limited to 300 cells, reducing the overall time of experimentation to several generations.

An improved chamber design, the microfluidic imaging matrix was developed by Falconet *et al.* [92], allowing for cultivation of up to 6000 yeast cells per chamber in a 4.4 x 260 x 684 μm monolayer chamber. While it allows tracking single cells over multiple generations, the overall experimental duration is limited by the chamber size. Moreover, random trapping leads to an unpredictable filling of the chamber potentially leading to overgrowing colonies, making the investigation of several colonies impossible.

Cookson *et al.* [93] developed one of the first open cultivation chamber systems, the so called “Tesla microchemostat” that permits single-cell fluorescence imaging of gene expression over many cellular generations of yeast. Within this design, several hundred cells are cultivated inside large cultivation chambers. Excess cells are pushed out of the cultivation chamber and are removed within the media stream. Uhlendorf *et al.* [94] used a similar open chamber concept (3.1 x 300 x 400 μm) for long-term model predictive control of gene expression of yeast colonies.

The same concepts were built for bacteria (Table 2.3). Chamber heights are between 0.9 and 1.2 μm to match the dimension of average bacteria width. The first reported systems did not allow for a controlled trapping and removal of single cells and were used to investigate colony behavior such as to characterize a general streaming instability occurring in a confined colony of nonmotile bacteria [95]. Cells near to the opening side are released as the colony expansion is restricted to one side. The released cells are removed by the media stream. Similarly, Volfson *et al.* [96] adapted the tesla mixer for the cultivation of bacteria (reduced the height from 4 μm to 1 μm). They investigated the biomechanical ordering of dense bacterial populations.

Ullman *et al.* [97] and Walden *et al.* [48] used monolayer chemostats based on the design of Mather *et al.* [95] to investigate cell length, growth and gene expression of single cells within a continuously growing microcolony. They analyzed the rate of gene expression at the level of single proteins over 3000 bacterial cell cycles. Grünberger *et al.* [98] have developed a hybrid system, using overflow channels to regulate the density of the cell colony.

Table 2.2: Monolayer growth chambers for the cultivation of yeast microcolonies.

Design category	Name	Organism	Dimension (h x w x l) μm	Main application	Key characteristics	Year	Reference
Continuous	Tesla microchemostat	<i>S. cerevisiae</i>	-	Monitoring dynamics of single-cell gene expression		2005	Cookson <i>et al.</i> [93]
Continuous		<i>S. cerevisiae</i>	5 x (160-600) x NA	Gene expression studies		2007	Paliwal <i>et al.</i> [99]
Closed	“Steve” valves imaging platform	<i>S. cerevisiae</i>	-	Dynamic analysis of MAPK signaling	Single-cell monolayer reached through PDMS valves	2008	Taylor <i>et al.</i> [91]
Closed	Microfluidic imaging matrix	<i>S. cerevisiae</i>	4.4 x 260 x 684	High-throughput tracking of single cells		2009	Falconnet <i>et al.</i> [92]
Closed	Linear arrays of chambers	<i>S. cerevisiae</i>	5 x 50 x 50	Growth propagation of yeast	Hybrid colony and channel design	2011	Wang <i>et al.</i> [100]
Continuous		<i>S. cerevisiae</i>	3.1 x ~300 x 400	Long-term predictive control of gene expression		2012	Uhlendorf <i>et al.</i> [94]
Continuous	Microfluidic dissection platform	<i>S. cerevisiae</i>	4 x 15 x 60	Whole lifespan analysis		2012	Lee <i>et al.</i> [101]
Continuous		<i>S. cerevisiae</i>	4 x 100 x 20	Aging in single yeast cells		2012	Xie <i>et al.</i> [102]
Closed	Falconnet <i>et al.</i> design	<i>S. cerevisiae</i>	2 x 165 x 434	High-throughput lineage tracking	Loading of different yeast strain/ different medium	2013	Ricicova <i>et al.</i> [103]
Continuous	Chemostat array	<i>S. cerevisiae</i>	5 x 260 x 300	Spatio-temporal analysis of the yeast proteome	Array of 1,152 microchemostats	2013	Dénervaud <i>et al.</i> [104]

Table 2.3: Monolayer growth chambers for the cultivation of bacterial microcolonies.

Design category	Name	Organism	Dimension (h x w x l) μm	Main application	Key characteristics	Year	Reference
Closed	Chambers	<i>E. coli</i>	NA x NA x 1.5	Self-organization in high-density bacterial colonies		2007	Cho <i>et al.</i> [105]
Continuous	Tesla microchemostat	<i>E. coli</i>	1 x NA x NA	Investigation of oscillation on single-cell level	Adapted from Cooksen <i>et al.</i>	2008	Stricker <i>et al.</i> [106]
Continuous	Tesla microchemostat	<i>E. coli</i>	1 x NA x NA	Biomechanical ordering of dense cell populations	Adapted from Cooksen <i>et al.</i>	2008	Volfson <i>et al.</i> [96]
Continuous		<i>E. coli</i>	NA x (80-100) x 100	Synchronized genetic clocks		2010	Danino <i>et al.</i> [107]
Continuous	Open traps and side traps	<i>E. coli</i>	1 x 200 x 2000	Streaming instability in growing cell populations		2010	Mather <i>et al.</i> [95]
Closed	Bacterial lobster traps	<i>Pseudomonas aeruginosa</i>	NA x NA x NA	Social behavior studies of bacteria		2010	Conell <i>et al.</i> [108]
Continuous		<i>Mycobacterium smegmatis</i>	1 x 7 x NA	Division, growth and aging behavior	Chamber height > bacteria diameter	2012	Aldridge <i>et al.</i> [109]
Continuous	Traps	<i>E. coli</i>	0.9 x 40 x 40	Gene expression analysis	Design comparable to Mather <i>et al.</i>	2013	Ullmann <i>et al.</i> [97]
Continuous	Sensing array	<i>E. coli</i> <i>Salmonella typhimurium</i>	1.65 x 85 x 100	Oscillation studies	Chamber height > bacteria diameter	2013	Prindle <i>et al.</i> [28]
Continuous	Picoliter bioreactor	<i>C. glutamicum</i>	1 x \emptyset 40	Growth and morphology studies		2013	Grünberger <i>et al.</i> [98]
Closed	Growth pockets	<i>E. coli</i>	1.2 x 60 x 120	Filamentation studies/ Manipulation		2013	Probst <i>et al.</i> [110]

The effectiveness of these colony based systems is strongly depends on the chamber height, chamber geometry and flow rate applied to the system. A chamber height larger than the organism leads either to the problem of losing cells during cultivation, or unpredictable and uncontrollable trapping procedure. In too narrow chambers, cell physiology can be influenced leading to reduced growth, “pancake formation” or shape deformation as demonstrated in sub- μm constrictions [111].

Single-cell channels

One alternative cultivation concept to overcome the limitation of exponential growth are single-cell growth channels (Table 2.4 and Figure 2.8). Compared to colony growth chambers this kind of cultivation devices were designed for long-term measurements of different cellular characteristics such as aging effects or oscillating gene expression. Growth channels allow for the cultivation of a fraction of cells for finitely many generations. Dead end growth channels (Figure 2.7A) allow the investigation of individual mother cells, whereas open growth channels (Figure 2.7B) allow investigation of individual cells with similar ages.

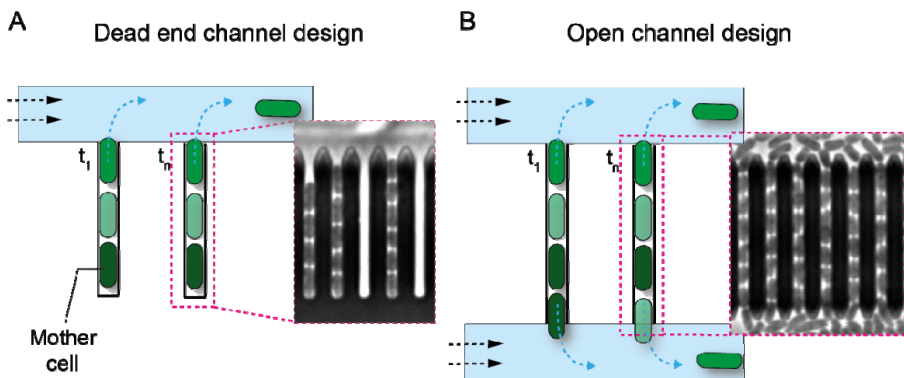


Figure 2.8: Schematic drawing of single-cell channel designs. (A) Dead-end growth channels allow the continuous investigation of mother cells. (B) Open channel designs allow the continuous investigation of individual cells with similar age.

One of the first systems was published by Balaban *et al.* [112]. In their system, individual bacteria cells were investigated under normal conditions and under antibiotic treatment. The developed devices consist of three layers, a first thin PDMS layer with thin $1.5 \times 0.5 \mu\text{m}$ lines. After pipetting bacterial suspension to the microfluidic structures, the lines were sealed with a permeable cellulose membrane and clamped with a large PDMS flow through channel system for medium exchange. Since several generations of cells can be investigated in the grooves, the history of “persister cells” could be recorded. In the presented study, the experimental time was limited to several generations (~ 10 hours of cultivation) and did not allow for continuous cultivation.

One of the first concepts, in which long-term tracking in one straight line was possible, was published by Rowat *et al.* [77], tracking lineages of single yeast cells. An

array of channels that have a constriction at one end was used to trap the “mother cell”. As soon as one cell is trapped, the flow is redirected and subsequent cells enter the bypass channel of the growth “chamber”, similar to the system reported by Tan *et al.* [113]. As cells divide in the narrow channel, they are constrained to grow in a line of a few cells, and can be analyzed regarding phenotypic variation within the cell lineage. The experimental time is limited to the channel length.

Several channel designs were published for bacteria. The first design was introduced by Jun and coworkers [114]. They presented a device that allowed long-term growth and division patterns of *E. coli* at a defined reproductive age. In dead end channels, single “mother cells” were trapped. The growth channels prevent the mother cell from moving around. Daughter cells are pushed out of the channel and are removed by the waste stream. Because of the narrow size, both motile and non motile cells can be captured. Since the filling is based on active diffusion, the original concept was restricted to the investigation of motile cells.

To reduce aging effects “open-end channel” designs were developed. This improved the loading procedure, when both ends are connected to separated main channels. Long *et al.* [58] changed the pressure on one main channel (pressure driven loading), which led to high trapping efficiency in most of the cells. After filling, both channels were operated with a small flow rate, to provide steady nutrient source.

A similar concept was developed by Moffitt *et al.* [115]. They used molded agarose to create linear tracks, separated by gutters. The hybrid PDMS agarose chip allowed first time to cultivate cells in linear channels, with the same abilities to agarose cultivations, and demonstrated that the exponential growth problem in conventional agar devices can be avoided. At the same time, cells still can communicate through the highly porous agarose walls, maintaining colony-like behavior. They demonstrated on two auxotrophic *E. coli* strains the cultivation of mixed microbial communities. However the porosity of agarose makes medium changes difficult and cultivation is far away from being defined and constant. Thus for co-cultivation studies this device is unique, but for medium changes and the investigation of influence of certain nutrient components this system should not be the method of choice.

Growth channels are used to investigate growth and aging [114], cell fate decision [116], product sensing [117], circadian oscillations [118], chromosome organization [119] and the measurement of physical properties [120, 121].

Generally speaking, growth channels allow for an easy automatable long-term growth pattern analysis. Currently the limitations are the necessity to adapt channel dimension to organism of interest. Furthermore, one major bottleneck is the filling procedure, which needs to be improved in the future.

Table 2.4: Overview of single-cell growth channels for yeast and bacteria.

Name	Organism	Dimension (h x w x l) μm	Application	System specific characteristics	Year	Reference
Microfluidic grooves	<i>E. coli</i>	1.5 x 0.5 x NA	Bacterial persistence during antibiotic treatment	Closed channels; PDMS – Membrane- PDMS stack	2004	Balaban <i>et al.</i> [112]
Single-cell lines	<i>S. cerevisiae</i>	5 x 5 x NA	Lineage tracking of single yeast cells	Dead end channels; Glass chip	2009	Rowat <i>et al.</i> [77]
Mother machine	<i>E. coli</i>	1 x 1 x 25	Long-term growth pattern analysis	Dead end channels	2010	Wang <i>et al.</i> [114]
Micro grooves	<i>E. coli</i>	3.0 x 1 x NA	Bacterial aging studies	Dead end channels	2012	Wakamoto <i>et al.</i> [122]
Single-cell chemostat	<i>E. coli</i> <i>B. subtilis</i> <i>E. faecalis</i>	(0.3 - 1.0) x (0.75 - 1.5) x (50 - 100)	Long-term growth and expression analysis; Co-cultivation	Open channel design PDMS agarose hybrid system	2012	Moffitt <i>et al.</i> [115]
Microfluidic chemostat	<i>E. coli</i>	(0.6 - 0.9) x 1.1 x 20	Growth rate and GFP expression	Open channel design	2013	Long <i>et al.</i> [58]
Small cavity	<i>S. cerevisiae</i>	3.3 x 6 x NA	Aging of yeast	Dead end channels	2013	Fehrmann <i>et al.</i> [123]
Troughs	<i>E. coli</i>	0.5 x 1.2 x NA	Four-dimensional imaging of bacterial nucleoid organization	Open channel design	2013	Fisher <i>et al.</i> [124]
Confined microchannels	<i>E. coli</i>	(0.5 x 10) x NA x NA	Antibiotic susceptibility testing	Open channel design; loading via nDEP	2013	Lu <i>et al.</i> [125]
V-shaped pockets	<i>S. cerevisiae</i>	4.8 x 10 x 10	Proof of principle		2013	Banaeiyan <i>et al.</i> [126]

Single-cell traps

Single-cell traps are modifications of the surface topography to capture single cells from a flow and trap them in a predefined position. In first instance they are intended to keep the cell at a certain position for dynamic metabolic measurements or defined lysis. The trapping structure dimension must therefore match to the size and shape of the cell.

Di Carlo *et al.* [127] presented one of the first single-cell array to investigate single-cell enzyme kinetics of human cell lines such as HeLa, Jurkat and 293 T-cell lines. This required the fabrication of traps with the dimension of 30 x 40 x 50 μm .

Similar principles were designed for single-cell investigation of yeast (Table 2.5). Ryley *et al.* [128] constructed so called yeast jails. They developed various trapping designs, in the range of a trapping area of 11 μm , with 4.5 μm spaces between jail bars. The size and geometry was designed, that during budding of the cells, the daughter cell would grow towards the outside of the jail. This assures to keep one cell in the jail, while the second one is removed. The prototype was used to study single-cell gene expression over time. A similar concept was reported by Rosa *et al.* [129].

According to Zhang *et al.* [130] such a device only works for the first few generations. As the size of mother and daughter grows with age, the daughter cells eventually jam the gates. Because of that Zhang *et al.* developed so called pensile columns. Basically, yeast cells are trapped between pillars of PDMS and the glass substrate. They tested different sizes of the column ranging from 20 x 20 μm to 80 x 80 μm in area in order to ensure that trapped cells stay underneath the column. The distance between PDMS and glass was optimized to 4 μm which is approximately the size of yeast cells. A similar concept was developed by Lee *et al.* [131].

Progress in sub- μm fabrication techniques (even 0.3 to 0.8 μm structures are reported [80]) even allowed the development of single-cell traps for bacteria. In 2011 the first system was reported for the trapping of one single bacteria cell (Table 2.6). The geometry of the single-cell trap, originally designed for larger cells, was adjusted for the trapping of bacteria [132], but no growth studies were performed. The first design demonstrating successful trapping and growth studies for isolated single bacteria cells was reported by Probst *et al.* [76] using sub- μm trapping structures.

Table 2.5: Overview of single-cell traps for yeast.

Name	Organism	Dimension (h x w x l) μm	Main application	Loading procedure	Year	Reference	Comments
Yeast jails	<i>S. cerevisiae</i>	Different designs	Variability of gene expression within yeast cells	Hydrodynamic trapping	2006	Ryley <i>et al.</i> [128]	
Cell-immobilization sites	<i>S. cerevisiae</i>	--	Proof of principle	Loading by negative pressure	2011	Zhu <i>et al.</i> [133]	Controllable immobilization and selective release of yeast
Pensile columns	<i>S. cerevisiae</i>	4 x (20 - 80) x (20 - 80)	Yeast aging	Loading by sudden injection with high velocity	2012	Zhang <i>et al.</i> [130]	Several cells are within the trapping region during observation
Hydrodynamic trap	<i>S. cerevisiae</i>	15 x 10 x 6	Gene expression of yeast cells	Hydrodynamic trapping	2012	Rosa <i>et al.</i> [129]	Similar concept as Ryley <i>et al.</i>
Microfluidic dissection platform	<i>S. cerevisiae</i>	(4 - 5) x 30 x 15	Long-term replicative aging studies	Hydrostatic pressure increase	2013	Lee <i>et al.</i> [101]	Several cells are within the trapping region during observation

Table 2.6: Overview of single-cell traps for bacteria.

Name	Organism	Dimension (h x w x l) μm	Main application	Loading procedure	Year	Reference	Comments
Conical nanopore array	<i>E. coli</i>	--	Capture and release of bacteria	--	2011	Guo <i>et al.</i> [134]	No growth studies performed
Micrometre-size sieves	<i>E. coli</i>	0.8 x 5 x 10	Proof of principle of trapping	Hydrodynamic cell loading	2011	Kim <i>et al.</i> [132]	Only trapping was reported, no growth studies.
Sub-micrometer traps	<i>E. coli</i>	1.5 x 2 x 1	Proof of principle trapping and long-term cultivation	Hydrodynamic cell loading	2013	Probst <i>et al.</i> [76]	Single-cell traps and double traps
Cell trap	<i>E. coli</i>	0.6 x 10 x NA	Analysis of single <i>E. coli</i> /lysates	Hydrodynamic cell loading	2013	Eyer <i>et al.</i> [135]	
Single microbe trap	<i>E. coli</i>	0.45 x 0.7 x 4	Single microbe trapping and release	--	2013	Vasdekis <i>et al.</i> [136]	No growth studies performed

2.1.6 Challenges and future directions

Despite the tremendous progress in the field of PDMS-glass single-cell cultivation devices, several aspects need to be improved, before the developed systems can be regularly used in application.

First, the filling procedures need to be standardized and improved. Many developed systems still lack the possibility of easy reproducible and repeatable filling. During the last two years, a tendency can be seen to fabricate agarose-PDMS hybrid chip systems (Table 2.7) to overcome this limitation. Cells are trapped between an agarose layer or a thin cellulose membrane and a glass slide. On top, PDMS channel systems are used for nutrient supply. These systems combine the advantage of both agar-pad systems and microfluidic perfusion. Cells can easily be trapped without complicated fabrication of trapping systems. At the same time, medium is continuously refreshed. The advantage of these systems is the investigation of motile bacteria strains, since the cells are restricted within their motility. Furthermore, cells can be investigated at reduced shear stress.

Table 2.7: Overview of hybrid agarose-PDMS single-cell cultivation systems.

Hybrid Characteristic	Organism	Main application	Year	Reference	Comments
PDMS - cellulose membrane	<i>S. cerevisiae</i>	Long-term fluorescent imaging	2008	Charvin <i>et al.</i> [137]	
PDMS - agarose	<i>M. xanthus</i> <i>E. coli</i>	Proof of principle	2009	Ducret <i>et al.</i> [138]	
PDMS - dialysis membrane - alginate gel	<i>M. smegmatis</i>	Proof of principle	2012	Golchin <i>et al.</i> [139]	Cells are not in one monolayer
PDMS - agarose	<i>Staphylococcus aureus</i>	Rapid antibiotic susceptibility testing	2012	Choi <i>et al.</i> [140]	Cells are not in one monolayer
PDMS + cellulose membrane	<i>M. smegmatis</i>	Dynamic persistence to antibiotics	2013	Wakamoto <i>et al.</i> [141]	
PDMS + polyacrylamide	<i>S. pombe</i> <i>E. coli</i>	Proof of principle growth studies	2013	Nghe <i>et al.</i> [142]	
PDMS + agarose	<i>E. coli</i> <i>Nitrosomonas europaea</i>	Morphology dynamics at antibiotic gradients	2014	Li <i>et al.</i> [143]	

Second, detailed analyses of the inherent trapping principle onto physiology of cells need to be performed. Until now, most of the systems were developed for the investigation of *E. coli* and *S. cerevisiae*. The impact onto physiological behavior of other species can so far only be estimated, but was reported to be critical.

Third, single-cell results have to be compared to large-scale and resulting differences need to be discussed and evaluated.

2.1.7 Conclusions

A wide range of novel single-cell cultivation systems were developed, revealing the high dynamics within this field. It is expected that the diversity of systems will still increase, but at the same time the systems will be increasingly used for detailed investigation and application.

The rapid development within the field of microfluidic single-cell cultivation technology will revolutionize the field of bacterial and yeast growth characterization in the next ten to twenty years. This survey is an attempt to capture a snapshot of the field at this critical stage. Of course traditional systems will still be an important research tool for the next years, however, the integration of single-cell technologies should certainly be considered to obtain additional information and interpret population based data from an another perspective.

2.2 Single-cell microfluidics for bioprocess development

This chapter gives an introduction into the field of single-cell cultivation systems that are applied for bioprocess and system biotechnological questions. Several application fields are discussed, pointing out the importance of novel microfluidic systems for future bioprocess optimization. The literature survey was conducted 2013. This chapter is based on a review that was published in *Current Opinion in Biotechnology* in spring 2014.

2.2.1 Abstract

Cell-to-cell heterogeneity in microbial biotechnological processes caused by biological (intrinsic) and environmental (extrinsic) fluctuations can have a severe impact on productivity. However, as yet little is known about the complex interplay between environmental reactor dynamics and cellular activity. A few years ago, innovative microfluidic systems were introduced facilitating the spatio-temporal analysis of single cells under well-defined environmental conditions allowing so far unachievable insights into population heterogeneity and bioreactor inhomogeneity. Examples of microfabricated systems include microfluidic cavities harbouring micropopulations of several thousand cells down to femtoliter-size structures entrapping individual bacteria. In well-defined perfusion experiments, central questions in biotechnology regarding, for example, growth, productivity, and heterogeneity on the single-cell level have been addressed for the first time. Microfluidics will take its place as a single-cell analytical technique in biotechnological process and strain characterization.

2.2.2 Introduction

“Biotechnology meets microfluidics”

The overall yield of the compound produced is central for the efficiency of a biotechnological production process utilizing microbial cells. However, it is the sum of all cellular activities which determines the productivity of an entire population [13]. This single cellular information is usually not unravelled during process development and relevant information is lost in conventional and average-based process analysis [144, 145].

It is well known that population heterogeneity can have a severe impact on production process efficiency, since individual cells may be in states other than the desired production phenotype [17, 146]. Even worse, it is expected that population heterogeneity as well as environmental reactor inhomogeneity will increase during scale-

up, often hindering successful transfer to industrial volumes [13, 15, 16, 147]. Neither intrinsic nor extrinsic reasons for cellular heterogeneity can be analyzed accurately under typical dynamic process conditions since they interplay in a complex and poorly understood manner.

For future improvements and developments in biotechnology and systems biology, downsizing of conventional bioreactor concepts [148, 149], flow cytometry approaches [150, 151], and droplet-based microfluidic systems [152] have to be complemented by microfluidic single-cell analysis to unravel the underlying mechanisms in population and environmental heterogeneity [29, 81, 153-157].

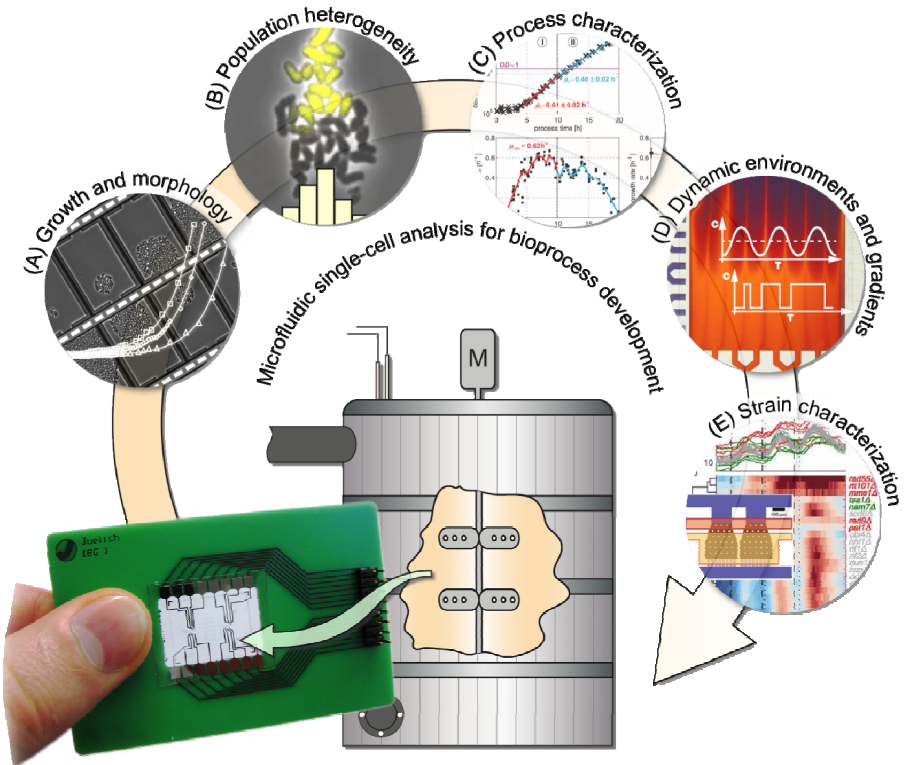


Figure 2.9: Microfluidic single-cell analysis as a new technology portfolio in biotechnological process development. Microbial single-cell analysis in microfluidic devices has shown proven potential in several fields of process and strain development: (A) Growth and morphology analysis; (B) Population heterogeneity of production strains regarding growth, fitness and single-cell productivity; (C) Optimizing process conditions and analysis of cellular response to defined constant environmental conditions (image reproduced and adapted with permission from [158]); (D) Cellular behavior and cell-to-cell heterogeneity at defined concentration gradients and dynamic environments (image courtesy of the Folch lab); (E) Highly parallelized systems for strain characterization and screening (image reproduced and adapted with permission from [104]).

Various physical principles have been exploited to trap, isolate and cultivate single cells from cell suspensions. Several reviews have addressed this spectrum of methods and

their applications, for example [20, 68, 69]. The present review covers recent innovative examples of simple microfluidic systems which specifically address central concerns of biotechnological process development and microbial strain characterization. In contrast to other surveys dealing with technical feasibility, the present review focuses on five biotechnological process fields (Figure 2.9), namely i) growth and morphology, ii) population heterogeneity, iii) process characterization, iv) dynamic environments and gradients, and v) strain characterization. Microfluidic single-cell analysis systems can be utilized to investigate cellular performance under very specific process conditions. First time, this allows correlation between environmental cause and single-cell reaction. Microfluidic single-cell analysis will undoubtedly become established as a novel analytical tool, in order to take a closer look at biotechnological process conditions aiming for improved understanding and, finally, optimization.

Microfluidics technology

Microfluidic single-cell cultivation systems can be used as analytical tools to emulate dynamic and complex large-scale microbial production processes at the picoliter scale. The crucial aspect is the change from complex and turbulent cultivation settings to laminar flow and diffusion-governed environments by ultimately downscaling to picoliter volumes and lower (Figure 2.10A). At that scale, cultivations benefit from the fast exchange of heat and mass, efficient diffusive mass transport and high feature density due to micrometer length scales. These microfluidic systems typically operate under continuous perfusion to maintain constant environmental conditions throughout cultivation. Single-cell cultivation, often combined with image-based analysis techniques, enables an analysis of individual cells with full spatial and temporal resolution in order to study complex interactions[159]. However, well-known sensor principles are no longer applicable at this scale. Instead, novel genetically encoded optical biosensors and optogenetic approaches are applied to derive cellular and environmental parameters in real time [160-162].

Four different types of simple perfusion microfluidics have been applied for microbial single-cell analysis so far. They can be classified according to the spatial directions in which single cells can propagate, namely 3D, 2D, 1D and 0D (Figure 2.10B, C and D). All these types can be operated continuously provided that fast cell removal is assured as soon as the cultivation cavities reach their maximum capacity. They can also be operated in batch mode or alternating modes if appropriate microfluidic fluid control is available, thereby mimicking more complex cultivation categories (batch, fed-batch, chemostat, turbidostat etc.). The smaller the number of cells per cultivation volume is, the more accurately the environment around the single cell can be controlled. In larger 3D as well as 2D planar populations, environmental inhomogeneity and gradients across the microcolonies are more likely than in 1D and 0D systems (Figure 2.10B) where the cultivation medium around the few cells is replenished very effectively.

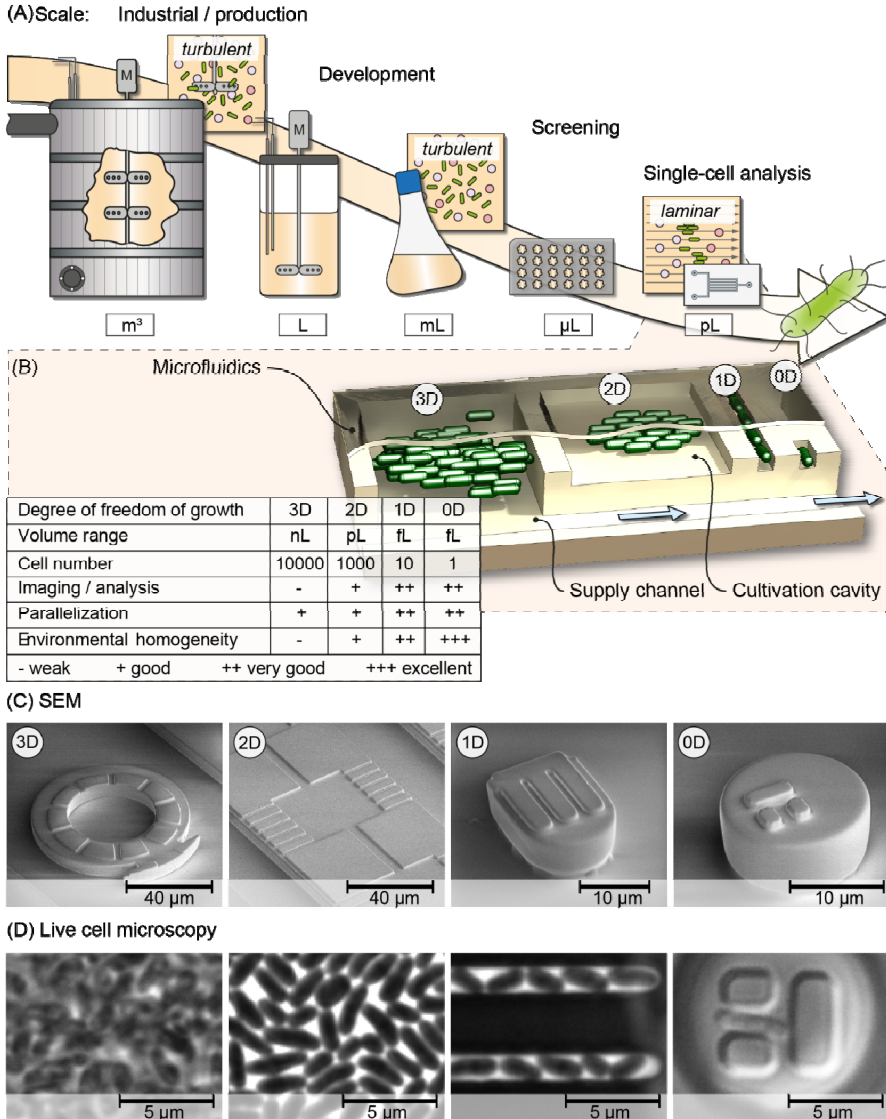


Figure 2.10: Microbial microfluidic single-cell analysis - a new scale in biotechnological cultivation. (A) Today cultivation systems in biotechnology range from an industrial shale of several m^3 down to systems of a few femtoliters with cutting-edge single-cell resolution for analytical purposes. (B) Various geometrical principles of micrometer dimensions have been introduced for microbial single-cell analysis covering: nanoliter cavities for 3D microcolonies, picoliter chambers for 2D cell monolayers, femtoliter channels for 1D linear single-cell rows and ultimately femtoliter single-cell traps. (C) Examples of scanning electron images of each single-cell cultivation principle. (D) Examples of live-cell imaging of each single-cell cultivation principle (0D SEM and live-cell microscopy image reproduced with permission from [76]; others own but unpublished results).

To this end, it is the biotechnological context and utilized microorganism which defines the appropriate microfluidic structure. Microbial single-cell analysis systems

handling sub-micron-sized cells necessitate several accompanying technologies, such as novel chip materials [163], novel fabrication methods in the sub-micrometer range [80, 164], characterization of transport phenomena in the miniaturized bioreactor system [165], as well as advanced imaging [166, 167] and image analysis techniques [168].

2.2.3 Application fields

Growth and morphology

Growth, one of the most important performance indicators in biotechnological production processes, is still one of the “most underexploited assays of cellular heterogeneity studies to date” [155]. Classically, agar pads are used for dynamic single-cell studies [55], but lack environmental control. In contrast, microfluidic cultivation systems can be continuously perfused with fresh medium without removing growing cells.

An early approach utilizing 10 μm high cultivation cavities (3D) in polydimethylsiloxane (PDMS) was used to analyze the growth of isogenic *Escherichia coli* JM 209 populations, although resolution was limited due to the 3D population growth [84]. In contrast, full single-cell resolution in various 2D growth configurations for clonal microcolonies was achieved when observing monolayers of *E. coli* [95, 97] and *Corynebacterium glutamicum* [169] under constant infusion of fresh growth media. An equivalent concept has also been published for larger yeast cells [101].

All 3D and 2D systems (Figure 2.10C and D) share the difficulty of reliable identification and tracking of individual cells especially in densely packed microcolonies, demanding sophisticated image recognition software. Moreover, careful cell size discrimination is needed when deriving growth rates simply by cell number, rather than cell area or volume. In larger and densely packed 2D microcolonies, gradients may extend throughout the colony leading to tremendous cell size variations as inner cells may face limiting conditions [95].

The “mother machine” concept was introduced as an elegant tool to continuously grow microbial cells in 1D dead-end microchannels thus reducing some previous limitations. The mother machine channels can accommodate a few cells in a row, whereas the mother cells remain trapped at the closed end of the channel (see also Figure 2.10C and D; 1D). Constant conditions are realized by continuous supply and very efficient media diffusion into the growth channels. Furthermore, the accurate alignment of multiple parallel growth channels greatly simplifies automated image analysis. *E. coli* strains were cultivated for more than 50 generations thereby deriving cell elongation rates and aging parameters from the locally immobilized mother cells. Fresh media was infused via 25-fold deeper supply channels to maintain constant conditions and to remove excess cells [114]. The same technical principle was also applied for the investigation of *Lactobacillus lactis* [80], *Bacillus subtilis* [116] and yeast [77].

The original mother machine design has recently been modified, and now incorporates two open ends instead of one in order to maintain a linear microcolony of homogeneous age since dividing cells are pushed out of both openings simultaneously. Experiments revealed reduced cell aging effects during cultivation compared to the original experiment within the mother machine [58] (Figure 2.11A). The open growth channel concept was also utilized to investigate single-cell growth dynamics of various bacteria strains, e.g., *B. subtilis*, *Enterococcus faecalis* [115], as well as *C. glutamicum* [117].

Similar to earlier single-cell trapping approaches for eukaryotic cells such as HeLa cells [127] and yeast cells [128], recently submicrometer barrier structures for trapping and cultivating individual bacteria have been demonstrated. These cultivation sites accommodate exactly one cell for analysis in perfectly controlled environments with minimal risk of environmental inhomogeneity [76] (Figure 2.10C and D; 0D).

Population heterogeneity

Understanding cellular metabolism to further optimize microbial metabolite production is crucial for all biotechnological production processes. Determining production rates at the single-cell level necessitates very special analytical approaches [170-173] or fluorescence-based enzyme cascades [174]. Genetically encoded fluorescence biosensor and reporter systems [175] are ideal tools for time-lapse imaging during microfluidic single-cell analysis, since single-cell production dynamics can be derived. In particular, transcriptional regulator based metabolite reporters have proven to be a versatile tool in monitoring intracellular metabolites [176, 177]. These reporter systems transform intracellular metabolite concentration into a detectable fluorescence readout and were used to investigate the single-cell production of amino acids under various environmental conditions [178]. Interestingly, under certain complex environmental cultivation conditions, isogenic microcolonies were imaged as they split into producing and non-producing subpopulations (Figure 2.11B).

While intracellularly accumulated metabolites can reach relatively high concentrations inside production organisms, very sensitive and fast approaches are required to determine low concentrations of secreted compounds within microfluidic environments [179]. Successful analysis may be rapidly counteracted by media convection, fast product diffusion and dilution. Nevertheless, product secretion is central for microbial production processes. In this context, the downstream secretion of GFP fusion proteins by single *Schizosaccharomyces pombe* cells in a continuous flow microfluidic cultivation configuration was successfully quantified by confocal microscopy [180].

Furthermore, geometrically isolated microwells used to minimize dilution and accommodate single methylotrophic yeast cells *Pichia pastoris* were exploited to analyze protein secretion. Population heterogeneity was then analyzed by fluorescence imaging.

Protein trafficking through the secretory machinery was found to be the rate-limiting step in single-cell productivity [181].

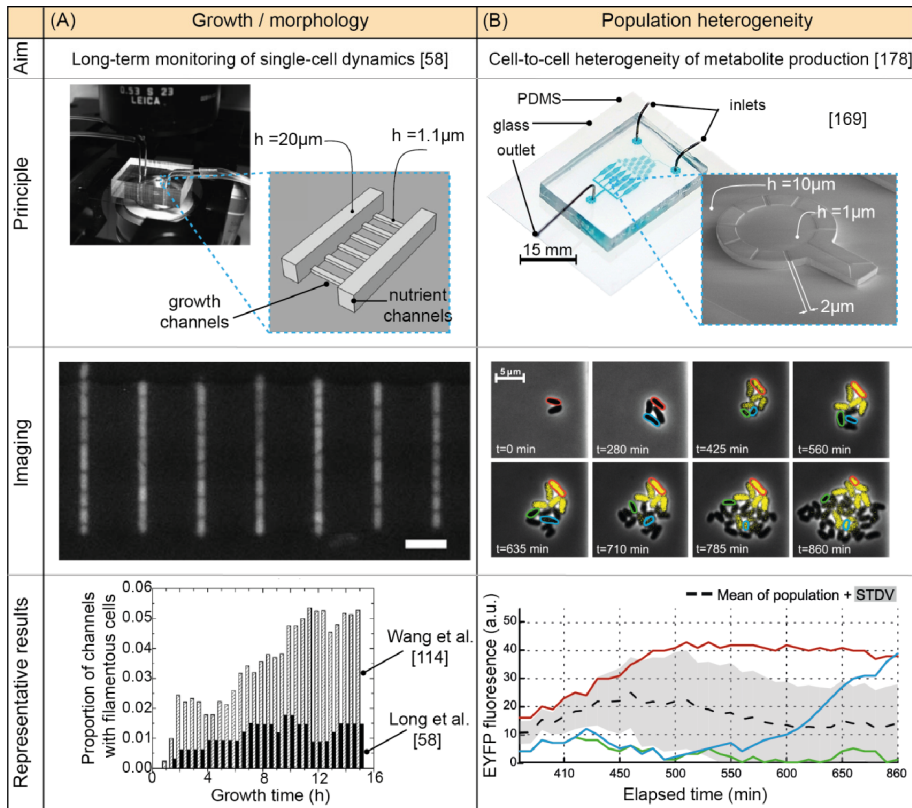


Figure 2.11: Microbial single-cell cultivation systems for growth and production analysis. (A) Long-term-growth studies of single *E. coli* cells in a high-throughput manner. The device features growth of single bacteria cells within parallel 1D growth channels maintaining linear microcolonies of similar age. Results show mean division times obtained from single-cell measurements of single *E. coli* cells with a PgyA-GFP reporter (images adapted and reproduced with permission from [58]). (B) Cell-to-cell heterogeneity studies of isogenic microcolonies inside perfused 2D picoliter bioreactors. Time-lapse images of *C. glutamicum* verified severe population heterogeneity and dynamic cell behavior under certain process conditions (images adapted and reproduced with permission from [169] and [178]).

Process characterization

Cell growth and production are the most important parameters in biotechnological production processes. However, they are simultaneously influenced by a diversity of process parameters. Unsurprisingly, microbial species grow faster in well-controlled microfluidic environments, since fresh media is continuously supplied to the cells. A few recent examples are given below.

Enhanced growth rates were revealed for several industrially relevant production strains. For example, *Hansenula polymorpha*, *Pichia pastoris* and *C. glutamicum* grew remarkably faster in controlled microfluidic environments. It was assumed that the

constant extracellular environment inside the microfluidic chip provides optimal conditions compared to shake flask systems in which cells are subjected to continuous concentration changes [73].

C. glutamicum strains exhibiting 1.5 fold improved growth rates were analyzed in more detail during microfluidic cultivations [98]. Utilizing the whole range of cultivation scales, from picoliter to liter, and accessible analytical systems, the constant availability of protocatechuate (PCA), typically added as an iron chelator, was identified as responsible for the elevated growth rates, rather than the continuous media flow itself [158]. It was discovered that PCA is continuously supplied and co-metabolized resulting in elevated growth rates. In contrast, the amount of PCA initially added to typical batch cultivations is rapidly depleted. The novelty of this work was to apply bioreactor supernatant from distinct cultivation time points. These different media samples were afterwards infused one at a time into the microfluidic cultivation device. Resulting single-cell performance could then be allocated to specific process conditions (Figure 2.12A). Microfluidics has thus contributed to understanding cellular metabolism under specific process conditions, which is a key to further optimization.

Dynamic environments and gradients

Gradients and fluctuating environmental conditions are omnipresent in large scale processes. Stable concentration gradients can be realized by the continuous infusion of adjacent laminar media streams into microfluidic geometries [182]. Lateral diffusion will then form well-defined concentration gradients, which have been mainly applied in chemotaxis and cultivation experiments for a variety of living cells [143, 183-185]. Furthermore, due to the low volumes, more complex but well-defined flow profiles, *e.g.*, pulsed flow or even oscillating conditions, can be realized. Here microfluidics offers new possibilities to emulate complex and dynamic biotechnological environments.

A first study showing the cultivation of Fischer rat thyroid cells within gradients combined with pulsing was reported in [156]. Cells were cultured inside a stable gradient of chloride channel activators or inhibitors. Cellular iodide influx was then initiated by rapid perfusion of iodide and the chloride channel activity was measured by YFP fluorescence.

Real-time gene expression control of single *Saccharomyces cerevisiae* was performed in dynamic microfluidic environments (Figure 2.12B). A model was applied to find the best possible osmotic pulse configuration to produce fluorescence levels as predicted. Cells were successfully controlled exhibiting a mean level of fluorescence depending on the applied target profile [94].

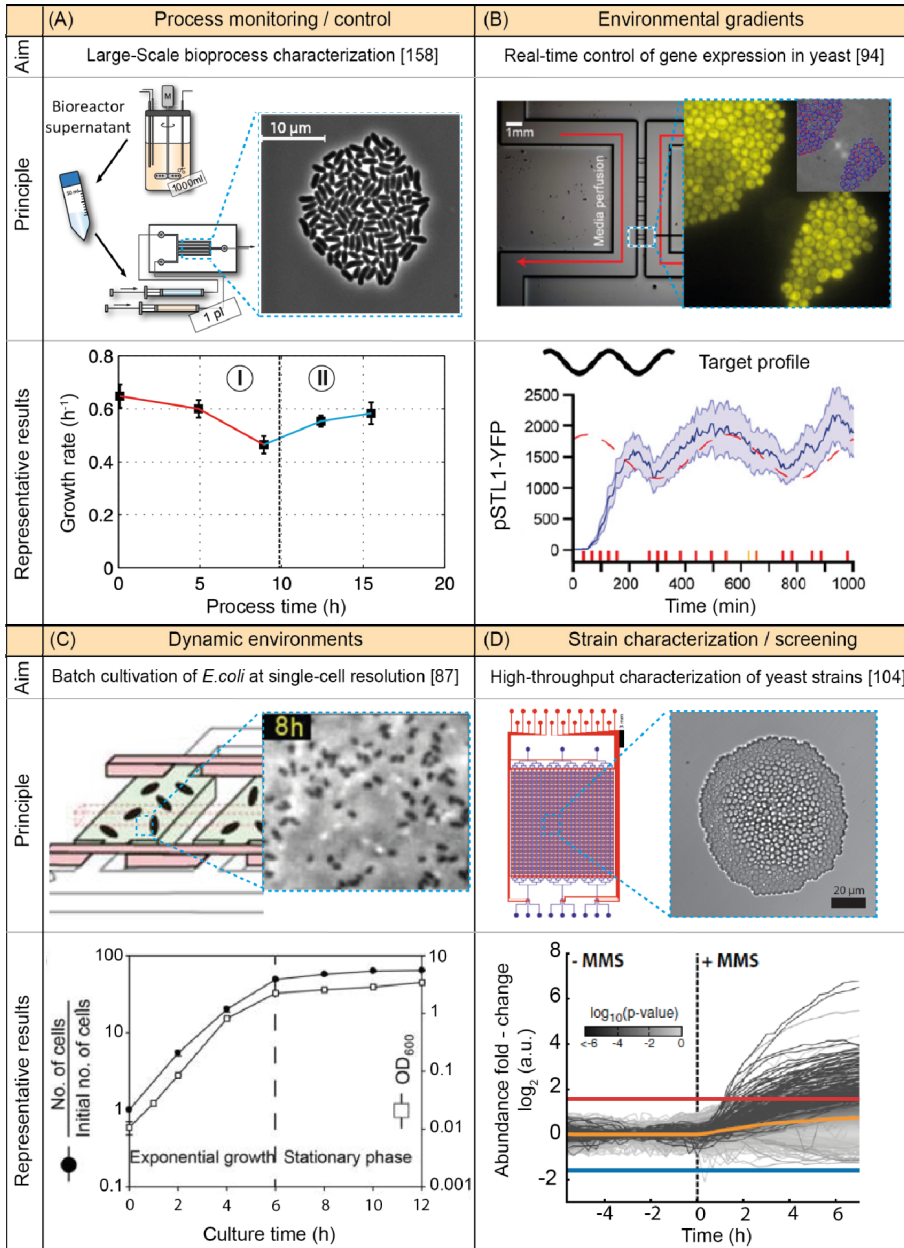


Figure 2.12: Microbial single-cell cultivation systems for process analysis, dynamic environments and high-throughput screening. (A) Microfluidic bioprocess characterization by microfluidic supernatant cultivations [158]. (B) Real-time control of yeast gene expression through positive feedback loop of fluorescence monitoring in a microfluidic single-cell perfusion system [94]. (C) Nanoliter microfluidic batch cultivation system for single-cell cultivations [87]. (D) High-throughput microchemostat array for the investigation of over 1000 yeast strains growing in parallel [104]; (Images adapted and reproduced with permission from [158], [94], [87], [104]).

In contrast to continuous perfusion systems with constant conditions, microfluidic batch compartments were developed incorporating PDMS valves. Single *E. coli* K12 cells were inoculated into chambers which were then mechanically closed and isolated from the supply stream to mimic realistic batch cultivation with nutrient depletion and metabolite accumulation [87] (Figure 2.12C).

Strain characterization

Conventionally, flow cytometry is used to investigate cell-to-cell heterogeneities [150], whereas medium optimization and microbial strain characterization is increasingly performed in microtiter cultivation systems [186]. For the first time, microfluidic single-cell cultivation systems offer both spatio-temporal growth and cell-to-cell characterization without the need for sampling. Moreover, due to the small structure size of a few micrometers, microfluidics favors massive parallelization and high-throughput applications [187]. For example, over 1000 different yeast strains were analyzed inside a single microfluidic device with a temporal resolution of 20 min to screen for protein abundance, providing a systematic view of the yeast proteome [104] (Figure 2.12D).

2.2.4 Conclusion

Microfluidics and single-cell analysis technology has matured and now taking its place among the other disciplines in biotechnological process characterization and development. After 20 years of microfluidics development, microsystems engineers are now able to share their know-how with colleagues from biology and biotechnology in highly interdisciplinary project consortia, which represent the key to future miniaturization of bioreactor concepts. Demonstrated advances have shown the feasibility of microfluidics in a variety of relevant fields thereby gathering information on industrially applicable production hosts, for the first time with single-cell resolution. This accurate single-cell data will allow more precise prediction of the large-scale biotechnological production processes and underlying cellular behavior.

3 Single-cell microfluidics: Development and validation

3.1 Microfabrication

This chapter provides the reader with all fabrication steps, which are necessary to build the microfluidic cultivation systems presented in this study. Starting from a short overview, all steps from design to final data analysis are explained. The chapter is based on the protocol published in 2013 in the *Journal of Visualized Experiments*.

3.1.1 Abstract

In this protocol, the fabrication, experimental setup and basic operation of the recently introduced microfluidic picoliter bioreactor (PLBR) is described in detail. The PLBR can be utilized for the analysis of single bacteria and microcolonies to investigate biotechnological and microbiological related questions concerning, *e.g.*, cell growth, morphology, stress response and metabolite or protein production on single-cell level. The device features continuous media flow enabling constant environmental conditions for perturbation studies, but in addition allows fast medium changes as well as oscillating conditions to mimic any desired environmental situation. To fabricate the single use devices, a silicon wafer containing sub micrometer sized SU-8 structures served as the replication mold for rapid Polydimethylsiloxane casting. Chips were cut, assembled, connected and set up onto a high resolution and fully automated microscope suited for time-lapse imaging, a powerful tool for spatio-temporal cell analysis. Here, the biotechnological platform organism *Corynebacterium glutamicum* was seeded into the PLBR and cell growth and intracellular fluorescence were followed over several hours unraveling time dependent population heterogeneity on single-cell level, not possible with conventional analysis methods such as flow cytometry. Besides insights into device fabrication, furthermore, the preparation of the pre-culture, loading, trapping of bacteria and the PLBR cultivation of single cells and colonies is demonstrated. These devices will add a new dimension in microbiological research to analyze time dependent phenomena of single bacteria under tight environmental control. Due to the simple and relatively short fabrication process the technology can be easily adapted at any microfluidics lab and simply tailored towards specific needs.

3.1.2 Introduction

Time-lapse microscopy is a powerful tool for studying living cells *in vivo* [159]. Meanwhile commercially available fully automated microscopy platforms including thermally induced focus drift compensation are commonly applied in biological research to study time-dependent phenomena, ranging from cancer and neuron cell research over tissue engineering and dynamic studies with single yeast or bacterial cells [127, 131, 188-190].

Typically transparent well plates, agar-pads or simply microscopy slides are applied to provide cell culture environments during time-lapse imaging [26]. Even though suitable for certain research, these simple systems have very limited control over environmental conditions and do not allow for more complex perturbations or well defined and fast medium changes. Disposable microfluidic chip devices produced by mass production have been introduced to the market recently but are mostly tailored towards larger eukaryotic cell types [131]. Although growth can be followed, well defined growth investigations concerning, *e.g.*, precise cell trapping, colony size, growth direction and the ability for cell removal are limited. Microfluidic habitats and reactors, in which bacteria are cultured in 3D environments have been developed [65, 84, 191], but have drawbacks when dealing with quantitative studies at the single-cell level. While overall population heterogeneity can be analyzed, many cell parameters cannot be determined accurately with single-cell resolution since growth is not restricted to monolayers.

This limitation triggered the development of micro systems enabling the cultivation of cells in well-defined channels and habitats with cells growing in flat monolayers with single-cell resolution and especially tight control over media supply and environmental conditions [95, 114, 127]. Few examples of microfluidic systems for the cultivation of bacterial cells have been demonstrated [48, 114, 169]. Bacteria typically exhibit very fast growth rates and require microfluidic structures in the range of few micrometers and below, especially when cell monolayers are desired for microscopy. Keymer *et al.* demonstrated growth and spreading of *E. coli* strains in microfabricated landscapes [192, 193]. Since they were interested in population dynamics they did not investigate with single-cell resolution.

We have developed the picoliter bioreactor (PLBR) [169], which is currently applied to investigate various biotechnological performance indicators such as growth [98] and fluorescence coupled productivity analysis on single-cell level [33, 177]. The present microfluidic device allows environmental reactor control at a defined culture volume of approximately one picoliter and continuous single-cell observation simultaneously. In comparison to open monolayer box systems [48, 95], where one or two sides are open to the media supply channel, the PLBR allows for controlled trapping and culturing. The design permits long term cultivation of bacteria without the risk of several adjacent colonies forming one large population. Furthermore, the system incorporates cultivation regions of 1 μm height (in the order of the cell diameter) to restrict bacteria growth to cell monolayers. In contrast, the supply channels are 10 fold deeper to minimize hydraulic resistance.

In comparison to miniaturized batch cultivation systems [194] the present system allows the cultivation with constant environmental parameters due to continuous media flow. Furthermore, environmental parameters such as medium composition, temperature, flow rates and gas exchange can be easily controlled and changed within seconds. This allows for specific investigations of cellular response to environmental changes concerning, for example, nutrient availability or stress stimuli. The demand for reduced

media volumes, namely in the range of few microliters only, enable researchers to perform novel studies, *e.g.*, the perturbation of cells during time-lapse imaging with supernatant of large-scale experiments unraveling cell response under these specific environmental conditions [98]. The picoliter bioreactor provides researchers with a robust system that tightly controls biophysical conditions and is operated using high precision syringe pumps and automated bright field and fluorescence microscopy for time-lapse imaging. Here, we report a complete protocol including device design, fabrication and exemplary applications.

3.1.3 Protocol

Wafer fabrication

- Design the microfluidic device containing inlets, outlets, main channels and the PLBRs (Figure 3.1A) using CAD software.
- The design presented in this protocol (Figure 3.2) consists of two seeding inlets, a gradient generator for mixing of two different substrates, one outlet, and six arrays of PLBRs. Each array contains 5 PLBRs, resulting in 30 parallel PLBRs inside one microfluidic device.
- Create a lithography photomask containing the desired chip layouts (Figure 3.1B). The photomask was produced in-house by electron beam writing with sub-micron resolution. The mask used was composed of a chromium layer on a 5 inch square glass plate.
- Note: perform all following steps under cleanroom class 100 conditions or better (a process flowchart is shown in Figure 3.1A and 3.1B).
- Clean a 4" silicon wafer with piranha (10:1 ratio of sulfuric acid and hydrogen peroxide) and hydrofluoric acid for several minutes (caution hazardous chemicals). Rinse with deionized (DI) water for approximately 10 s.
- Dehydrate wafer for 20 minutes at 200 °C.
- Spin coat 1 μm SU-8 2000.5 photoresist onto the wafer (1st layer) (4 mL resist, spin 10 s with, $v = 500$ rpm and $a = 100$ rpm/s, spin 30 s with $v = 1000$ rpm and $a = 300$ rpm/s).
- Place the coated wafer on a hotplate at 95 °C to drive off excess solvent (1.5 min at 65 °C, 1.5 min at 95 °C and 1 min at 65 °C; ideally use two hotplates).
- Insert 1st layer photomask (here the trapping regions of the picoliter reactors) and wafer inside the mask aligner and expose wafer to 350-400 nm (vacuum contact, 64 mJ/cm², $t = 3$ s, $I = 7$ mW/cm²).
- Perform post exposure bake on a hotplate at 95 °C to initiate the polymerization of SU-8 (1 min at 65 °C, 1 min at 95 °C and 1 min at 65 °C). Note: after this step the structures in the SU-8 layer can be seen.
- Place the wafer in a SU-8 developer bath for 1 min and transfer the wafer into a second container with fresh SU-8 developer for few seconds.

- Rinse the wafer in isopropanol to remove SU-8 developer and dry wafer using nitrogen flow of wafer spinner.
- Hard bake the wafer for 10 min at 150 °C.
- Spin coat 9 μm SU-8 2010 photoresist onto the wafer (2nd layer) (dispense 4 mL resist, spin 10 s with $v = 500$ rpm, $a = 100$ rpm/s and spin 30 s with $v = 4000$ rpm, $a = 300$ rpm/s).
- Place the wafer with SU-8 on a hotplate at 95 °C to drive off excess solvent (15 min at 65 °C, 45-60 min at 95 °C and 10 min at 65 °C). Note: attention has to be paid to wrinkles and bubbles. If the wafer is heated too fast to 95 °C, evaporated solvent may be encapsulated in tiny gas bubbles.
- Insert photomask with the desired layout (here main channels for nutrient supply) and the wafer into the mask aligner and expose to 350-400 nm (hard contact, 64 mJ/cm², $t = 10$ s, $I = 7$ mW/cm²)
- Perform post exposure bake on a hotplate at 95 °C to finalize the polymerization of SU-8 (5 min at 65 °C, 3:30 min at 95 °C, 3 min at 65 °C). Note: after this step the structures in the SU-8 layer can be seen.
- Place the wafer in a SU-8 developer bath for 45 s, transfer the wafer into a second container with fresh SU-8 developer and develop for 60 s.
- Rinse the wafer 20 s with isopropanol to remove any SU-8 developer residue and dry wafer using pressured nitrogen.
- Finally hard bake the wafer at 150 °C. As a result the final wafer (Figure 3.1C) is obtained, which will be used as master mold for PDMS molding.
- Perform profilometer measurements (Figure 3.3C) to validate SU-8 structure heights. Note: inaccuracies in structure height may result in inefficient cell trapping or loss of cells during cultivation.

Polydimethylsiloxane chip fabrication

- Note: All following steps should be ideally performed under laminar-flow conditions to prevent dust particles interfering with the fabrication procedure (a process flowchart is shown in Figure 3.4).
- Prepare a mixture of polydimethylsiloxane (PDMS) base and curing agent in a 10:1 ratio. Mix carefully until a homogenous solution is achieved which looks opaque. Prepare as much as required for the desired layer height (here 3 mm).
- Degas the PDMS mixture for approximately 30 minutes under slight vacuum until all bubbles have disappeared.
- Prepare molding device (or petri dish) with appropriate SU-8 wafer and pour the PDMS mixture into it (Figure 3.1D).
- Bake the PDMS for 3 hrs. at 80 °C in the oven.
- Carefully peel off the PDMS slab from the wafer. Cut the slab into single chips using a clean and sharp scalpel.

- Wash the chips in an n-pentane bath for 90 minutes, followed by two acetone washing baths (90 min each). Dry the chips overnight to remove any solvent residue. Caution: perform the PDMS washing under a fume hood. Note: during the n-pentane wash, monomers and dimers are removed from the cured PDMS and the chip size may temporarily double during washing procedure.
- Store the microfluidic PDMS chips in close containers until the final experiment.
- Just before the experiment, punch the inlet and outlet holes into the PDMS chip using a needle (or hole-puncher) with a slightly smaller diameter than the connectors that are used to connect tubing with PDMS chip.
- Clean the microfluidic PDMS chip carefully with isopropanol and use scotch tape to remove any dust particles which might stick on the structured PDMS side. Use the scotch tape several times until no particle can be seen on the chip.
- Clean a 170 μm thin glass slide with acetone and isopropanol successively. Finally clean with deionized water and dry with pressurized nitrogen.
- Before plasma-activation, warm up the plasma cleaner and run the plasma for approximately 300 s. Plasma-oxidize glass slide and PDMS chip (Power 50 W, Time = 25 s, oxygen flow rate = 20 sccm).
- Align the PDMS and glass chip before bonding. Finally, place the PDMS chip carefully onto the glass slide (Figure 3.1E). PDMS and glass will bond within seconds. Note: do not push with tweezers onto the top of the PDMS chip during the bonding process. This may lead to so called roof-collapsing of the channels and small structures.
- In order to strengthen the bond, bake the final PDMS-glass chip for 10 s at 80 $^{\circ}\text{C}$.

Preparation of the bacterial culture

- Note: All cultivations should be prepared in sterile filtered medium to prevent accumulation of undesired particles, which may interfere during cultivation.
- Use an agar plate containing the desired organisms (here, *C. glutamicum* ATCC 13032) and inoculate one colony into 20 mL of fresh BHI medium, incubate overnight (\approx 8 -14 hrs.) at 30 $^{\circ}\text{C}$ on a rotary shaker (120 rpm).
- Transfer 10 μL of the preculture into the desired medium (here CGXII [195]) which will be used during microfluidic cultivation and let the cell grow overnight at 30 $^{\circ}\text{C}$ on a rotary shaker (120 rpm).
- Transfer the desired amount of cell suspension (between 10 μL and 500 μL , depending on the start of the experiment) into the desired medium (here CGXII [195]) which will be used during microfluidic cell cultivation. Note: the best is to use cells from the early logarithmic phase for seeding. For *C. glutamicum* culture the best optical density (OD_{600}) for seeding was between 0.5 and 2.
- Transfer 1 mL of the bacterial culture into a sterile 2 mL tube. Note: this should be done right after the microfluidic PDMS chip was assembled to minimize transfer time between shake flask and microfluidic cultivation. Typically the transfer time is

around 15 minutes and should be kept as small as possible to prevent impact on metabolism caused by oxygen limitation and temperature changes.

Experimental setup

- Note: All steps are performed with an inverted microscope.
- Start microscope incubator 2 hrs. before the experiment to warm-up the system. Note: the microscopy should be equipped with a full-size incubator to control temperature and if desired gas flow. Additional humidity control is not necessary since the chip system is continuously infused with media.
- Open incubator system, select the desired objective and if required add immersion oil onto the objective.
- Mount the chip inside the chip holder. If required fix the glass plate with adhesive tape in order to avoid chip any movement during stage operation.
- Center the sample on the microscope and focus onto the PLBR arrays.
- Connect inlets and outlets with appropriate tubing (Figure 3.1F). Connect tubing to a waste reservoir. A representative chip can be seen in Figure 3.4D.
- Insert syringes into pumps and start media flow. Use medium, buffer or if necessary coating solution and rinse the microfluidic channels for approximately 1 hr. Note: coating solution is used to coat channel walls to prevent unspecific cell adhesion.
- For *Escherichia coli*, 0.1% solution of BSA is used to coat the channel walls. For *C. glutamicum* no coating is necessary. After the coating procedure flush the chip with medium prior cell seeding.
- Before cell seeding and cultivation, check that no leakage occurs and that the temperature is constant.

Seeding of bacterial cells into the microfluidic device

- Make sure the desired bacterial suspension is available in appropriate syringes connected to tubing.
- Disconnect buffer or coating solution and connect the cell suspension to the chip. To minimize death volume, undesired air bubbles and to reduce experimental time, change the complete needle as well as tubing, rather than only the syringes.
- Infuse the cell suspension into the channels at a volumetric flow rate of 200 nL/min until most of the PLBRs are filled with the desired amount of cells (Figure 3.5A). Note: optimal seeding results depend on the bacterial strain, OD₆₀₀, and growth medium of the preculture. These parameters have to be adapted to increase trapping efficiency and time until a sufficient number of cells are trapped in the reactor structures. For *C. glutamicum*, a cell suspension of OD₆₀₀ 0.5-2 was used; for *E. coli* the OD₆₀₀ was between 0.5 and 1.
- If only a small number of PLBRs are filled, increase the flow rate to 800-1200 nL/min.

- Disconnect the cell suspension and connect the growth medium to the chip (Figure 3.5B). Make sure that no air bubble is introduced during the medium change. Perfuse with fresh growth media at 100 nL/min.

Time-lapse imaging

- Select specific PLBRs for time-lapse imaging. PLBRs are chosen that contain a single mother cell at the beginning of an experiment. The number of regions of interest that can be investigated in one experiment depends on the desired frame rate and microscopic setup.
- Select an appropriate frame rate depending of number of PLBRs. Make sure that the microscope can handle the desired amount of ROIs in the time-lapse interval.
- Choose appropriate filter sets (here YFP). Automatically close the shutter during stage movement and after each time-lapse measurement to prevent chromophore bleaching.
- Configure the time-lapse microscopy sequence and start the experiment.
- After all PLBRs are overgrown, the experiment can be stopped, the microfluidic PDMS chip can be discarded and the experiment can be evaluated.

Analysis

- Note: The following steps or parts of the procedure can be performed manually or by image analysis programs such as Image J etc.
- Determine PLBRs of interest where the cultivation fulfills all desired criteria, *e.g.*, number of mother cells, position of the mother cells, etc.
- To determine the growth rate of one microcolony count the number of cells in each time frame.
- Calculate the maximum growth rate by plotting time vs. $\ln(\text{cell number})$. The slope of the plot represents the growth rate in $[1/h]$ (see Figure 3.6).
- Fluorescence data analysis strongly depends on the performed experiment. In this report, an example was chosen to illustrate colony-to-colony and cell-to-cell heterogeneity between different isogenic microcolonies (see Figure 3.7).

A complete list of materials and equipment used within this project can be found in Appendix A.1.

3.1.4 Representative results

Device fabrication

The microfluidic PLBR system is fabricated by one layer of PDMS bonded onto a thin glass chip suited for high resolution microscopy. The fabrication consists of two main steps: Firstly the fabrication of the replication master (Figure 3.1A, B and C) and secondly the chip fabrication (Figure 3.1D, E and F). According to the protocol, standard

photolithographic microfabrication techniques are used to create the master mold. Laboratories without cleanroom facility can acquire commercially available customized SU-8 master molds. Using repetitive PDMS molding (Figure 3.1A, B and C) hundreds of disposable chips can be produced. PDMS molding and chip assembly can be done in any lab and do not require cleanroom facilities, however, laminar airflow workplaces are favorable.

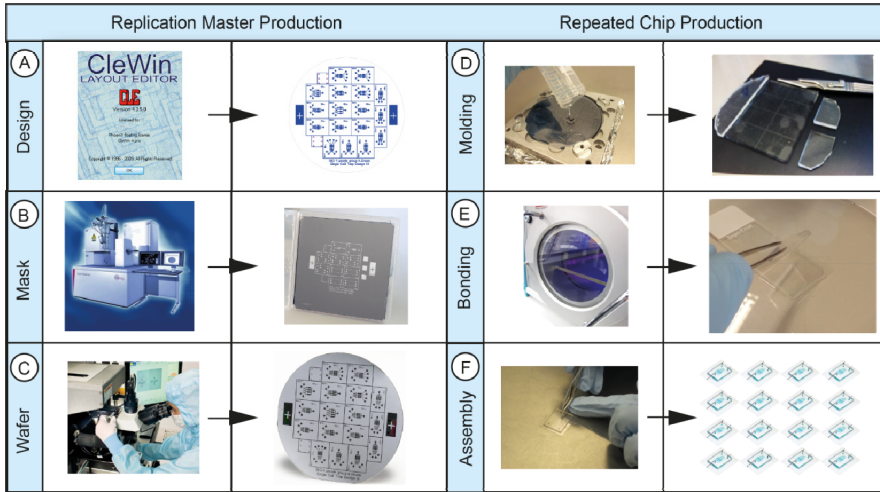


Figure 3.1: Overview of PLBR chip production process. Master mold fabrication: starting with (A) design, (B) lithography mask fabrication and (C) wafer production. PDMS-glass chip production: starting with (D) PDMS molding followed by (E) glass and PDMS bonding and (F) final chip assembly.

The process starts with the design of the microfluidic chip system. CAD software is used to design the microfluidic chip (Figure 3.1A). After CAD, a mask is generated by an e beam writer (Figure 3.1B) with submicron resolution. In the present study a 5” chromium mask was created which was used for the SU-8 wafer lithography. The final silicon-SU 8 wafer is used for PDMS molding (Figure 3.1D). After a baking step the PDMS slab is cut into chips which are irreversibly bonded onto the glass slides (Figure 3.1E). Finally the tubing is connected (Figure 3.1F).

Figure 3.2 visualizes the design of the microfluidic system in detail. It consists of two seeding inlets, a gradient generator for mixing of different substrates or media and one outlet. The main channels have a dimension of $50 \mu\text{m} \times 10 \mu\text{m}$ (W x H). Each device consists of six arrays of PLBRs, containing 5 PLBRs each. This results in 30 parallelized reactors inside one microfluidic device.

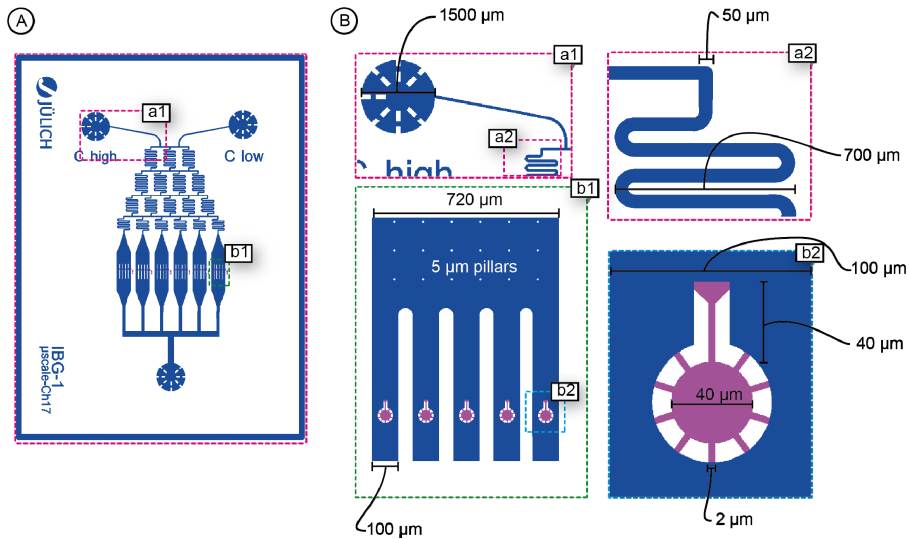


Figure 3.2: Design of the PLBR chip. (A) CAD drawing of the whole microfluidic chip. (B) Magnification of selected layout positions: The layout contains two medium inlets (a1), a gradient generator with mixing channels (a2) and 6 parallel PLBR arrays (b1). Figure b2 shows one PLBR, which is embedded in a fluid channel with a width of 100 μm . The PLBR has an inner diameter of 40 μm and nutrient channels with 2 μm in width. The seeding inlet has a length of 40 μm . Pink color represents the first layer (trapping and cultivation region) and blue color represents the second layer (fluid transport).

Figure 3.3 illustrates the replication master production. As described in detail in the protocol, a first SU-8 layer is fabricated by SU-8 lithography (Figure 3.3A). A similar procedure is applied for the second layer (Figures 3.3B). To check the channel geometry we investigated the height of the PLBRs and main channels using a profilometer. In the example shown in Figure 3.3C, the first layer (the cultivation layer) was measured. Here the layer has a consistent height of 1200 nm, suitable for the cultivation of *C. glutamicum* in BHI medium.

Figure 3.4 illustrates the PDMS molding procedure starting with PDMS mixing (Figure 4A) followed by the molding process (Figure 3.4B) and finally the bonding step (Figure 3.4C). Figure 3.4D displays the final microfluidic chip incorporating the 170 μm thick glass plate, PDMS chip (3 mm in height) with inlets and outlets and steel needles connected to tubing. After the experiment the chip can be disposed and no extensive cleaning is necessary. Furthermore, it is easy to assemble and handle. No complex and difficult filling procedure is necessary.

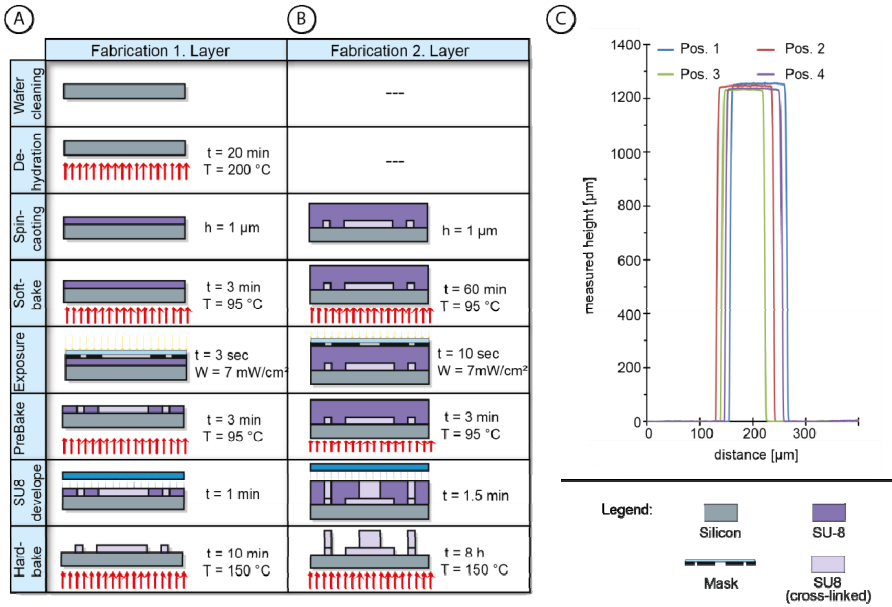


Figure 3.3: Illustration of two layer wafer fabrication process. (A) Fabrication of the first layer containing trapping structures; (B) Fabrication of the second layer containing fluid channels, inlets and outlets (C) representative surface profiles of the first layer. In this case the height of the first layer was 1200 nm and is used for the cultivation of *C. glutamicum* in complex medium.

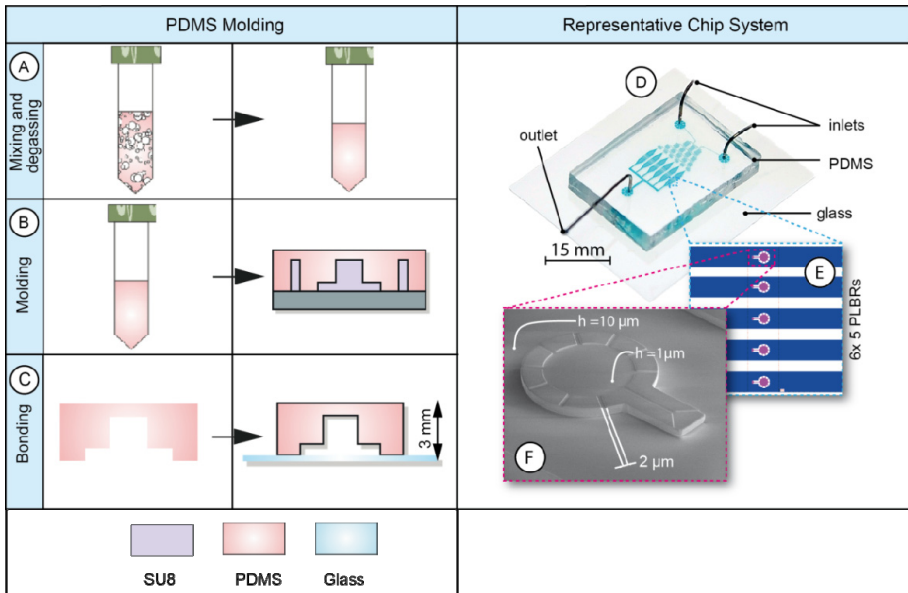


Figure 3.4: Device fabrication and representative chip. Illustration of the PDMS molding process: (A) PDMS mixing and degassing; (B) PDMS molding; (C) mold release, cutting and chip bonding. Final chip (Reproduced with permission of the Royal Society of Chemistry) [169]: (D) photograph of the PDMS chip

with 2 inlets and 1 outlet; (E) CAD image of six parallel arrays containing 5 PLBRs each; (F) SEM image of one PLBR.

Device principle

Figure 3.5 shows the working principle of the reactor system. Cells are infused into the microfluidic device and individual cells remain trapped inside the PLBR simply by cell-wall interactions. Due to the difference in hydrodynamic resistance of channel and PLBR, only minimal flow occurs inside the PLBR. After seeding of the PLBR (Figure 3.5A), the growth and observation phase is initiated with a change from bacterial suspension to growth medium (Figure 3.5B). After the PLBRs are overgrown (Figure 3.5C) the experiment is typically stopped and time-lapse images can be analyzed. For more details on the trapping mechanisms and flow profile within the PLBR the reader is referred to Grünberger *et al.* [169].

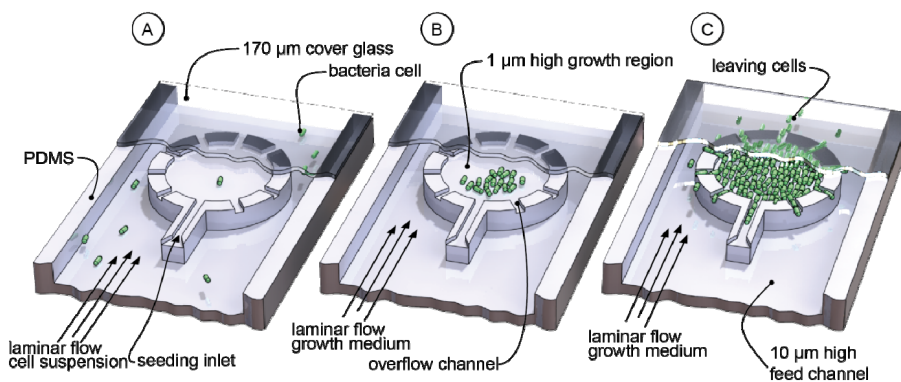


Figure 3.5: Working principle of the PLBR system. (A) Seeding phase; (B) growth phase of the bacterial microcolonies; (C) overflow phase. Reproduced with permission of the Royal Society of Chemistry [169].

Growth rate analysis

The present system can be applied to study various bacterial species with respect to different biological parameters such as growth, morphology or a fluorescent signal. In a first example *C. glutamicum*, an industrially relevant production organism was cultured under standard cultivation conditions ($T = 30\text{ }^{\circ}\text{C}$, CGXII medium [195]). Figure 6A shows the growth curves derived from three isogenic microcolonies. Exponential growth is maintained until the PLBRs are filled indicating that no nutrient limitation occurs. Figure 3.6B displays four DIC time-lapse microscopy images of a growing *C. glutamicum* colony.

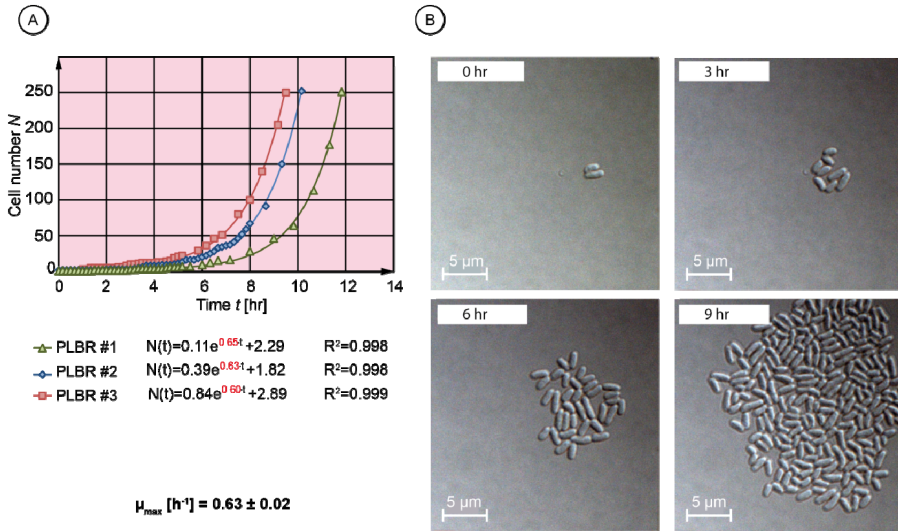


Figure 3.6: Growth rate determination of *C. glutamicum* WT microcolonies. (A) Growth plot of three PLBR cultivations and resulting exponential curves (Parts reproduced with permission of the Royal Society of Chemistry)[169] (B) Time-lapse images of a growing *C. glutamicum* colony.

Fluorescence analysis

For single-cell fluorescence microscopy, researchers often make use of specific fluorescent proteins, for example GFP or derivatives, to couple a specific phenotype of interest to a measurable output (a fluorescent signal). To demonstrate the applicability of the PBLR for fluorescence based time-lapse studies, we investigated the fluorescence emission of a *C. glutamicum* strain producing a plasmid-encoded YFP-TetR fusion protein under control of the P_{tac} promoter (pEKE x_2 -*yfp-tetR*) [33, 196]. In the presence of low inducer (IPTG) concentrations, expression from P_{tac} is known to lead to significant cell-to-cell variation in isogenic bacterial populations. Starting from one preculture, the growth and single-cell fluorescence was followed for several isogenic microcolonies. As it can be seen in Figure 3.7, we observed phenotypic heterogeneity between different microcolonies and heterogeneity at the single-cell level within colonies starting from one mother cell. One colony (Figure 3.7B, PLBR 1) showed almost no fluorescence emission, whereas cells of PLBR 2 exhibited a low fluorescence emission due to basal *yfp-tetR* expression from the P_{tac} promoter. In PLBR 3 fluorescence emission was considerable strong compared to the other colonies and a broad distribution of the population was observed. This example demonstrates the applicability of the PBLR for time-lapse fluorescence microscopy studies. In comparison to flow cytometry, in which the fluorescence of single cells can be determined at one time point, the present systems allows the tracking of cells and the study of single-cell fluorescence in real time over many generations.

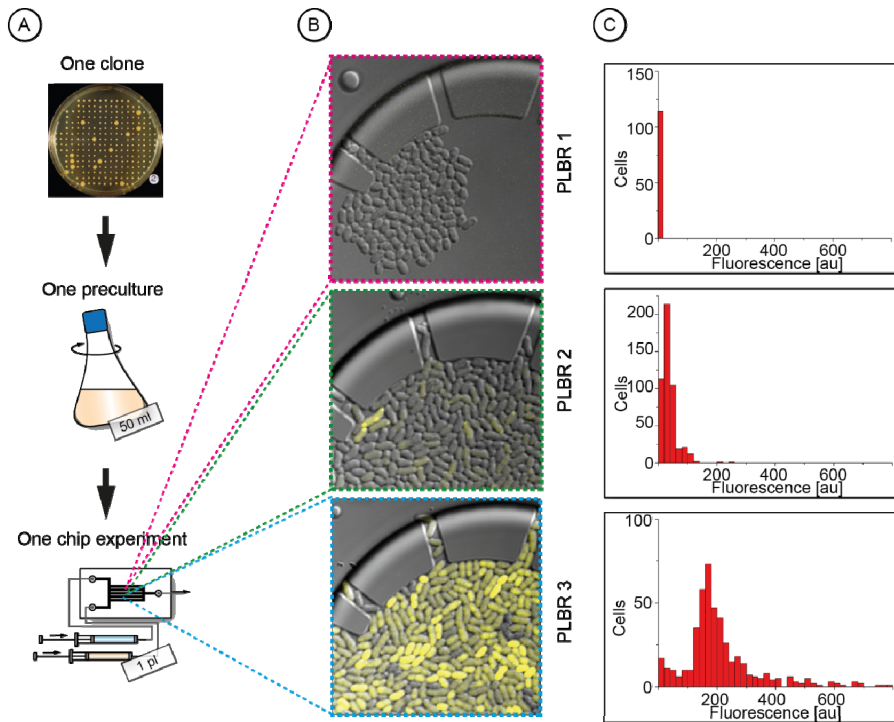


Figure 3.7: PBLR-based analysis of population heterogeneity. Shown is *C. glutamicum* expressing a *yfp-tetR* fusion under the control of the P_{lac} promoter ($pEKEx2$ -*yfp-tetR*) in the absence of the inducer IPTG. (A) Experimental workflow; (B) three isogenic microcolonies showing colony-to-colony heterogeneity and cell-to-cell heterogeneity; (C) distribution of single-cell fluorescence within the respective microcolonies.

3.1.5 Discussion

We have described the fabrication, experimental setup and related operation procedures of a microfluidic PDMS device containing several PLBRs for single-cell analysis of bacteria.

Microfabrication using soft lithography techniques allows fast adjustments of device dimensions for various sizes and bacteria morphologies. Currently we are optimizing the picoliter bioreactor regarding the cultivation of different microbial organisms and cultivation throughput. In order to increase the trapping efficiency, also the reactor geometry is under optimization. Figure 3.8 shows four new PLBR devices which are currently validated. In all figures the seeding channel was redesigned with regards to width and shape. In practice, this seems to have an effect on the number of cells that are trapped, but needs further investigations. Significant improvements regarding the trapping efficiency were also achieved by the incorporation of additional overflow channels leading to higher convective flow through the reactor and more cells

being trapped. However, at the same time one increases the risk to wash out cells during cultivation.

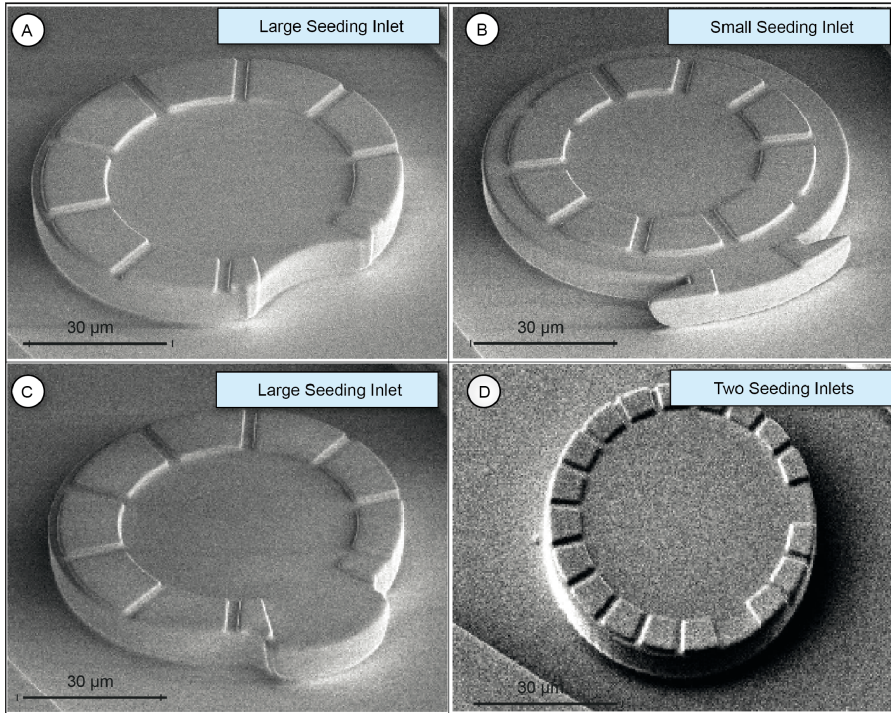


Figure 3.8: Scanning electron images of different PLBRs. SEM images showing seeding inlets for the optimization of trapping efficiency. (A) Larger seeding inlets. (B) Smaller seeding inlets. (C) Larger “open” seeding inlets. (D) Two seeding inlets.

The device is an interesting alternative to macroscale cultivations that have been used for decades to investigate growth and production processes on single-cell level. However, it has some important requirements: For parallel monitoring of several picoliter bioreactors a high resolution and fully motorized microscopic setup with focus drift compensation is mandatory. In addition an incubation system is needed to maintain the desired cultivation temperature constant throughout the measurements.

We achieve a 95% success rate in device fabrication. Main problems are related to inefficient PDMS-glass bonding, PDMS roof collapse or fluid leakage (see Appendix A.2 for troubleshooting of most occurring problems). Although the experimental work is done partially under non-sterile conditions, we rarely see contamination during experiments, due the closed fluidic system. PDMS microfluidic devices are optically transparent, therefore, can be used for high resolution *in vivo* imaging. Although PDMS seems to be perfect for the application, it has a high affinity for hydrophobic molecules, making the use of solvents which are widely used in whole cell biocatalytic processes limited.

However, suitable coatings are available to adapt the protocol to these kinds of applications.

The proposed PLBR is well suited for spatio-temporal analysis of cellular and even sub-cellular events of various kinds of bacteria. A major advantage of the present approach lies in the ability to quantify microcolony growth directly in contrast to conventional methods. Furthermore, the PLBR allows for culturing under defined and constant conditions. Because the system facilitates the use of small amounts of reagents or materials it carries the advantages of being inexpensive, customizable and amenable to high-throughput. In traditional methods average values of the whole population are considered when analyzing microbial cultivation. Furthermore, existing methods need manual sampling which can lead to degradation of samples and thus to errors in the measurement. The PLBR offers new perspectives for bioprocess development and population heterogeneity analysis in microbiology. The PLBR is a promising tool for various applications within bioprocess development and could be applied in various fields of research, *e.g.*, analysis of cell-to-cell heterogeneity, analysis of specific cell clusters within cell-lineages, screening of microbial production strains and real-time investigation of cell phenotypes.

3.2 Picoliter bioreactors

This chapter describes the successful realization of the first picoliter bioreactor for single-cell cultivation studies. A short description of the design will be given. Selected examples demonstrate, how the developed system can be used to investigate biotechnologically relevant questions. The results show, how the system can be used to gather information which was not possible to obtain with conventional cultivation systems. The chapter is based on a publication in *Lab on a Chip* published in 2012.

3.2.1 Abstract

In the continuously growing field of Industrial Biotechnology the scale-up from lab to industrial scale is still a major hurdle to develop competitive bioprocesses. During scale-up the productivity of single cells might be affected by bioreactor inhomogeneity and population heterogeneity. Currently, these complex interactions are difficult to investigate. In this report, design, fabrication and operation of a disposable picoliter cultivation system is described, in which environmental conditions can be well controlled on a short time scale and bacterial microcolony growth experiments can be observed by time-lapse microscopy. Three exemplary investigations will be discussed emphasizing the applicability and versatility of the device. Growth and analysis of industrially relevant bacteria with single-cell resolution (in particular *Escherichia coli* and *Corynebacterium glutamicum*) starting from one single mother cell to densely packed cultures is demonstrated. Applying the picoliter bioreactor, 1.5-fold increased growth rates of *C. glutamicum* wild type cells were observed compared to typical 1l lab-scale batch cultivation. Moreover, the device was used to analyze and quantify the morphological changes of an industrially relevant L-lysine producer *C. glutamicum* after artificially inducing starvation conditions. Instead of a one week lab-scale experiment, only 1 hour was sufficient to reveal the same information. Furthermore, time-lapse microscopy during 24 hours picoliter cultivation of an arginine producing strain containing a genetically encoded fluorescence sensor disclosed time dependent single-cell productivity and growth, which was not possible with conventional methods.

3.2.2 Introduction

Industrial biotechnology is concerned with the production of chemicals, pharmaceuticals and proteins by using microorganisms growing on sustainable resources. Growth and production are the two key factors in biotechnological production processes which underlie continuous optimization. Assuming isogenic starting populations, optimal reactor control and mixing, a uniform cell behavior during growth might be expected.

However, it has emerged in recent years that isogenic bacterial populations can be physiologically heterogeneous [112, 144, 197-201], *e.g.*, comprising producing and non-producing cells. Hence there is strong demand to gain knowledge on population heterogeneity impacting industrial-scale cultivation.

Population heterogeneity may have two reasons: First, cellular heterogeneity, caused by either a) emerged genetic differences [202], b) general stochastic effects [203], and c) population based phenomena like quorum sensing [204], and second, environmental heterogeneities at the microscale level, caused by insufficient process control and mixing. Particularly, cells are continuously exposed to fluctuating conditions as they travel through the various zones of bioreactors. Clearly, such heterogeneity directly effects cell metabolism [13, 18]. Typically, cellular as well as environmental heterogeneities occur at the same time, leading to the problem that phenotypic screening and characterization is hard to accomplish. Until now, mainly due to missing experimental and analytical techniques, detailed knowledge on population heterogeneity and its impact on production processes is not available [144, 147].

To date, most of the heterogeneity studies are based on large cell populations, containing several billions of cells to collect statistically reliable data. To investigate the behavior of individual cells of such populations, a well-established method is fluorescence activated cell sorting (FACS) [27]. FACS is an ideal high-throughput tool for screening and sorting of populations up to 80,000 cells per second [205]. However, FACS as well as other cytometric methods like Coulter counters are offline methods implying elaborate sampling routines prior to analytics. Furthermore, FACS is a snapshot analysis device and possibilities for investigating time dependent processes on single-cell level are limited. For example, FACS does not facilitate individual cell tracking, to determine proliferation, cell cycle events, growth rates and time dependent production.

Due to its simplicity and applicability with conventional microscopes, cell culturing on small agar pads is frequently applied. It enables time-lapse investigations of microcolonies with single-cell resolution, however, at very low throughput and minimal environmental control [55]. To overcome some of these limitations, automated microscopy and image recognition software has been applied to analyze multiple bacteria microcolonies on a single agar pad [26]. Nevertheless, lack of environmental and spatial cell growth control remain major drawbacks.

In contrast to FACS and agar pads, microfluidics and lab-on-a-chip devices do allow for long term cell analysis with the possibility to perform environmental and cell growth control [206]. Microfluidics offers homogeneous and well controllable microscale environments due to laminar flow and diffusion based mixing. Furthermore, due to massive parallelization of micrometer sized components, microfluidics has the potential for high-throughput bacterial cell analysis.

Two approaches have been described in literature so far: First, miniaturization of common bioreactor technology down to nanoliter volumes with integrated sensors for

various process parameters. These microfluidic bioreactors allow environmental control but do not facilitate single-cell resolution for longer time periods [207]. Second, microfluidic devices for biotechnological single-cell studies including, *e.g.*, phenotypic population heterogeneity [88] and single-cell growth [66]. Our intention is a combination of both approaches, to be specific, a microfluidic device allowing environmental reactor control at a defined culture volume and continuous single-cell observation simultaneously.

To accomplish single-cell analysis in microfluidic devices, cell trapping is essential. Different methods for single-cell trapping have been applied so far, including contactless and contact based methods [68, 69]. However, most methods were applied to eukaryotic cells [127]. Evidently, the 10-100 times smaller prokaryotic cells used in Industrial Biotechnology necessitate more precise micro fabrication and well device control. Hence, only a few microfluidic methods for single bacteria analysis have been demonstrated till now. Keymer *et al.* and Mannik *et al.* developed microfluidic systems to investigate growth and motility of bacteria populations [111, 193]. Wang *et al.* applied hundreds of 1 μm wide dead-end channels to determine the growth rate of individual *E. coli* cells over more than 200 generations, but no investigations on complete colonies were possible [114]. Kortmann *et al.* used elaborate dielectrophoretic (DEP) trapping to determine growth rates of single yeast cells and bacteria cells [66]. Walden *et al.* developed parallel trapping regions for bacteria cultivation of up to 300 cells in a monolayer [48]. The latter allows for population heterogeneity analysis of larger bacterial microcolonies. Unfortunately, the layout does not allow controlled spatial cell growth and could result in inaccurate growth rate quantification.

In this study a novel microfluidic bioreactor is presented allowing parallel analysis not only of individual bacteria but also of multiple microcolonies of up to 500 cells inside 1 pL sized bioreactors (PLBRs). The system was developed for single use with a focus on simplicity. In contrast to previously reported systems, single cells simply remain trapped inside the shallow bioreactor, not relying on sophisticated cell trapping mechanisms, and cells grow in a monolayer ideal for time-lapse microscopy. Analysis can be performed on many PLBRs in parallel by automated and image based microscopy. An innovative reactor design with overflow capability allows for continuous and non-restricted cell cultivation and observation, ideal for bioprocess investigations. Furthermore, it allows for steady medium infusion maintaining constant environmental conditions as well as defined medium switches within seconds to induce various cell reactions. Moreover, the high potential for parallelization makes the system an ideal tool to collect statistically trustworthy data.

This paper covers device principle, design, basic fabrication aspects and focusses on typical applications in biotechnological research, where other methods reach their technological limits. Three exemplary biotechnological investigations are presented indicating the versatility of the device. First, as a proof of principle, the cultivation of two industrially relevant organisms, *E. coli* and *C. glutamicum* was performed under constant

conditions. By determining growth rates of three picoliter bioreactor cultivations, biocompatibility and reproducibility was investigated as a necessary step for further experiments. Second, defined short time medium changes were applied, to assess the biological response of the growing bacteria colony under starving conditions. Third, a first example of combined growth and production studies with genetically encoded fluorescence reporters for *C. glutamicum* is shown. Utilizing one microfluidic system, we could investigate important bioprocess parameters, e.g., cell growth, morphology, and productivity at the same time.

3.2.3 Device principle and design

The presented microfluidic device is intended for the analysis of bacteria cells on single-cell level. We aim for the investigation of microcolonies of up to 500 cells. In contrast to previously reported systems, the device described in this report has been designed for non-motile bacteria. For this purpose, novel picoliter sized bioreactors, in this paper referred to as PLBR, were designed and implemented into a microfluidic chip. The device can incorporate up to several hundred PLBRs connected to various inlet and outlet channels for supplying growth medium and waste removal. To minimize hydrodynamic resistance but enforce cells to grow in a monolayer, two different channel heights were included: The supply and waste channels have an app. height of 10 μm , whereas the shallow cell cultivation region is app. 1 μm high. This 1 μm culturing region restricts cell growth to a monolayer, ideal for image based live-cell and time-lapse microscopy. As illustrated in Figure 3.9, each PLBR consists of a circular plateau with radially arranged channels. The front channel is elongated thereby forming the cell seeding inlet. The PLBR is located inside the centre of the supply channel, enabling a medium flow around the trap and reduced flow through the cultivation region (as evident from Appendix B.1).

As illustrated in Figure 3.9 the experiment can be divided into three phases:

a) During the “seeding phase”, the device is infused with a cell suspension as shown in Figure 3.9A. Cells are randomly seeded into the PLBRs with the fluid flow dragging cells through the seeding inlet into the circular reactors. Cells simply remain trapped in between the glass cover and reactor plateau, not relying on sophisticated trapping methods. Ideally each reactor is seeded with one single mother cell, leading to isogenic microcolonies during cultivation.

b) As soon as a single cell is seeded into the reactor, fresh growth medium is infused. This initiates the “growth phase”, as illustrated in Figure 3.9B. During this phase the growth of each microcolony can be followed over several generations by image based time-lapse microscopy.

c) Depending on the size and shape of the cultivated organism, a maximum capacity of app. 500 cells can be reached, until geometric constraints lead to the “overflow phase” of the PLBR. Excess cells are pushed out of the reactor chamber via the overflow

channels and are continuously dragged away by the medium stream (Figure 3.9C). This design allows for continuous cultivation and analysis.

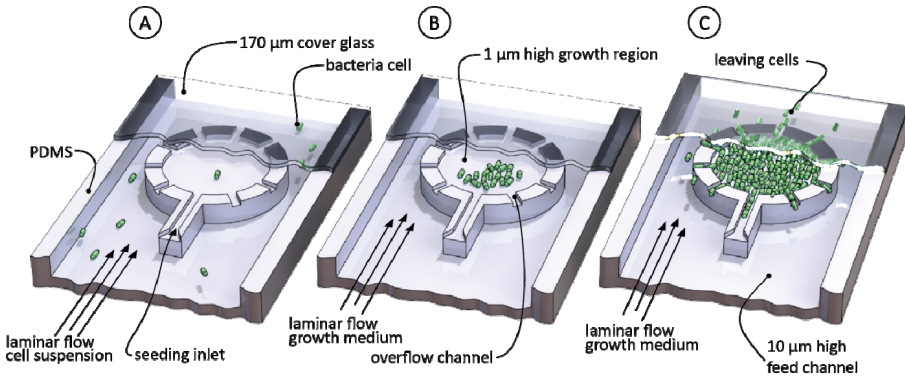


Figure 3.9: Illustration of the picoliter bioreactor (PLBR) for cultivation of bacteria. The shallow circular PLBR has radially arranged channels and is placed inside a deeper supply channel. (A) During the “seeding phase” single cells are seeded into the PLBR. (B) Once a single cell is seeded, growth medium is infused initiating the “growth phase”. (C) As soon as the reactor is fully packed, cells are pushed out of the overflow channels during the “overflow phase”. Illustration is not to scale.

Each device consists of a microfabricated polydimethylsiloxane (PDMS) chip bonded onto a 170 µm thick glass slide suitable for high resolution microscopy. Total processing time, including lithography for the mask as well as the chip fabrication, is usually accomplished within several days allowing for short innovation cycles. Since PDMS chips can be fabricated rapidly the system is designed for single use only and to be discarded after application. Hence elaborate cleaning and extensive autoclaving procedures can be omitted. A successfully fabricated device is shown in 3.10A. Each chip is 4 mm thick, 15 mm wide and 20 mm long. The total interior fluid volume is approximately 200nl. As depicted, dispensing needles are connected to the device inlets and waste outlet. Six interconnected channel arrays (Figure 3.10B) containing 5 PLBRs chambers each (30 PLBRs in total) can be flushed with specific medium simultaneously. A gradient generator channel network was implemented, however, was not utilized during this project and is intended for further studies. To verify structure resolution of the molded PDMS chips, scanning electron microscopy (SEM) was performed prior to chip bonding with an SEM image of one PLBR shown in Figure3.10C.

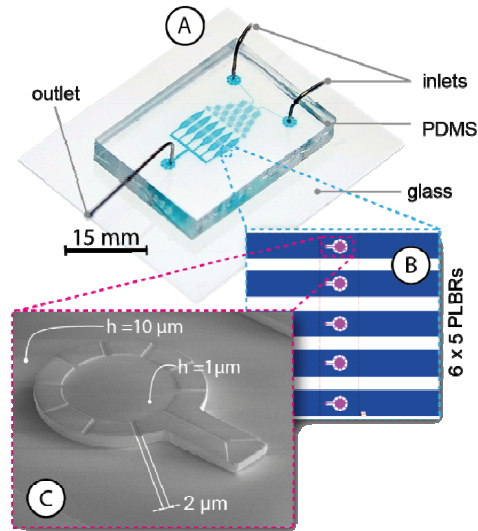


Figure 3.10: Images showing the fabricated microfluidic chip device. (A) The PDMS microfluidic chip was bonded to a $170\ \mu\text{m}$ glass slide and connected to silicone tubing. For purpose of illustration, the chip was filled with ink. Each chip is $4\ \text{mm} \times 15\ \text{mm} \times 20\ \text{mm}$ (height \times width \times length) in size. The device consists of two inlets, one outlet, a microfluidic gradient generator for future studies and 6 linear arrays containing 5 PLBRs each (30 PLBRs in total). (B) CAD image of one PLBR array, containing 5 PLBRs in parallel. (C) SEM of a single PLBR with $1\ \text{pL}$ cultivation volume. The height of the PLBR is app. $1\ \mu\text{m}$ and the supply channel height is app. $10\ \mu\text{m}$. Seeding and overflow channels have a width of $2\ \mu\text{m}$.

3.2.4 Material and methods

Chip fabrication

To fabricate the mold for PDMS casting, a two layer SU-8 process was carried out on a silicon wafer. For processing parameters the reader is referred to the literature [79]. In this report, only major processing steps and parameters are given.

Processing was performed under class 100 cleanroom conditions. A 4-inch silicon wafer was thoroughly cleaned in piranha solution, deionized water and eventually spin dried. Prior to resist spinning a 30 minute dehydration bake at $150\ ^\circ\text{C}$ was performed. A $1200\ \text{nm}$ thick layer of negative photoresist SU-8 (SU-8 2000.5/2010 mixture=12:100, MicroChem Corp.) was spincoated onto the wafer. This layer was pre-baked for 1 minute at $90\ ^\circ\text{C}$. To achieve the desired structure resolution, an electron beam written $5''$ lithography mask was fabricated and applied during wafer exposure. Exposure time was optimized with respect to SU-8 thickness, structure resolution and mask aligner lamp intensity (SÜSS MicroTec AG, Garching, Germany), and was typically below 4 seconds carried out in vacuum contact mode. After a 1 minute post exposure bake at $90\ ^\circ\text{C}$ the wafer was developed in resist developer (mrdev 600, Micro Resist Technology GmbH, Germany) and eventually hard baked at $120\ ^\circ\text{C}$. A second SU-8 layer ($10\ \mu\text{m}$, SU-8 2010) was spin coated onto the wafer. Lithography was carried out similar to the first layer and

in accordance with the manufactures specifications. Processing resulted in a two layer relief structure ready for PDMS casting.

Molding was carried out under conventional lab conditions. Polydimethylsiloxane (PDMS) (Sylgard 184 Silicone Elastomer, Dow Corning Corporation, Midland, USA) was mixed with cross linker in a 10:1 ratio and degassed under slight vacuum. The liquid PDMS was casted over the mold and thermally cured for 3 hours at 65 °C. The cured PDMS slab was cut into several chips. Uncured PDMS monomer residue was removed by washing the PDMS chips in pentane, acetone and eventually followed by a drying step overnight in accordance with Wang and co-workers [114]. Holes for the inlets and outlet were manually punched into the chip using sharp dispensing needles. The PDMS chip and a 170 µm thin glass plate (D263 T eco, 30 mm x 25 mm x 0.17 mm, Schott AG, Germany) were thoroughly rinsed with isopropanol ensuring sterile culturing conditions after assembly. After drying with nitrogen the PDMS chip and the glass plate were placed in oxygen plasma for 25 seconds at 50 watts (Femto Plasma Cleaner, Diener Electronics, Germany) and permanently bonded to the glass slide. Bonding was strengthened through two minute incubation at 65 °C. The inlet and outlet of the microfluidic chip were connected to silicone tubing (Tygon S-54-HL, ID=0.25 mm, OD=0.76 mm, VWR International) via dispensing needles (ID=0.2 mm, OD=0.42 mm). Chips were immediately used for microfluidic cultivation after fabrication.

Experimental setup, procedure and analysis

1 mL sterile glass syringes (ILS Innovative Labor Systeme GmbH, Germany) were used for medium supply. Medium flow control was realized with high precision syringe pumps (neMESYS, Cetoni, Germany). The chip was placed inside an in-house fabricated incubator for temperature and atmosphere control. The incubator was placed on a fully motorized inverted microscope (Nikon Eclipse Ti) suitable for time-lapse live-cell imaging. In detail, the setup was equipped with a focus assistant (Nikon PFS) compensating for thermal drift during long term microscopy, Apo TIRF 100x Oil DIC N objective, NIKON DS-Vi1 colour camera, ANDOR LUCA R DL604 camera, Xenon fluorescence light source for fluorescence excitation and high quality filters for the proper excitation of the chromophore eYFP and detection of its emission. Additionally, the objective was heated with an objective heater (ALA OBJ-Heater, Ala Scientific Instruments, USA).

The microfluidic device was flushed with fresh medium for 30 minutes prior to each cell seeding phase. A cell suspension with an optical density between 1 and 3, just transferred from a pre-culture at exponential growth phase, was infused to the system. Flow was stopped when satisfying amounts of PLBRs were seeded with a single cell. After seeding the flow was switched from bacterial suspension to growth medium, with a flow rate of app. 10 nl/min per PLBR device (300 nl/min in total), to initiate the growth experiment. This flow rate was optimized to ensure stable trapping of the seeded mother

cells inside the PLBRs. Medium switching was done manual as soon as the desired colony size was observed.

Time-lapse images of individual PLBRs were acquired in 10 minute time intervals. DIC microscopy images as well as fluorescence images were captured and analyzed using the Nikon NIS Elements AR software package. Image analysis and data acquisition for the growth experiments was done as follows: The number of bacteria in each reactor chamber was counted and cell size measured manually at different time steps.

Additional methods and protocols for microfluidic experiments, bacteria sample preparation and bench-scale cultivation can be found in Appendix B.1-B.4.

3.2.5 Results and discussion

The *E. coli* strain BL21 is one of the most frequently used microbial hosts for recombinant protein production [208]. This strain is genetically modified to disable flagella functionality, and thus unable to move or migrate during cultivation. Likewise, *C. glutamicum* is one of the most important hosts for industrial amino acid production [6, 23, 209]. This bacterium is naturally non-motile. Therefore, both bacteria are suited for our PLBR single-cell seeding principle, where cell migration is undesirable. Motile bacteria might actively leave the PLBR zone, and prevent proper cell counting studies.

Picoliter cultivation of *E. coli* BL21

A proof of principle experiment was performed to demonstrate the device functionality. During our microfluidic experiments *E. coli* BL21 was cultivated in complex LB-Medium at 37 °C (± 0.2 °C) under aerobic conditions. We expect variations in oxygen to be minor in our device because of the high gas permeability of the PDMS, large surface area to volume ratio and the continuous influx of fresh growth medium. Recent studies suggest that even with bigger reactor chambers and more bacteria sufficient oxygen supply is guaranteed [85, 210]. As expected we observed the three phases as explained in the device principle section.

a) As depicted in Figure 3.11A, the suspension of *E. coli* BL21 pre-grown in LB-medium was infused and within minutes the PLBRs were seeded with bacterial cells. Since filling was performed randomly, roughly 25% of the PLBRs were seeded with one single cell as desired. Since each device incorporates many PLBRs, enough PLBRs were available for microscopy and analysis. Chip designs with hundreds of PLBRs and improved seeding efficiency are currently being under development. After switching to growth medium, a short adaption phase was observed and then the single mother cells started to grow. In Figure 3.11D the first division event is resolved in more detail.

b) During the growth phase (Figure 3.11B) the microcolony could be analyzed with respect to, e.g., cell morphology, division rate, fluorescence related productivity, stress reactions and population heterogeneities on single-cell level. The constant environmental conditions and the possibility to induce instantaneous changes

make this microfluidic system ideal for single-cell analysis and bioprocess characterization. Performing image analysis cell division was followed over several generations until the reactor was filled and eventually the overflow started, as shown in Figure 3.11C.

c) During the overflow phase cells were continuously pushed out of the reactor and eventually dragged away with the medium stream. If culture growth and cell removal are in balance, a nearly constant cell density can be maintained inside the PLBR, suitable for bioprocess studies. However, depending on the organism's growth rate an ongoing increase in cell density inside the PLBR can be observed instead. Hence, in contrast to the relatively low cell density during the growth phase, the overflow phase can result in extremely high cell densities. At these high densities, individual cells are difficult to analyze. However, due to rapid chip production the overflow channels and reactor size can be easily tailored to specific requirements.

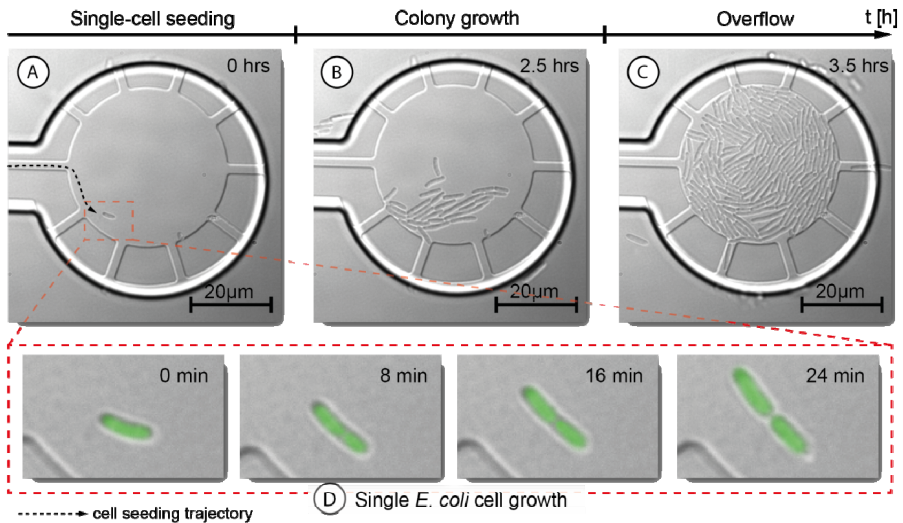


Figure 3.11: Time-lapse microscopy images showing the cultivation of *E. coli* BL21 inside a PLBR (see also supplemental video S1 of [169]). (A) A single *E. coli* cell was seeded into the PLBR and complex LB growth medium was infused. (B) After 2.5 hours of cultivation at $T=37^\circ\text{C}$ a microcolony of app. 30 cells was formed. (C) After 3.5 hours of cultivation the overflow phase was reached. Cells were pushed continuously out of the PLBR maintaining a constant density. (D) Time-lapse image series showing the growth of the single mother cell after initiating the growth phase. (For purpose of illustration the dividing *E. coli* cell was artificially colored afterwards by image processing software). (A-C) The overflow channels have different lengths due to a slight misalignment during the two layer photolithography process. The functionality was not affected by this misalignment.

Growth quantification of *C. glutamicum*

For long-term growth rate experiments, defined constant and non-toxic environmental conditions have to be guaranteed. Therefore, it was essential to investigate the influence of our system on the physiological state of the cells, in this report indirectly measured by the growth rate. PLBR cultivation was performed with the wild type of

C. glutamicum in minimal medium CGXII at 30 °C. For comparison the growth rates of three PLBR colonies on one chip were derived from time-lapse microscopy images by single-cell counting. It can be seen in Figure 3.12 that colonies grew exponentially with equivalent growth rates. It appeared that the growth curves are slightly shifted. This is potentially due to initially different cell-division cycle states of the captured “mother” cells and the adaption to the new environment. The maximum growth rate determined during our experiments was $\mu_{\max} = 0.63 \pm 0.02 \text{ h}^{-1}$ (n=3).

To the best of our knowledge this is the first study investigating growth of *C. glutamicum* on single-cell level in microfluidic devices. Literature values derived during shake flask cultivations are in the range of $\mu_{\max} = 0.40 \text{ h}^{-1}$ [211]. Applying a sophisticated continuously infused turbidostat bioreactor system only Bäumchen *et al.* observed a nearly comparable growth rate of $\mu_{\max} = 0.58 \text{ h}^{-1}$ [212].

The high PLBR growth rate of $\mu_{\max} = 0.63 \pm 0.02 \text{ h}^{-1}$ supports our assumption that bacteria remain in good physiological state in our microfluidic system. Actually, it also suggests that the microfluidic system offers better growth conditions than in typical lab-scale experiments. This is probably due to the continuous medium flow leading to more homogeneous conditions and the removal of secreted by-products. This aspect will be further investigated in more detailed future experiments.

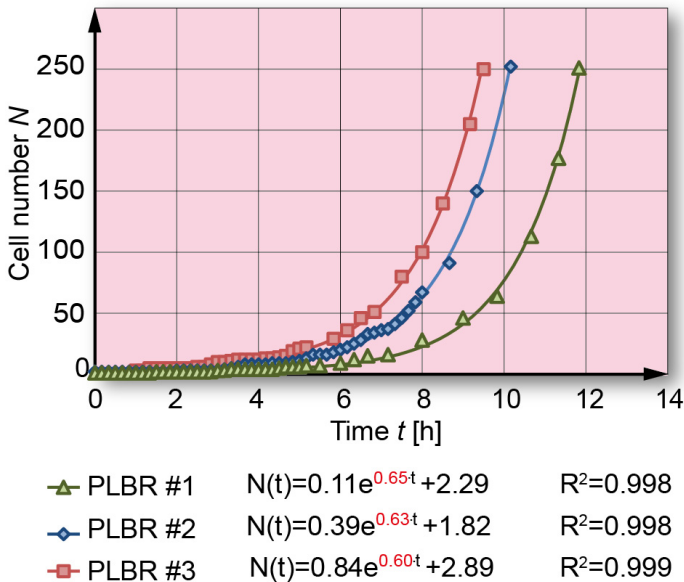


Figure 3.12: Growth curves of *C. glutamicum* wild type microcolonies cultivated in three different PLBRs on one chip. Growth was followed by single-cell counting of time-lapse microscopy images. The average maximal growth rate (μ_{\max}) and corresponding doubling time (t_d) was determined by exponential data fitting as $\mu_{\max} = 0.63 \pm 0.02 \text{ h}^{-1}$ (n=3) and $t_d = 66 \text{ min}$.

Induced Stationary phase during PLBR Cultivation of *C. glutamicum* DM1800

In the following section, a comparison of a batch cultivation (1 liter) with our PLBR (10^{-12} liter) is shown. Results obtained during 1 liter cultivation will be discussed first, followed by our PLBR results.

A batch cultivation can be characterized by three phases, as illustrated in Figure 3.13A. The process starts with the lag-phase, in which freshly seeded cells adapt to the new environmental conditions. The lag-phase is followed by the exponential growth phase where the maximum growth rate under the applied conditions is derived. Eventually, available nutrients are consumed and metabolic side products have increased, inducing the stationary phase. During this phase negligible growth is normally measured followed by cell degradation and cell death. Morphological variability of *C. glutamicum* has been known from prior microscopic observations, but no systematic process and time dependent investigations have been done so far [23].

In a lab-scale batch cultivation (1 liter cultivation: details see materials and methods in supplemental part) of the L-lysine producing strain *C. glutamicum* DM1800, cellular heterogeneity during the stationary and late stationary phase was observed (Figure 3.13). Two different sub-populations were seen as determined by the applied Coulter counter system, namely: cells larger than 1.3 μm and cells smaller than 1.3 μm in length. As depicted in Figure 3.13B, over the entire cultivation time single cells larger than 1.3 μm and cells smaller than 1.3 μm in length can be observed. There is a pronounced change in the ratio of these two cell classes, with a clear predominance of small cells in the stationary phase. Similar results were obtained using *C. glutamicum* wild type (data not shown). The quantitative assessment of population heterogeneity required elaborate lab-scale cultivation, sample preparation and Coulter counter based cell counting. As can be seen in Figure 3.13B, samples were taken, prepared and analyzed during more than 160 hours of cultivation. Despite the high relevance and interest in the observed population heterogeneity and its possible impact on industrial-scale cultivation, it becomes clear that processing time and effort is inappropriate for more detailed studies at lab-scale.

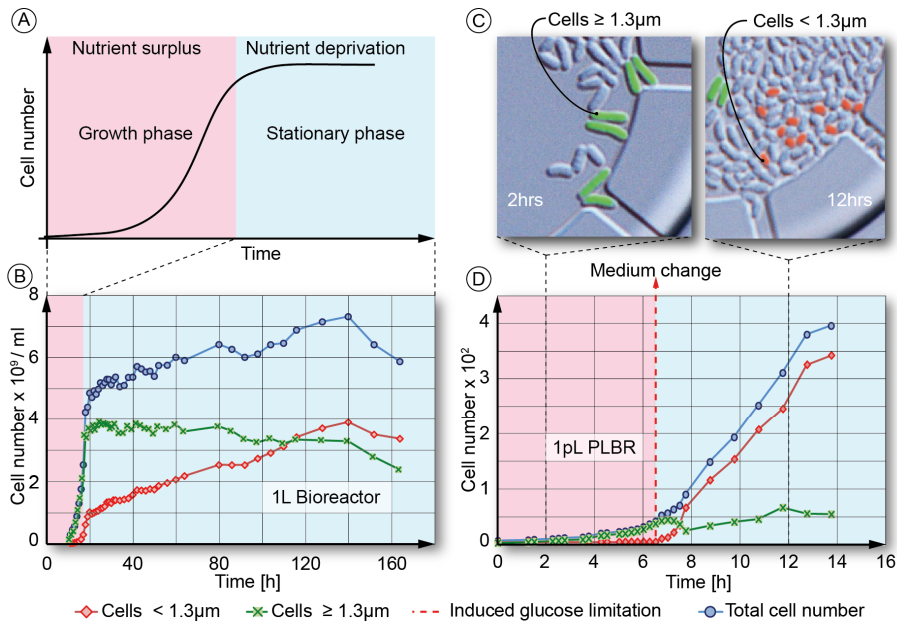


Figure 3.13: Growth and morphology analysis of *C. glutamicum* DM1800 during 11 lab-scale batch cultivation and under PLBR cultivation after inducing an artificial stationary phase: (A) Typical growth curve during batch cultivation. (B) Experimentally derived growth curve of a 1L batch cultivation of *C. glutamicum* DM1800 following the exponential and late stationary growth phase. The number of small cells exceeded the number of larger cells after app. 100 hours after reaching the stationary phase. (C) Time-lapse microscopy images showing the cell population at 2 hrs. and after 12 hrs. experimental time inside the PLBR. Few cells were artificially colored exemplarily for purpose of illustration. (D) Experimentally derived growth curve of an isogenic microcolony inside the PLBR; The number of small cells exceeded the number of larger cells in app. 45 minutes after artificially inducing the stationary phase.

At this stage the developed microfluidic PLBR was applied to perform the same investigations during the late stationary phase. Obviously, our chip device that is continuously infused with fresh medium cannot be directly compared to a batch cultivation process. However, it can be used to artificially induce different environmental conditions within seconds simply by changing the medium and for instance mimic the stationary growth phase.

The chip was infused with the *C. glutamicum* DM1800 cells and PLBRs were seeded with single cells. The growth phase was initiated with fresh minimal medium CGXII at 30 °C. During the growth phase the measured maximal growth rate $\mu_{\max_PLBR} = 0.56 \pm 0.02 \text{ h}^{-1}$ was again significantly higher than the growth rate of $\mu_{\max_LS} = 0.37 \text{ h}^{-1}$, which was experimentally derived during the lab-scale batch cultivation described above. These findings are in accordance with previous PLBR cultivations and prove that better growth conditions can be maintained not only for the *C. glutamicum* wild type but also for the industrially utilized L-lysine producing strain DM1800. After reaching app. 50 cells inside the PLBR, medium was changed to medium lacking glucose thereby artificially inducing the stationary phase. Time-lapse microscopy images revealed the

same phenotypic differentiation as observed during 1 liter lab-scale cultivation. Although no carbon source was available, the absolute cell number increased. Whereas one part of the culture almost stopped growing, the other part still continued to divide but into remarkable smaller cells, as exemplarily shown in Figure 3.13C. A possible reason could be the formation of carbon storage pools like, e.g., glycogen in some cells during the growth period under carbon excess. These storage pools are then used under carbon limiting conditions to continue growth for several generations. The amount of cells larger than 1.3 μm dropped notably after inducing the stationary phase, as shown in Figure 3.13D. It can be seen that our PLBR system reduced the required experimental time drastically. Within 45 minutes of chip cultivation after inducing the stationary phase, the amount of cells smaller 1.3 μm equaled the quantity of cells larger than 1.3 μm . In contrast to that, 120 hours of sheer experimental time were needed to obtain the same results at lab-scale batch cultivation. In particular the experimental time was reduced 160 fold. The slight increase of cells larger than 1.3 μm after app. 8 hours could be due to inaccurate cell measurement, as it became difficult to measure accurately 1.3 μm at densely packed colonies, as evident from Figure 3.13C (12 hours). Growth inside the PLBR completely stopped beyond 14 hours of cultivation, which was comparable to the results obtained during 1 liter cultivation.

Fluorescence based production studies

As described in the introduction, FACS is an ideal high-throughput system to sort and analyze microorganisms based on a fluorescence signal. However, FACS is limited to snap-shot analysis and time dependent analysis is impossible. In contrast, our microfluidic system allows fluorescence based productivity analysis on a single-cell level for long time periods (here over 30 hours) and tracking of individual cells is possible by image analysis.

As a proof of principle we cultivated the L-arginine producing *C. glutamicum* pSenLysTKP-*argB*(fbr) strain in our PLBR device. This wild type derivative contains a plasmid-encoded metabolite sensor, enabling yellow fluorescence protein (EYFP) expression in response to enhanced intracellular L-arginine concentration (Binder *et al.* [33]). The plasmid contains in addition a feed-back resistant acetylglutamate kinase, resulting in weak extracellular L-arginine accumulation as observed in shake flask cultivations. Using PLBR, constant environmental conditions were applied to analyze the characteristics of this strain with respect to the growth and EYFP signal. Figure 3.14 shows a time-lapse image series of the isogenic microcolony inside the PLBR. Clearly an interesting change in cellular fluorescence and cell growth can be observed. It can be realized that the two cells in focus start to emit fluorescence after an adaptation phase apparently required to synthesize sufficient endogenous L-arginine to induce expression of the genetically encoded L-arginine sensor. EYFP emission continues up to 22 hours, although some heterogeneity with respect to fluorescence intensity becomes apparent. With significant growth ($\mu_{\text{max}} = 0.46 \text{ h}^{-1}$) beginning after 22 hours the number of fluorescent cells decreases, and at 30 hours no single cell is fluorescent. A similar

behavior of fluorescence and growth was observed in additional PLBR cultivations, too, but not observed with a control carrying a vector devoid of *argB(fbr)*. Currently, we cannot explain conclusively the time dependent fluorescence observed. One reason could be the rather weak production of the strain available. However, the experiment demonstrates the applicability of our system to investigate more complex biological phenomena such as time dependent production processes which was not possible before.

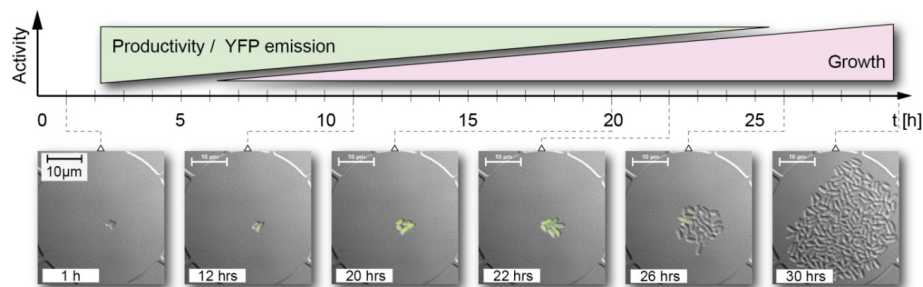


Figure 3.14: Time-lapse image series showing the growth and production of *C. glutamicum* pSenLysTKP-*argB(fbr)* during PLBR cultivation. The strain contains a metabolite sensor enabling EYFP expression in response to enhanced intracellular L-arginine concentration. The seeded mother cell starts to emit fluorescence after 12 hours indicating production of L-arginine. While undergoing a change to maximum cell growth EYFP emission declined.

3.2.6 Conclusions

This report demonstrates an innovative microfluidic device for cultivation of bacteria on single-cell level. A PDMS device was designed and fabricated for trapping of single bacteria cells in picoliter volume bioreactors (PLBR). The PLBR has a few important key characteristics: The system is a disposable low cost product, no intensive cleaning is required and the risk for contamination is minimal. Due to an innovative design, bacteria are being trapped simply by the shallow bioreactor region, not relying on sophisticated technical cell trapping methods, and grow inside confined reactor regions allowing continuous analysis. Once the bioreactor is filled, radially arranged overflow channels provide well controlled cell removal not limiting experimental time. Moreover, fast medium changes facilitate to mimic every desired environmental situation of a lab-scale process. Due to picoliter volumes, low cell numbers and short response time, a fraction of experimental time is required for otherwise elaborate and time-consuming investigations. Furthermore, the high potential for parallelization makes the system an ideal tool to collect statistically trustworthy data.

The presented system is not limited to the analysis of cell growth under standard conditions, but could be applied to investigate many environmental changes, *e.g.*, medium composition, pH changes, temperature fluctuations and flow rates. Furthermore, if time-lapse images are recorded at appropriate time intervals, also division events of individual

cells could be analyzed in detail, rather than just counting cell populations. In-depth studies are planned to investigate population heterogeneity effects in more detail.

Additionally, the device carries great potential if combined with appropriate analytical techniques, for analysing substrate consumption and (by)-product formation of resulting microcolonies. Hence future studies will also concentrate on quantifying the PLBR upstream regarding the cells exometabolome by untargeted (GC-TOF-MS) and targeted (LC-MS/MS) approaches as well as protein secretion by fluorescence labelling techniques.

As a final conclusion, our microfluidic PLBR is well suited for population heterogeneity studies on single-cell level and future bioprocess optimization strategies.

3.3 High-throughput single-cell cultivation

This chapter presents the successful realization and characterization of a parallelized single-cell cultivation platform for high-throughput growth studies. As proof of principle, the spontaneously induced stress response of *C. glutamicum* was investigated in detail. The results shown in this chapter were performed in close cooperation with Arun Nanda (Population heterogeneity group, IBG-1: Biotechnology), Stefan Helfrich and Birgit Stute (Modeling and Simulation group, IBG-1: Biotechnology). Lineage tree visualization was performed by S. Helfrich and CFD simulations were performed by B. Stute. A. Nanda conducted the FACS study.

3.3.1 Abstract

Cell-to-cell heterogeneity typically evolves during cultivation due to a manifold of biological and environmental factors. Especially rare cellular events occurring within less than 1% of the total population can be relevant for the fate of the whole population but hard to detect during analysis. Flow cytometric methods offer the possibility to sort and analyze rarely evolving phenotypes at high-throughput. However, it is not possible to investigate single-cell dynamics. In the present study, we demonstrate a microfluidic single-cell cultivation (MSCC) platform that incorporates monolayer growth chambers (MGC). Up to several hundred isogenic microcolonies growing in a cell monolayer can be tracked by automated time-lapse microscopy with spatio-temporal resolution. This high-throughput approach enables well defined single-cell studies to elucidate cell-to-cell heterogeneity more specifically compared to FC, and records single-cell dynamics. In fact, we have utilized the system to analyze lineage trees, division events of single-cell, morphological phenotypes and rare biological events. The occurrence of spontaneously induced stress in *Corynebacterium glutamicum* cells was investigated by analyzing strains with genetically encoded reporter systems visualizing SOS response. The experiments revealed a spontaneous induction in 0.07-0.5% of the total population which is comparable to results obtained from large-scale cultivation in combination with flow cytometry. These results demonstrate the importance of novel high-throughput microfluidic single-cell cultivation systems for exploring rare events in isogenic bacteria microcolonies at the single-cell level.

3.3.2 Introduction

Flow cytometry (FC) is state of the art when analyzing the distribution of single-cell heterogeneity of cell populations and offers a tremendous throughput of up to 80,000 cells per second [33]. FC and in particular fluorescence activated cell sorting (FACS) are

applied in many cell biology applications, for example, to unravel cell-to-cell heterogeneity in isogenic populations [27, 151, 213] and to identify and sort subpopulations from a mixed culture [214, 215]. Identifying rarely occurring cells that for example, survive antibiotic treatment is even more challenging since its occurrence is often below 1% or even smaller [216, 217].

At that point, high throughput is of importance to analyze statistically reliable cell numbers. However, temporal resolution of individual cells during perturbation studies becomes another prerequisite, which is nearly impossible to obtain with conventional flow-through analytics. To overcome this limitation, microfluidic single-cell cultivation devices have been developed [21, 155, 218, 219] and applied in microbiology, offering cultivation and analysis under well-defined environmental conditions [220, 221]. Moreover, microfluidic single-cell systems allow for the control of the environment, for example, by fast medium switches and the ability for long-term cultivations. Performing time-lapse microscopy dynamic events such as cell lysis can be followed [178], offering information that would be lost using conventional technologies. Several microfluidic studies were reported to identify persister cells during the treatment with antibiotics, revealing origin and temporal behavior of rare cell events evolving in microbial populations [112, 141]. Moreover, microfluidic systems were developed to capture rare cell types [222]. These studies showed, that cells comprising less than 1% of a total population can have a significant impact on the fate of the whole population [219]. Therefore, it is of utmost importance to understand the mechanisms which enable small subpopulations to survive or dominate over the majority of cells.

Compared to their isogenic descendants, derived individual cells may exhibit no significantly different phenotype. Using fluorescence-based reporter systems, differences within cells can be visualized [223], allowing to screen for and to identify occasional cellular events [224].

The detection of rare cell events occurring below 1% of the total cell number, requires several thousands of cells to be monitored in parallel to gain statistically reliable data and to draw biologically relevant conclusions. In the present report, we demonstrate the capabilities of a disposable microfluidic microbial cultivation system for the screening of rare cell events and lineage tree analysis. The system fulfills the following important prerequisites:

- Support of full microcolony growth to derive lineage information since all cells are trapped inside the cultivation chamber
- Single-cell resolution since bacteria grow in monolayers
- Spatio as well as temporal single-cell resolution due to high resolution time-lapse microscopy
- High-throughput (>100.000 cells/run)
- Full environmental control

Convective and diffusive mass transport were analyzed by computational fluid dynamics (CFD), validating stable environmental conditions during cultivation and fast medium switches in the order of seconds. *Corynebacterium glutamicum* was chosen as model organism due to its high relevance in biotechnological applications and its relation to the pathogenic relative *Mycobacterium tuberculosis* [225, 226]. Several studies reported cell-to-cell heterogeneity within *C. glutamicum* populations, including cell-to-cell heterogeneity in viability, membrane potential and growth activity [40]. Furthermore, biological diversity is reported on growth and production [178], as well as on the occurrence of exceptional cellular events in spontaneous phage induction [196, 227], making *C. glutamicum* a promising organism for the screening of rare events.

C. glutamicum wild type and mutant strains equipped with a genetically encoded SOS reporter system [227] were analyzed to benchmark the microfluidic system. The chosen fluorescence-based reporter system allows for a dynamic investigation of infrequently appearing cell events, for example, individual cells encountering DNA damage and undergoing SOS response. The results revealed, that 0.07-0.5% of the cells showed an increased reporter output under standard cultivation conditions. This fits well with results obtained by conventional flow cytometric methods in combination with shake flask cultivations.

3.3.3 Materials and methods

Device fabrication and setup

High resolution PDMS soft lithography was carried out to manufacture single-use microfluidic devices with integrated channel heights of 10 μm and 1 μm , respectively. The device fabrication and the experimental setup can be found in more detail in previous publications [98, 169].

Microfluidic device characterization

Fundamental microfluidic flow characterization was performed by infusing fluorescently labeled latex beads with

- I. 200 nm (yellow-green fluorescent 505/515),
- II. 1 μm (blue fluorescent 350/440) and
- III. 2 μm (red fluorescent 535/575).

The FluoSpheres[®] are carboxylate-modified microspheres (2% solids) and were purchased from Molecular Probes. 200 nm and 1 μm beads were applied for online flow characterization, 1 μm and 2 μm beads were applied to emulate cell trapping. Prior flow characterization, the microfluidic channels were primed with a BSA solution (0.1%) for 60 minutes at a total flow-rate of 700 nl/min to minimize unspecific bead adhesion. All fluorescent latex beads suspensions were diluted 1:1000 in 0.1% BSA solution.

Fluorescence exposure time was set to 10 s to capture flow trajectories if not stated differently.

Bacterial strains and pre-cultivation

C. glutamicum ATCC 13032 was used for proof of principle experiments. *C. glutamicum*/pJC1-*P_{recA}-e2-crimson* was used to perform the detailed investigation of spontaneously stress induced cells during microcolony growth. Detailed information regarding the construction of More details *C. glutamicum*/pJC1-*P_{recA}-e2-crimson* can be found in Nanda *et al.* [227].

CGXII was used as standard mineral medium for *C. glutamicum* consisting of (per liter): 20 g (NH₄)₂SO₄, 5 g urea, 1 g K₂HPO₄, 1 g KH₂PO₄, 0.25 g MgSO₄·7H₂O, 42 g 3-morpholinopropanesulfonic acid (MOPS), 10 mg CaCl₂, 10mg FeSO₄·7H₂O, 10 mg MnSO₄·H₂O, 1mg ZnSO₄·7H₂O, 0.2 mg CuSO₄, 0.02 mg NiCl₂·6H₂O, 0.2 mg biotin, 0.03 mg of protocatechuic acid. The medium was adjusted to pH 7, and 4% glucose was added as carbon source. All chemicals were purchased from Carl Roth and Sigma Aldrich. The medium was autoclaved and additionally sterile filtered (0.22 μm pore size filters) prior to cultivation of the pre-cultures and MSCC experiments to prevent clogging of the microfluidic channels.

Prior to all main cultures, cells were pre-cultured as 20 mL cultures in 100 mL baffled Erlenmeyer flasks on a rotary shaker at 120 rpm with orbital shaking at 30 °C. A primary pre-culture in BHI complex medium was inoculated to a second pre-culture in CGXII mineral medium, which was finally inoculated to an OD₆₀₀ of 0.05 to the main cultures for MSCC experiments.

Microfluidic cultivation

For detailed description of the MSCC setup, operation and equipment, the reader is referred to [98, 169]. In the following, only noteworthy changes to the previously published protocols are described.

Prior to MSCC experiments, the device was flushed with fresh sterile filtered CGXII medium. After that, the chip was flushed with the bacterial suspension and the trapping phase was initiated. Bacterial suspensions were taken from the main culture at exponential phase at OD₆₀₀ between 0.5 and 1. Filling was done according to Appendix C.1 and Appendix Figure C.1-C.3). As soon as sufficient single mother cells were entrapped inside the cultivation chambers, CGXII was infused instead.

Time-lapse imaging

Phase contrast and fluorescence time-lapse images of evolving microcolonies were captured every 10 to 20 minutes. Fluorescence images were recorded using an ANDOR LUCA R DL604 CCD camera with an exposure time of 200 ms. Crimson chromophores were excited using a 300 watt Xenon light source (Lambda DG-4 Sutter Instruments) at maximum intensity and appropriate optical filters (excitation: HQ 600/37, dichroic:

DM630, emission: HQ 675/67; Chroma). Between different experiments settings were not changed to allow the direct comparison of fluorescence intensities.

Image analysis and data visualization

Growth pattern analysis was performed semi-automatically, using the commercially available software package NIS-Elements AR (Nikon Instruments), by counting the cell number, cell length and mean fluorescence value of individual cells in each growth chamber at different time points. These datasets were used for software based lineage tree visualization and growth analysis. The software tool has been developed in-house to generate lineage trees annotated with additional, phenotypic information (Helfrich, unpublished).

For the quantification of spontaneously induced *C. glutamicum*, specific cells exhibiting two, five or 15 times higher mean fluorescence than the average uninduced cells were classified as SOS response positive. An average final cell number of 750 cells per cultivation chamber was assumed, based on the cell count of 10 cultivation chambers, to derive the percentage of SOS response positive cells.

Flow cytometry

Flow cytometry was performed on a FACS Aria II (Becton Dickinson, San Jose, USA) flow cytometer with 488 nm excitation by a blue solid-state laser and 633 nm excitation by a red solid-state laser. Forward-scatter characteristics (FSC) and side-scatter characteristics (SSC) were detected as small- and large-angle scatters of the 488 nm laser, respectively. E2-Crimson fluorescence was detected using a 660/20 nm band-pass filter. About 100,000 cells were analyzed to determine SOS response at different time points, if not stated differently. Cells with a fluorescence output 12 to 18 fold higher than the average and above were counted as SOS response positive.

Computational fluid dynamics

Computational fluid dynamics (CFD) was performed with COMSOL multi physics. For further information, the reader is referred to Appendix C.2.

3.3.4 Results

Device layout and principle

The present microfluidic system (Figure 3.15A) is intended for high-throughput single-cell cultivation and analysis of evolving isogenic microcolonies. Each device consists of a polydimethylsiloxane (PDMS) chip (3 mm thick, 15 mm wide and 20 mm long) with incorporated microfluidic channels bonded onto a 170 μm thick glass slide (cover glass) suitable for high-resolution microscopy. Since PDMS chips can be fabricated rapidly, the system is intended for single-use only, avoiding elaborate device cleaning and autoclaving.

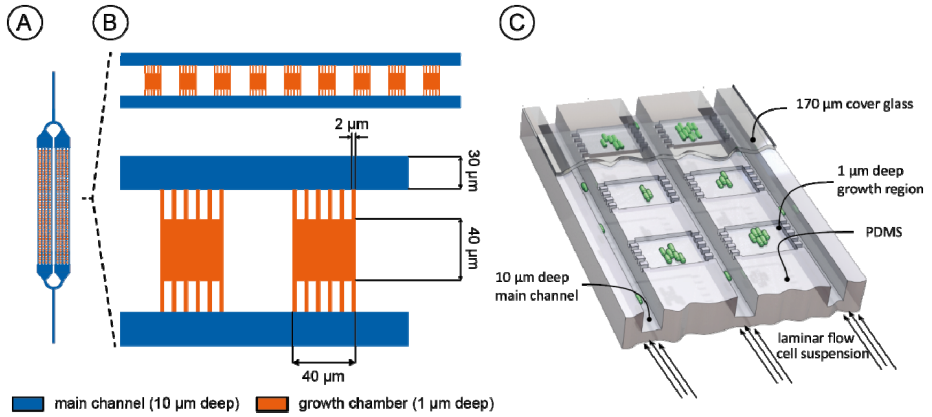


Figure 3.15: Device layout and schematic overview of the microfluidic single-cell cultivation (MSCC) system. (A) CAD drawing of the MSCC system, containing ten arrays of monolayer growth chambers (MGC). (B) Close up view of one array of parallelized MGCs (top). Each MGC (orange) is $40\ \mu\text{m} \times 40\ \mu\text{m}$ in size and $1\ \mu\text{m}$ in height. Each MGC is connected to two main channels (blue) with a cross section of $30\ \mu\text{m} \times 10\ \mu\text{m}$. (C) Cultivation principle of the MSCC. Microcolonies are growing inside the MGC while medium is infused continuously through the main channel. This allows the cultivation at constant environmental conditions.

The chip incorporates 400 parallel monolayer growth chambers (MGC) (Figure 3.15B) connected with inlet channels to supply growth medium and a single outlet channel for fluid disposal. Each MGC of $40\ \mu\text{m} \times 40\ \mu\text{m} \times 1\ \mu\text{m}$ (width \times length \times height) can accommodate one microcolony of approximately 750 individual bacteria (Appendix C.5). The uniform MGC height of $1\ \mu\text{m}$ restricts microcolony growth to a cell monolayer, facilitating continuous image-based analysis of individual cells by time-lapse microscopy. MGCs are arranged in between two ten-fold deeper supply channels ($10\ \mu\text{m}$ depth \times $30\ \mu\text{m}$ width) with laterally interconnected micrometer sized channel arrays as depicted (Figure 3.15B). Throughout the cultivation, medium is fed continuously at identical flow-rates via each supply channel. Thus, zero pressure difference occurs across each MGC, leading to solely diffusive mass transport into and inside the MGC. Therefore, cultivated cells are not negatively affected by convective flow, shear stress or pressure gradients. Experimental flow tracer studies as well as computational fluid dynamics analysis were performed to characterize fluid dynamics inside the MGCs.

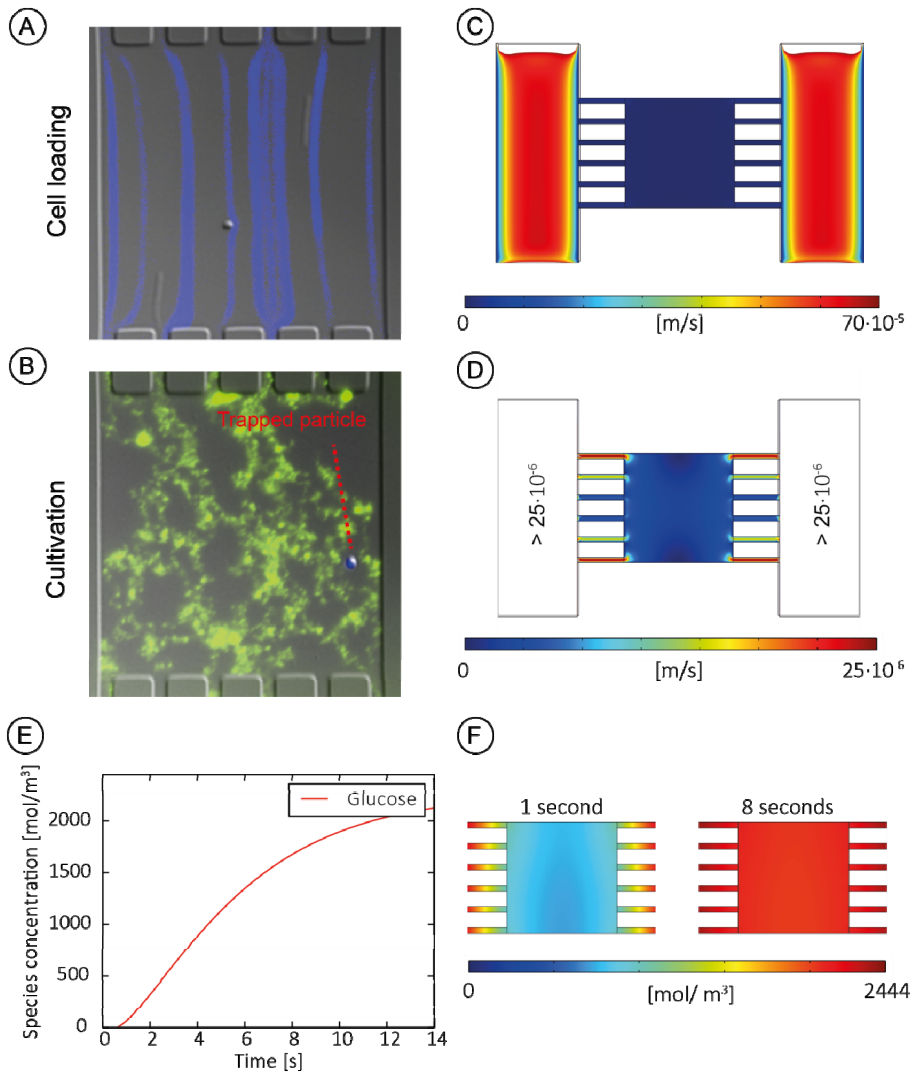


Figure 3.16: Characterization of flow and trapping profile within the MGCs. (A) Fluorescence traces of 1 μm polystyrene beads illustrating the horizontal flow profile during cell trapping and (B) behavior of 200 nm beads during cultivation conditions, illustrating diffusion based transport. (C) Flow profile in the main channel compared to the MGC. (D) Flow profile within the cultivation chambers obtained by CFD simulations, showing a strong domination of diffusion based material transport compared to the main channel, where convection is the main transport phenomenon (color bar one magnitude smaller). (E) Nutrient supply after medium change. Within seconds the medium can be changed, guaranteeing excess of nutrients during MSCC. (F) Glucose concentration profile during medium change illustrated for 1 s and 8 s after medium change.

Flow tracer analysis

The microfluidic system was characterized experimentally using fluorescence beads. Firstly, the filling procedure was characterized using 1 μm polystyrene beads thereby emulating cells of similar size. Figure 3.16A shows the flow profile of blue

fluorescent beads flowing through the monolayer cultivation chamber (blue traces) during cell loading. Some of the 1 μm beads are randomly trapped between glass and PDMS. In a typical experiment, the cells are seeded and the growth phase is then initiated with a medium switch from bacterial suspension to growth medium with a flow rate of 300 nl/min in total. This procedure was now emulated by 0.2 μm sized green fluorescent beads supplemented into the fluid flow. Figure 3.16B shows the trapped 1 μm beads (blue) and the 0.2 μm green fluorescence beads distributed inside the MGC. The green fluorescent beads inside the MGCs moved solely by diffusion, whereas the large beads remain trapped (no tumbling). This approach experimentally proved stable cultivation conditions compared to “open” monolayer growth chambers, where cells might get lost during the cultivation due to partial convective flow within the chamber (Appendix C.6).

CFD simulations

CFD simulations were performed to validate the experimental findings and optimize structure geometry. CFD simulation confirmed a solely diffusive flow behavior inside the MGCs with a negligible convective flow (Figures 3.16C and D). The characteristic time of diffusive media exchange ($t_{\text{diffusion}}$) between the main channels and the MGCs (assumed distance = 50 μm) for small molecules such as glucose is $t_{\text{diffusion}} = 1.8 \text{ s}$ (diffusion coefficient $D_{\text{Glu}} = 7 \cdot 10^{-10} \frac{\text{m}^2}{\text{s}}$ at 25 °C). These estimations were confirmed by results of the CFD calculations, simulating the exchange of medium after initiating the growth phase. Within four seconds, half of the maximum concentration is reached. This indicates that cells are supplied continuously with substrate (Figures 3.16E and F). Compared to the glucose consumption of one single cell, which is in the range of atto- and femtomol per cell per second [228], the system offers excess nutrient supply and limitations can be excluded under standard cultivation conditions (CGXII; 30 °C). It is known from previous studies that cells actively change their environment and under glucose excess conditions (as predominant in the MSCC) cellular overflow metabolism leads to excretion of by-products such as ethanol, acetate or lactate [229]. Therefore, the removal of secreted products and by-products of the system was simulated additionally. As demonstrated in Appendix C.7, secreted products and by-products are continuously removed, preventing accumulation, and remain at a low concentrations compared to the provided substrate. Cells are solely exposed to metabolite concentrations produced by neighboring cells, compared to a batch system, where by-product and product concentration can reach mM range [229].

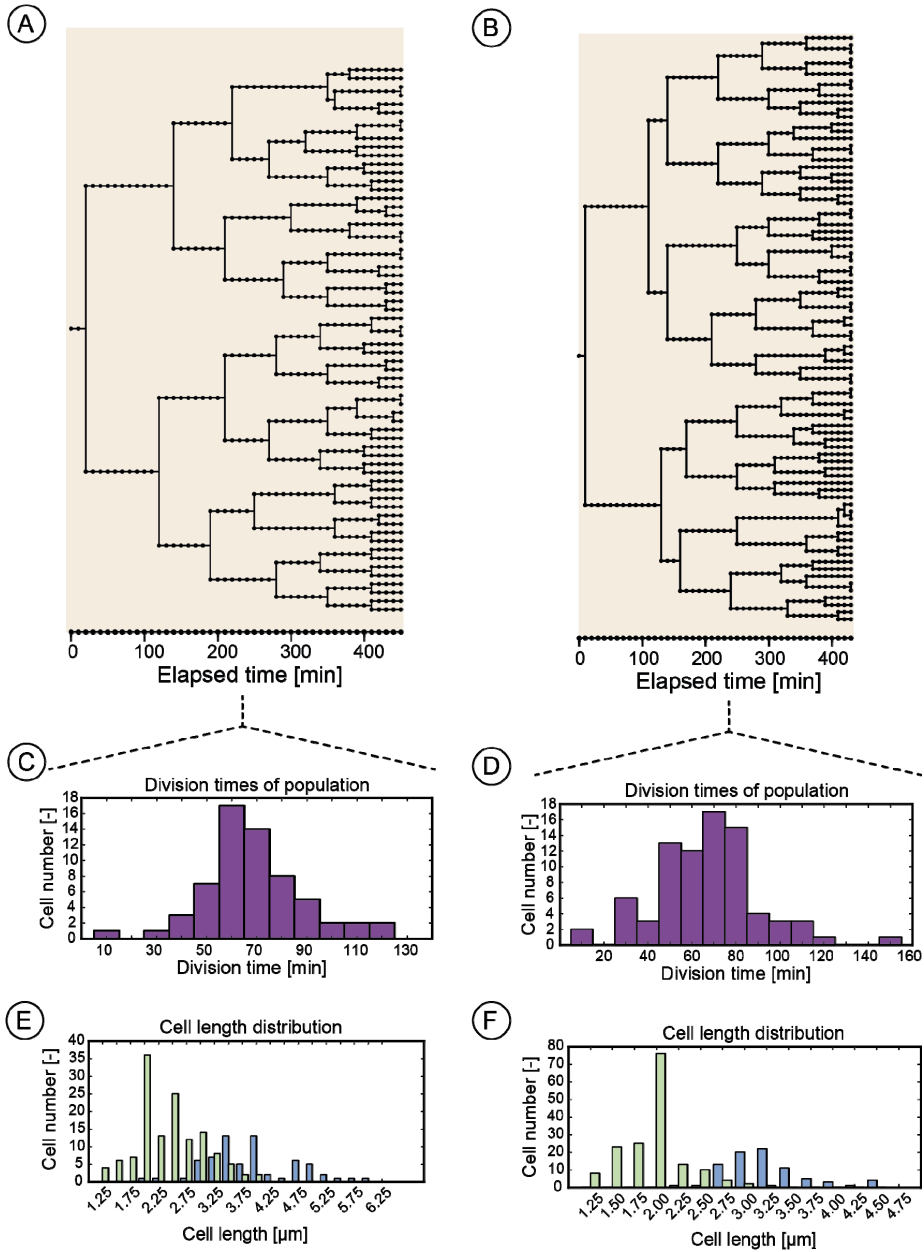


Figure 3.17: Analysis of growth heterogeneity of two isogenic microcolonies of *C. glutamicum*. (A+B) Lineage trees showing the overall growth and division behavior. (C+D) Division time distribution and (E+F) cell length distribution before (blue) and after division (green) derived from lineage trees showing in Figure A and B.

Single-cell bacterial growth pattern analysis of isogenic microcolonies

Standard growth experiments with *C. glutamicum* ATCC 13032 were performed. Appendix C.8 shows a growth rate distribution of different colonies under the same growth conditions for 60 colonies. The overall microcolony growth behavior is comparable and shows a normal distribution. Observed variations within the microcolony growth could be related to differences of individual cells and cell clusters, potentially affecting the population's performance and leading to differences in the overall growth rate.

Figure 3.17A, 3.17B and Appendix C.9 visualize three different colony lineage trees with comparable maximum colony growth rates ($\mu_{\max, \text{Col } 1} = 0.58 \text{ h}^{-1}$, $\mu_{\max, \text{Col } 2} = 0.61 \text{ h}^{-1}$, $\mu_{\max, \text{Col } 3} = 0.65 \text{ h}^{-1}$). Figure 3.17C-F shows the corresponding single-cell doubling times as well as length before and after division. The distribution reveals that division times range from 10 minutes up to over 160 minutes with an average of 63 min (67 min) for the two illustrated examples. Similar results can be found for the length distribution before and after division, ranging from 2.6 μm to 5.8 μm and an average cell size of 3.2 μm before division. After division, cells have an average cell size of 1.95 μm , ranging from 1.2 μm in minimum to 3.7 μm as maximum.

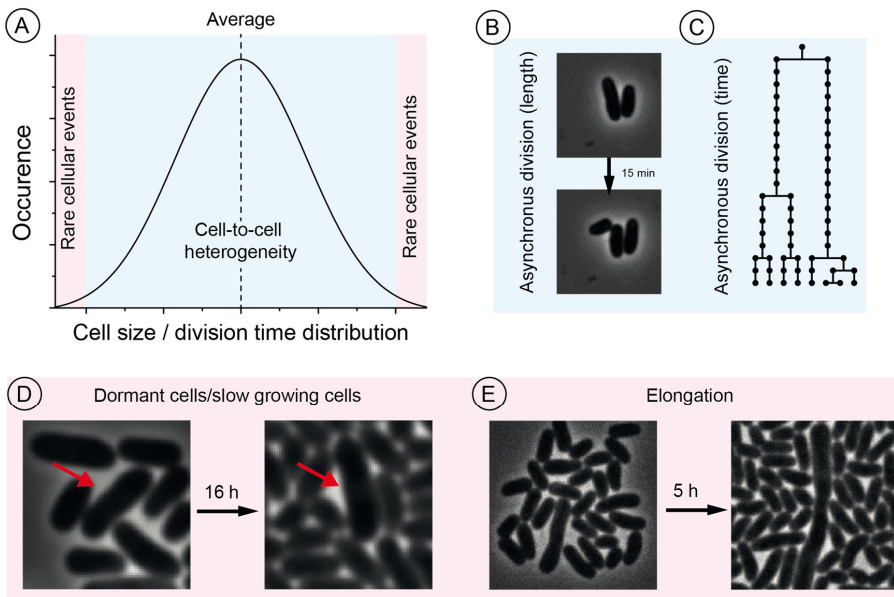


Figure 3.18: Overview of single-cell heterogeneity and rare events during *C. glutamicum* growth under standard conditions. (A) Probability distribution function, illustrating cell-to-cell heterogeneity as well as rare cellular events. (B+C) Asynchronous division led to a spread in the Gauss distribution in cell size and division time. (D+E) Rare events can be found in both, temporal and structural context. (D) Slow growing as well as dormant cells can be found (red arrow). (E) Elongation, as well as other morphological deformed cell shapes (see also Appendix C.10) can be detected.

Identifying rare cellular events in *C. glutamicum*

The distributions of cell size and cell division show variability between individuals, commonly referred to as “population noise” in the literature [19] (for schematic illustration see Figure 3.18A). Figure 3.18B and 3.18C display population noise caused by asynchronous division times as well as asynchronous division length. However, even elongated cells (Figure 3.18E), morphological deformed cells (Appendix Figure C.10A), branched cells (Appendix Figure C.10B) as well as slow growing or putative “dormant” cells have been observed (Figure 3.18E). From here on, these “outliers” are referred to as “rare events”. Especially, the latter case is difficult to identify during exponential growth conditions. These events are rarely seen and affect populations in less than 1% of the cells (e.g., one cellular division event with 160 min (cf. Figure 3.18D)).

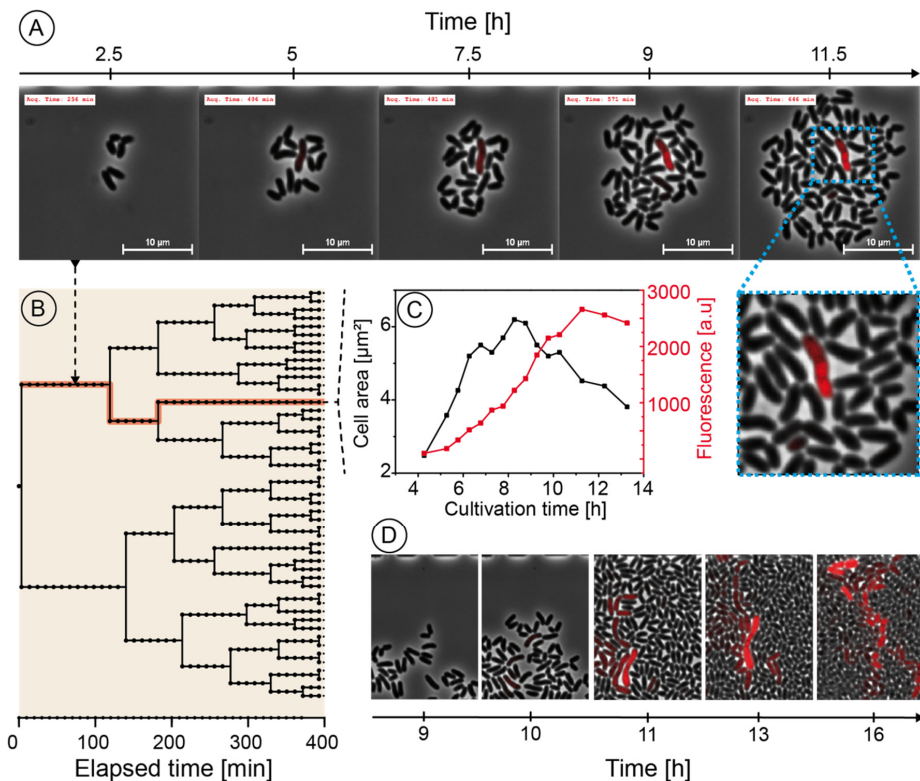


Figure 3.19: Dynamic SOS response of *C. glutamicum* cells. (A) Representative *C. glutamicum* colony, containing one single cell showing a SOS response during cultivation under normal conditions. (B) Lineage tree showing a homogeneous growth profile, except one cell that stops growth. (C) Fluorescence and cell area profile over time, which show a correlation between reduction in cell area/growth and reporter output. (D) Microcolony containing a SOS positive cell cluster. Cells continue to grow, but with reduced growth rate and changed morphology.

Dynamic studies of rare cellular stress events in *C. glutamicum*

The reliable quantification of rare events as classified in Figure 3.19 requires a “measurement output” which correlates to specific characteristics of the rare events. Elongation or reduced growth can be indicators for the induction of cellular stress responses [230]. Thus, a genetically encoded reporter system which is able to perceive a cell’s response to DNA damage was used for further studies (further denoted as “SOS reporter”). The reporter gives a visual output for the transcription of the gene encoding the single-strand binding protein RecA. In response to DNA damage, RecA binds ssDNA, catalyzes the autoproteolytic cleavage of the repressor LexA and thus leads to its own activation [227] (further denoted as “SOS+ cells”).

C. glutamicum/pJC1- P_{recA} -*e2-crimson* was cultivated under the same environmental conditions as described in the previous section. Here, rare events showing the characteristics such as morphological changes or inhibition of cell division were observed. Typically, the identified cells showed a strong continuous SOS reporter signal. Figure 3.19A displays an isogenic *C. glutamicum*/pJC1- P_{recA} -*e2-crimson* colony, where one single cell stops dividing, whereas all sister cells showed continued growth (see lineage tree Figure 3.19B). At the same time, the cell’s SOS reporter signal is increased (Figure 3.19C), allowing the direct identification of these cells inside the microcolony. In this particular case, the cell did not resume to grow, and seemed irreversibly damaged. As expected, cells that grow and divide exhibit no irreversible SOS signal (Figure 3.19B). Figure 3.19D illustrates stressed cells of another colony, that in fact resume growth, showed a pulse of the SOS signal but resumed growth, indicating that the cell was able to overcome this stress by the SOS-induced repair mechanisms despite having an increased SOS reporter output. As seen in the corresponding image sequence, most of the cells undergoing SOS response belong to a cell cluster originating from two common ancestors.

High-throughput screening of rare cellular events

Recently, intensive FACS studies were used to quantify the amount of cells that expressed a spontaneous SOS response in *C. glutamicum* [227]. Figure 3.20A shows the quantification of the SOS response of shaking flask cultivation combined with FACS analysis, resulting in 0.05-1.25% of spontaneously induced cells as reported, depending on gating and the number of analyzed cells (Appendix Figure C.11 and C.12). Again, *C. glutamicum*/pJC1- P_{recA} -*e2-crimson* was cultivated in the MGCs under standard conditions. An endpoint determination of spontaneously induced cells of 300 MGCs was performed after the chambers were filled. Similar to the shake flask experiments, 0.07-0.5% of cells showed an increased stress response. Figure 6B shows that the average number of cells per microcolony with an increased reporter output, which lies at around three to four cells per cultivation chamber. This can significantly vary, depending on the investigated chamber and the method of quantification (Appendix C.13).

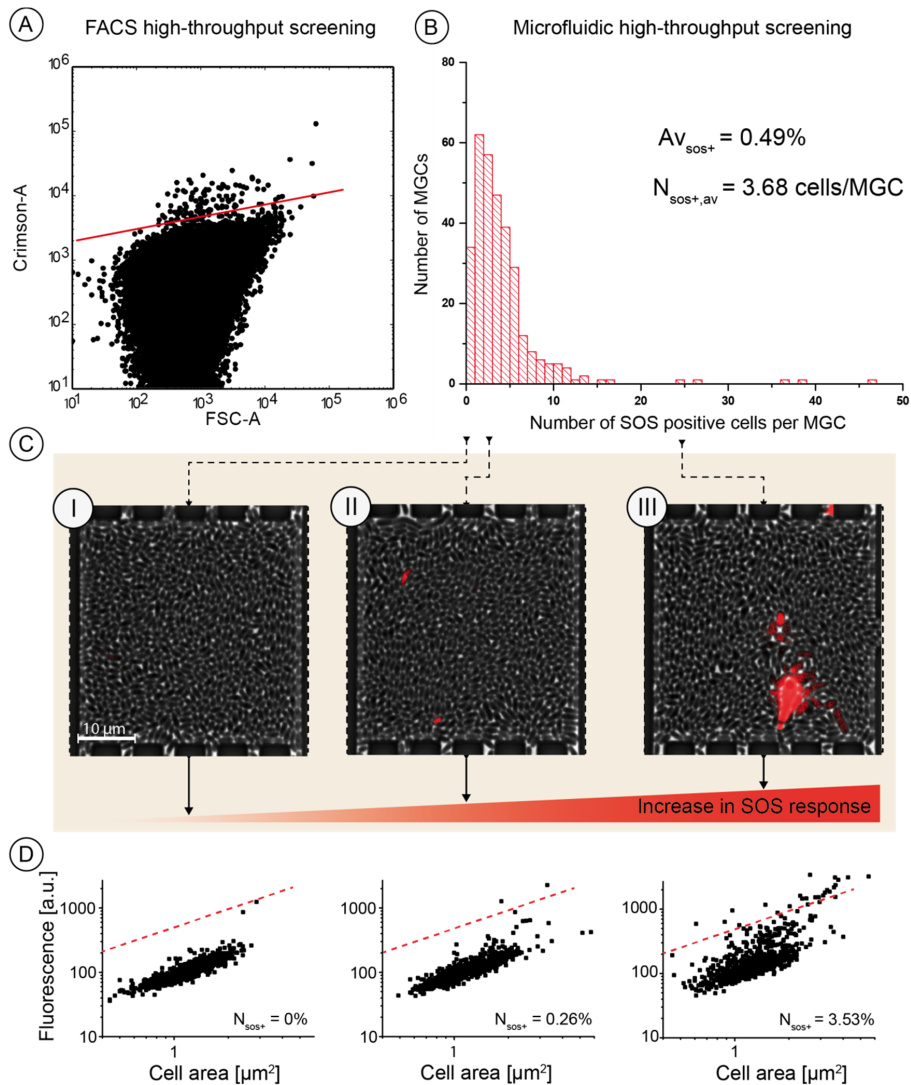


Figure 3.20: Quantification of SOS response during MSCC high-throughput screening. (A) FACS plot obtained by flow cytometric data of shaking flask cultivations. 0.07% of cells are showing spontaneous SOS response. (B) Number of cells that show SOS signal occurring in each of the 300 chambers. The distribution shows an average of approximately three to four spontaneously induced cells per chamber, corresponding to 0.07-0.5% percent of cells. (C) Image of three colonies at the end of the cultivation: (I) Colony containing no cell with increased SOS signal. (II) Colony shows two cells with an increased SOS signal. (III) Colony shows several cells with a positive SOS signal. (D) Area-fluorescence dot-plot obtained through MSCC of the three colonies shown in C.

In Figure 3.20D, three different subpopulations are shown. The cellular characteristics (cell area vs. overall fluorescence signal) of all individual cells in the colony were plotted. Population I harbors 850 cells with zero cells expressing a positive SOS reporter signal. Population II contains several outliers, exhibiting a higher SOS-reporter signal

with two SOS+ cells resulting in 0.26% of stressed cells. In Population III, 25 cells show an increased signal. In this exceptional case, over 3% of spontaneously induced cells can be found under standard cultivation conditions. Appendix C.14 presents the difference in SOS+ cells for different quantification methods.

3.3.5 Discussion

In the first part of this study (Chapter 3.3.1), a novel microfluidic system for parallelized growth studies at the single-cell level was presented. The high degree of parallelization enables the generation of statistically reliable information, a prerequisite for the investigation of rare cellular events at the single-cell level.

The flow profile and medium exchange of the MGCs for the cultivation of isogenic microcolonies were characterized in detail. Medium exchange can be performed within seconds, allowing for the investigation of population heterogeneity at constant environmental conditions. This was confirmed by CFD simulations showing a complete exchange of the chamber volume within seconds.

Proof of principle simulations were performed to characterize the environmental conditions in more detail regarding flow regime and mass transfer. The accumulation of secreted by-products is minimized during MGC cultivation and steady-state cultivation conditions can be assumed throughout the first generations of cellular division. It is expected, that accumulation of by-products and gradient formation is promoted in parts of the colony, when it reaches the dimensions of the MGC. No indication for impaired growth was observed within the presented study, however, more detailed studies are currently being performed to investigate this phenomenon. Furthermore, accurate simulations require reliable single-cell parameters, such as single-cell production and single-cell substrate uptake. This information is currently not available and is derived from average data of bulk analytics [231], which neglects single-cell behavior and thus leads to imprecise simulations. Furthermore, cellular growth kinetics might not solely be limited to the main carbon source as simulated in this work (see Unthan *et al.* [158]). More elaborate simulations are necessary to take these constraints into account and to allow for accurate prediction of stable cultivation conditions within MSCC.

During the cultivation of *C. glutamicum* wild-type cells under standard cultivation conditions, individual cells showed untypical behavior concerning division, growth and morphology. These events were observed in less than 1% of the cells, despite constant cultivation conditions. Especially when these rare cells occurred at the early stages of cultivations, the overall colony behavior was affected. This is impressively seen in the lineage tree shown in Appendix C.9, where the lag-phase of one single cell changes significantly the overall appearance of the lineage tree.

One reason for the observed rare cellular events in the form of dormant cells and cells with elongated morphologies could be the induction of the SOS response, triggered by severe DNA damage [227, 232]. This was investigated in more detail, cultivating

C. glutamicum/pJC1-*P_{recA}-e2-crimson* in the developed MGC system. Cells showing an increased SOS reporter output were quantified and contributed to 0.07-0.5% of the population.

The implementation of the MGC system for systematic single-cell studies requires the validation that the SOS response is not triggered by the microfluidic cultivation conditions. Several studies using microfluidics report of a significant impact of the cultivation principle onto physiology of the cells (cf. Supplement material of [118]). This hypothesis is currently under debate [70]. A comparison of the SOS response of cells cultivated in shaking flasks (SOS+ cells = 0.07-1.25%) showed no significant difference compared to MSCC experiments (SOS+ cells = 0.07-0.5%). These findings confirm that the MGC cultivation conditions used in the present study have no significant impact on cellular physiology. Nevertheless, inherent cultivation principles cannot be fully excluded as a trigger for the SOS response and need further investigations. Nanda *et al.* [227] reported an increase of SOS positive cells within the early exponential phase. It was assumed that the intrinsic DNA damage rises in this phase of accelerated growth, caused by the native DNA polymerase. In the presented MGC cultivations, cells continuously grew at their maximum growth rate, which is most comparable to early exponential conditions [98, 158] in batch cultivation. This might be an additional explanation for the occurrence of SOS positive cells.

Using conventional cultivation systems in combination with FACS allows for snapshot analysis of rare events. Furthermore, the history and lineage of cells undergoing SOS response cannot be investigated. The MGC has proven to be useful for investigating small sub colonies and interestingly revealed both, spontaneously induced single cells as well as spontaneously induced cell clusters (cf. Figure 3.20D). This offers completely new insights in the mechanisms of rare bacterial cellular events. Moreover, rare event screening using microfluidics allows for direct observation of cellular events over time. A detailed discrimination of different SOS+ cells can be performed. This includes the quantification of cells, showing a reversible SOS response.

Similar to FACS studies (Appendix C.8), the accuracy of the quantification depends on the investigation of absolute cell numbers. Within this study, rare events occurred at a frequency between 0.07 and 0.5%, but even rare events with much lower occurrence could be investigated in principle. Especially with a low image sampling frequency, the total number of cells imaged could be increased to probably 10^6 cells per experiment.

The capabilities of the MGC discussed in this work provide the foundation for developing an automated high-throughput analysis platform for bacteria microcolonies and statistical data analysis of bacterial lineage trees. Currently, the limiting steps for wide-range use in biotechnology and bioprocess engineering remains the automatic quantitative analysis of the microcolonies through image-based analysis tools such as provided by Sliusarenko *et al.*[233] and Youssef *et al.*[234]. Progress in these methods

will provide an easy to handle and robust system for high-throughput investigation of bacterial rare events.

3.3.6 Conclusion

The presented technology allows for the systematic investigation of rare cellular events with high statistical significance, an important prerequisite for systematic cell-to-cell heterogeneity studies, as biological variance can be high at the single-cell level. Future integration of these techniques for the cultivation and analysis at the single-cell level will expand the understanding of cell-to-cell heterogeneity in various biological processes, ranging from antibiotic screening [235] and adaption processes [236, 237] to new insights for applied fields such as food microbiology [238]. Especially for the investigation of cellular processes in the early exponential and lag-phase [239], suitable tools are still missing. The MGC offers a novel technique for the future investigation of these phenomena.

3.4 Systematic comparison of single-cell cultivation technologies

The first results indicated that the physiology of cells was not significantly affected in the PLBR or MGC. This chapter compares three different single-cell cultivation technologies and their individual impact on the physiology of *C. glutamicum*. This study was performed in close cooperation with Christian Dusny (Laboratory of Chemical Biotechnology; TU Dortmund). nDEP and agarose pad cultivations were performed by Christian Dusny. The “manuscript” was prepared by Christian Dusny and the author of this thesis. Detailed contributions are listed at the end of the chapter.

3.4.1 Abstract

Single-cell analysis has become an indispensable tool for modern (Systems) Biology. The analysis of living single cells provides fundamental insight into the dynamic architecture of a population and the origin of cellular heterogeneity. Although microfluidic technologies for single-cell cultivation are increasingly employed for dissecting physiological dynamics of individual microbes, little is known about the inherent impact of the cultivation technology itself on cellular function.

This study comprises a systematic comparison of three inherently different technologies for single-cell cultivation on the basis of physiological and morphological characteristics. We characterized microfluidic negative dielectrophoresis (nDEP), microfluidic monolayer growth chamber (MGC) systems with agarose-based cultivations in terms of specific volume growth rates, division rates and morphological characteristics of *Corynebacterium glutamicum* ATCC 13032 as a bacterial model organism. We developed a method for the description of the specific volume growth rate μ_{\max} based on the cell volume increase over time, which was universally applied to all systems. With this method we were able to follow microbial volume growth at the single-cell level with high temporal resolution.

Interestingly, single-cell volume growth rates were robust and conserved for several generations with all three technologies. However, division rates and cell length distribution of individual cells grown on agarose pads deviated by up to 50% respectively, while with nDEP and MGC, division rates and cell morphology were highly consistent. This indicated a significant effect of agarose cultivation on cellular traits.

This study quantifies the effect of the cultivation technology on basal physiological parameters for the first time and underlines the importance of a careful selection of the

cultivation technology in order to allow for an unbiased analysis of cellular behavior at the single-cell level.

3.4.2 Introduction

The accurate description and clarification of the origin of cell-to-cell heterogeneity is fundamental for understanding various biological phenomena such as stress response [26, 55] adaptation processes [240-242], and robustness [114] of bacterial populations. Such processes are traditionally investigated at a bulk level by measuring activity and responses of whole populations to certain external stimuli. Yet, cell-to-cell differences and phenotypic plasticity are masked by the population average, hiding the fate of the single cell [144]. To properly evaluate differences and dynamics beyond the bulk, several technologies for single-cell analysis have been developed during the past decades. Such technologies range from simple agarose pads to complex microfluidic single-cell cultivation concepts, allowing for analyses at high spatial and temporal resolution. A main driver for the development of the more complex microfluidic cultivation approaches is the control of the extracellular environment, allowing targeted perturbations of the cultivated cells [22, 29, 155]. This is achieved by matching the structural dimensions of the device to the physical scale of the microorganisms. In combination with microfluidic perfusion, a rapid removal of secreted metabolites is possible, leading to virtually gradient-free extracellular environments that can be precisely manipulated [66, 243]. However, as manifold as the conceivable applications for microfluidic single-cell cultivation are, as diverse are in turn the technological approaches that have been developed [20, 29]. These approaches range from optical [61, 110], acoustic [63], magnetic [64], nDEP [65, 180] and hydrodynamic trapping [67], with a multitude of different designs within each category. From the vast quantity of published microfluidic approaches, two technologies stand out: First, contactless methods like dielectrophoresis traps, which offer selectivity and active control during cell capturing, selection and the cultivation process [244]. Second, contact-based methods using hydrodynamic barrier structures and chambers for high-throughput single-cell cultivation [22]. Both technologies have shown to be valuable for investigating cell-to-cell heterogeneity and phenotypic plasticity in many studies [22, 73]. However, the comparison and interpretation of results obtained with such different cultivation technologies are difficult since knowledge about intrinsic influences of the respective cultivation method itself on cellular physiology is limited.

Our purpose here is to perform a systematic evaluation of cell trapping with negative dielectrophoresis (nDEP), monolayer growth chambers (MGC), and agarose pad based cultivation technologies. This evaluation includes (i) a detailed analysis of characteristic features of the cultivation technologies on the basis of technology-specific parameters and (ii) systematic growth and morphology analysis, using wild-type *C. glutamicum* in order to clarify the impact of the respective cultivation technology on cellular physiology.

To our knowledge, this is the first systematic comparison of quantitative single-cell growth studies with different single-cell cultivation technologies. *C. glutamicum* was chosen as model system because of its broad application in biotechnology [245] as well as its close relation to the pathogens *Mycobacterium tuberculosis* and *Corynebacterium diphtheriae* [246]. Furthermore, *C. glutamicum* features a “snapping” cell division that allows employing the microorganisms as a 3D sensor for the characterization of spatial degree of freedom within the respective cultivation device.

3.4.3 Materials and methods

Strains and media for nDEP and agarose pad cultivations

Corynebacterium glutamicum ATCC 13032 was stored in brain heart infusion (BHI) medium supplemented with glycerol to a concentration of 20% (v/v) at -80 °C. All precultures, main cultures and single-cell experiments of *C. glutamicum* ATCC 13032 were performed in BHI medium, containing 37.5 g L⁻¹ of BHI extract. The medium was adjusted to a pH of 7.0 with sodium hydroxide. The conductivity of the BHI cultivation medium was adjusted to 1 S m⁻¹ with sterile dH₂O (approximate dilution of 5%). Cells from cryocultures were incubated on BHI agar plates at 30 °C and stored for no longer than 48 h at 4 °C to prevent nutrient depletion. From the agar plates, an individual colony was taken and transferred to 100 mL baffled shake flasks filled with 20 mL sterile BHI medium. The shake flask cultures were incubated in an Edmund Bühler shaker KS-15 at 300 rpm and 30 °C (Edmund Bühler GmbH, Germany). Cells were grown to mid-exponential growth phase prior to cultivation in the nDEP system and on agarose pads. The culture was diluted with fresh BHI medium to a final OD₆₀₀ (Thermo Scientific, Germany) of 0.01 and introduced to the nDEP chip or seeded onto the agarose pads.

Strains and media for MGC cultivations

C. glutamicum ATCC 13032, obtained from the same cryoculture as used for nDEP experiments were cultivated in BHI medium, containing 37.5 g L⁻¹ of BHI extract. The medium was adjusted to a pH of 7.0 with sodium hydroxide. For preculture, 20 mL of sterile cultivation medium in a 100 mL baffled shake flask was inoculated with a cryogenic culture bead (Roti-Store®, Carl Roth GmbH) and incubated in and rotary shaker at 30 °C and 120 rpm overnight. The main culture was prepared by inoculation with 500 to 1000 µL of the preculture. The main culture was used for microfluidic seeding with an OD₆₀₀ between 0.1 and 1 in the early exponential growth phase.

Preparation of agarose pads

5 mL of freshly prepared BHI medium was supplemented with 75 mg low-melt agarose (1.5% (w/v)) and repeatedly heated until the agarose was dissolved. 800 µL of warm agarose solution was pipetted onto a clean standard microscope cover glass slide (18 mm², 175 µm thickness) and immediately covered by another glass slide to create an even and bubble-free agarose layer of 4-5 µm thickness between the two cover slides.

After cooling for 45 min at room temperature, the top cover slide was carefully removed. 2 μL of cell suspension with a cell density of $\text{OD}_{600} = 0.01$ was pipetted onto the agarose layer to introduce single cells. The cell suspension on the pad was allowed to settle and dry for 15 min at room temperature. The agarose pad was subsequently flipped and placed on a custom petri dish equipped with a glass bottom (thickness 175 μm). The petri dish was sealed and mounted on the microscope stage to follow bacterial growth. All experiments were performed at 30 $^{\circ}\text{C}$.

Single-cell trapping and cultivation with the nDEP

The microfluidic nDEP chip was employed for contactless cultivation of isolated single-cells and isogenic micropopulations in precisely controlled environments [65]. For device design, details on chip manufacturing, system setup, cleaning procedure, cell seeding and cultivation conditions, the reader is referred to previous studies [73].

Single-cell trapping and cultivation with the MGC

A single-use polydimethylsiloxane (PDMS) microfluidic chip was utilized to cultivate isogenic microcolonies. For further information about fabrication procedure, setup and operation the reader is referred to Grünberger *et al.* [98]. For details about the design and characterization of the used monolayer growth chambers (MGC) the reader is referred to Chapter 3.3.

System-independent determination of specific volume growth rates and division rates

Cells were generally observed with 100x oil immersion objectives and time-lapse images were used to derive specific volume growth rates and division rates. For the analysis of volume growth, a universally applicable model for the description of the cell volume at the single-cell level was developed. The central assumption behind the determination of the specific volume growth rates based on cell volume increase is a constant cell density of the cell ρ_{cell} , which is expressed by the ratio of cell mass M_{cell} [kg] to cell volume V_{cell} [m^3] [247].

$$\rho_{\text{cell}} = \frac{M_{\text{cell}}}{V_{\text{cell}}} = \text{const.} \quad (3.1)$$

With this, the specific volume growth rate μ can be described by

$$\frac{dV_{\text{cell}}}{dt} = \mu \times V_{\text{cell}} \quad (3.2)$$

where V_{cell} [μm^3] is the volume of a single cell or the sum of cell volumes of a population [μm^3], t is the cultivation time [h] and μ is the specific growth rate [h^{-1}]. The specific growth rate μ can also be described by

$$\mu = \frac{\ln 2}{t_{d,V}} \quad (3.3)$$

with $t_{d,V}$ [h] the time for the doubling of the cell volume. The specific growth rates of the trapped cells in the nDEP as well as MGC were calculated on the basis of the given equations. Cellular dimensions were obtained from image cytometry data obtained by time-lapse microscopy. Individual cells were measured with the AxioVision Rel. 4.8.2 interactive measurement software modules (Carl Zeiss Microimaging GmbH, Germany) or NIS-Elements AR (Nikon Instruments, Germany). The continuous rotation of the cells trapped with nDEP allowed to precisely measure the cellular dimensions. The actual cell volume was calculated based on a mathematical volume approximation of a segmented club-shaped solid for *C. glutamicum* ATCC 13032 according to

$$V_{cell} = \frac{2}{3}\pi r_1^3 + \frac{2}{3}\pi r_2^3 + \pi r_1^2 \times (l_1 - r_1) + \pi r_2^2 \times (l_2 - r_2) \quad (3.4)$$

with r_1 and r_2 [μm] denoting the radii of the spherical poles and l_1 and l_2 [μm] denoting the lengths of the halves of a cell (Figure 3.21).

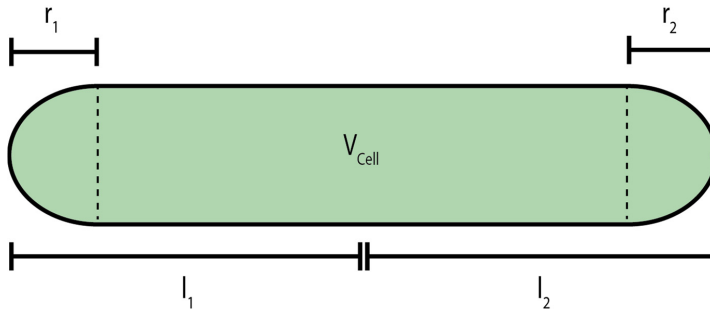


Figure 3.21: Mathematical approximation of cell volume from time-lapse microscopy images. Cells were segmented into four solid bodies (two central cylinders and two hemispheres for the pole caps) to approximate the cell volume and account for the club shape of single cells. Full mathematical description see Equation 3.4.

The division rate v [h^{-1}] was also derived from time-lapse microscopy by counting the number of cells N [-] at the respective time-points. The rate of division can be denoted as

$$\frac{dN_{cell}}{dt} = v \times N_{cell} \quad (3.5)$$

or by

$$v = \frac{\ln 2}{t_{d,N}} \quad (3.6)$$

with $t_{d,N}$ [h] as the time for doubling of the cell number.

3.4.4 Results

Systematic evaluation of conceptual differences in nDEP, MGC and agarose pads

On the basis of their inherent properties and special features, we investigated how the cultivation technology itself determines its applicability to answer specific biological questions.

In contrast to conventional population-based cultivation approaches, all technologies share the advantage of allowing to investigate cellular dynamics with single-cell resolution. Nevertheless, significant differences in terms of cell trapping, mass transfer as well as device dimensions and fabrication are discussed and illustrated in Figure 3.22.

1) Cell trapping principle and application

For the systematic comparison, we focused on the most significant difference, the mode of cell trapping. Here, nDEP enables a contactless retention of the cell within a dielectrophoretic force field. This force field is generated by an arrangement of eight equidistant electrodes (see Figure 3.22A a1). Periodical switching of the electrode drive pattern induces a dipole at the cell surface which creates a repelling force on the cell. As a result of this force, the cell is trapped and levitates at the point of lowest field intensity. This method allows for a selective isolation of any cell from a whole population. The technology was shown to be applicable for cultivating a broad range of different cell types, including mammalian cells, bacteria and several different yeast species [65, 66, 73, 180, 243].

The second technology under investigation, the MGC system employs mechanical cell trapping in growth chambers (Figure 3.22B b1). The chambers are restricted in height and match the average width of the investigated cell type. This spatial confinement forces the trapped cells to grow in a monolayer. The actual cell isolation process relies on the stochastic distribution of the introduced cells across the microchambers. Such microfluidic microchamber-based cultivation approaches have been already applied for answering numerous biological questions at a single-cell level [95, 97, 98, 110, 158, 169, 177, 178].

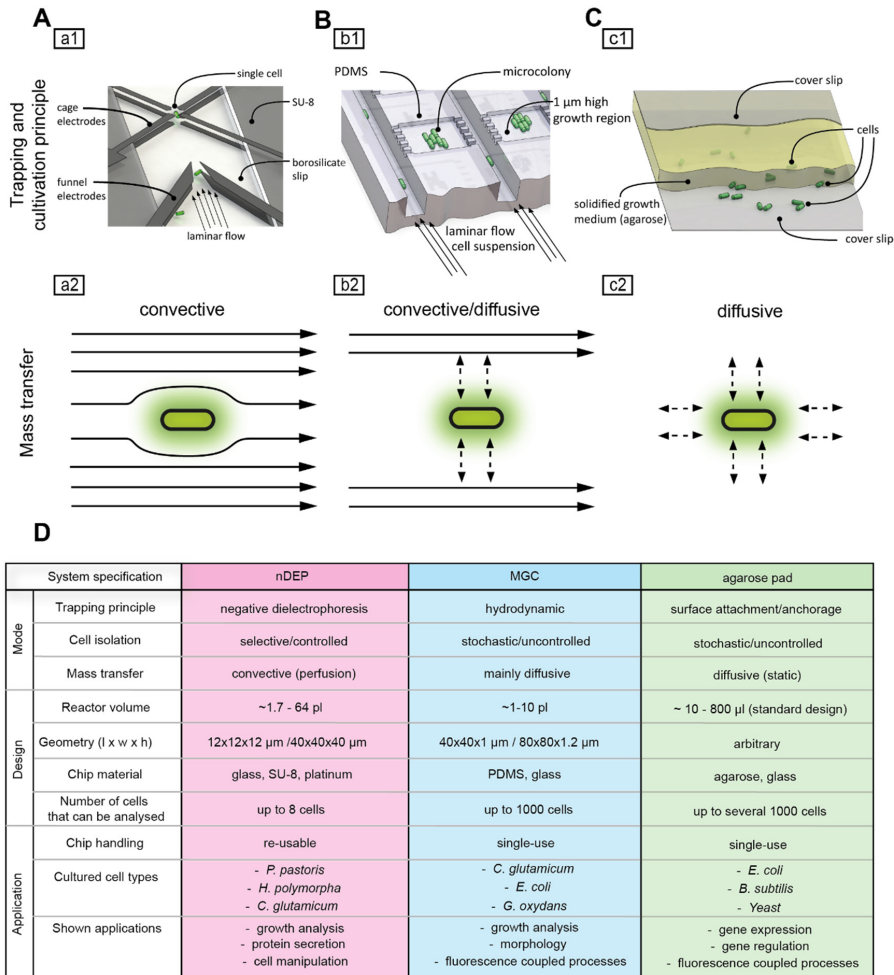


Figure 3.22: Design and functional principles of the compared single-cell cultivation systems from a macroscopic and microscopic point of view. (A) Operating principle of the nDEP for single-cell isolation and trapping, with cells guided into the electrode cage by funnel electrodes under continuous perfusion (a1). Convective mass transfer is dominant in nDEP system (a2). (B) Illustration of PDMS-based MGC chip with single-cell seeding and cultivation (b1). Mass transfer in MGC in the cell cultivation is mainly driven by diffusion (b2). (C) Casted sandwich agarose pad with a layer of solidified growth medium between two glass cover slides. Cells are located between agarose pad and bottom glass cover slide (c1). Mass transfer in agarose pads is exclusively facilitated by passive diffusion. (D) Key numbers and characteristics of nDEP, MGC and agarose pads.

The third technology constitute agarose pads, where single-cells are entrapped between a layer of semi-solid growth medium and a glass cover slide (Figure 3.22C c1). Cells are randomly spread on the agarose pad by applying an appropriately diluted cell suspension. As with MGC, cells are also forced to grow in one focal plane. Numerous studies employed agarose pads to study the dynamics of gene expression and cellular stress responses to external perturbations (*e.g.*, [26, 248, 249]).

Resulting from the respective cell trapping principle, the three systems offer inherently different degrees of control over the extracellular environment. This comparison yielded a distinct application profile for each of the three cultivation technologies.

nDEP is particularly suitable for the targeted isolation of certain phenotypes from a population and allows for retrieving cells afterwards. Furthermore, nDEP also works for all types of unicellular microorganisms. Another characteristic of nDEP is the free levitation and rotation, which excludes cell-surface interaction and allows the observation of the cells from multiple perspectives.

In terms of the number of cells that can be analyzed in parallel, the use of nDEP is typically restricted to the analysis of a single to few cells. The maximum number of cells that can be trapped inside a $20\ \mu\text{m} \times 20\ \mu\text{m} \times 20\ \mu\text{m}$ electrode cage depends on cell dimensions. For bacteria and smaller yeast species, up to 30 cells can be retained in the field cage. Quantification of growth is restricted to a maximum of eight cells.

For higher throughput single-cell cultivations and analysis, MGC is well suited. 200 cultivation chambers can be observed in one experiment; hence highly parallelized analysis can be performed. Micropopulations of up to 1000 cells can be grown in a single cultivation chamber with the dimension of $60\ \mu\text{m} \times 60\ \mu\text{m} \times 1\ \mu\text{m}$. A cultivation chamber with a maximum volume of 10 pL, can be seen in Figure 3.22B. Cells are forced to grow in a monolayer, which allows for automated image acquisition. However, the cell isolation process is stochastic and neither enables a targeted isolation of specific phenotypes nor a subsequent release of cultivated cells.

Agarose pads allow parallelized high-throughput analyses with cells growing in one focal plane and allow to simultaneously follow the development from single cells to microcolonies consisting of several hundred cells. Cell isolation relies on stochastic distribution of cells and confinement is largely independent of the cell dimension and type.

II) Mass transfer

Mass transfer with nDEP systems is dominated by convective flow and eddy diffusion as a result of direct cell perfusion. This provides a steady supply of nutrients and also guarantees fast removal of secreted metabolites from the extracellular microenvironment. Fluctuations in concentration in the direct surrounding of the cell are therefore minimized [66]. Further, a rapid and accurate chemical perturbation of the cells is given.

Similar to nDEP, mass transfer in MGC relies on a combination of convective and diffusive mass transfer. Each microchamber is connected to 10 x deeper supply channels which are continuously flushed with fresh medium, allowing for swift diffusion of nutrients into the cultivation area (Chapter 3.3).

In contrast to nDEP and MGC, agarose pads exhibit a static environment, where mass transfer is exclusively facilitated by diffusion. Here, nutrients can deplete locally when the consumption rate is higher than the rate of resupply by diffusion. Moreover, produced metabolites may accumulate in the direct vicinity of the cell. Combination of both, agarose and microfluidic based medium supply has been reported as well [115, 139]. The trapping principle and mode of medium supply are illustrated in Figure 3.22A.

III) Platform design, setup and periphery

There are substantial differences in design, fabrication and periphery of the respective cultivation technologies. For operating nDEP devices, a rather complex periphery is required, consisting of a radio frequency generator that drives the electrodes and a temperature control system using peltier elements for cooling. The nDEP system consists of the actual microfluidic glass chip mounted to a support plate, which also includes contact pads for connecting the generator to the chip electrodes). Rapid and reliable connection of the external fluidics to the microchannel structures is realized with a customized pressure-based fluidic block [66]. This fluidic block also acts as a cooling block for transferring heat from the peltier elements. The chip fabrication process is comparably complex and involves several lithography and etching steps for creating channel structures and electrode geometries. The fabrication process yields robust microfluidic chips that can be thoroughly cleaned after cultivation experiments, which allows for a repeated use of the chips [66].

In contrast, MGC fabrication process and periphery is rather simple. The microfluidic chip consists of a glass plate that adheres to a PDMS slap. Because of the cheap materials and the simply molding process, MGC systems are disposed after usage. The MGC structures are created by soft lithography, which enables creating multiple chips from one mold. Fluidic connections are established by punching holes. Temperature of the chip and surrounding periphery is controlled by an incubation system.

The simplest technology in terms of design, fabrication and needed periphery is the agarose pad, which is usually prepared within in a short time period of only a few hours. It is made of standard materials that are in stock in every standard bio(techno)logical laboratory. Temperature control can be performed with a microscope incubator or by simply moving the microscope system to a temperature-controlled incubation room. Features that all three cultivation technologies have in common, as well as respective unique characteristics are illustrated in Figure 3.23.

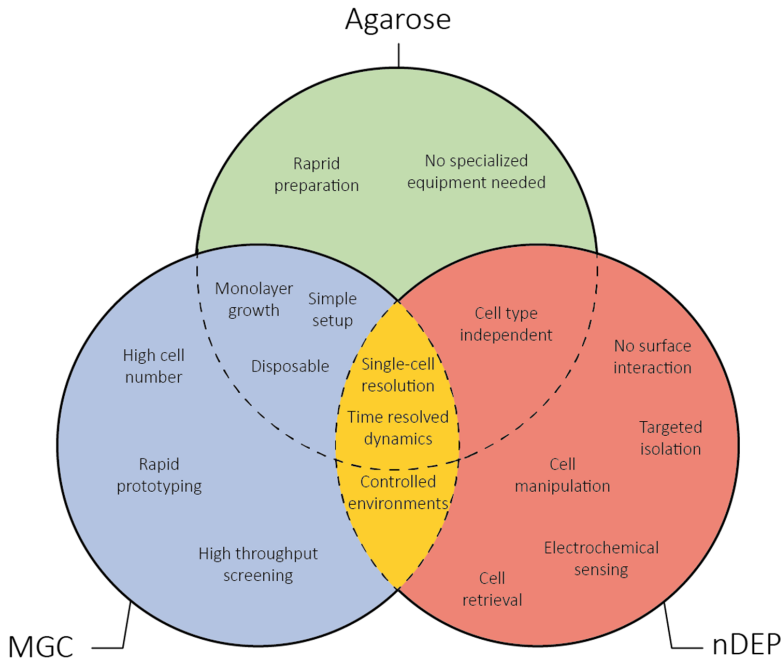


Figure 3.23: System evaluation of nDEP, MGC and agarose pads. The Venn diagram illustrates the common properties as intersections and unique properties of each method (nDEP = red, MGC = blue, agarose pad = green).

Specific volume growth rates and division rates of *C. glutamicum* ATCC 13032 cells at the single-cell level

We cultivated *C. glutamicum* starting from one cell at standard growth conditions (Figure 3.24 A-C). In general, growth immediately commenced without any detectable lag-phase upon introduction of the cells into the respective cultivation system. These growth characteristics could be observed independently of the applied cultivation technology. Measured maximal specific volume growth rates of micropopulations were consistent with a mean value of μ_{\max} of $0.6 \text{ h}^{-1} \pm 0.03$ for nDEP cultivations and $0.61 \text{ h}^{-1} \pm 0.06$ for cells cultivated with the MGC. Specific volume growth rates of micropopulations cultivated with agarose pads were $0.57 \text{ h}^{-1} \pm 0.05$. All investigated micropopulations followed a strictly exponential volume increase (Appendix D.1). The frequency plots of the measured specific growth rates revealed a normal distribution for all three systems (Figure 3.24D-F).

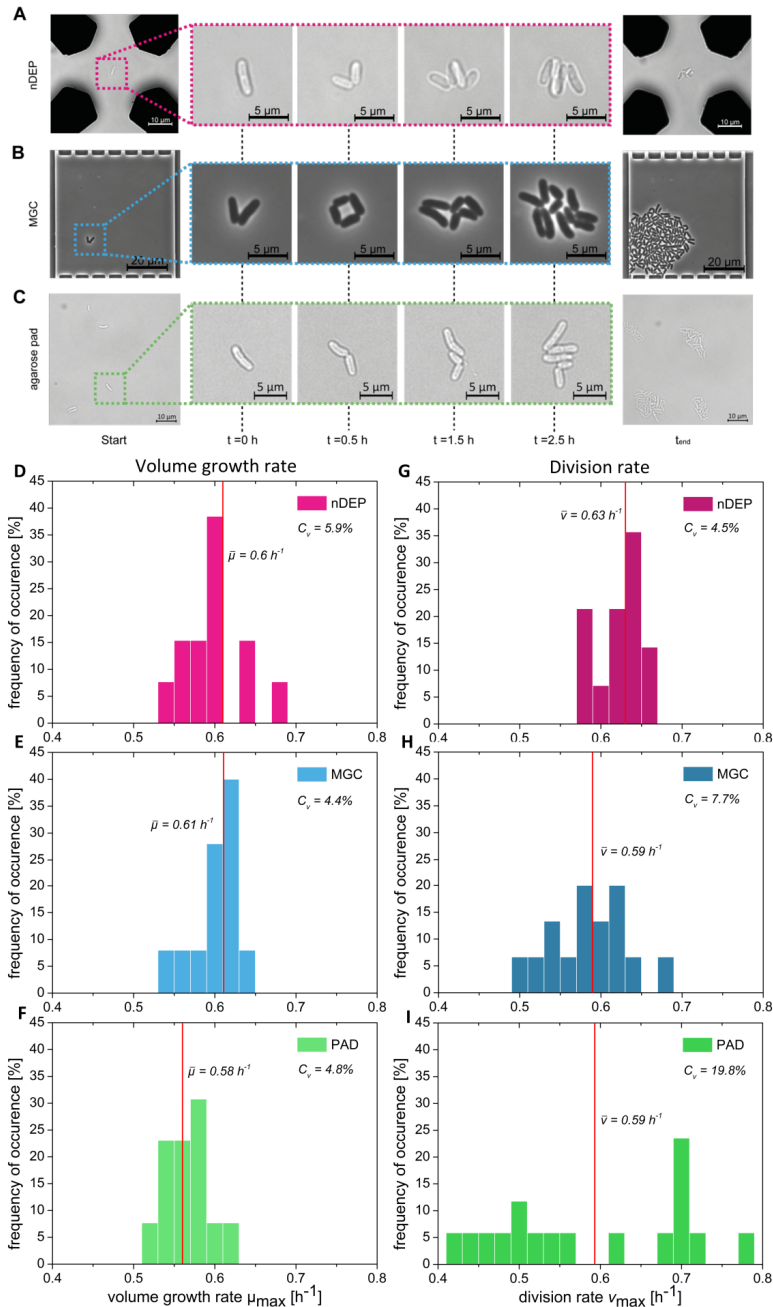


Figure 3.24: Cultivation of *C. glutamicum* with nDEP, MGC and agarose pad. (A-C) Trapped and growing cells in the center of the octupole cage by nDEP, in the MGC and on agarose pad. Image sequence of a typical experiment ($t = 0$ until $t = t_{\text{end}}$). (D-F) Frequency distribution of single-cell volume growth kinetics (μ_{\max}) derived by image analysis. (G-I) Frequency distribution of division rates (ν_{\max}) of single cells and micropopulations cultivated with nDEP, MGC and agarose pads. All experiments were conducted under the same growth conditions ($T = 30 \text{ }^\circ\text{C}$, BHI growth medium). For device specific parameters see Materials and Methods section.

In addition to volume growth, we also assessed specific cell division rates of individual cells and micropopulations (Figure 3.24 G, H, I). Surprisingly, cells displayed significantly scattered division rates with coefficient of variance ($C_{V, PAD} = 19.8\%$) on agarose pads. In comparison to the respective measured volume growth rates, the mean of all measured specific division rates corresponded to the mean specific volume growth rate ($v_{PAD} = 0.59 \text{ h}^{-1} \pm 0.11$). Mean specific cell division rates matched the mean specific volume growth rates ($v_{nDEP} = 0.63 \text{ h}^{-1} \pm 0.03$, $v_{MGC} = 0.59 \text{ h}^{-1} \pm 0.05$) for nDEP and MGC (Figure 3.25). However, in comparison to nDEP cultivations, a minor increase in variation of specific division rates was observed with the MGC ($C_{V, nDEP} = 4.5\%$, $C_{V, MGC} = 7.7\%$).

The observed irregularities in terms of division rate consistency indicate an inherent influence of the agarose pad technology on cellular physiology of *C. glutamicum*.

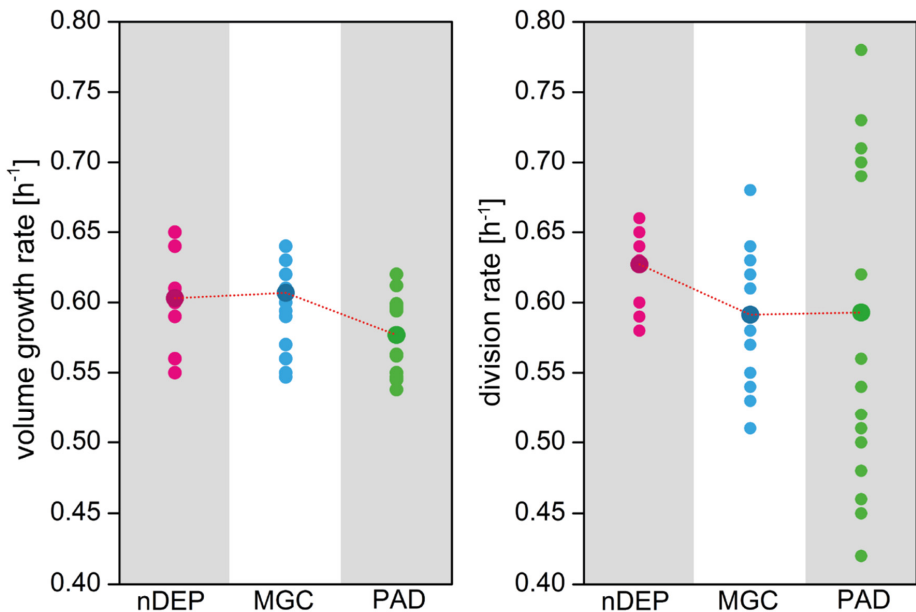


Figure 3.25: Scatter plot of measured specific volume growth rates (left) and specific division rates (right) for nDEP, MGC and agarose pads.

Analysis of morphology and snapping division during single-cell cultivations of *C. glutamicum*

The observed irregular division rates of *C. glutamicum* might be caused by deviating cell morphology during cultivation.

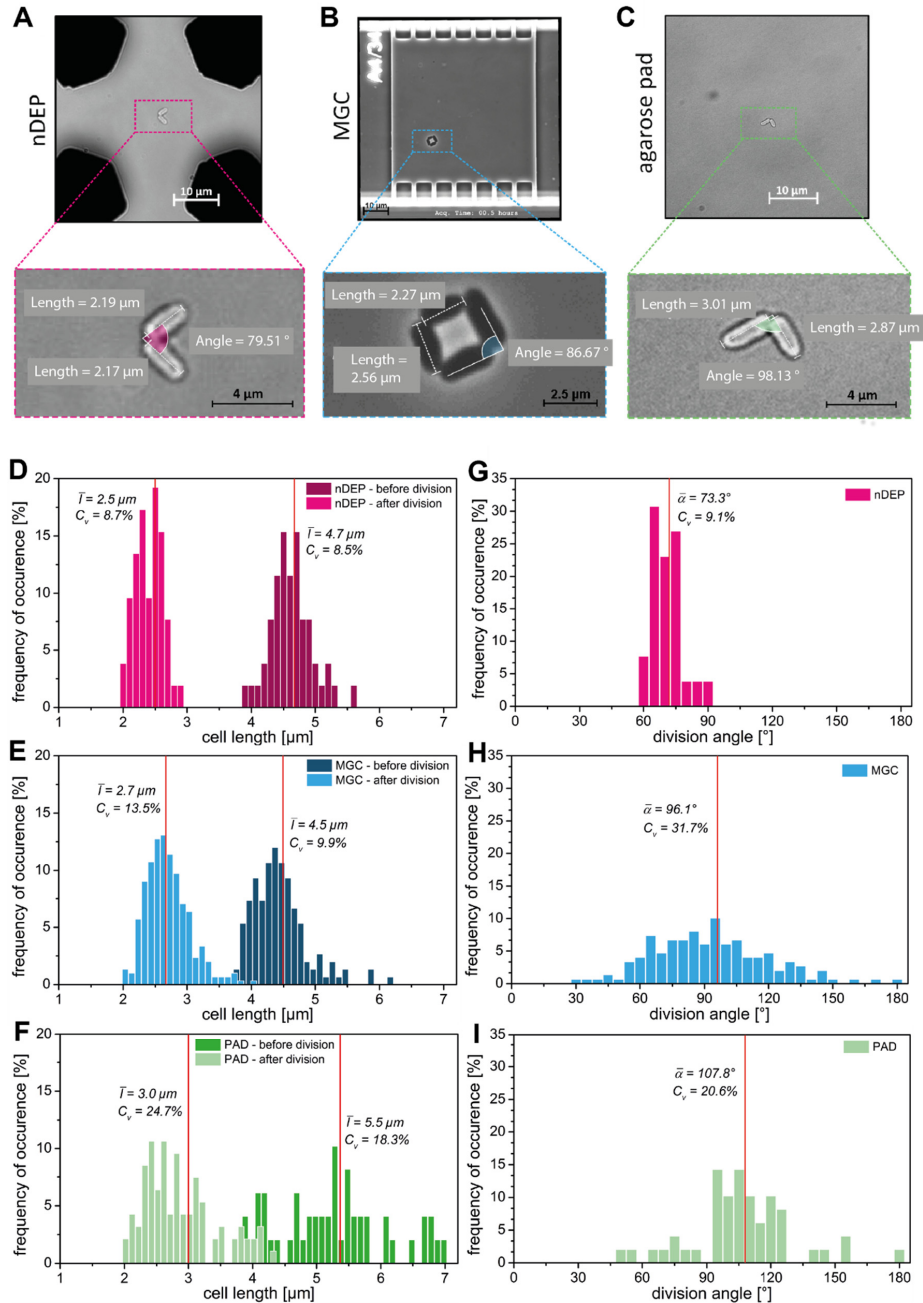


Figure 3.26: (A-C) Determination of cell lengths and division angles based on cytometric data. (D-F) Frequency distribution of cells length before and after cell division with the nDEP, MGC and agarose pad. (G-I) Comparison of the division angle distribution of *C. glutamicum* ATCC 13032 cell poles cultivated in with nDEP, MGC and agarose pad. The respective division angles were measured immediately after snapping division events. The dotted lines represent the Gaussian distribution of the determined cell lengths and division angles.

Therefore, cell morphology was investigated in detail during cultivation. The distributions of cell lengths just before and after division for nDEP, MGC and agarose pad-based cultivations are illustrated in Figure 3.26 D-F. For nDEP and MGC cultivations average cell lengths are in good agreement with $4.68 \mu\text{m} \pm 0.4$ ($C_v= 8.4\%$) and $4.42 \mu\text{m} \pm 0.44$ ($C_v= 12.8\%$) before and $2.45 \mu\text{m} \pm 0.21$ ($C_v= 8.7\%$) and $2.67 \pm 0.36 \mu\text{m}$ ($C_v= 13.4\%$) after the division event, respectively. Only 2% of the cells cultivated with MGC had lengths above $6 \mu\text{m}$ before cell division. With nDEP, all cells divided before reaching $6 \mu\text{m}$ in length. Cell length distributions follow a normal distribution with the nDEP and MGC technologies ($P>0.05$).

For cells grown on agarose pads, a higher tendency towards elongation in comparison to nDEP and MGC cultivations was observed. This inclination towards elongation was pronounced with 23% of the cells reaching lengths of more than $6 \mu\text{m}$ right before cell division. Average cell length before division was $5.44 \mu\text{m} \pm 1.16$ ($C_v= 21.6\%$) and $3.04 \mu\text{m} \pm 0.75$ ($C_v= 24.7\%$) after division, with both distributions exhibiting significant variance. Cell lengths distributions were heavy-sided towards increased cell lengths, rather than following a normal distribution. Cells grown on agarose pads also exhibited a stronger tendency towards asymmetric division, pointing to a disturbance in the placement of the division septum (Figure 3.27).

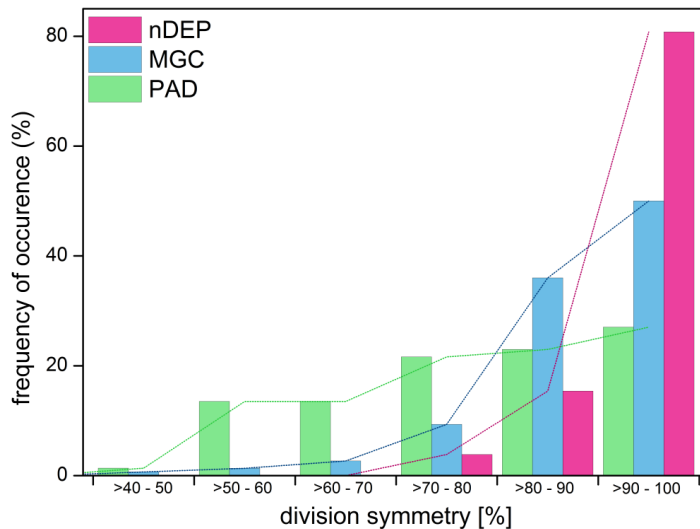


Figure 3.27: Division symmetry of *C. glutamicum* is influenced by cultivation technology. Cells tend to divide in a more asymmetric fashion on agarose pads. Division symmetry was measured as the ratio of short to long cell pole directly after the cell division event.

We concluded from these results that the physiology of cells cultivated on agarose pads is subjected to stress caused by the mode of trapping or environmental conditions.

In addition to cell lengths, we also assessed division angles of single cells directly after the division event. Cells of *C. glutamicum* exhibit a distinct V-shaped shape after

the cell division as a result from the snapping postfission movement (snapping division) [250, 251]. The snapping division involves a sudden swing, during which the outer membrane of the two emerging cell poles is still interconnected at their proximal ends. This feature is particularly well suited for evaluating the effect of spatial restriction or an applied external force on the cells during the cultivation in the respective cultivation system. For a quantitative description, the angular arrangement of the cells immediately after the division event was used.

With an average angle of $73.2^\circ \pm 6.6$ ($C_v=9.1\%$) the division angle of cells cultured in nDEP is 22% smaller than of cells cultured with the MGC system with an average angle of $96.1^\circ \pm 30.5$ ($C_v=31.7\%$) (Figure 3.26 G-I). A tendency towards higher division angles was observed for cells cultivated with agarose pads, with cells exhibiting an average division angle of $107.8^\circ \pm 22.2$ ($C_v=20.6\%$). The frequency distribution of division angles was very sharp and normally distributed with the nDEP system. A broader distribution of division angles was observed with the MGC system and agarose pads. Division angles were broadly distributed in a more random fashion compared to the nDEP system, which may result from an inhomogeneous adhesion of the cells to adjacent surfaces and local variations in the extent of the spatial constriction.

3.4.5 Discussion

Technical discussion

Here, we present a comparative study that provides new insight into the inherent influences of single-cell trapping and cultivation methods on microbial physiology.

We performed a systematic evaluation of the three different single-cell cultivation methods in terms of functionality and applicability. The evaluation revealed a distinct application profile for each cultivation principle. nDEP systems generally enable a highly selective isolation of specific phenotypes from whole populations and avoids cell-surface contact, which may trigger changes in the cellular phenotype. In addition, continuous cell perfusion allows an unprecedented control over the extracellular environment and enables rapid chemical perturbation of the cells.

In contrast to this, the MGC principle stands out for its possibility to perform experiments with high throughput while still allowing for environmental control and chemical perturbation. Moreover, the system allows tracking microcolonies of up to thousand cells per chamber. MGC systems are usually easy to fabricate and allow for rapid prototyping within weeks. Agarose pads also allow for high-throughput analysis of a large number of cells and resulting colonies in parallel, while precise control of the cellular environment and chemical short-term perturbation are not possible.

Biological discussion

However, besides these technological characteristics, inherent influences of the cultivation technology itself on cellular physiology of *C. glutamicum* could be clearly demonstrated. The analysis of growth revealed highly consistent specific volume growth rates of single-cells and micropopulations for all three investigated systems despite distinct differences in trapping principle and the type of environment (nDEP: levitation – liquid medium – continuous perfusion; MGC: surface contact – liquid medium – mainly diffusion; agarose pad: surface adhesion/embedding – semi-solid medium – diffusion). Throughout all performed growth experiments, the measured specific growth rates exceeded those of populations cultivated with bulk systems like shake flasks [73]. This indicated that during cultivations of at least 2 h, growth conditions were provided that allowed the cells to exploit their maximal biological capacity in terms of growth rate. We deduce from these results that stress resulting from adaptation to changing environmental conditions, which inevitably occurs in bulk cultivations and was previously shown to impair growth, is minimized in all three systems [18, 252]. Only such state of equilibrium between the cell and its extracellular environment enables an unbiased analysis of the true response of cellular physiology to exogenic stimuli.

In addition to elevated and robust specific volume growth rates, none of the cultivated single cells showed a detectable lag-phase after introduction into the cultivation devices. This observation was especially surprising for agarose pad cultivations, since recent population-based studies reported that a change from liquid medium to semi-solid medium involves stress resulting in temporary growth arrest in bacteria [253]. However, despite differences of agarose pads and agar plates in terms of cell exposure to ambient air, our data on single-cell growth suggest to study this phenomenon in detail. Our results clearly demonstrate the superiority of the employed single-cell cultivation systems in comparison to bulk approaches when it comes to an accurate description of fundamental biological parameters. Our work also introduces a reliable and universal method for the quantitative description of specific growth rates at a single-cell level, which is of high practical relevance for biological single-cell analyses.

A further important implication of our work is that the dielectrophoretic force during nDEP trapping does not affect cellular physiology of *C. glutamicum* with the chosen trapping parameters. The origin for previously reported adverse effects of nDEP trapping on cellular viability [254] is thus to be sought elsewhere, for example in insufficient compensation of temperature effects induced by resistive joule heating.

However, in contrast to the consistent volume growth rates, division rates of cells grown on agarose pads significantly deviated from nDEP and MGC cultivations. Analysis of cellular morphology during this study disclosed significant irregularities during cultivation of *C. glutamicum* on agarose pads. Differences in division rate could be clearly assigned to elongation on agarose pads. Cells continually inclined towards an elongated cell shape, while cells grown with nDEP and MGC did not show such behavior. The process of cell elongation in *C. glutamicum* was shown to be induced by multiple stresses,

for example, DNA damage or nutrient starvation during stationary phase. It has been speculated that an alteration of the usually tightly regulated cell morphology represents a protective strategy of many microorganisms against antibiotic activity, solvent stress or starvation [255]. Remarkably, specific volume growth rates of single cells were steady and not influenced by cell elongation, whereas division rates were significantly reduced. A further remarkable observation was the tendency of *C. glutamicum* towards asymmetric division on agarose pads, since several studies revealed that *C. glutamicum* exhibits a symmetric type of cell division [40]. Asymmetry in cell division points to a disturbance in chromosome segregation, which is responsible for the tightly controlled midcell division positioning [256].

Even though reasons for the elongation and deviating division symmetry of *C. glutamicum* on agarose pads cannot be unambiguously disclosed on the basis of our data, it can be yet narrowed down to two central aspects. Both, the static environment which is influenced by the metabolic activity of the cell as well as tight embedding of cells in between the agarose layer and glass cover slip clearly distinguish agarose pads from the other two systems.

We therefore utilized the snapping movement of *C. glutamicum* upon cell division as a three dimensional sensor in order to evaluate the extent of spatial restriction of the cells for each of the cultivation systems. Significant spatial restriction, resulting in increased snapping angles after cell division, suggests a strong spatial restriction of cells embedded in the agarose pads. Since influences of the extracellular environment would be manifested in decreased specific growth rates, we speculate that the spatial restriction of the cells on agarose pads is the origin of stress that triggers elongation. In comparison to nDEP trapping, an increased division angle distribution could be also observed for cells cultivated with the MGC system. This indicates an elevated degree of spatial restriction in the MGC system in comparison to agarose pads, which is however sufficiently low to prevent elongation.

To our knowledge, this work represents the first systematic characterization and evaluation of single-cell cultivation technologies. We have demonstrated that the cultivation technology itself influences fundamental cellular characteristics, *e.g.*, division rate and morphology. Our results imply the need of thoroughly characterizing the cultivation technology to be used in terms of inherent influences on cellular physiology. Furthermore, we developed a universal and straightforward method that allows deriving specific volume growth rates of single cells from any time-lapse microscopy data. In terms of versatility and practicability, this method is comparable to measurements of optical density at the bulk level. We therefore anticipate that growth analysis may be included as a tool for quantitative single-cell analysis by default to enable comparison with growth rates obtained at the population level.

Author contribution:

Designed the experiments: Christian Dusny (C.D.) and Alexander Grünberger (A.G.)

Performed the experiments: A.G. performed MGC experiments
C.D. performed nDEP and agarose pad experiments

Analyzed the data: A.G. analyzed MGC experiments
C.D. analyzed nDEP and agarose pad experiments

Wrote the manuscript: A.G.:

- Introduction
- Material and methods of MGC experiments
- Parts of the systematic evaluation
- Results of MGC
- Technical comparison in the Discussion

C.D.:

- Abstract
- Material and methods of nDEP/agarose pad
- Determination of volumetric/division growth rates
- Parts of the systematic evaluation
- Results of nDEP and agarose pad
- Biological part of the Discussion

Figures: A.G. created Figure 3.21, 3.22, 3.23 and 3.24 (A+B)
C.D. created Figure 3.24(C-I), 3.25, 3.26 and 3.27

Both authors finally edited and proofed the text.

4 Single-cell analysis in bioprocess development

4.1 Growth rate investigation I: Cultivation at different scales

During the first single-cell cultivations unexpected high growth rates for *C. glutamicum* were obtained. In this chapter, a systematic comparison of different cultivation scales was performed, revealing higher growth rates for *C. glutamicum* at highly diluted environments. The chapter is based on a publication published 2013 in *Biotechnology and Bioengineering*. The work was performed in close cooperation with Jan van Ooyen and Nicole Paczia (Bioprocesses and Bioanalytics group, IBG-1: Biotechnology).

4.1.1 Abstract

Fast growth of industrial microorganisms, such as *Corynebacterium glutamicum*, is a direct amplifier for the productivity of any growth coupled or decoupled production process. Recently, it has been shown that *C. glutamicum* when grown in a novel picoliter bioreactor (PLBR) exhibits a 50% higher growth rate compared to a 1 liter batch cultivation [169]. We here compare growth of *C. glutamicum* with glucose as substrate at different scales covering batch cultivations in the liter range down to single-cell cultivations in the picoliter range. The maximum growth rate of standard batch cultures as estimated from different biomass quantification methods is $\hat{\mu} = 0.42 \pm 0.03 \text{ h}^{-1}$ even for microtiter scale cultivations. In contrast, growth in a microfluidic perfusion system enabling analysis of single cells reproducibly reveals a higher growth rate of $\hat{\mu} = 0.62 \pm 0.02 \text{ h}^{-1}$. When in the same perfusion system cell-free supernatant from exponentially grown shake flask cultures is used the growth rate of single cells is reduced to $\hat{\mu} = 0.47 \pm 0.02 \text{ h}^{-1}$. Likewise, when fresh medium is additionally supplied with 5 mM acetate, a growth rate of $\hat{\mu} = 0.51 \pm 0.01 \text{ h}^{-1}$ is determined. These results prove that higher growth rates of *C. glutamicum* than known from typical batch cultivations are possible, and that growth is definitely impaired by very low concentrations of by-products such as acetate.

4.1.2 Introduction

Importance of maximum growth rate

The maximum growth rate (μ_{\max}) is the key characteristic for describing the phenotype of a microbial cell population. The knowledge of μ_{\max} for a certain microorganism and cultivation condition builds the basis for, e.g., optimizing media compositions for growth and production [257, 258], characterizing the effect of genetic manipulations by metabolic engineering tasks [259], and describing cellular metabolism by kinetic models [260].

Moreover, μ_{\max} is one of the most important parameters for industrial production processes utilizing microorganisms. On the one hand this directly relates to all processes, which are known to work well in a growth-coupled manner, *e.g.*, the production of amino and organic acids [261] as well as recombinant proteins [262]. On the other hand it is also of great interest for all processes where the growth and production phase is decoupled and hence fast generation of high cell densities have a high impact on the overall economic feasibility of a certain production process. In fact, this holds true for all processes based on biotransformations using whole cells or cell extracts, which are in competition with cell-free synthetic approaches in the near future [263].

However, until now, it is impossible to precisely predict μ_{\max} for a given media composition in a typical batch process. This is simply due to the fact that growth under batch conditions is usually greatly affected by a combination of substrate excess, higher cell densities, heterogeneities caused by insufficient mixing and accumulation of possible toxic side-products [264].

Clearly, if the growth rate of an organism can be raised in a production process, this has an immediate impact on its overall productivity. It will be shown below that maximum growth rates published for common production organisms might not be the upper limit.

Single-cell investigation versus classical culture

Nowadays, in order to gain more insight into the mechanism of microbial growth microfluidic tools are being developed that also allow investigations on the single-cell level [66, 84, 207]. In a recent study we reported on the development of a novel picoliter bioreactor (PLBR) for cultivation of single bacterial cells [169]. Surprisingly, the application of the PLBR for cultivation of the *C. glutamicum* wild type, a model organism of white biotechnology, showed a 1.5-fold higher exponential growth rate compared to a 1 liter batch cultivation. Higher growth rates in microfluidic systems compared to typical lab-scale batch approaches were also reported for *E. coli* [114] and supports the hypotheses of faster cell growth under constant environmental conditions.

In general, it can be argued that the overall culture conditions in a microfluidic system are more optimal for fast growth compared to the conventional approaches, *e.g.*, bioreactor or shake flask. It is already known for a long time that several inhomogeneity factors including gradients in chemical and physical properties (*e.g.*, media and gas supply) have a major impact on cell population growth. Clearly, this is most pronounced in cultivations applying high cell densities where growth of distinct cells is likely to be impaired by short-term limitations of, *e.g.*, substrate or oxygen supply leading to a decrease in the overall growth rate of the cell population. For more details the reader is referred to [13, 15, 186, 265].

Interestingly, detailed studies of the impact of cultivation modes as well as biomass measurements on the maximum growth rate estimation have not been systematically performed so far.

Estimation of maximum growth rate

In the following we provide some definitions related to the estimation of μ_{\max} to allow a precise formulation of the major questions that we will address within this paper.

The time dependent specific growth rate $\mu(t)$ of a bacterial cell population X in a closed system (batch culture) is calculated as:

$$\mu(t) = \frac{\dot{X}}{X} \quad (4.1)$$

From Eq. (4.1) the “true” maximum growth rate in the time interval $0 \leq t \leq T$ of cultivation is derived as:

$$\mu_{\max} \stackrel{\text{def}}{=} \max_{0 \leq t \leq T} \mu(t) \quad (4.2)$$

Clearly, μ_{\max} is not accessible as the underlying biomass quantification methods are not accurate enough to allow for a statistical trustworthy calculation of the time-derivatives in Eq. (4.1).

Nevertheless, an estimation of μ_{\max} can be realized by assuming a constant exponential growth behavior over some time interval $T_1 \leq t \leq T_2$. Integration of Eq. (4.1) then leads to an average growth rate $\bar{\mu}$ that is, *per definition*, a lower boundary for μ_{\max} . Since from Eq. (4.1) it follows

$$\ln(X_2) = \ln(X_1) + \int_{T_1}^{T_2} \mu(t) dt$$

the exact solution of Eq. (4.1) at time T_2 is given by

$$X_2(T_2) = X_1(T_1) \cdot e^{\bar{\mu} \cdot (T_2 - T_1)} \quad (4.3)$$

with the average growth rate

$$\bar{\mu} = \frac{1}{T_2 - T_1} \int_{T_1}^{T_2} \mu(t) dt \leq \mu_{\max}$$

As an alternative, the exponential growth rate μ can be directly estimated when the growth rate is constant over the time interval $T_1 \leq t \leq T_2$ as is, *e.g.*, the case in the exponential growth phase of a batch culture. In that case Eq. (4.3) reads:

$$X_2(t) = X_1(T_1) \cdot e^{\mu \cdot (t - T_1)} \quad (4.4)$$

with

$$\mu = \mu(t) = \text{const.}$$

Thus fitting this exponential function to the biomass measurements $X(t_i)$ by applying, *e.g.*, the well-known method of least squares

$$\hat{\mu} = \arg \min_{\mu} \kappa(\mu) \leq \mu_{\max}$$

with

$$\kappa(\mu) = \sum_{i=1}^n \|X(t_i) - \hat{X}(t_i)\|_{\sum X(t_i)}^2 \quad (4.5)$$

a reliable estimate $\hat{\mu}$ of the exponential growth rate is obtained if the constant growth assumption is correct. Fortunately, this assumption can be checked by inspecting the goodness of fit. This method has the main advantage that multiple biomass measurements including its randomly distributed errors $\sum_{X(t_i)}$ are utilized to give a more robust estimation of μ_{\max} .

Assuming that the average size and volume of single cells grown in a population does not change during the time of investigation, the increase in cell density is proportional to the increase in cell concentration. In that case an under-estimation of μ_{\max} in terms of one or the other variable leads to the same results. However, as already shown in several studies with different microorganism, the average size and volume of cells can vary considerably in dependence of the cultivation conditions [266-268]. In turn, this has a direct influence on the estimation of μ_{\max} based on cell density, which is then different from the maximum rate estimate from cell concentration measurements.

Aims of this study

In this study we comprehensively compare the growth of *C. glutamicum* wild type on CGXII glucose medium applying well-defined cultivation experiments at different cultivation scales. Moreover, several biomass quantification methods related to cell concentration and bacterial cell density are applied to safely answer the following two questions:

- 1) Has the cultivation scale and underlying technical devices a direct influence on the estimation of the maximum growth rate?
- 2) Is the constant growth rate in the exponential phase of a batch culture equal to the maximum possible growth rate under the pre-defined conditions?

Furthermore, we show how miniaturized batch systems such as microtiter plates in combination with microfluidic systems can be used to test the influence of selected medium components onto growth and production formation of industrially relevant microorganism.

4.1.3 Material and methods

Medium and pre-cultivations

The mineral medium used for *C. glutamicum* was CGXII consisting of (per liter): 20 g $(\text{NH}_4)_2\text{SO}_4$, 5 g urea, 0.5 g K_2HPO_4 , 1 g KH_2PO_4 , 0.25 g $\text{MgSO}_4 \cdot 7\text{H}_2\text{O}$, 42 g 3-morpholinopropanesulfonic acid, 10 mg CaCl_2 , 10 mg $\text{FeSO}_4 \cdot 7\text{H}_2\text{O}$, 10 mg $\text{MnSO}_4 \cdot \text{H}_2\text{O}$, 1 mg $\text{ZnSO}_4 \cdot 7\text{H}_2\text{O}$, 0.2 mg CuSO_4 , 0.02 mg $\text{NiCl}_2 \cdot 6\text{H}_2\text{O}$, 0.2 mg biotin, 0.03 mg of protocatechuic acid adjusted to pH 7, and 4% glucose as carbon and energy source. To prevent growth artifacts, the same medium batch was used for all cultivations. First, the mineral medium was prepared and sterile filtered without 3-morpholinopropanesulfonic acid and aliquots for bioreactor experiments were taken. For shake flask, Biolector and microfluidic chip experiments sterile 3-morpholinopropanesulfonic acid was added.

Prior to all main cultures, cells were pre-cultured as 50 mL cultures in 500 mL baffled Erlenmeyer flasks on a rotary shaker at 120 rpm with orbital shaking at a diameter of 25 cm at 30 °C. A first pre-culture in LB complex medium was inoculated to a second pre-culture in CGXII mineral medium, which was then inoculated to an OD_{600} of 1 to the main cultures of shake flask, bioreactor, microtiter plates and microfluidic chip experiments.

Shake flask cultivations

C. glutamicum was grown as 50 mL cultures in 500 mL baffled Erlenmeyer flasks on CGXII medium and growth was monitored by measuring the optical density at 600 nm (OD_{600}).

Bioreactor cultivations

The 1.4 l bioreactors (Multifors Multi-Fermenter System with 4 independently controllable bioreactors, Infors, Einsbach, Germany) contained 600 mL CGXII medium with 4% (w v^{-1}) glucose, but without the buffer substance 3-morpholinopropanesulfonic acid. The bioreactors were sparged with 0.9 l min^{-1} air. Oxygen saturation was measured online with a polarimetric oxygen electrode (Mettler Toledo, Giessen, Germany) and was held permanently over 30% by gradually increasing stirrer speed from 600 rpm up to 1000 rpm. The pH was determined online using a standard pH electrode (Mettler Toledo) and adjusted to pH 7 with 3 M Sodium hydroxide and 3 M hydrochloric acid. Foam formation was suppressed automatically by titration of 25% (v v^{-1}) Antifoam 204/water suspension (Sigma-Aldrich, Steinheim, Germany).

Microtiter plate (MTP) cultivations

MTP cultivations were carried out in 48 well Flowerplates (m2p-labs, Aachen, Germany) incubated in a BioLector (m2p-labs, Aachen, Germany), each well filled with 1 mL with the same inoculated CG XII medium as in shake flasks. Wells with not inoculated media were analyzed as negative controls in the same MTP. MTPs were

incubated at 30 °C with a relative humidity above 80% avoiding evaporation. In addition, MTPs were shaken at 1200 rpm with a shaking diameter of 3 mm. To minimize evaporation but allow feasible gas transfer MTPs were sealed with gas permeable films (m2p-labs, Aachen/Germany). Biomass was analyzed with backscatter measurement at 600 nm and gain 20. The two cultivation parameters pO₂ and pH were measured with immobilized indicator substances, so called optodes, inside each flowerplate well.

Microfluidic chip cultivations

To investigate single-cell growth behavior of *C. glutamicum* at different culturing parameters, the previously reported PLBR was used [169]. The microfluidic device is intended for the analysis of bacteria on single-cell level. Starting from one single “mother” cell, microcolonies of up to 500 cells can be investigated. The device is continuously infused with fresh media, resulting in constant environmental conditions over the whole experimental time. The device can incorporate up to several hundred PLBRs connected to various inlet and outlet channels for supplying growth medium and waste removal. The 1 μm culturing region restricts cell growth to a monolayer, ideal for image based live-cell and time-lapse microscopy. For fabrication and detailed device principle, the reader is referred to [169].

The chip was placed inside an in-house manufactured incubator for temperature and atmosphere control and connected to 1 mL sterile glass syringes (ILS Innovative Labor Systeme GmbH, Germany) for continuous media supply. Media flow was controlled with high precision syringe pumps (neMESYS, Cetoni, Germany). The incubator was mounted onto a fully motorized inverted microscope (Nikon Eclipse Ti) suitable for time-lapse live-cell imaging. In detail, the setup was equipped with a focus assistant (Nikon PFS) compensating for thermal drift during long term microscopy, Apo TIRF 100x Oil DIC N objective, NIKON DS-Vi1 color camera and ANDOR LUCA R DL604 camera. Additionally, the objective was heated with an objective heater (ALA OBJ-Heater, Ala Scientific Instruments, USA).

The microfluidic device was purged with fresh CGXII-medium for 30 minutes prior to each cell seeding phase. A cell suspension with an optical density between 1 and 3, transferred from a pre-culture at exponential growth phase, was infused to the system. Flow was stopped when satisfying amounts of PLBRs were seeded with a single cell. After successful cell seeding with bacterial suspension, instead the growth medium was infused at approx. 10 nL min⁻¹ per PLBR to initiate the cultivation.

DIC microscopy images of individual PLBRs were captured in 10 min time intervals and resulting time-lapse images were recorded as well as analyzed employing the Nikon NIS Elements AR software package. To derive growth rates, the number of bacteria was counted and the area of evolving microcolony was measured for each PLBR and corresponding time-lapse images, respectively.

Offline analytics

Optical density (OD₆₀₀) was measured at 600 nm (Shimadzu, PharmaSpec UV 1700) against 0.9% (w v⁻¹) NaCl. Glucose was measured using an enzymatic analysis system (EBIO compact, Eppendorf AG Hamburg). Cell count and cell size were monitored offline via a Coulter counter equipped with a 45 µm capillary (CASY® 1 Modell TT, Roche Diagnostics).

For fluorescence activated cell sorting (FACS) analytics cells were carefully diluted to an optical density below 0.1 and immediately analyzed by a FACS ARIA II high-speed cell sorter (BD Biosciences) using excitation lines at 488 and 633 nm and detecting fluorescence at 660 ± 10 nm at a sample pressure of 70 psi. Data were analyzed using BD DIVA 6.1.3 software. The sheath fluid was sterile filtered PBS. Non-bacterial particles were excluded by electronic gating on the basis of forward versus side scatter area. To obtain precise cell numbers an exact number of fluorescent beads (BD TruCOUNT Tubes, BD Biosciences) was added to the samples for internal calibration. In one experiment targeted and untargeted analysis of the culture supernatant was performed by HPLC [269] and GC-ToF-MS [270] measurements, respectively.

4.1.4 Results and discussion

Maximum growth rates at different cultivation scales

Growth of *C. glutamicum* wild type on CGXII glucose was followed by applying a series of experiments at different cultivation scales. A special device is the single-cell cultivation system PLBR. In this system single cells are trapped in a microfluidic channel (Figure 4.1), allowing for constant perfusion with fresh medium and microscopic inspection of growth. An example of a time-lapse video is included as supplemental video S1 in [98], which served to derive the triplicate growth rate data of these first experiments. Starting from one identical CGXII glucose pre-culture cultivations of *C. glutamicum* were done as outlined in Figure 4.2, ranging from 600 mL bioreactor scale over 50 mL shake flask scale and 1 mL microtiter plate scale down to 1 pL PLBR scale. Most importantly, each cultivation experiment was performed in at least three biological replicates.

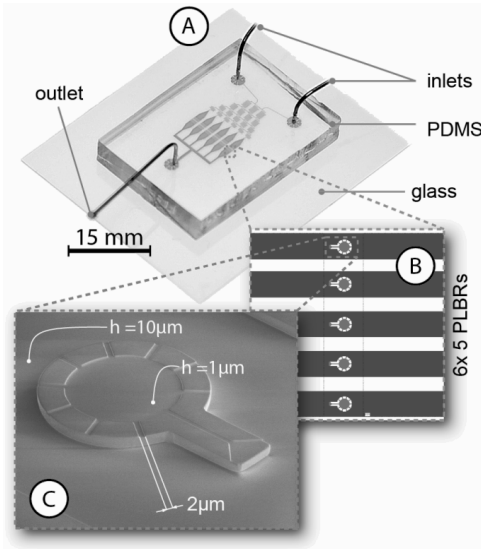


Figure 4.1: Picoliter bioreactor system (PLBR) used for perfusion growth studies. (A) Fabricated microfluidic chip device. (B) Magnification of one growth array containing 5 PLBRs in parallel. (C) Scanning electron microscopy image of a single PLBR with 1 pL cultivation volume. The height of the PLBR is approx. 1 μm and the supply channel height is approx. 10 μm . Seeding and overflow channels have a width of 2 μm . Figure is taken from [169]. Reproduced with permission of the Royal Society of Chemistry.

In order to test and reproduce possible effects on the estimation of μ_{max} when based on different measurements of either cell concentration or cell density we applied different quantification methods including cell number, optical density, backscatter, cell volume and colony area. Values for μ_{max} were then estimated for each culture and quantification method by fitting an exponential function to the measurement data in the time window of exponential growth (cf. Eq. (4.4) and (4.5)).

The maximum growth rate during the exponential phase of bioreactor cultivations is estimated in an overall range of $0.37 \text{ h}^{-1} \leq \hat{\mu} \leq 0.41 \text{ h}^{-1}$ if all rate estimates from the different measurements are covered by one standard confidence interval (Figure 4.2A and Appendix Figure E.1). The determined exponential growth rate from the shake flask experiments lies within a range of $0.40 \text{ h}^{-1} \leq \hat{\mu} \leq 0.47 \text{ h}^{-1}$, showing some tendency to higher growth rates (Figure 4.2B and Appendix Figure E.2). The volume reduction in microtiter plates as compared to the bioreactor is by a factor of 10^3 . However, no significant influence on exponential growth is observed in the microtiter plates and the growth rate determined is identical to the shake flask experiment (Figure 4.2C and Appendix Figure E.3). Most interestingly, growth in the microfluidic chip is much faster as compared to all other experiments showing a rate between $0.60 \text{ h}^{-1} \leq \hat{\mu} \leq 0.65 \text{ h}^{-1}$ (Figure 4.2D and Appendix Figure E.4). In that case the working volume is reduced by a factor of 10^{12} .

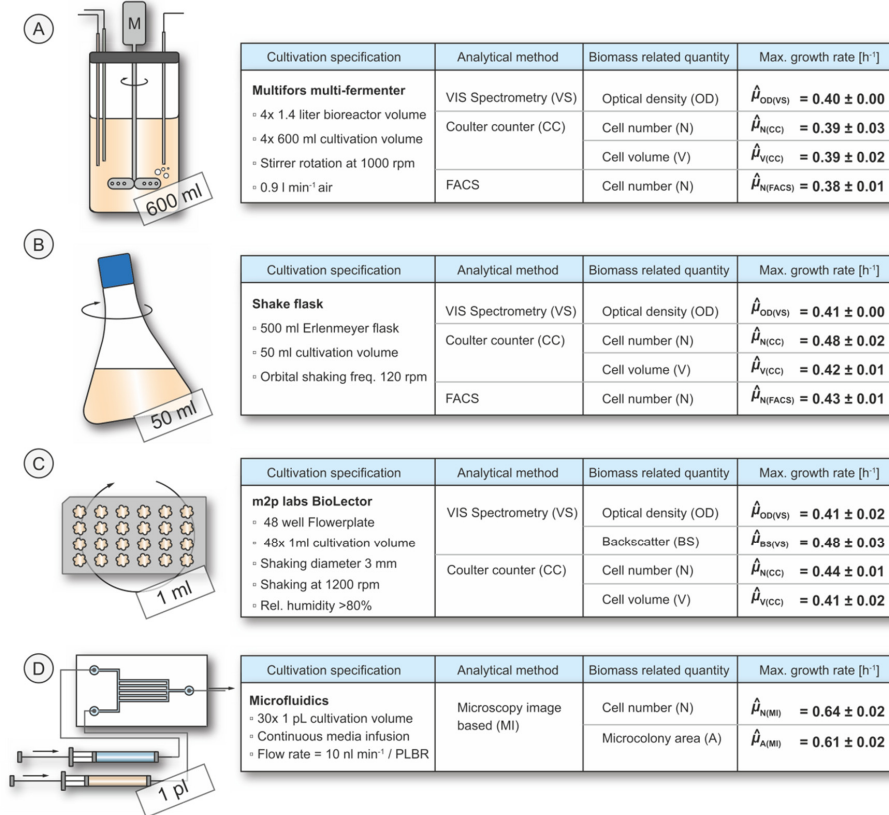


Figure 4.2: Growth of *C. glutamicum* wild type at different cultivation scales on CGXII glucose medium. (A-D) In each case maximum growth rates were estimated during the exponential phase and based on different methods for biomass determination. Mean values and standard deviations are calculated from at least triplicate cultures.

Reproducibility of maximum growth rate estimation

To the best of our knowledge this is also the first report which uses biological replicate cultivations and several biomass measurements techniques to prove the reproducibility of maximum growth rate estimations for a model organism in industrial biotechnology. Depending on the measurement method and cultivation condition the relative standard deviation from at least triplicates varies between $1\% \leq \sigma_{\text{rel}} \leq 10\%$ (cf. Figure 4.1). Moreover, our results clearly demonstrate that under the conditions tested, there are no significant differences between the maximum growth rate estimates based on cell concentration and bacterial cell density measurements, respectively. Although there is no superior biomass quantification method regarding reproducibility it has to be pointed out that the microscopy image based method in combination with the microfluidic chip is currently the only direct quantification method for cell concentration and bacterial cell density.

General impact of the micro-environment

The surprising result of a 50% increase in the maximum growth rate of *C. glutamicum* when cultivated under the PLBR conditions consequently asks for a rational explanation behind this observation. Clearly, cells cultivated in the PLBR are not growing under batch conditions. Due to the specific design of the PLBR, cells are growing in a monolayer with continuous supply of fresh media [169]. Hence all growth essential nutrients are provided in excess for each cell of the microcolony. This also holds true for the essential gas components oxygen and carbon dioxide, which are instantaneously supplied by direct diffusion through the gas permeable PDMS layer and taken up by the cells monolayer via a large cell surface area. Regarding the cells micro-environment, the conditions are comparable to a continuously operated bioreactor at high dilution rates (e.g., chemostat or turbidostat).

In a recent study the effect of increased dissolved carbon dioxide concentrations (p_{CO_2}) on the maximum growth rate of *C. glutamicum* in a 1.5 l bioreactor under turbidostat conditions with glucose or lactate as single carbon sources was investigated [212]. In that case the growth rate was derived indirectly by calculating the mean dilution rate from the glucose consumption rate, which was necessary to hold a constant biomass concentration of 2 g l^{-1} inside the bioreactor. Most interestingly, a comparable high maximum growth rate of $\mu_{\text{max}} = 0.58 \text{ h}^{-1}$ on glucose was reported under standard p_{CO_2} -levels (corresponding to atmospheric pressure) as shown here for the PLBR cultivations. However, no growth accelerating effect of higher p_{CO_2} -levels was detectable during growth on defined glucose media.

In fact there is a common striking feature between the turbidostat and our PLBR, which relies on a continuous removal of secreted by-products via the dilution with fresh media solution. Moreover, in all other experimental setups tested here, the classical batch-mode was applied, which is known to provoke pyruvate overflow metabolism under conditions of carbon excess resulting in typical by-products like acetate or pyruvate in

prokaryotes like *C. glutamicum* [23]. Hence it can be readily concluded that the formation of by-products and/or its re-uptake somehow directly impairs growth through toxicity effects or on the other hand is much more energy demanding than currently believed.

In order to test for a negative effect of growth due to by-product formation we conducted experiments in the microtiterplate scale as well as in the microfluidic scale.

Influence of by-product dilution on growth

In one experiment we investigated the potential impact of “by-product dilution” on the maximum growth rate in microtiter plates, starting from the same pre-culture as mentioned above and performing a log-dilution series, each in three-fold biological replicates. The resulting growth curves show a direct dependency on the initial cell concentration (Figure 4.3A). By comparing the cultivation times needed to reach a certain threshold backscatter signal, a shift towards lower initial cell densities is found where growth accelerates faster within the first hours of cultivation.

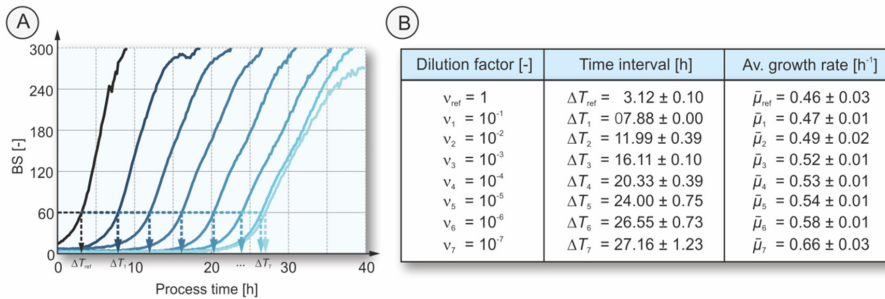


Figure 4.3: Influence of by-product dilution on growth of *C. glutamicum* wild type in microtiter plates on CGXII glucose medium. (A) Log-dilution series were generated from three reference cultures and grown in parallel. For each cultivation mean backscatter signals are shown. (B) Corresponding time intervals after reaching the threshold backscatter signal of BS = 60 were determined and used for the estimation of average growth rates according to Eq. (4.3). Standard deviations are calculated from the triplicate cultures.

Since the backscatter measurements in the diluted cultures are below the upper limit of quantification at the beginning of the cultivation the data cannot be directly used for a maximum growth rate estimation following the standard procedure as stated above. For that reason we applied Eq. (4.3) to estimate average growth rates $\bar{\mu}_i$ for each diluted culture i . Here the variable $X_{2,i} = BS_{60}$ is set to a threshold backscatter signal of BS = 60. The initial biomass values $X_{1,i} = BS_{ref,0} \cdot v_i$ are estimated from the backscatter signal of the undiluted reference cultures $BS_{ref,0} = BS_{ref}(t = 0)$ of each replicate series and the dilution factor v_i .

Following this approach, the calculated average growth rates show a clear increase along the dilution series (Figure 4.3B). Most interestingly, starting with only few cells an average growth rate of $\bar{\mu}_7 = 0.66 \pm 0.03 \text{ h}^{-1}$ is reached, which resembles the maximum growth rate of the PLBR cultivation experiment (cf. Figure 4.1D). Obviously, the final

dilution ($v_7 = 10^{-7}$) is in the range of only a few single cells and possible effects of, e.g., less active or dead cells are much more pronounced. Eventually, this leads to a higher variation in the obtained growth curves (cf. Appendix Figure E.5) and therefore the estimated growth rate shows a higher standard deviation. Nevertheless, it has to be kept in mind that the calculated average growth rates always represent underestimations of the true maximum growth rate (cf. Eq. (4.3)) and hence the true μ_{\max} -value is likely to be higher in the first phase of the cultivation.

In contrast, no systematic effect on the maximum growth rate is observed in the later exponential phase, *i.e.*, providing in each case a sufficiently high biomass concentration and hence signal to noise ratio for rate estimation according to Eq. (4.4) and (5). This observation can be again explained by the fact, that at low cell density the possible growth impairing by-products are greatly diluted in the cell's surrounding, while at higher cell density, proportional to biomass, the secreted by-product concentration is much higher.

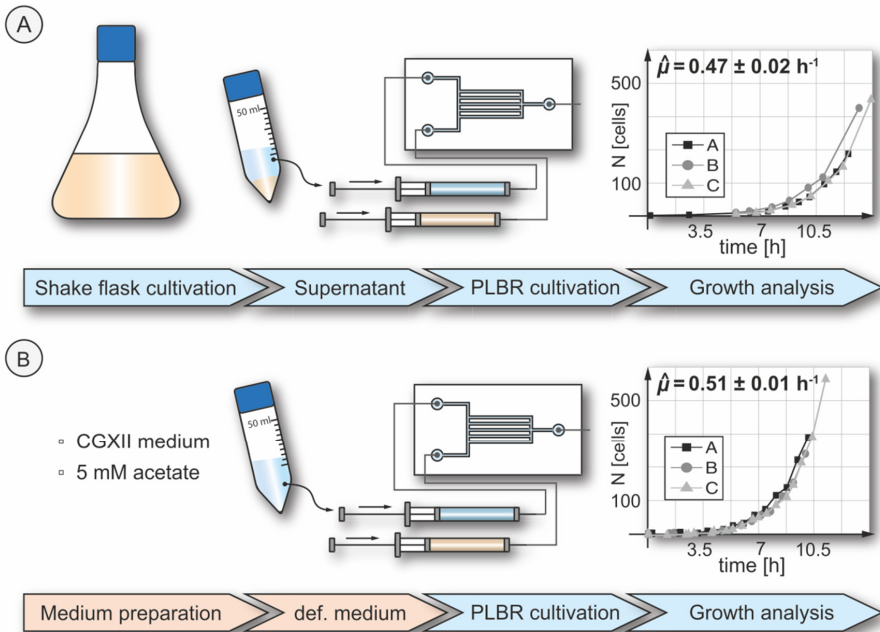


Figure 4.4: Influence of secreted by-products on growth of *C. glutamicum* wild type cultivated under PLBR conditions. (A) Cells are grown on undefined cell-free supernatant from exponentially grown shake flask cultures. (B) Cells are grown on CGXII glucose medium supplemented with 5 mM acetate. Cell counts from microscopic images are used for exponential growth rate estimation. Mean values and standard deviations are calculated from triplicate cultures.

Influence of secreted by-products on growth

In two further experiments we directly addressed the question whether secreted by-products negatively influence the growth of *C. glutamicum* under PLBR conditions. For that purpose *C. glutamicum* cells were fed with either undefined cell-free supernatant from exponentially grown shake flask cultures ($OD_{600} = 5$) or CGXII glucose medium supplemented with 5 mM acetate, a well-known by-product of glucose grown *C. glutamicum* cells [271] (Figure 4.4 and Appendix Figure E.6 and E.7). In both cases growth is significantly slower compared to the reference cultivation (cf. Figure 2D). Moreover in the cell-free supernatant medium the estimated growth rate lies within the range of the standard batch-approaches (cf. Figure 4.2A-C), whereas in the acetate media the rate is still significantly higher.

The acetate concentration in the cell free supernatant was detectable (> 0.05 mM) by HPLC analytics, but below the upper limit of quantification (< 0.5 mM). Additionally, untargeted GC-ToF-MS analyses was performed to identify possible other by-products in the cell-free supernatant, but no further differences were found in comparison to non-inoculated medium (data not shown). Interestingly, when *C. glutamicum* cells are grown in defined media with glucose and acetate as carbon sources the glucose consumption rate decreases to 50% compared to cells grown with glucose as sole carbon source [272]. The effect on growth can thus partly be explained with accumulation of by-products or even autoinducers [273] in the culture supernatant.

Macroscopic view of batch growth

To sketch up a qualitative picture on how by-product formation possibly effects the specific growth rate in a batch culture we formulated a simple unstructured model allowing for by-product formation, inhibition as well as its coutilization. For more details on the model structure see the Appendix E.1.

The model is applied to simulate the time dependent changes in all process variables and the resulting dynamics are shown in Figure 4.5. The cells initially grow very fast on the primary substrate with a significantly higher maximum growth rate. However, with an increasing by-product concentration also growth on the primary substrate is inhibited and the resulting specific growth rate greatly decreases until a steady-state is reached where by-product formation and coutilization are balanced. Consequently, the following exponential growth phase is determined by a specific growth rate that does not equal the maximum growth rate from the beginning, but a constant rate resulting from coutilization of substrate and by-product as well as constant by-product inhibition. Noteworthy, the model simulations also reflect the current understanding of glucose induced acetate metabolism in *C. glutamicum* from the macroscopic point of view.

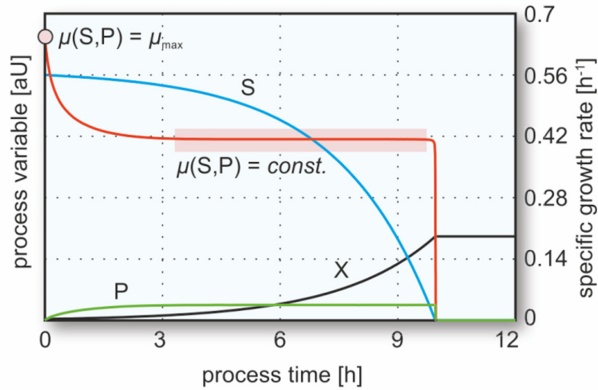


Figure 4.5: Dynamics of a batch process as a function of cell (X), substrate (S) and by-product concentrations (P). Cell population growth is determined by a balance of by-product formation and coutilization of the primary substrate and the by-product. The following model parameter values are used for simulation: $X_0 = 0.1 \text{ g l}^{-1}$, $S_0 = 20 \text{ g l}^{-1}$, $P_0 = 0 \text{ g l}^{-1}$, $\pi_P = 0.75 \text{ g l}^{-1} \text{ h}^{-1}$, $\mu_{\max,S} = 0.65 \text{ h}^{-1}$, $\mu_{\max,P} = 0.28 \text{ h}^{-1}$, $K_S = K_P = 0.01 \text{ g l}^{-1}$, $Y_{X/S} = 0.41 \text{ g g}^{-1}$, $Y_{X/P} = 0.29 \text{ g g}^{-1}$, $k_I = 0.015 \text{ g l}^{-1}$.

4.1.5 Conclusions and outlook

From our results we can conclude that the exponential growth rate of *C. glutamicum* wild type on CGXII glucose medium is not directly depending on the cultivation scale and underlying technical devices (*e.g.*, stirred-tank bioreactor, shake flask, microtiter plate). In fact, it is a function of the pre-defined (start medium and mode of operation) and resulting (medium with by-products) cultivation conditions. On the one hand, in all tested conventional approaches, the chosen mode of operation was batch where at a certain threshold cell density the concentration of specific by-products (*e.g.*, acetate) is high enough to exert a growth impairing effect. On the other hand, under conditions of low by-product concentrations, *i.e.*, as a result of cell washing in the PLBR (comparable to a continuously operated bioreactor) or very low cell densities at the initial batch phase (*e.g.*, BioLector), growth is not impaired and hence most likely maximal for the specific medium composition under investigation.

The results show, that the PLBR as well as the BioLector approach can be used to unravel “true” maximum growth rates. Hence both setups can be used in future screening studies for determining growth influencing factors focusing mainly on medium components. The main advantage of the PLBR compared to classical lab-scale approaches relies in the instantaneous observation of the cell’s response to specific environmental stimuli. Hence experiments can be carried out to directly relate a strain’s genotype and its growth phenotype (including morphology) in dependence of underlying nutritional conditions. These studies can then be combined with experiments in microtiter plates to test and optimize candidate factors in a high-throughput manner.

4.2 Growth rate investigation II: What triggers faster growth?

Using different techniques, ranging from different analytical tools to various cultivation scales, PCA was identified as main factor for higher growth rates in minimal medium. This chapter demonstrates, how the single-cell cultivation devices can successfully be used and integrated for future bioprocess development studies. The outcome of this work was published 2013 in *Biotechnology and Bioengineering*. The work was performed in close cooperation with Simon Unthan (Bioprocesses and Bioanalytics group, IBG-1: Biotechnology).

4.2.1 Abstract

In a former study we showed that *C. glutamicum* grows much faster in defined CGXII glucose medium when growth was initiated in highly diluted environments [98]. Here we studied the batch growth of *C. glutamicum* in CGXII at a comparable low starting biomass concentration of $OD \approx 0.005$ in more detail. During bioreactor cultivations a bi-phasic growth behavior with changing growth rates was observed. Initially the culture grew with $\hat{\mu} = 0.61 \pm 0.02 \text{ h}^{-1}$ before the growth rate dropped to $\hat{\mu} = 0.46 \pm 0.02 \text{ h}^{-1}$.

We were able to confirm the elevated growth rate for *C. glutamicum* in CGXII and showed for the first time a growth rate beyond 0.6 in lab-scale bioreactor cultivations on defined medium. Advanced growth studies combining well-designed bioreactor and microfluidic single-cell cultivations (MSCC) with quantitative transcriptomics, metabolomics and integrative *in silico* analysis revealed protocatechuic acid as a hidden co-substrate for accelerated growth within CGXII.

The presented approach proves the general applicability of MSCC to investigate and validate the effect of single medium components on microorganism growth during cultivation in liquid media, and therefore might be of interest for any kind of basic growth study.

4.2.2 Introduction

Corynebacterium glutamicum is a Gram-positive bacterium, originally isolated from soil [245], and nowadays frequently applied as production host for chemicals, materials and fuels [6]. This organism can utilize a variety of different carbon sources and shows monophasic growth for many substrate mixtures, except for combinations of glucose and glutamate or glucose and ethanol [274, 275].

C. glutamicum serves as a platform for Metabolic Engineering and as a model organism for Systems Biology due to its importance for industrial biotechnology and its close relation to the host-pathogen *Mycobacterium tuberculosis* [225, 226, 276]. For both areas a well-defined medium composition for biomass growth and production is essential, in order to allow for valuable data generation and, hence, reliable comparison of strain properties and performances.

One of the earliest published media for *C. glutamicum* with a clearly defined composition, contained only glucose as carbon and energy source as well as different sources for nitrogen, phosphate, sulfur, vitamins, mineral salts and trace elements (Table 4.1, [277]). Interestingly, this medium, denoted as CGVIII, also contained high amounts of calcium carbonate (CaCO_3), which was shown to be beneficial for cell population growth.

Table 4.1: Selected media compositions for cultivation of *C. glutamicum* under defined conditions. All amounts refer to 1 liter.

	Cremer <i>et al.</i> [277] CGVIII	Keilhauer <i>et al.</i> [195] CGXII	Bäumchen <i>et al.</i> [212]	Kind <i>et al.</i> [278]
D-glucose	40 g	40 g	10 g	10 g
(NH ₄) ₂ SO ₄	20 g	20 g	10 g	15 g
Urea		5 g		
KH ₂ PO ₄	0.5 g	1 g	1 g	7.7 g
K ₂ HPO ₄	0.5 g	1 g	2 g	24.98 g
MgSO ₄ •7H ₂ O	0.25 g	0.25 g	0.25 g	0.2 g
MOPS		42 g		
CaCl ₂		10 mg	10 mg	
FeSO ₄ •7 H ₂ O	10 mg	10 mg	10 mg	20 mg
MnSO ₄ •H ₂ O	10 mg	10 mg	10 mg	2 mg
ZnSO ₄ •7H ₂ O	1 mg	1 mg	1 mg	0.5 mg
CuSO ₄ •5H ₂ O	0.2 mg	0.2 mg	0.31 mg	
NiCl ₂ •6H ₂ O		0.02 mg	0.2 mg	
Biotin	0.2 mg	0.2 mg	0.2 mg	0.5 mg
Protocatechuic acid		0.3 mg (later corrected to 30 mg)	30 mg	30 mg
CaCO ₃	20 g			
NaCl				1 g
Na ₂ B ₄ O ₇ •10H ₂ O				0.2 mg
(NH ₄) ₆ Mo ₇ O ₂₄ •4H ₂ O				0.1 mg
Thiamine-HCl				1 mg
CaCl ₂ •2H ₂ O				0.2 mg
CaCl ₂ •H ₂ O				55 mg
FeCl ₃ •H ₂ O				2 mg

In 1989 Liebl *et al.* found that in the absence of CaCO_3 , iron chelating compounds are required for growth of *C. glutamicum* and proposed 3,4-dihydroxybenzoic acid (or protocatechuic acid, PCA) for standard use in defined media [279]. Later Keilhauer *et al.* substantially modified CGVIII by adding the iron chelator PCA [195] and exchanged CaCO_3 by very low amounts of an alternative calcium source (CaCl_2 , cf. Table 4.1). This medium is commonly referred to as CGXII minimal medium and, depending on the

cultivation system, either used with or without 3-(N-morpholino)propanesulfonic acid (MOPS) as pH regulating buffer.

Since CGXII had been formulated, it became the standard for Metabolic Engineering and Systems Biology with *C. glutamicum* and, until now, the publication by Keilhauer *et al.* has been cited more than 250 times (Google Scholar). In addition, the usage of other PCA containing minimal media is even more widespread in the scientific community, since some reports for *C. glutamicum* refer to other publications (cf. Table 4.1, [212, 278]).

In a previous study we determined the exponential growth rate of *C. glutamicum* wild type in CGXII medium at different cultivation scales. At standard initial cell densities a growth rate of $0.39 - 0.45 \text{ h}^{-1}$ was found, independent from the cultivation scale and underlying technical devices. In contrast, when growth was initiated in highly diluted environments a greatly elevated growth rate in the range of $0.60 - 0.64 \text{ h}^{-1}$ was reproducibly determined [98]. In further investigations it was found that by-products such as acetate can impair growth already at very low concentrations. More generally, we supposed that any condition leading to sufficient by-product dilution enables cell population growth with the “true” maximum growth rate as predefined by the initial medium composition.

In this study we investigated the relationship between initial cell densities, medium composition, batch growth and maximum growth rates in more detail.

4.2.3 Materials and methods

Medium preparation

Cultivations were performed on the defined medium CGXII, containing per liter of distilled water: 20 g $(\text{NH}_4)_2\text{SO}_4$, 1 g K_2HPO_4 , 1 g KH_2PO_4 , 5 g urea, 13.25 mg $\text{CaCl}_2 \cdot 2\text{H}_2\text{O}$, 0.25 g $\text{MgSO}_4 \cdot 7\text{H}_2\text{O}$, 1 mg $\text{FeSO}_4 \cdot 7\text{H}_2\text{O}$, 1 mg $\text{MnSO}_4 \cdot \text{H}_2\text{O}$, 0.02 mg $\text{NiCl}_2 \cdot 6\text{H}_2\text{O}$, 0.313 mg $\text{CuSO}_4 \cdot 5\text{H}_2\text{O}$, 1 mg $\text{ZnSO}_4 \cdot 7\text{H}_2\text{O}$, 0.2 mg biotin and 10 g D-glucose. The concentration of protocatechuic acid (PCA) was 30 mg l^{-1} in standard medium, but was varied during growth studies in the range of $0.6 \text{ mg l}^{-1} - 2.5 \text{ g l}^{-1}$. Medium for cultivation in bioreactors or microtiter plates was supplemented with 3% ($v v^{-1}$) AF204 antifoam agent or 42 g l^{-1} MOPS buffer, respectively. During medium preparation, some substances were added sterile after autoclaving (D-glucose, PCA, biotin, trace elements and AF204) and 4 M NaOH was used to adjust pH 7.0. All chemicals used were purchased from SIGMA Aldrich.

Bioreactor cultivations

Bioreactor cultivations of *C. glutamicum* wild type (ATCC 13032) were carried out in 1.5 l reactors (DASGIP AG, Jülich, Germany). Cultivations were performed in batch mode at constant temperature ($30 \text{ }^\circ\text{C}$) and air flow (1 vvm). Aerobic process conditions were controlled via stirrer speed (200 – 1200 rpm) to maintain 30% dissolved oxygen

concentration (DO). The pH of the culture was regulated to pH 7.0 with 4 M HCl and 4 M NaOH. Online measurements were taken for pH (405-DPAS-SC-K80/225, Mettler Toledo), DO (Visiform DO 225, Hamilton) and exhaust gas composition (GA4, DASGIP AG, Jülich, Germany).

All bioreactor cultivations were inoculated directly from cryo culture aliquots, which had been prepared from a CGXII shaking flask culture of exponentially growing *C. glutamicum*. For preparation the cells were harvested at $OD_{600} = 10$, washed with 0.9% (w v⁻¹) NaCl and stored at -80 °C in NaCl solution containing 20% (v v⁻¹) glycerol. From these cryo culture aliquots, 0.5 mL were added to 1 l bioreactor cultivations to obtain a comparable low inoculum ($OD_{600} \approx 0.005$).

Growth of batch cultures at such low initial biomass concentration was tracked with the Coulter Counter Multisizer 3 (Beckmann Coulter, Inc.) equipped with a 30 µM capillary. Culture samples were diluted with CasyTon (Roche Diagnostics GmbH) if necessary, and measured for cell concentration as well as distribution of cell volumes. Data of total biovolume (BV) was moreover used to determine specific uptake rates in the cultures. These rates were related to cell dry weight (CDW) using the linear regression function $CDW [g] = 0.474 \cdot BV [ml]$.

Microtiter plate cultivations

Cultivations in microtiter plates were performed using the BioLector device (m2p-labs, Baesweiler, Germany). The BioLector allows the time-dense tracking of culture parameters (pH, DO) and biomass concentrations (backscatter) of 48 parallel cultivations in one FlowerPlate® (m2p-labs, Baesweiler, Germany). The wells of these FlowerPlates are baffled to enable high oxygen transfer rates, comparable to bioreactor scale.

For cultivations, 1 mL inoculated culture was filled in each well of a Flowerplates, which was closed with a gas permeable sterile foil. The BioLector was operated at 1000 rpm, 30 °C and 95% humidity. Backscatter signals were measured at gain 20 and later normalized by the blank value of each well separately.

Microfluidic single-cell cultivations

The in-house developed polydimethylsiloxane microfluidic system enables the spatio-temporal analysis of growing microcolonies with single-cell resolution by automated high resolution time-lapse microscopy. Due to continuous media perfusion environmental conditions are maintained constant, ideal for perturbation studies. Each chip device contains 400 microfluidic cultivation chambers of 1 µm x 60 µm x 60 µm (height x length x width) connected to media supply channels. Mass transport inside the cultivation chambers is based on diffusion only. For chip fabrication details and further information the reader is referred to the publications by Grünberger *et al.* [98, 169].

The microfluidic chip was mounted onto a motorized inverted microscope (Nikon Eclipse Ti, Nikon microscopy, Germany) equipped with an incubator for temperature and atmosphere control. The cell suspension with an OD_{600} between 0.5 and 1, transferred

from the pre-culture at exponential growth phase, was infused into the chip to inoculate the microfluidic cultivation chambers with single cells. Growth medium was infused at approx. 100 nL min^{-1} after cell inoculation. CGXII medium was prepared as described before and additionally sterile filtered to prevent particle agglomeration during microfluidic cultivation.

Supernatant samples of the lab-scale bioreactor cultivation were instantly filtered ($0.22 \text{ }\mu\text{m}$ pore size) to remove cells and prevent degradation, and were stored at $-20 \text{ }^\circ\text{C}$ for microfluidic experiments.

Time-lapse phase contrast microscopy images of the growing microcolonies were recorded every 10 minutes over 24 h of microfluidic cultivation. Afterwards, cell numbers, cell length and growth rates were derived by image analysis utilizing the Nikon NIS Elements AR software package.

GC-ToF-MS and LC-MS/MS analysis

Untargeted metabolome screening in culture supernatants was performed via an Agilent 6890N gas chromatograph coupled to a Waters Micromass GCT Premier high resolution time of flight mass spectrometer. For details regarding sample preparation, MS operation and peak identification the reader is referred to [229].

PCA concentrations in culture supernatants were measured by HPLC (X-LC 3000 Series, Jasco) coupled to a mass spectrometer (API 4000, ABSciex) equipped with a TurboIon spray source. For the analysis a C18 column (Synergy Hydro, Phenomenex) was used with eluent A (10 mM tributylamine aqueous solution adjusted pH to 4.95 with 15 mM acetic acid) and eluent B (methanol) at a temperature of $40 \text{ }^\circ\text{C}$. The elution was isocratic with a A/B ratio of 70/30, a flow rate of 0.45 mL min^{-1} and an injection volume of $10 \text{ }\mu\text{l}$. For more details regarding MS operation see [229].

Transcriptome analysis

For transcriptome analysis, cells were cultivated in four bioreactors in standard CGXII medium as described before. Each culture was harvested either during first or second growth phase at $\text{OD} = 0.2$ or $\text{OD} = 2$, respectively. Global gene expression was analyzed independently following two biological replicates for each condition. RNA and the synthesis of fluorescently labeled cDNA were prepared as described before [280].

The custom-made DNA microarrays were obtained from Agilent Technologies (Waldbronn, Germany). Agilent's eArray platform was used to assemble custom 4x44K 60mer microarray designs (<https://earray.chem.agilent.com/earray/>). The custom design included oligonucleotides for the annotated protein-coding genes and structural RNA genes of the bacterial genomes from *C. glutamicum*, *Escherichia coli*, *Gluconobacter oxydans*, and *Bacillus subtilis* for genome-wide gene expression analysis. For *C. glutamicum*, the genome annotation by Kalinowski and co-workers [243] (accession number NC_006958) was used, listing 3057 protein coding genes and 80

structural tRNA and ribosomal RNA genes. In the custom design the *C. glutamicum* genes are represented by one, two or three oligonucleotides, which were employed to determine the relative RNA level. The custom array design also included the Agilent's control spots. Purified cDNA samples to be compared were pooled. The prepared two-color samples were hybridized on 4x44K arrays at 65 °C for 17 h using Agilent's gene expression hybridization kit, Agilent's hybridization chamber, and Agilent's hybridization oven. After hybridization, the arrays were washed using Agilent's wash buffer kit according to the manufacturer's instructions. Fluorescence of hybridized DNA microarrays was determined at 532 nm (Cy3-dUTP) and 635 nm (Cy5-dUTP) at 5 µm resolution with a GenePix 4000B laser scanner and GenePix Pro 6.0 software (Molecular Devices, Sunnyvale, USA). Fluorescence images were saved to raw data files in TIFF format (GenePix Pro 6.0).

Quantitative TIFF image analysis was carried out using GenePix image analysis software and the Agilent's gene array list (GAL) file. The results were saved as GPR-file (GenePix Pro 6.0). For background correction of spot intensities, ratio calculation and normalization, as well as generation of diagnostic plots for array quality control, GPR-files were processed using the BioConductor R-packages *limma* and *marray* (www.bioconductor.org). For further analysis, the processed and loess-normalized data as well as detailed experimental information according to MIAME [281] were stored in the in-house DNA microarray database [282]. To search the data for differentially expressed genes by the processed Cy5/Cy3 ratio reflecting the relative RNA level, the criteria flags ≥ 2 (GenePix Pro 6.0) and signal/noise ≥ 5 for Cy5 (F635Median/B635Median, GenePix Pro 6.0) or Cy3 (F532Median/B532Median, GenePix Pro 6.0) were used. If the signal/noise of Cy5 and of Cy3 were < 3 , then signals were considered as too weak to analyze the Cy5/Cy3 ratio of a gene. Furthermore, p-values were calculated by a paired Student's *t* test comparing the relative RNA levels of a gene in the replicates to the relative RNA levels of all other genes in the replicates.

4.2.4 Results and discussion

Bi-phasic growth of *C. glutamicum* in CGXII medium

The batch growth of *C. glutamicum* was studied under controlled bioreactor conditions in standard CGXII medium and low initial cell densities. Each cultivation was inoculated at a comparable low cell concentration of $N(t=0) = 1.3 \cdot 10^6 \pm 2.1 \cdot 10^5$ cells ml⁻¹, which corresponds to an optical density (OD₆₀₀) of OD₆₀₀ ≈ 0.005 and a cell dry weight (CDW) of CDW ≈ 0.002 g l⁻¹. The cultivations were performed in ten biological replicates, in order to allow for a reliable estimation of specific growth rates. Noteworthy, the biomass growth was tracked by a sensitive Coulter Counter method, since the limit of quantification (LOQ) for the commonly applied OD₆₀₀ and CDW measurements are much higher (LOQ_{OD} ≈ 0.5 , LOQ_{CDW} ≈ 1 g l⁻¹, results from preliminary experiments).

As shown in Figure 4.6A, the batch cultivation follows two growth phases with a metabolic switch at $t \approx 10$ h and a corresponding $OD_{600} \approx 0.5$. For both phases, the exponential growth rates were determined. For the first phase the exponential growth rate is estimated as $\hat{\mu} = 0.61 \pm 0.02 \text{ h}^{-1}$, which matches the higher growth rate of *C. glutamicum* when cultivated in the microfluidic perfusion system [98]. In contrast, the exponential growth rate during the second phase with $\hat{\mu} = 0.46 \pm 0.02 \text{ h}^{-1}$ is much lower, and close to the growth rate estimate of $0.42 \pm 0.03 \text{ h}^{-1}$ presented in our former study. Noteworthy, in former experiments the cells were inoculated at $OD_{600} = 1$ and therefore cultivated at higher densities during exponential growth (see supplementary information in [98]). In the actual experiments such cell densities are reached after 14 h of cultivation (cf. Figure 4.6A).

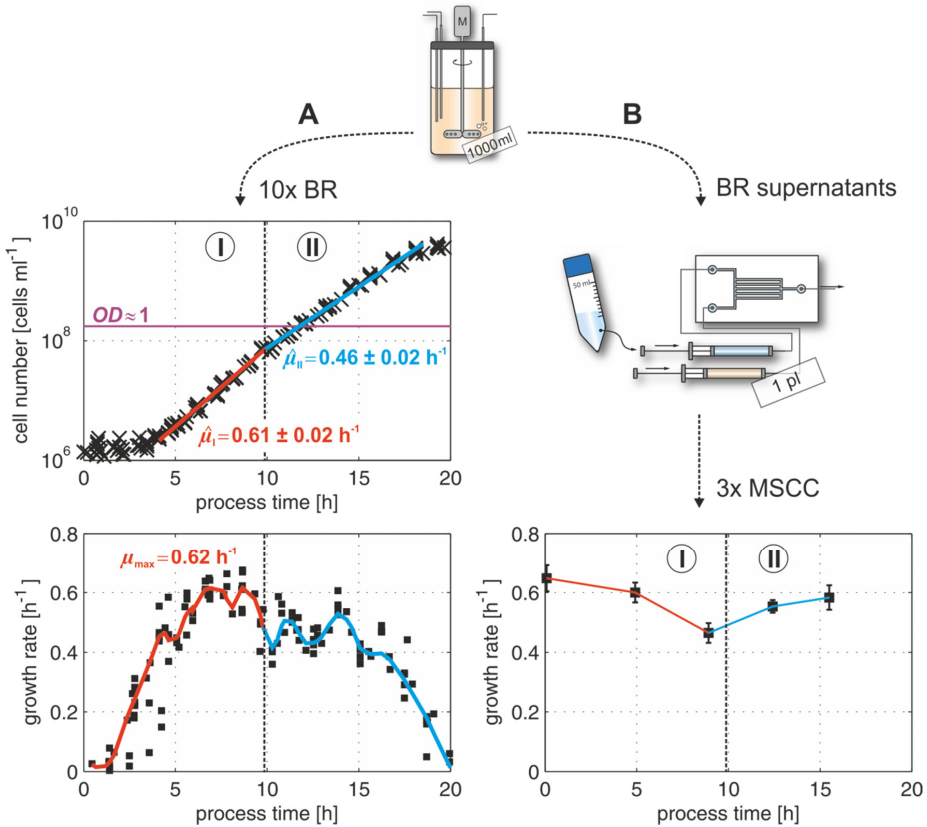


Figure 4.6: Batch cultivation of *C. glutamicum* in standard CGXII glucose medium in 1 l bioreactors reveals a bi-phasic growth behavior. (A) Two distinct growth phases were identified in ten biological replicates, of which the first was characterized by a higher growth rate of $\hat{\mu} = 0.61 \pm 0.02 \text{ h}^{-1}$. For comparison the graph depicts the initial biomass density ($OD_{600} \approx 1$) applied in our former bioreactor experiments [98]. (B) Filtrated culture supernatants of distinct time-points from the bioreactor were used as growth medium during MSCC. Abbreviations: BR, bioreactor; MSCC, microfluidic single-cell cultivation.

The growth curves were further analyzed to exclude any misinterpretation in the distinction between the two observed growth phases. Firstly, the differential growth rates along the cultivation were determined to evaluate the division of the growth curve into two phases (cf. Figure 4.6A, bottom). A clear drop of differential growth rates at 10 h cultivation time supported the time-dependent metabolic switch. Secondly, we checked if the observed changes in growth rates which are based on cell number measurements, were distorted by underlying dynamic changes in cell sizes. Therefore, the overall cell volume (biovolume) and the mean single-cell volume were followed along all cultivations (see Appendix Figure F.1). As expected, the biphasic growth behavior was again reproduced from the biovolume measurements. Moreover, after inoculation the cells first grew in size (lag-phase with respect to cell division) and then, eventually after reaching a maximum cell size, continuously became smaller with decreasing substrate availability. This observation is consistent with previous results, where *C. glutamicum* was cultivated in a long-term batch following prolonged carbon limitation and decreasing cell sizes [229].

The observed metabolic switch in CGXII batch cultures occurring at a certain threshold cell density that leads to decreasing growth rates, can result from the accumulation of inhibiting by-products or the limitation of specific media components. However, to discriminate between both effects, the instantaneous growth phenotype in response to the changing media composition has to be measured and all side-effects resulting from the cultivation history must be safely excluded.

Here microfluidic single-cell cultivation (MSCC) is a powerful technique that can be used to access growth phenotypes (including division rates and morphology), which are predominantly resulting from the medium components in the inflow. The continuous dilution with fresh medium prevents any by-product accumulation in the cultivation chamber and therefore excludes any potential growth impairing effect of such compounds [98]. Moreover, MSCC allows direct online monitoring of growing cell populations and therefore higher accuracy in growth rate estimation.

Biosensing of culture supernatants with MSCC

We applied MSCC to determine the growth phenotype of *C. glutamicum* in cell free supernatant samples from bioreactor cultivations (Figure 4.6B). The supernatant from the beginning of the bioreactor cultivation, which nearly equals the original CGXII medium, resulted in growth rates of $\hat{\mu} = 0.65 \pm 0.04 \text{ h}^{-1}$, essentially reproducing our former results. Within the subsequent supernatant samples, the growth rate first decreased until a minimum of $\hat{\mu} = 0.46 \pm 0.03 \text{ h}^{-1}$ was reached and then increased again to significantly higher values. Noteworthy, also the mean cell size of *C. glutamicum* follows the same pattern, pointing to a link between medium composition, growth rate and cell size (see Appendix Figure F.2). The bi-phasic growth characteristics, observed in the bioreactor cultivation, could therefore be reproduced by MSCC.

The re-switch to higher growth rates found during MSCC on bioreactor supernatants from late exponential phase could be explained by differences in the growth environment and time-scale between both cultivation systems. In the bioreactor the cells grow in batch mode on glucose excess and, hence, the cultivation broth is likely to be enriched with significant amounts of intracellular metabolites [229]. During this process the extracellular environment is dynamically changing, which most likely forces the cells to continuously adapt their metabolism. This energy demanding adaption will directly affect growth rates which are, moreover, the estimated averages from a heterogeneous cell population in different stages of adaption. In contrast, during MSCC only a few cells are cultivated and the growth medium, here in form of a culture supernatant, is continuously flushed to provide a constant extracellular environment. As a result, the cells can adapt for multiple hours to the unique composition of each particular supernatant sample from the batch reactor. Hence, even small amounts of co-metabolites might significantly improve cellular growth, after a time-dependent adaption to the complex composition could take place. In conclusion, a MSCC approach shows the maximal possible growth rate in a given medium composition and might thereby be significantly higher than found in the dynamic environment in a batch culture.

The observation of a growth rate minimum around the metabolic switch following MSCC rather excludes an accumulation of inhibiting by-products like, *e.g.*, acetate as reason for lower growth rates during bioreactor batch cultivation. In such a case one would not expect increasing growth rates on supernatant samples taken from the second growth phase. Moreover, in our former study acetate was already tested as potentially inhibiting by-product and provoked decreased growth rates under MSCC conditions when supplemented next to glucose [98].

Consequently, the MSCC data strongly points to a limitation of a media component as the key factor for the bi-phasic growth behavior. To further test this hypothesis, we analyzed the time dependent changes in the composition of culture supernatants during bioreactor batch cultivation.

Potential growth effectors in culture supernatants

In a first approach we applied an untargeted metabolome screening via GC-ToF-MS, focusing on supernatant samples from the bioreactor cultivation started at low initial cell density. It was observed that the medium components urea and PCA decreased extracellular, and PCA completely vanished from the medium during the first growth phase (Appendix Figure F.3). While the absence of urea in the CGXII medium had no effect on growth (data not shown), it was already shown that PCA or a comparable iron chelator like, *e.g.*, catechol or citrate, is necessary to initiate cell division in *C. glutamicum* [279, 283].

Hence, in the following we concentrated on PCA and performed quantitative, targeted LC-MS/MS analysis of the same supernatant samples (Figure 4.7A). As a result, PCA was completely consumed by the cells within 10 h of cultivation and the time point

of PCA depletion coincided with the subsequent start of the second growth phase. In accordance to this observation, recent reports have broadened the potential function of PCA from a sole iron chelator to an alternative substrate, as *C. glutamicum* was able to grow on PCA as single carbon source [284-286].

Differential transcriptome analysis

With PCA as potential target compound at hand, we continued with a differential transcriptome analysis to quantify gene expression changes, accompanied with the growth rate reduction in the second growth phase.

For transcriptome analysis, two bioreactor samples were taken from each growth phase, *i.e.*, 2 h before and 1.5 h after the drop in the growth rates. The resulting mean ratios of selected mRNA levels are shown in Figure 4.7B. A complete list of significantly up or down-regulated genes can be found in Table F.1 of the Appendix.

As a main result, a significant up-regulation of nearly all genes encoding for the β -ketoacid pathway was determined during the first growth phase (Figure 4.7C and D). Within this pathway, PCA is taken up by the 4-hydroxybenzoate transporter *pcaK* [286] and then degraded within six enzymatic steps to the tricarboxylic acid (TCA) cycle intermediates acetyl-coenzyme-A (AcCoA) and succinyl-CoA (SuCoA) [287].

Interestingly, several genes (*iolB*, *iolC*, *gntP*, *pobA*, *catA1*) encoding for catabolic degradation of substances typically found in soil (inositol, gluconate, benzoate, catechol) were also found to be greatly up-regulated in the first growth phase (cf. Appendix Table F.1). This finding might reflect a more global transcriptomic response of *C. glutamicum* to the presence of substrates occurring in its natural habitat.

In addition, a two-fold up-regulation was observed for the genes *nifS2* (cg1761), *sufC* (cg1762), *sufB* (cg1764) and a putative transcriptional regulator (cg1765) which build the operon of essential [Fe-S]-cluster biosynthesis [288]. Noteworthy, different [Fe-S]-cluster containing enzymes are linked to PCA degradation, its further downstream catabolism and, more general, are required for fast growth. This holds true for protocatechuate dioxygenase (PcaGH in Figure 4.7D), the TCA-cycle enzymes aconitase, succinate-dehydrogenase as well as the cytochrome *bc₁* complex, involved in respiratory energy metabolism [23].

In contrast, during the second growth phase no distinct transcriptomic response with regard to the absence of PCA was found and especially the expression of genes related to the iron starvation response in *C. glutamicum* [289] was unaltered.

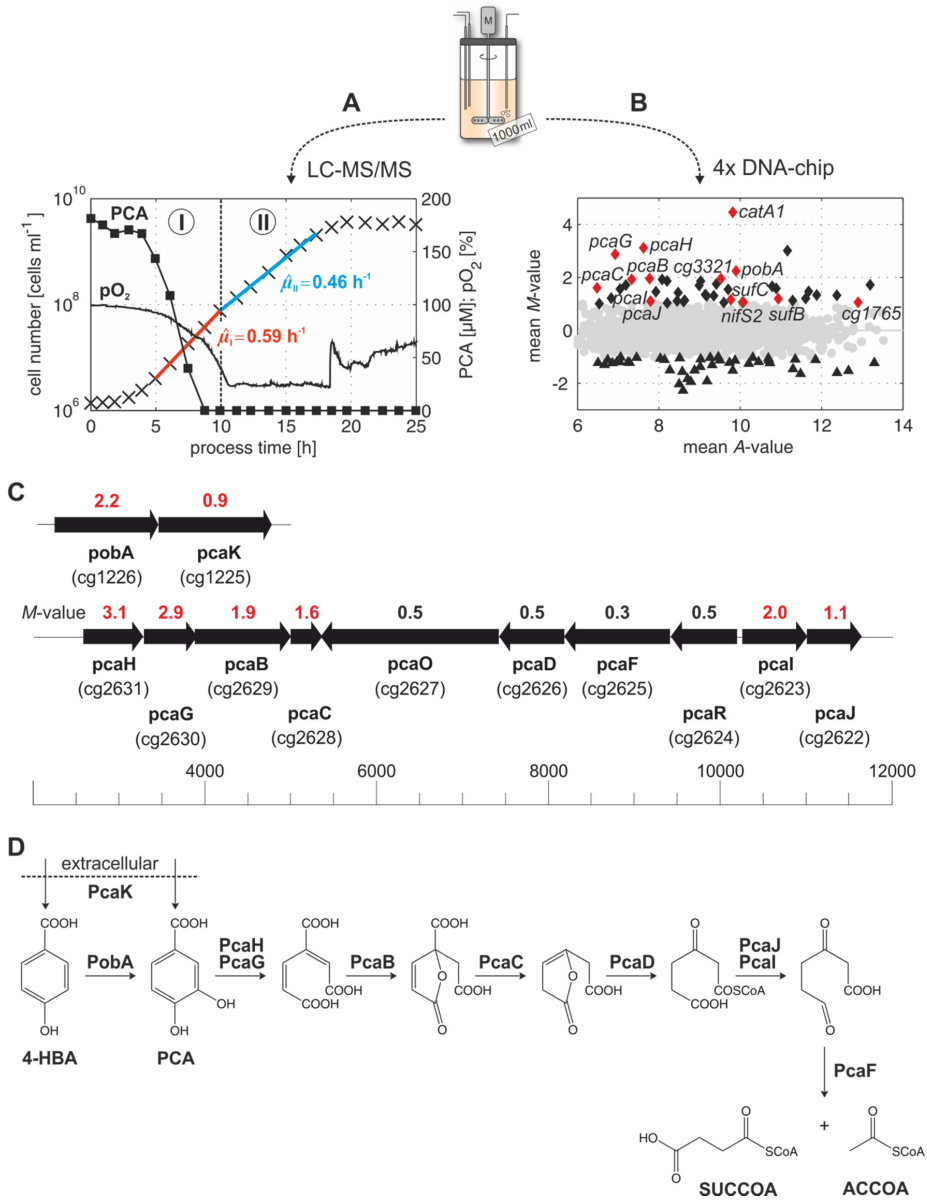


Figure 4.7: In-depth analysis of bi-phasic growth behavior of *C. glutamicum* when cultivated in CGXII glucose medium. (A) LC-MS/MS analytics revealed a decreasing concentration of the iron chelator PCA in the supernatant. After PCA completely vanished ($t \geq 9$ h), the switch from first to second growth phase was observed. (B+C) In a differential transcriptomics study it was shown, that multiple genes encoding for the β -ketoadipate pathway were higher expressed in the first growth phase. (D) Illustration of the PCA catabolism in *C. glutamicum*, resulting in the TCA intermediates succinyl-CoA and acetyl-CoA.

Growth response to varying PCA concentration

The results from metabolome and transcriptome analysis strongly indicated that PCA is actively catabolized by *C. glutamicum* in standard CGXII medium, what can only be observed at comparable low cell densities. In the following, the effect of PCA availability on the growth of *C. glutamicum* was investigated in more detail by a specially designed series of batch and MSCC experiments.

C. glutamicum was grown in two batch cultivations in CGXII medium with and without PCA inoculated at a standard cell density of $OD_{600} \approx 0.5$ (Figure 4.8). Both cultures showed growth demonstrating that *C. glutamicum* can initiate cell division also in the absence of PCA, when inoculated at sufficient cell densities. However, the PCA containing culture immediately grew exponentially, while the PCA-free culture showed a delayed growth phase in the beginning. This observation could either point to a growth enhancing effect of PCA during early culture stages or simply indicate that *C. glutamicum* needs to adapt to PCA-free medium (lag-phase). A potential adaption would, however, not be expected when the cells were grown in a PCA-free pre-culture.

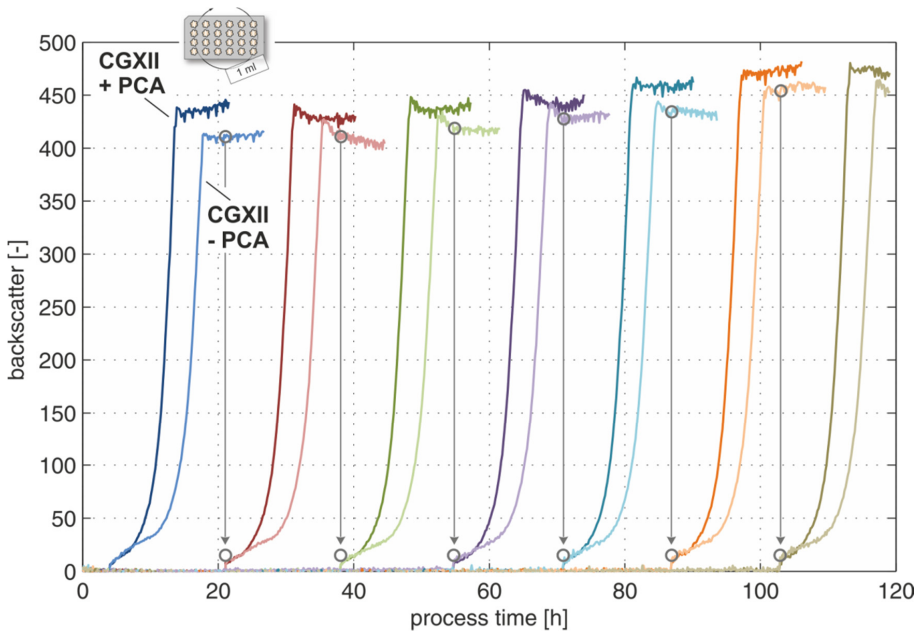


Figure 4.8: Growth of *C. glutamicum* in microtiter plates containing CGXII medium with and without PCA. Cells from the PCA free culture were used to inoculate subsequent cultivations on both medium variants. In PCA free medium a delayed growth pattern was observed. However, later growth rates were comparable to cultures on PCA containing medium. In six following repetitive batch cycles the growth pattern was found unchanged and thereby, no cellular adaption to PCA free medium was found.

Therefore, a series of six repetitive batch cycles was performed in which cells from the previous PCA-free culture were used to inoculate subsequent cultivations with and without PCA (cf. Figure 4.8). As a result, all PCA containing cultures immediately grew

exponentially, while the PCA-free cultures showed a conserved delayed growth behavior. Hence, it can be concluded that the amount of PCA that is initially available per single cell directly influences early cell population growth. In the later growth phase all repetitive batch cultures showed the standard exponential growth rate ($\hat{\mu} = 0.46 \pm 0.01 \text{ h}^{-1}$) independently from initial PCA availability.

Next we studied the effect of PCA surplus when *C. glutamicum* is grown in CGXII medium in batch cultures with glucose inoculated at $\text{OD}_{600} \approx 0.5$ (Figure 4.9A). In a culture with 16.3 mM PCA (*i.e.*, 83-times the standard concentration) the elevated growth rate of $\hat{\mu} = 0.61 \text{ h}^{-1}$ was now maintained up to higher cell densities of $\text{OD} \approx 3$. In accordance with the faster growth during the first phase, the dissolved oxygen (DO) concentration decreased much faster until the PCA was fully consumed. After complete PCA consumption a step-increase in the DO-signal was observed, which clearly indicated a metabolic switch to the PCA-free phase and standard exponential growth on glucose.

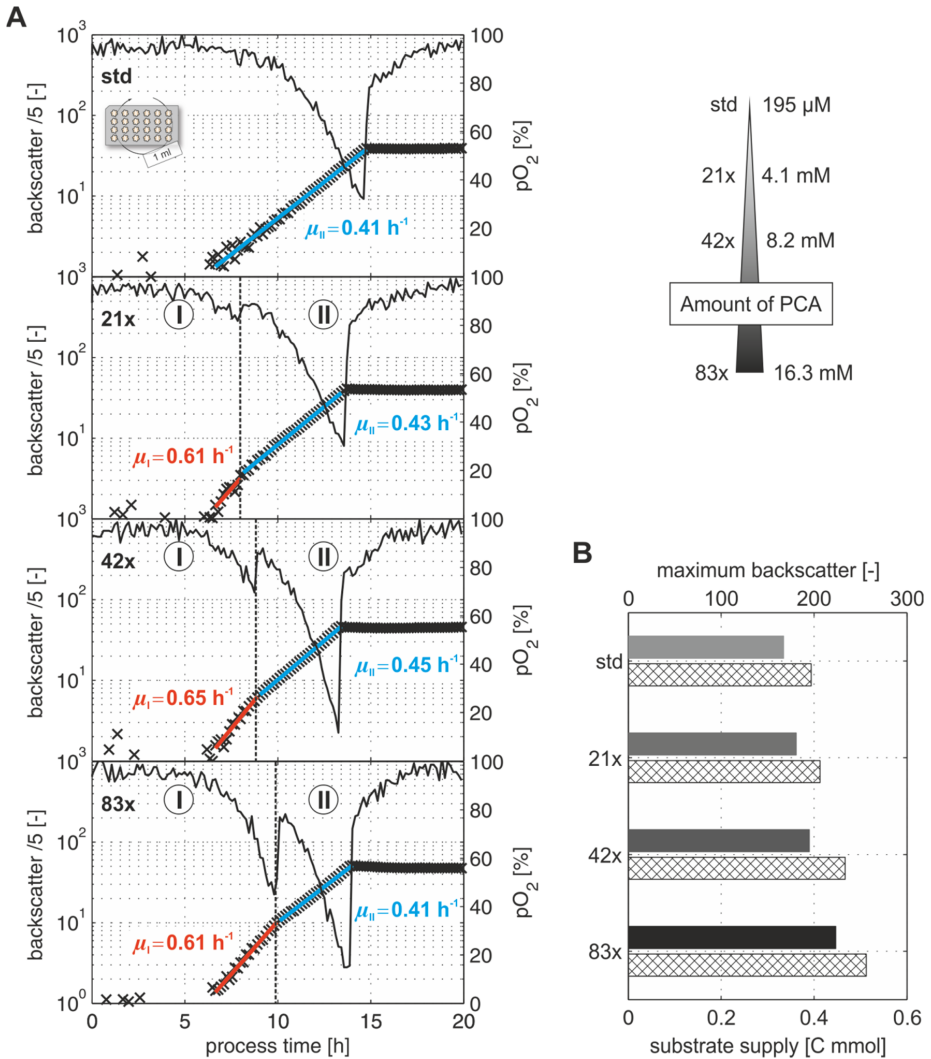


Figure 4.9: Influence of PCA surplus on growth of *C. glutamicum* during batch cultivation in CGXII medium with 10 g l^{-1} glucose. (A) Microtiter plates were inoculated at $OD_{600} \approx 0.5$ and the standard (std) PCA concentration of $195 \mu\text{M}$ was increased step-wise up to a final concentration of 16.3 mM (83x). Growth was monitored online via backscatter and dissolved oxygen (pO_2) measurements. At higher PCA concentrations the phase of elevated growth rates could be prolonged and thereby established until higher biomass concentrations of $OD_{600} \approx 3$. (B) Correlation between maximum backscatter from batch cultivation and total carbon supply in the medium, which was changed by increasing PCA concentrations.

To further evaluate the role of PCA as an additional C-source the final biomass density (backscatter signal) was analyzed with respect to carbon availability in the used growth media (Figure 4.9B). While glucose concentration was kept constant, the total carbon fraction was altered from PCA variation in the different medium compositions. The final biomass densities in those growth media showed a proportional increase to

elevated PCA concentrations, supporting once more the role of PCA for biomass generation.

Finally, microfluidic experiments confirmed that *C. glutamicum* can grow on PCA as single carbon source and, most interestingly, the resulting maximum growth rates are directly depending on the amount of PCA supplied via the continuous feeding rate (Figure 4.10A).

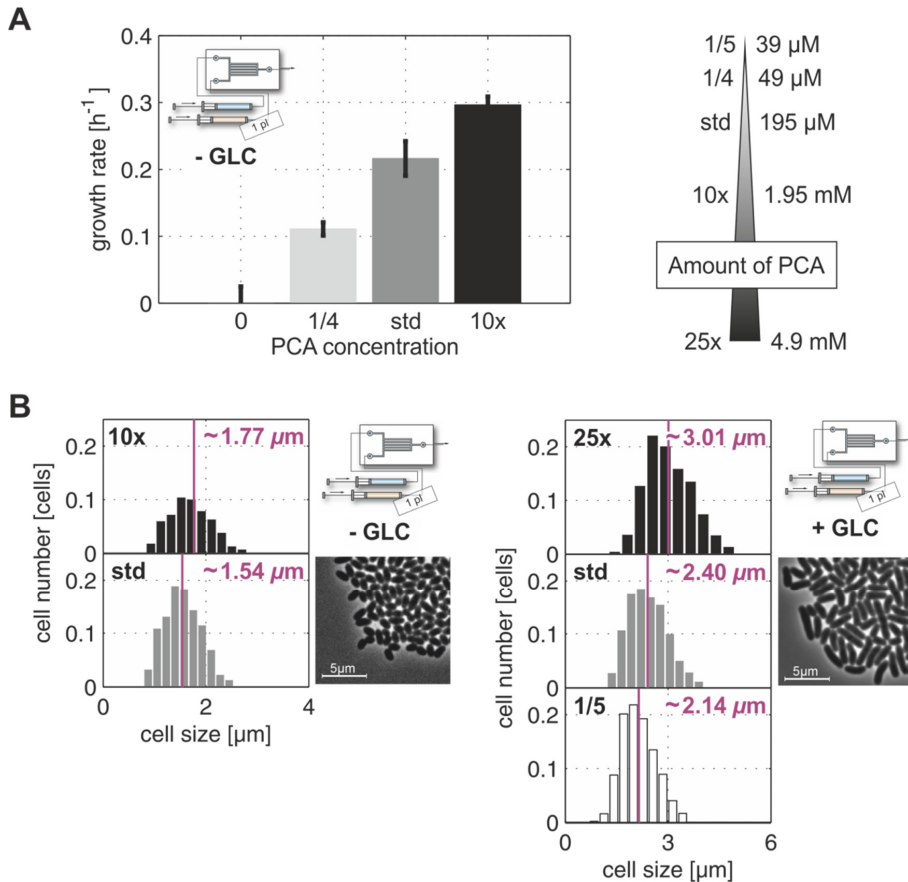


Figure 4.10: Growth of *C. glutamicum* on PCA as sole carbon source and its impact on cell morphology. (A) Growth in CGXII without glucose was observed during microfluidic cultivation when PCA was added and the observed growth rates were a direct function of PCA concentration. (B) Correlation between PCA supply and cell size of *C. glutamicum* during MSCC in CGXII with and without glucose at varying PCA concentrations.

Moreover, a strong correlation between PCA supply, specific growth rate and cell size was found for growth in CGXII medium with and without glucose throughout all performed experiments (Figure 4.10B). This result is in agreement with the cell size pattern observed during the biosensing experiments (cf. Appendix Figure F.2), and

generally strengthens the hypothesis of a direct linkage between nutrient availability, cell size and growth rate in microorganisms [268, 290].

***In silico* analysis of PCA catabolism**

To specify the carbon source function of PCA, we performed flux variability analysis (FVA) using a genome scale model of *C. glutamicum* [291]. In short, FVA is applied to simulate the minimum and maximum flux for each reaction in the network while maintaining the maximal possible growth rate under the predefined network constraints. For more details regarding the FVA method the reader is referred to [292].

The specific uptake rates for glucose ($\text{upt}_{\text{GLC}} = 4.42 \pm 0.54 \text{ mmol g}_{\text{CDW}}^{-1} \text{ h}^{-1}$) and PCA ($\text{upt}_{\text{PCA}} = 2.04 \pm 0.20 \text{ mmol g}_{\text{CDW}}^{-1} \text{ h}^{-1}$) were calculated from one batch experiment using the standard CGXII medium composition (cf. Figure 4.7A) and taken as network constraints for FVA.

Figure 4.11 depicts one possible intracellular flux distribution within the central carbon metabolism of *C. glutamicum* that results in a maximum growth rate prediction of $\hat{\mu} = 0.55 \text{ h}^{-1}$ and thus resembles the situation during the first growth phase (cf. Figure 4.6A and Appendix Figure F.1). In contrast, when only glucose is supplied as carbon and energy source, the maximum growth rate is predicted as $\hat{\mu} = 0.39 \text{ h}^{-1}$, which is in the range of the experimentally determined value during the second growth phase.

In both cases the absolute value of the simulated growth rate is lower than the measured one, which might be due to the underlying network parameterization including precursor and ATP demand for biomass synthesis. As the accuracy of absolute rate estimation using a pure stoichiometric network approach is limited, we focused on the interpretation of the relative changes in the following.

The predicted increase in growth rates from additional consumption of PCA ($\Delta\mu \approx 0.15 \text{ h}^{-1}$) is in good correlation to the increase in growth rates found experimentally. For some selected reactions the relative flux ranges allowing for the two optimum solutions are represented. As expected, the metabolization of PCA leads to a significantly higher carbon flux along the TCA-cycle, providing not only a surplus of the biomass precursor α -ketoglutarate and oxaloacetate, but also of energy and reduction equivalents. With regard to the NADPH generation, the flux along the pentose phosphate pathway tends to be down-regulated in response to the higher TCA-cycle flux and a potential activity of the malic enzyme.

Clearly, the latter finding needs further confirmation by trying more elaborate flux estimations via ^{13}C -metabolic flux analysis (^{13}C -MFA, [293]). The anaplerosis of *C. glutamicum* comprises 5 reactions that potentially operate in parallel [23], and thereby cannot be resolved in a quantitative manner even with ^{13}C -MFA [294]. This is again reflected in the broad flux range estimated for all anaplerotic reactions when applying the FVA approach (cf. Figure 4.11).

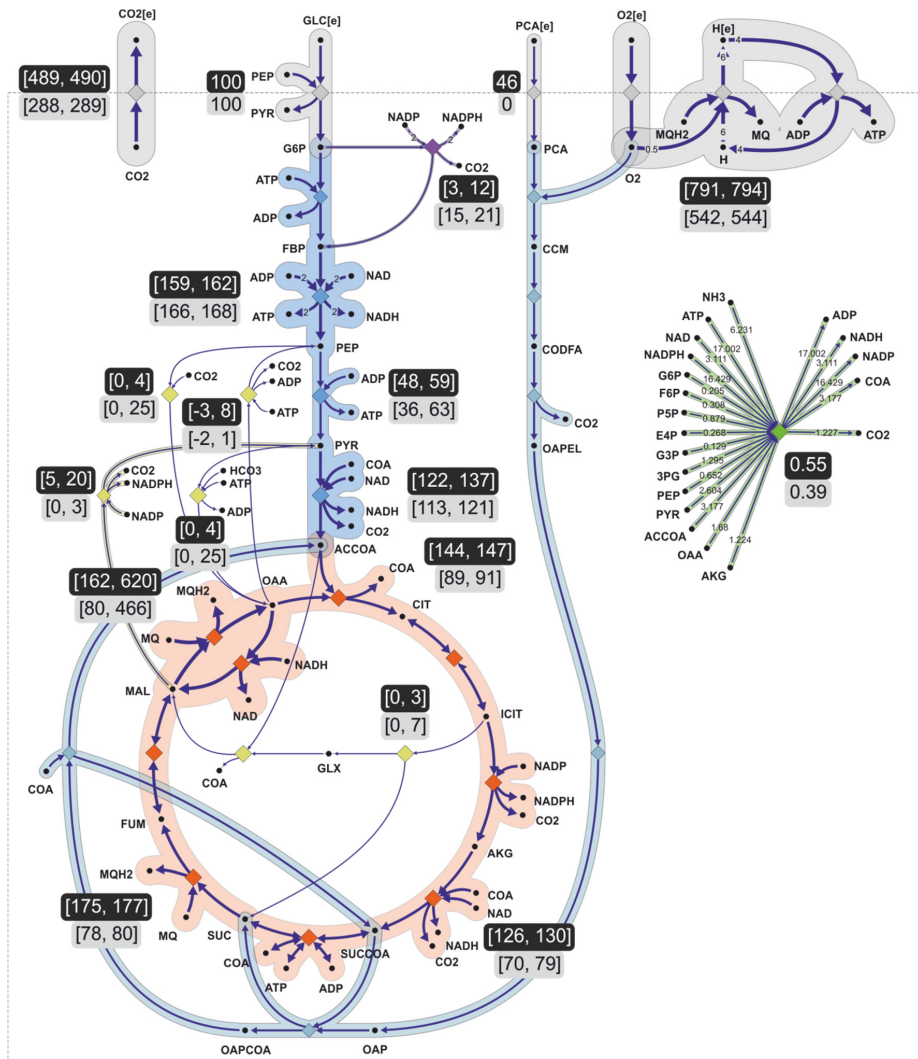


Figure 4.11: Coarse-grained simulation of metabolic fluxes in *C. glutamicum* during co-metabolism of PCA and glucose. The values represent the minimum and maximum fluxes resulting from flux variability analysis (FVA). For FVA the measured uptake rates for both substrates were fixed during the simulation and biomass growth was applied as optimization criteria. The simulation was repeated for growth on sole glucose (assuming no PCA uptake) and the corresponding flux ranges are represented in the lower boxes.

Role of PCA as iron chelator

The *in silico* results can only support the carbon function of PCA but not its role for iron uptake, since until now the complex machinery of iron utilization in bacteria is not fully understood and hence also not covered by the *C. glutamicum* model.

To further clarify the impact of iron chelating agents like PCA we tested the alternative chelator deferoxamine (DFA) performing MSCC experiments. It was found

that *C. glutamicum* can grow on glucose CGXII medium supplemented with DFA at a growth rate of $\hat{\mu} = 0.57 \pm 0.03 \text{ h}^{-1}$ (Appendix Figure F.4). Surprisingly, reproducible growth was also observed on DFA as single carbon and energy source ($\hat{\mu} = 0.09 \pm 0.01 \text{ h}^{-1}$). DFA is a quite complex molecule and to the best of our knowledge no information on a potential degradation mechanism for this compound in any microorganism exists so far. In summary these results showed that it is very difficult to clearly differentiate between the function as carbon source and iron chelator of a substance since its uptake is likely to be accompanied by its catabolization.

With regard to this experimental restriction, we evaluated the potential iron chelating function of PCA based on our former results on PCA uptake and the iron demand for *C. glutamicum* biomass formation. Liebl *et al.* measured the total content of iron in *C. glutamicum* cells grown in CGXII medium in a range of $0.3 - 0.5 \text{ mg}_{\text{Fe}} \text{ g}_{\text{CDW}}^{-1}$ [279]. In our bioreactor experiments the amount of biomass produced until PCA depletion was estimated as $\Delta \text{CDW} \approx 0.2 \text{ g l}^{-1}$ (compare Figure 4.7A). By assuming that each mole of PCA (from an initial concentration of $195 \mu\text{M}$) transports one mole of iron into the cell, the total iron content at the end of the first growth phase would add up to $\approx 55 \text{ mg}_{\text{Fe}} \text{ g}_{\text{CDW}}^{-1}$. As this value is more than two orders of magnitude higher compared to the iron demand, we argue that the predominant function of PCA is its direct utilization as carbon and energy source.

Moreover, we showed experimentally that *C. glutamicum* grows at rates around $\mu \approx 0.45 \text{ h}^{-1}$ in PCA depleted cultures as well as in PCA-free medium (cmp. Figure 4.7A and Figure 4.8). Therefore, one might reconsider previous assumptions about the role of PCA as iron chelator and, more generally speaking, if cultivation media for *C. glutamicum* must be supplemented with iron chelating agents.

4.2.5 Conclusions

In general, biphasic growth of microorganisms is not expected when cultivated in a defined minimal medium. For cultivation of *C. glutamicum*, CGXII is the commonly used defined medium, which is assumed to contain only one growth limiting carbon source namely D-glucose.

Our results prove that protocatechuic acid is co-utilized next to glucose and provokes rapid cell division during the initial phase of cell population growth. Moreover we conclude that the channeling of carbon from PCA into the TCA-cycle is the predominant cause for elevated growth rates of *C. glutamicum* in CGXII medium. Consequently, one has to be careful in speaking of “glucose as the sole carbon and energy source” in CGXII.

In a batch cultivation started at standard inoculum ($\text{OD}_{600} \geq 0.5$) the initial amount of PCA is consumed very fast and thus no significant impact on the results of a phenotypic characterization is expected. However, the resulting growth can be significantly

influenced by the co-utilization of both substrates when *C. glutamicum* is cultivated at low cell density or grown under conditions of continuous media supply (e.g., fed-batch and chemostat cultures).

As another result we found that *C. glutamicum* grew in size with rising PCA concentrations. Changes in cell size and morphology will result in different specific cell volumes and must thereby be kept in mind when aiming for the quantification of intracellular metabolite concentrations [295].

From our data we cannot rule out a combined effect on the observed growth rates of PCA catabolism and iron transport into the cell. Nevertheless, when taking the cellular demand of iron and the comparably high PCA uptake rate into account, the effect of iron transport should be negligible.

As a variety of other benzoic acids and phenols are catabolized in the β -ketoacid pathway, we see the potential of new substrate mixtures to improve total biomass productivity. However, these co-substrates need to be purchased at reasonable costs, as industrial products of *C. glutamicum* are often bulk chemicals that achieve relatively low prices. Here, lignin hydrolyzates from lignocellulosic biomass might be a promising candidate, which contain multiple aromatic compounds like vanillic, p-coumaric as well as protocatechuic acid [296].

Combining bioreactor and microfluidic single-cell cultivation experiments, we could rapidly narrow the key factor for bi-phasic growth down to the culture supernatant. This shows the potential of the MSCC approach to validate medium compositions, as the fluid is exchanged at a high dilution rate and therefore the cells are analyzed in a quasi-stationary state without significant changes in their environment (accumulation or consumption of components). Vice versa, when performing such microfluidic experiments where the overall growth strongly depends on the starting medium composition, one carefully has to prepare the medium to prevent the loss of any essential nutrient, e.g., by precipitation.

4.3 Carbon source dependent cell size and growth of *C. glutamicum*

Single-cell based experimental results are important for the modeling of bioprocesses. This chapter demonstrates how the MSCC can successfully be used as a screening tool for growth investigations at different defined medium compositions. Most of the data presented in this chapter were part of the Master project of Johanna Heinrich.

4.3.1 Abstract

Systems Biology requires quantitative experimental data to model bioprocesses. Traditionally, the same behavior for all cells is assumed, ignoring existing cell-to-cell heterogeneity. This leads to uncertainties and systematic errors within resulting biological models. Unfortunately, single-cell characteristics such as cell volume and intracellular metabolite concentrations are hardly available. In this work, phenotypic parameters such as growth rate and morphology were systematically determined under constant environmental conditions at the single-cell level. The response of *Corynebacterium glutamicum* to more than 30 defined environmental parameters was investigated. The presented data allow to draw several conclusions on the linkage between growth rate and morphology, which is not possible under dynamically changing cultivation conditions at large-scale. The example illustrates the potential of microfluidic single-cell cultivation (MSCC) for the extraction of system biological relevant parameters for population heterogeneity studies. This lays the foundation for further characterization of different industrially used production strains, necessary for the validation and improvement of models.

4.3.2 Introduction

Systems Biology covers the understanding of complex cellular systems with application in different disciplines such as microbiology and industrial biotechnology. These approaches rely on the description of biological processes through elaborate mathematical models [260]. Therefore, quantitative data related to intracellular processes such as metabolite concentrations as well as macroscopic parameters like specific growth rate and substrate uptake rates are required. Most information for the biological process under investigation is currently derived from the application of classical molecular biological methods (bulk measurements such as cell dry weight (CDW) or optical density (OD₆₀₀)). These measurements are used to calculate single-cell volume or to obtain intracellular concentrations [231]. Such assumptions introduce systematic errors that may exceed 10% [268].

First studies have investigated cellular parameters, such as single-cell volume, using flow cytometry or microscopic techniques, in which cells undergo extensive preparation procedures. These techniques allow first insights into cell-to-cell heterogeneity of cultivation processes. Volkmer *et al.*[268] investigated the relationship between OD₆₀₀, cell concentration and cell size for *E. coli* at more than 20 different cultivation conditions. They showed that changing cultivation conditions led to different cell volume for *E. coli*.

In most of the biological cultivation processes, environmental parameters are continuously changing [13], leading to changing cellular responses over time. Cellular parameters at well-defined environmental conditions are difficult to obtain by conventional experimental methods.

Live-cell imaging [297] in combination with novel microfluidic cultivation systems can be used to monitor cells with spatio-temporal resolution at well-defined environments. Single-cell technologies are enabling comprehensive molecular and functional characterization of heterogeneous cell populations and will therefore contribute to an improved understanding in Systems Biology. Novel experimental microfluidic technologies, such as microfluidic single-cell cultivation (MSCC), offer unique techniques to acquire cellular parameters (cell size, cell area, cell growth) at the single-cell level within defined environments [22]. These MSCC conditions differ significantly from conventional cultivations. The pre-defined medium composition and concentration of the different compounds determines the cultivation condition over the complete cultivation time. Products and by-products are permanently removed while fresh nutrients are continuously supplied, ensuring constant environmental condition. Various systems for the investigation of yeast and industrially relevant bacteria strains have been developed and applied for basic growth studies and growth coupled production processes [22, 29].

In a detailed study, different single-cell cultivation technologies were used to analyze growth and cellular parameters of *C. glutamicum* wild type under complex medium conditions (Chapter 3.4). Noack and coworkers investigated the growth behavior of *C. glutamicum* cells, when bioreactor supernatant was used as a growth medium for MSCC [98, 158]. Dynamic changes in of growth rate and cell size were detected along a typical bioreactor cultivation.

In the present study the growth and morphology of *C. glutamicum* under various cultivation conditions were investigated in more detail at the single-cell level. The growth behavior of isogenic microcolonies at different carbon sources, ranging from glucose to intermediates of the tricarboxylic acid cycle (TCA) were tested (Figure 4.12). To the best of our knowledge, no systematic screening of different medium conditions on single-cell level was done before.

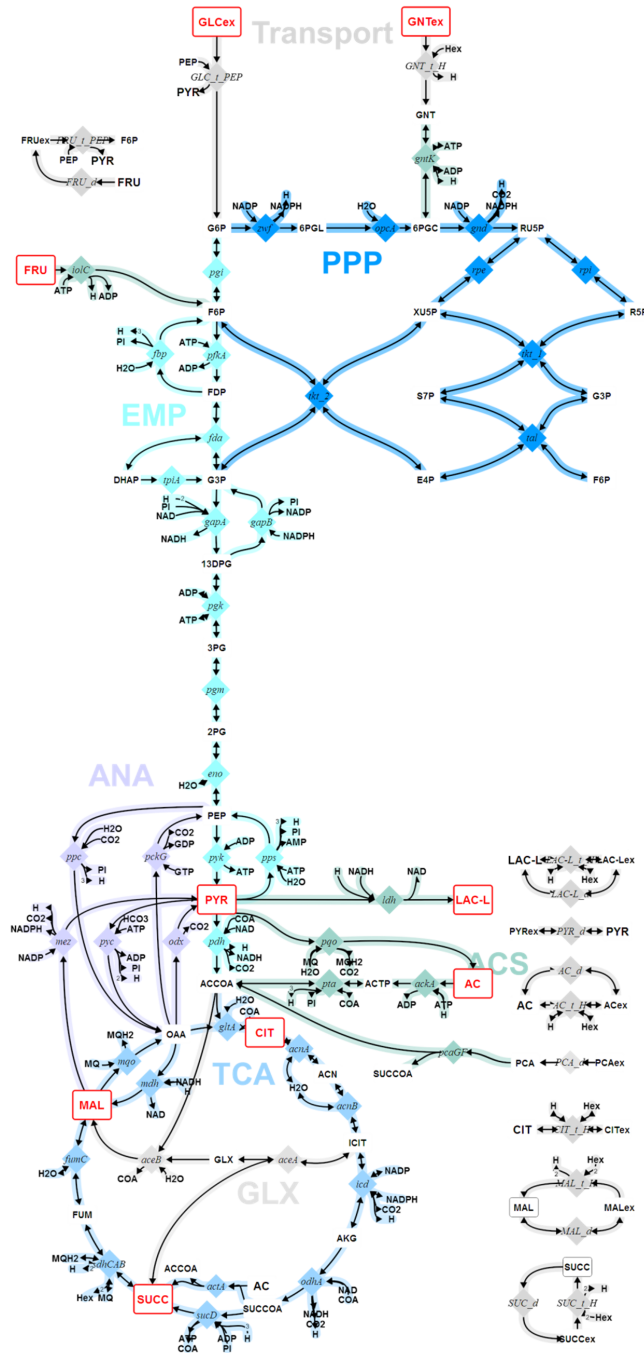


Figure 4.12: Central metabolism of *C. glutamicum* with EMP, PPP, TCA-cycle and glyoxylate-cycle. MSCC investigations were carried out for different C-sources, which are glucose, fructose, gluconate, pyruvate, lactate, acetate, citrate, malate and succinate (highlighted in red). The metabolic network was kindly provided by Elisabeth Zelle (Modeling and Simulation group, IBG-1: Biotechnology).

4.3.3 Materials and methods

Strain and storage

C. glutamicum ATCC 13032, obtained from DMSZ, was used for all experiments performed within this study. *C. glutamicum* was stored in Roti® store cryo beads at – 80 °C.

Media and sample preparation

The mineral medium used for *C. glutamicum* was CGXII consisting of (per liter) [195]: 20 g (NH₄)₂SO₄, 5 g urea, 1 g K₂HPO₄, 1 g KH₂PO₄, 0.25 g MgSO₄·7H₂O, 42 g 3-morpholinopropanesulfonic acid (MOPS), 10 mg CaCl₂·2H₂O, 10 mg FeSO₄·7H₂O, 10 mg MnSO₄·H₂O, 1 mg ZnSO₄·7H₂O, 0.2 mg CuSO₄, 0.02 mg NiCl₂·6H₂O, 0.2 mg biotin, 0.03 mg of protocatechuic acid adjusted to pH 7, and 4% glucose as carbon and energy source.

For MSCC experiments, CGXII medium was supplemented with different C-sources as presented in Table 4.2 and the amount was adjusted to achieve equal molar concentration of carbon in each medium. Either protocatechuic acid (PCA) (0.2 mM) or deferoxamine (DFA) (0.02 mM) was used as chelating agent. Furthermore, for the citrate medium, 5 mM CaCl₂ was added to increase citrate uptake [298, 299]. Whereas all precultures were done in CGXII containing MOPS, one set of MSCC cultivations was conducted without the addition of MOPS (see Results). The pH of each C-source stock solution (1M) was adjusted to pH 7 with either NaOH or HCl. Prior to use, all media were sterile filtered (0.22 μm pore size).

Table 4.2: C-sources of precultivation and MSCC experiments.

C-source	Precultivation	Microfluidic experiment
Glucose	80 mM D-glucose	27 mM D-glucose
Gluconate	80 mM D-gluconate	27 mM D-gluconate
Fructose	80 mM fructose	27 mM D-fructose
Acetate	80 mM acetate	80 mM acetate
Pyruvate	80 mM D- pyruvate	53 mM pyruvate
Lactate	20 mM D-glucose + 60 mM L-lactate	53 mM L-lactate
Citrate	40 mM D-glucose + 40 mM citrate +	27 mM citrate +
	CaCl ₂ (10 mM)	CaCl ₂ (5 mM)
Succinate	20 mM D-glucose + 60 mM succinate	40 mM succinate
Malate	20 mM D-glucose + 60 mM malate	40 mM malate

A three step precultivation procedure was performed and all cultivations were done on a rotary shaker at 120 rpm with orbital shaking at 30 °C. First, cells were cultivated in

brain heart infusion (BHI) medium containing 37.5 g L⁻¹ of BHI extract. This medium was adjusted to a pH of 7.0 with sodium hydroxide. 20 mL of sterile cultivation medium in a 100 mL baffled shake flask was inoculated with one Roti® store cryo bead. The second preculture was inoculated from the first preculture to an OD₆₀₀ of 0.1 and the medium under test. The main culture for final chip seeding was inoculated with cells from the second preculture to an OD₆₀₀ of 0.05 and harvested between 0.1 and 0.5.

Chip fabrication and design

A single-use polydimethylsiloxane (PDMS) microfluidic chip fabricated as described previously [98] was utilized to cultivate isogenic microcolonies on single-cell level. A single chip (Figure 4.13A) contained several hundred monolayer growth chambers (Figure 4.13 B-D) (dimension: 1 μm x 40 μm x 60 μm), similar to the design presented in Chapter 2.4, facilitating high-throughput single-cell analysis. Each growth chamber was interconnected by two parallel 10-fold deeper supply channels. Throughout operation, all nutrient supply channels were infused with identical volume flow rates of different medium. This resulted in solely diffusion based mass transport across the shallow cultivation chambers.

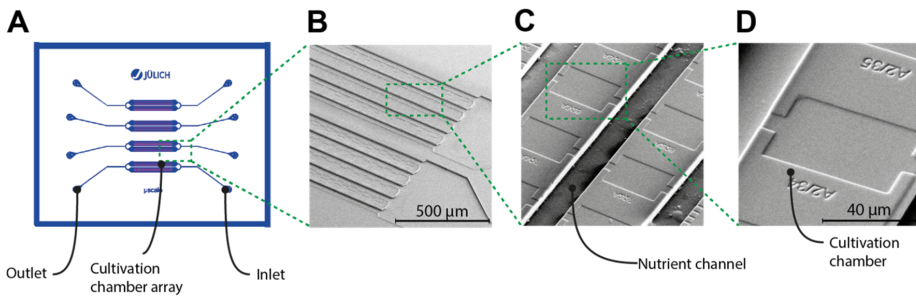


Figure 4.13: Overview of the MSCC device used in this study. (A) CAD drawing of the chip design, containing four identical cultivation arrays. (B) SEM picture of one cultivation array. Each array consists of 2 x 4 chamber arrays. (C) Cultivation chamber array separated by nutrient channels. (D) Cultivation chamber with the dimension of 1 μm x 40 μm x 60 μm.

Microfluidic cultivation

The microfluidic chip was mounted onto a motorized microscope (Nikon Eclipse Ti) equipped with an in-house developed incubator and a heated Nikon Apo TIRF 100x Oil DIC N objective (ALA OBJ-Heater, Ala Scientific Instruments, USA) for temperature control. Furthermore, the microscope was equipped with a Nikon perfect focus system compensating for thermal drift, and an ANDOR LUCA R DL604 EMCCD camera (Andor Technology plc., Belfast, UK).

The aforementioned prepared cell suspension was infused at 200 nL min⁻¹ using 1 mL disposable syringes and high precision syringe pumps (neMESYS, Cetoni, Germany) to randomly inoculate single mother cells into the growth chambers. After sufficient

individual cells were trapped, the chambers were infused with fresh medium at 100 nL min^{-1} .

Time-lapse imaging and data analysis

Phase contrast and fluorescence microscopy images of multiple colonies were captured in sequence every 10 min by automated time-lapse microscopy, thereby facilitating image based single-cell analysis with spatio-temporal resolution. Final image sequences were analyzed with the Nikon NIS Elements AR software package to determine cell number for growth rate determination and cell length distributions. Growth rates were determined according to the methods published by Grünberger *et al.* [98].

4.3.4 Results

MSCC with different C-sources were performed to determine C-source specific maximum growth rates ($\mu_{\max, C\text{-Source}}$). C-sources that are most commonly applied for *C. glutamicum* and relevant for industrial application were selected. All C-sources were tested with three different medium compositions: CGXII medium containing the desired C-source, including either (i) 3-(N-morpholino)propanesulfonic acid (MOPS) and PCA (ii), PCA or (iii) MOPS and DFA. The first set of MSCC experiments was chosen according to flask experiments, where MOPS is added as buffer component and PCA as iron chelator. In the second case, MOPS was omitted, because continuous perfusion during microfluidic cultivations does not need any additives to actively buffer changing pH-values. Products and by-products are continuously removed leading to constant pH-values. In the third case, PCA was replaced by DFA, to take into account the potential co-metabolization of the added iron chelator [158]. Appendix G.1 summarizes the different growth conditions, the resulting maximum growth rates and the number of single-cell colonies analyzed.

The growth rates obtained for each set of C-sources showed some similarities (Figure 4.14). Under glucose standard conditions (+ MOPS, + PCA) a growth rate of $\mu_{\max, \text{Glc}} = 0.59 \pm 0.03 \text{ h}^{-1}$ was obtained. The maximum growth rate without MOPS was $\mu_{\max, \text{Glc}_{-}\text{MOPS}} = 0.66 \pm 0.03 \text{ h}^{-1}$. Growth on DFA resulted in slightly lower growth rates of $\mu_{\max, \text{Glc}_{-}\text{DFA}} = 0.50 \pm 0.04 \text{ h}^{-1}$. A nearly identical growth pattern was obtained for cultivation on gluconate as C-source ($\mu_{\max, \text{GNT}} = 0.57 \pm 0.01 \text{ h}^{-1}$; $\mu_{\max, \text{GNT}_{-}\text{PCA}} = 0.60 \pm 0.03 \text{ h}^{-1}$; $\mu_{\max, \text{GNT}_{-}\text{DFA}} = 0.52 \pm 0.01 \text{ h}^{-1}$). Smaller growth rates, but with similar growth pattern (see Figure 4.14) were obtained for C-sources such as pyruvate, lactate, acetate, citrate, succinate and malate. Only the growth of fructose showed an alternate growth pattern with $\mu_{\max, \text{FRU}} = 0.24 \pm 0.05 \text{ h}^{-1}$; $\mu_{\max, \text{FRU}_{-}\text{MOPS}} = 0.51 \pm 0.02 \text{ h}^{-1}$; $\mu_{\max, \text{FRU}_{-}\text{DFA}} = 0.30 \pm 0.03 \text{ h}^{-1}$. The maximum growth rate on fructose containing MOPS were significantly reduced compared to the cultivation performed without MOPS. Most interestingly growth without a main C-source, containing either PCA or DFA resulted in growth rates $\mu_{\max, \text{PCA}} = 0.21 \pm 0.03 \text{ h}^{-1}$; $\mu_{\max, \text{PCA}_{-}\text{MOPS}} =$

$0.27 \pm 0.04 \text{ h}^{-1}$; $\mu_{\max, \text{DFA}} = 0.09 \pm 0.02 \text{ h}^{-1}$, which is in agreement with values reported before [158].

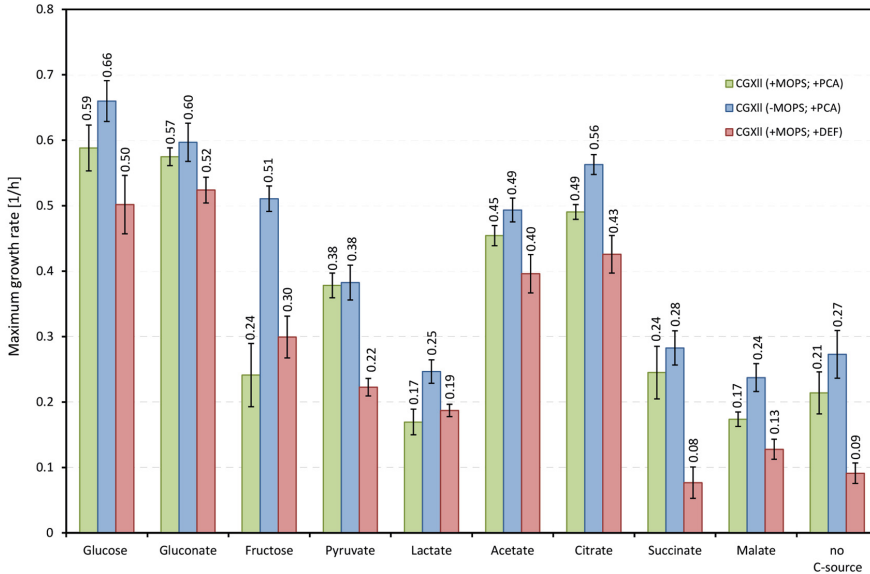


Figure 4.14: Maximum growth rates of *C. glutamicum* grown on CGXII with different C-sources and without the addition of a main C-source. Three different medium compositions are presented (CGXII (+MOPS; +PCA); CGXII (-MOPS; +PCA); CGXII (+MOPS; +DFA)).

Besides the growth rate, morphological parameters such as cell length and cross-sectional cell area are further characteristics which can vary under different environmental conditions. MSCC offers the unique possibility for direct image-based online monitoring of the influence of different media on morphology. The analysis revealed that *C. glutamicum* showed large variations within average cell sizes when growing on the different C-sources. Figure 4.15 and 4.16 display representative colonies (left) and corresponding cell size distributions (right). The corresponding individual cell size of three independent colonies was measured, as soon as the colony size has reached approximately 150 cells.

The average cell length (L_{av}) of cells grown on complex medium (here BHI) was $L_{\text{AV, BHI}} = 3.4 \pm 0.74 \mu\text{m}$. L_{av} for one experimental set with defined C-sources (-MOPS; + PCA) varied between $L_{\text{AV, AC}} = 2.98 \pm 0.62 \mu\text{m}$ for acetate to $L_{\text{AV, LAC}} = 1.61 \pm 0.37 \mu\text{m}$ for lactate. Figure 4.15E shows the cell length distribution for *C. glutamicum* cells, which were grown on standard CGXII medium for 14 hours, before stationary phase was initiated artificially by removing the main C-source (for experimental detail see [98]). This led to a similar cell length distribution as seen for cultivation without a main C-source (Figure 4.16D), but can vary depending on initial colony size and duration of the artificial stationary phase (data not shown).

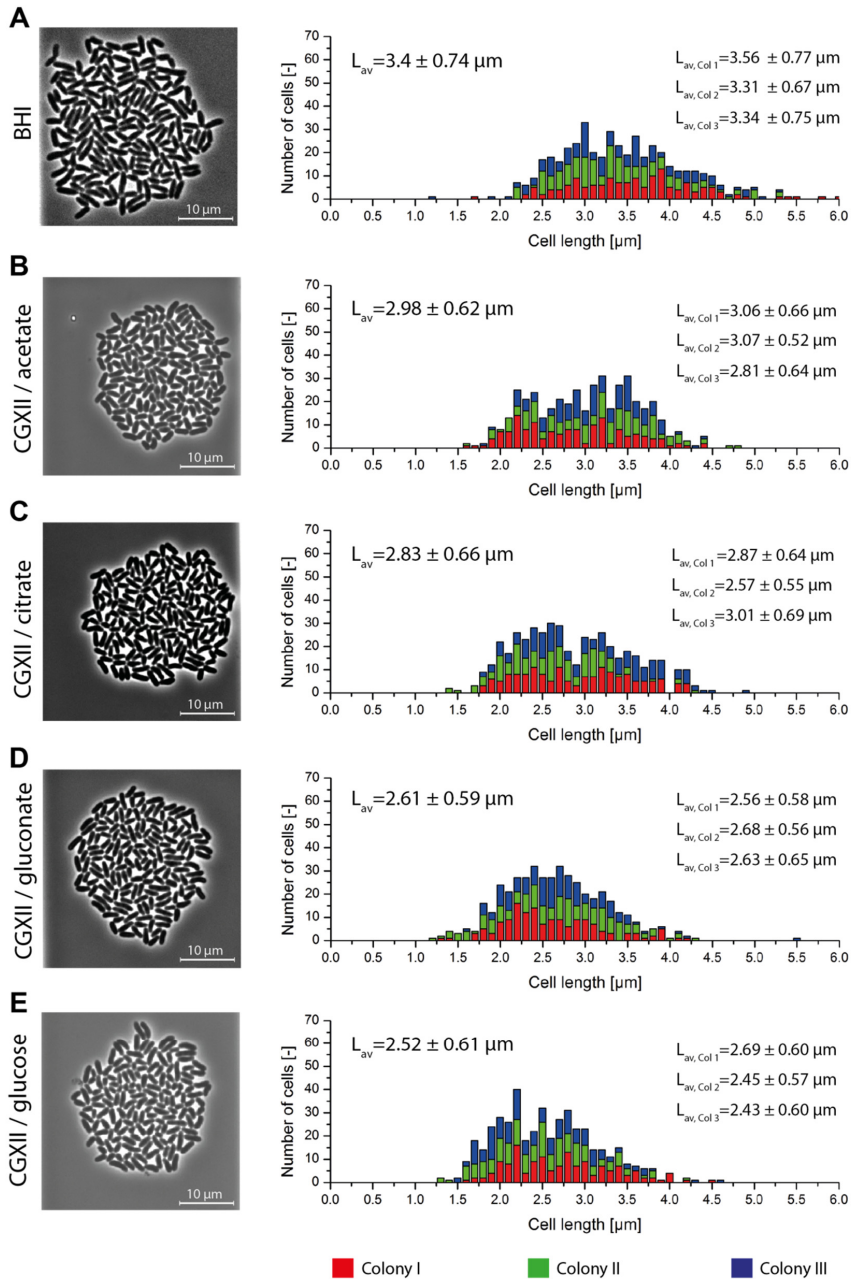


Figure 4.15: Morphology of *C. glutamicum* grown on different C- sources. (left) Microcolony of approximately 150 cells. (right) Cell size distribution of colonies cultivated with (A) BHI in contrast to CGXII (-MOPS; + PCA) and the addition of (B) acetate; (C) citrate; (D) gluconate and (E) glucose.

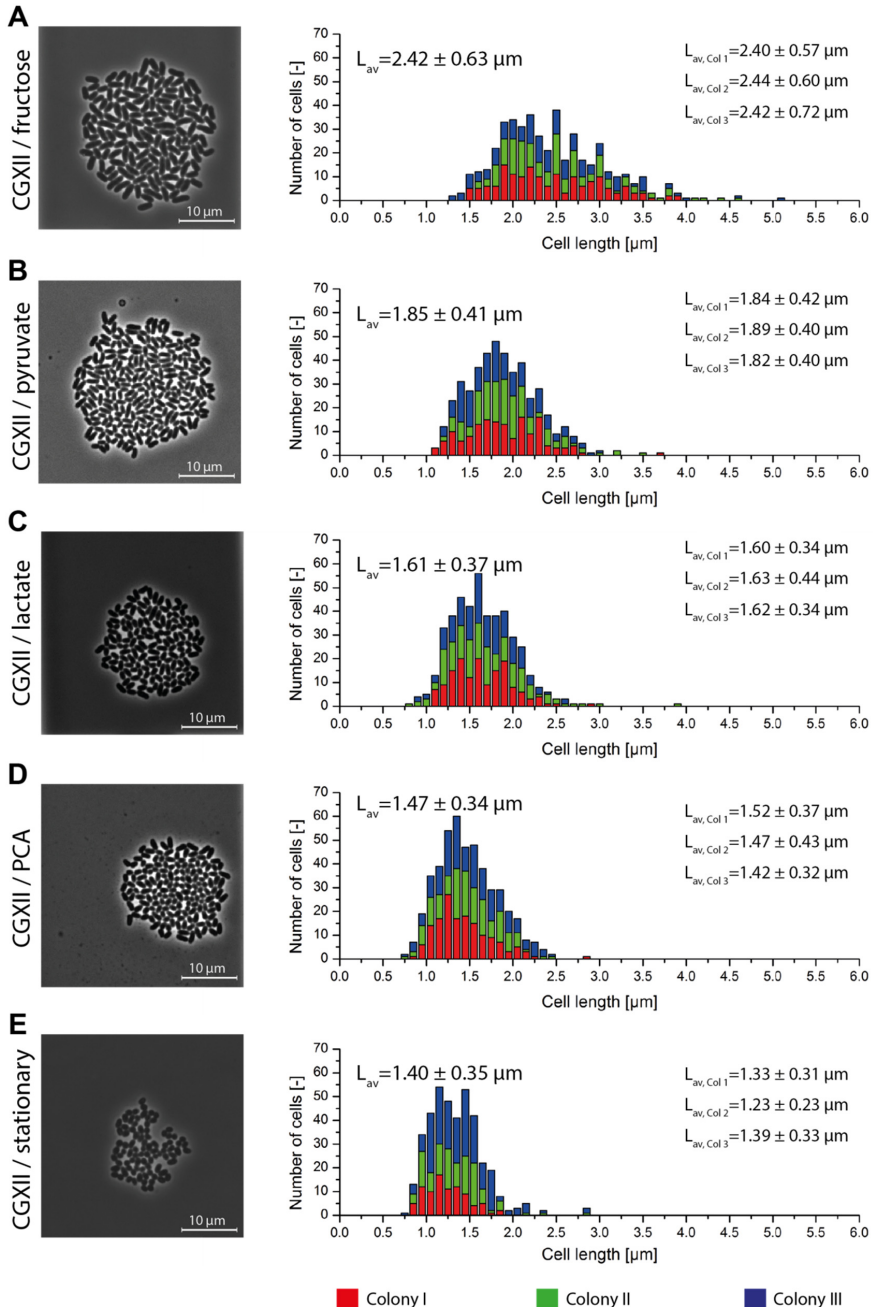


Figure 4.16: Morphology of *C. glutamicum* grown on different C-sources. (left) Microcolony of approximately 150 cells. (right) Cell size distribution of colonies cultivated with CGXII (-MOPS; + PCA) and the addition of (A) fructose, (B) pyruvate, (C) lactate, (D) no additional C- source and (E) cells under artificially induced carbon starvation.

Figure 4.17 shows the average cell length of the microcolonies versus growth rate for the set of cultivations with PCA but without MOPS. Here, a clear correlation between growth rate and average cell length was found, showing higher growth rates for larger cells. An exception is given by acetate exhibiting increased average cell length in comparison to the other C-sources under investigation.

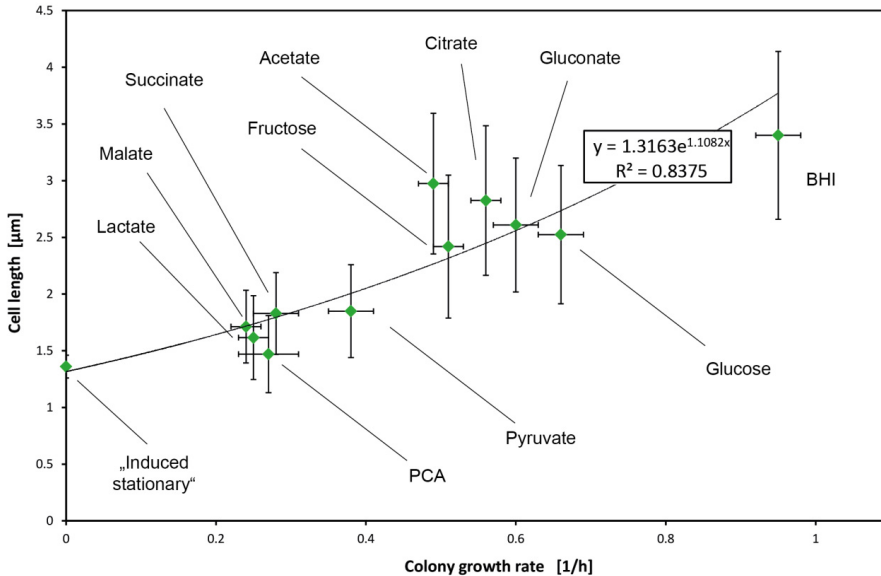


Figure 4.17: Cell length vs. maximum growth rate for microcolonies of *C. glutamicum* grown on BHI and CGXII (-MOPS +PCA) without main C-source as well as different C-sources as indicated. Mean cell length values and standard deviations were taken from the data shown in Figure 4.16 and 4.17. Mean colony growth rates and standard deviations were estimated from the respective replicates as listed in Appendix G.1.

4.3.5 Discussion

MSCC enables the analysis of cellular parameters such as growth and growth coupled processes under defined and constant environmental conditions. Pioneering studies have successfully demonstrated that this technology can be used to investigate growth [98] and production [178]. Here, a systematic screening study was performed, investigating the impact of different C-sources onto growth and morphology of *C. glutamicum*.

The experiments demonstrate that medium with and without the buffer substance MOPS as well as variations in the iron chelator (PCA vs. DFA) can have significant effect onto colony growth rates. MSCC containing MOPS revealed slightly smaller growth rates under most conditions tested. One reason could be a change in osmolality, which might affect substrate uptake rates. Whether increased growth rates in the absence of MOPS are due to a change in osmotic pressure could be tested by adding sorbitol instead of MOPS

into the cultivation medium. Another explanation could be given by assuming the uptake of MOPS and its cleavage by sulfatases [300]. In this case the resulting fragment of the molecule (4-ethyl morpholine) could accumulate in the cells and hence exert a negative influence on cell growth. In order to investigate such an effect, a mutant strain lacking sulfatases could be constructed for more detailed studies.

In the case of fructose, however, significant differences were observed for the cultivation with and without MOPS. This finding might result from interactions of the buffer compound with the transporter system for fructose, inhibiting the PTS fructose uptake and thus the overall growth rate. Increasing the fructose concentration in the MSCC experiment in combination with different buffer compounds could give further insights for this hypothesis.

In Figure 4.18, the obtained colony growth rates from MSCC experiments are compared to literature values obtained from traditional shake flask or bioreactor experiments (for an overview of literature values see Appendix G.2). Except for lactate the growth rates obtained in this study are all significantly higher [$\Delta\mu = 0.1 - 0.2 \text{ h}^{-1}$]. This finding can be explained by the co-metabolization of PCA and DFA during microfluidic cultivations [158].

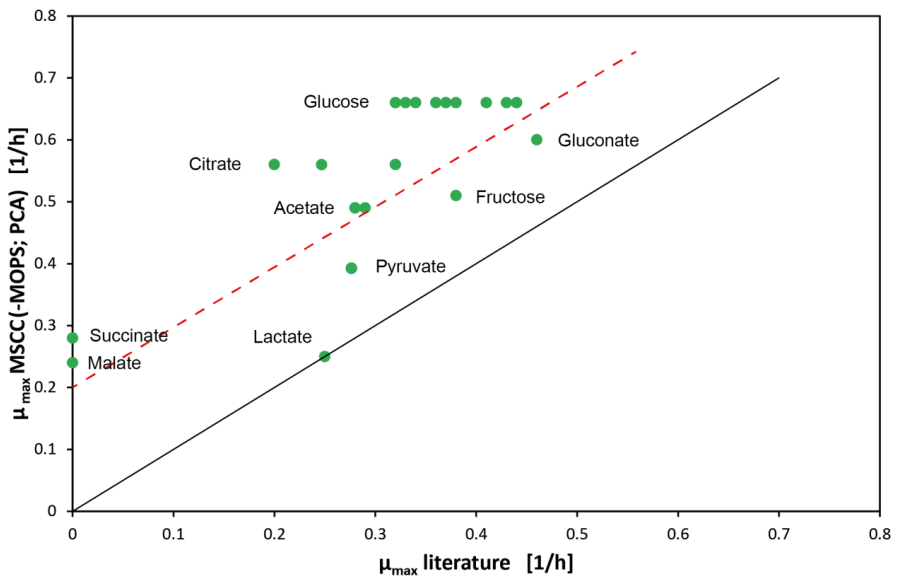


Figure 4.18: Comparison of maximum growth rates of *C. glutamicum* grown on CGXII (-MOPS; +PCA) with different C-sources in MSCC with published values obtained by typical flask and bioreactor experiments.

The lactate growth rates obtained in MSCC need further investigation. One reason for the comparable growth rates obtained in MSCC and lab-scale could be a reduced co-metabolization of PCA, leading to the metabolization of lactate as sole carbon source and

thus the same growth rates. Another explanation could be differences within the precultivation protocols. In this study, a three-step precultivation (BHI-CGXII-CGXII) was performed, compared to a two-step precultivation (BHI-CGXII) reported by Rittmann *et al.*[301]. The history of the cells can strongly determine MSCC and is currently under detailed investigations. Even higher growth rates for chemostat cultivations using lactate as sole C-source and varying CO₂ concentrations were reported ($\mu_{\max} = 0.37 - 0.47 \text{ h}^{-1}$; [212]). A comparison of the obtained results and detailed studies regarding the role of CO₂ within MSCC is not yet possible. Up to now, concentration profiles and the availability of dissolved compounds such as O₂ and CO₂ can only be estimated and need detailed characterization studies in future.

No growth on succinate and malate as sole C-source was reported for *C. glutamicum* WT before [302, 303]. This leads to the conclusion that the obtained growth on succinate and malate in this study is solely based on the metabolization of the corresponding iron chelator such as PCA or DFA.

The morphological investigations revealed a correlation between colony growth rate and average cell length (Figure 4.17). Nutrient dependent cell size control was reported for several bacteria species [304]. Currently, research focuses on the detailed understanding of bacterial growth control mechanisms leading to cell division and the regulation of the maximum cell size [305]. A more detailed analysis of the presented data regarding single-cell division time, cell-length before and after division (rather than average cell size distributions) could reveal new insights into single-cell growth and single-cell division of *C. glutamicum*. Especially, the comparison of single-cell growth rates obtained by volume increase compared to the growth rates obtained by increase in cell number might be a promising link for detailed studies on single-cell level. This remains a fascinating question for future studies.

4.3.6 Conclusion

This study represents a first important step towards the systematic determination of growth rates and cell morphology at defined medium conditions. These information is currently difficult to obtain. In this study, the “average” population behavior, rather than behavior of single-cell division events was measured. Further analysis will be needed to examine the relation between single-cell growth, division and morphological characteristics which are ultimately required. Advanced image-analysis software tools are necessary to extract the desired information.

5 Future application

This chapter summarizes ongoing research topics of single-cell analysis for bioprocess development. An overview in the field of novel single-cell designs and potential application fields is given.

5.1 Optimization of single-cell designs

The established single-cell technology has proven to be a promising tool to further understand bioprocesses. The easy adaptability of the fabrication processes allows the development of novel designs in reduced manufacturing cycle times (< 4 weeks). In addition to the presented colony-based single-cell cultivation systems such as PLBR and MGC (Chapter 3), single-cell devices were also designed to allow long-term cultivation (Chapter 5.2.1). Moreover, miniaturization was continued to enable the investigation of small bacterial subcolonies (<10 cells) (Chapter 5.2.2) and even single bacteria cells (Chapter 5.2.3), as presented in the following chapters briefly.

5.1.1 Continuous colony reactor

The PLBR and MGC systems presented in Chapter 3 allow for the cultivation of maximally 11 generations. For the long-term investigation of growth and metabolic processes the design has to be changed. For this purpose the MGC design was adapted similar to the systems presented by Mather *et al.* [95] (see also Chapter 2.1 for design principle). This modification allows for long-term monitoring of subcolonies of approximately 1000 cells depending on the chamber size and organism under investigation.

Figure 5.1A shows a SEM picture of a continuous colony reactor (CCR). The trapping principle is similar to the protocol described in Chapter 3. Cells can be cultivated for several generations (> 11 generations). Especially time-delayed induction of metabolic processes compared to cellular growth behavior can be investigated, which was limited with the original designs (PLBR and MGC). As an example, Figure 5.1B illustrates long-term growth and induction process of protein expression in *E. coli* Tuner(DE3)/pRhoHi-2-LacI-EYFP [306] with 40 μ M IPTG. In the described example, fluorescence as well as cell-to-cell heterogeneity increase over time. Systematic studies are necessary to understand the underlying reasons.

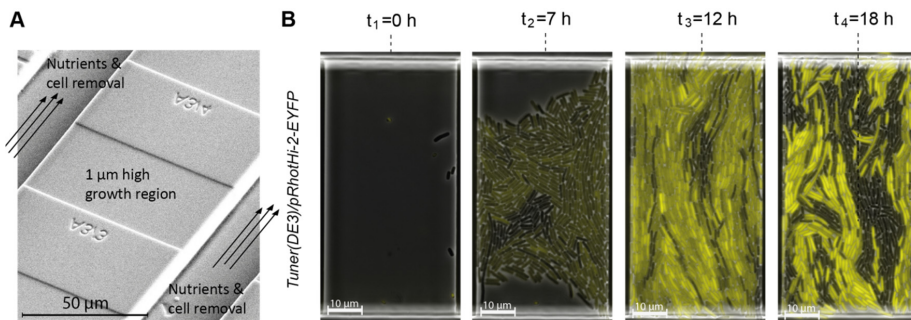


Figure 5.1: Continuous colony reactor. (A) SEM picture of an open continuous colony reactor. (B) Time-lapse series of IPTG-induced gene expression of *E. coli* Tuner(DE3)/pRhoHi-2-LacI-EYFP.

Especially for long-term studies, the CCR system offers new experimental procedures to analyze slow induction processes, adaption processes and robustness of growth. Furthermore, long-term cell-to-cell heterogeneity studies at constant and changing environmental conditions can be performed.

5.1.2 Single-cell growth channels

Single-cell growth channels are often used for long-term investigations of small sub-colonies (Chapter 2.1) [22, 154]. Figure 5.2A-C points out three special geometries developed during this thesis. All designs allow for long-term investigation (Figure 5.2D-F) of single-cell division (Figure 5.2G) as well as dynamic single-cell growth (Figure 5.2H). Design I and II are dedicated for growth investigations of single mother cells with a limited number of descendants. In contrast, in design III the descendants of a “mother cell pool” with approximately five mother cells can be investigated.

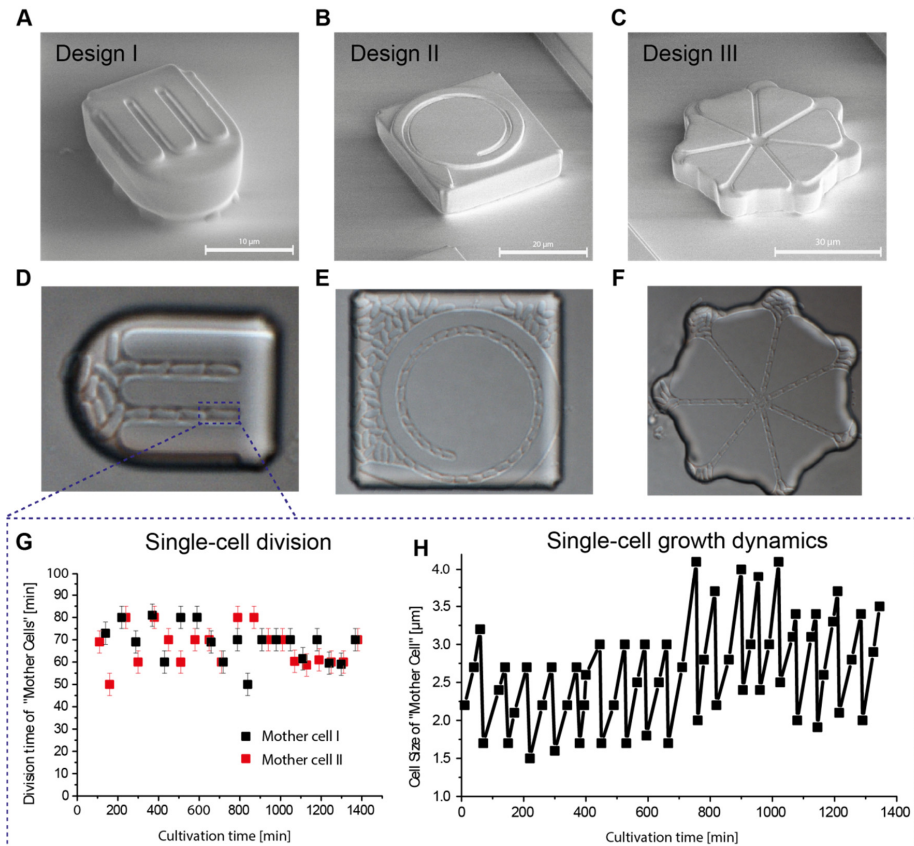


Figure 5.2: Single-cell growth channels. (A-C) SEM figures of different single-cell growth channel designs. Design I and II are dead end growth channels. In contrast, design III is an open end design. (D-F) Representative image of *C. glutamicum* ATCC 13032 cultivated in design I-III (G) Single-cell division times of *C. glutamicum* of two mother cell-lines. (H) Dynamic growth study of one “mother” cell.

As a proof of principle, single-cell growth of *C. glutamicum* ATCC 13032 was investigated in more detail in the new systems. With a doubling time of $t_d = 76 \pm 8$ min of the mother cells, the results correspond well to doubling times obtained by colony growth experiments at the single-cell level (see Chapter 3 and 4). All cultivations were performed according to protocol presented in Chapter 3.1.

5.1.3 Single-cell traps

The reactor size has to be reduced to the dimension of one single cell to perform “real” single-cell analysis. Figure 5.3A shows an SEM picture of a single-cell trap for the cultivation of single bacteria cells. Cells are trapped hydrodynamically inside the PDMS-glass barrier structure (Figure 5.3B). After trapping, the cell is continuously perfused with fresh medium. Similar to the single-cell growth channels, division and growth of single cells can be investigated (Figure 5.3C), however, completely isolated from any neighboring cells. After division, daughter cells are immediately dragged away by the fluid stream. For further information the reader is referred to [307].

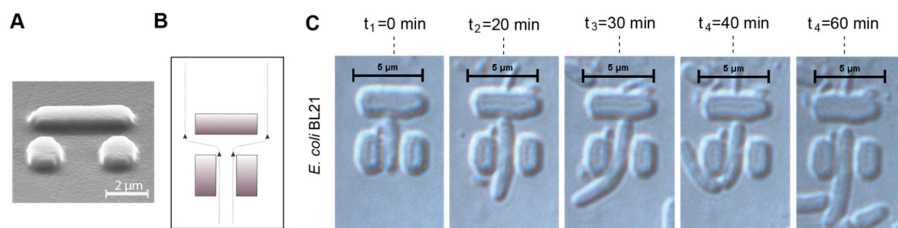


Figure 5.3: Sub μ -meter bacterial single-cell traps. (A) SEM image of one single-cell trap. (B) Flow profile of a single-cell bacteria trap. (C) Time-lapse images of a single growing *E. coli* BL21 cell, showing a division event between 30 and 40 minutes.

5.2 Further fields of application

5.2.1 Optimization for industrial platform organisms

Establishing single-cell cultivation systems as platform technology requires the ability to apply the technology to a wide range of organisms and strains. As single-cell reactors are in the same order of magnitude in respect to the size as the organisms under investigation, systems have to be adapted to the specific characteristics of the organisms such as size, morphology, morphogenesis and division mechanisms. This chapter describes ongoing efforts to transfer the developed workflow to other industrial important platform organisms.

Further bacterial systems

Bacteria species vastly differ in size and shape. Depending on the bacterial strain and cultivation parameters (see Chapter 4.3), the optimized height of the MGC and PLRB was found to be between $0.9 \mu\text{m}$ and $1.2 \mu\text{m}$. We have demonstrated the successful

trapping and cultivation of various *C. glutamicum* as well as *E. coli* strains (Chapter 3). Furthermore, the systems were tested for the cultivation of *Vibrio harveyi* ATCC 33867 (Figure 5.4A) and *Gluconobacter oxydans* subsp. *suboxydans* DSM 2343 (ATCC 621H) (Figure 5.4B) and *B. subtilis* (Figure 5.4C). Figure 5.5 shows the image sequence of one isogenic colony of each organism, respectively. The morphology and growth pattern differ significantly between the organisms and chosen cultivation parameters.

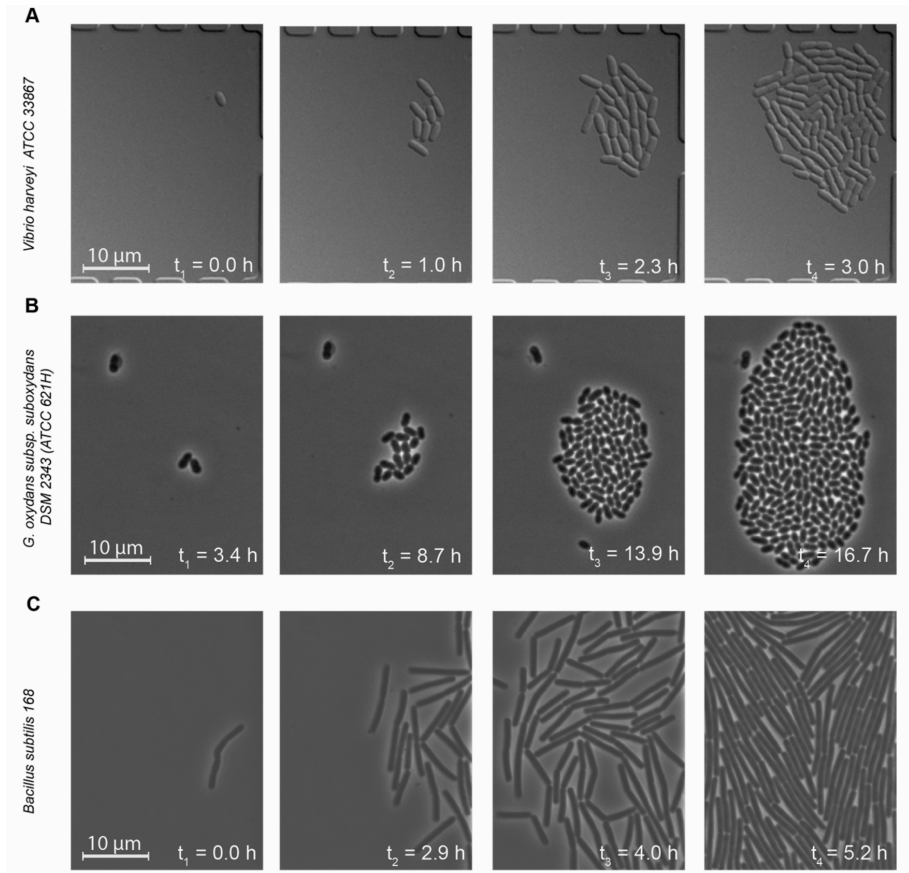


Figure 5.4: Overview of cultivated bacteria. (A) Colony growth of *Vibrio harveyi* ATCC 33867 (DSM 6904). (B) Colony growth of *G. oxydans* subsp. *suboxydans* DSM 2343 (ATCC 621H). (C) Colony growth of *B. subtilis* 168.

Single-cell studies of fungal systems

As “industrial cell factories” filamentous fungi are of biotechnological interest for various economically important metabolites used for detergents, refinement of food and beverages, as well as pharmaceutical compounds [308]. Unfortunately, the morphogenesis of filamentous microorganisms is often the bottleneck for productivity in industrial production processes [309]. A better understanding of the underlying mechanisms inducing fungal morphogenesis is required to improve bioprocesses.

Filamentous fungi significantly change their size and morphology during a lifespan in several orders of magnitude. Fungal growth starts from simple spherical spores (typically smaller than 10 μm in diameter) which then form germ tubes developing into multi-branched hyphal structures ($< 100 \mu\text{m}$). Finally, these structures can form complex mycelia, which may reach sizes up to several millimeters in diameter.

So far, only few microfluidic systems for the analysis of single fungi over the entire lifespan have been reported. The first system described by Spohr *et al.* [310] was used for the online monitoring of fungal growth. Advances in automated life-cell imaging and microfluidic fabrication techniques, led to the development of advanced microfluidic systems for fungi. Nicolau and coworkers presented a device for probing dynamic behavior of filamentous fungi in a microfluidic system [311]. Recently, a first microfluidic device for growth analysis of spores was reported focusing on the investigation of spore germination at different environmental conditions [312].

Within this project a simple microfluidic system was developed (Figure 5.5A-C) and the morphogenesis of different growth states were investigated in detail. Figure 5.6 shows an overview of application fields that were investigated, ranging from spore swelling (Figure 5.6A) to, septation (Figure 5.6B), hyphal growth (Figure 5.6C) as well as mycel and pellet formation (Figure 5.6D and E). For further information, especially the trapping and cultivation principle, the reader is referred to [313].

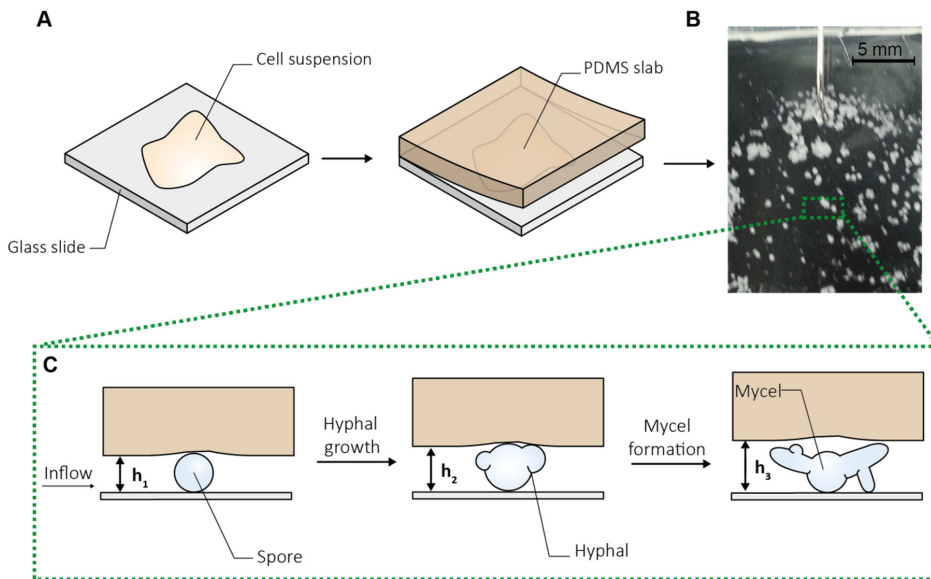


Figure 5.5: Device principle. (A) PDMS-glass microfluidic perfusion system for the cultivation of filamentous fungi. (B) Bird perspective of the chip system after several days of cultivation. (C) Schematic illustration of trapping and cultivation of a fungus in different morphological states within the flexible PDMS glass device. During growth the height partly adapts to the height (h_1 - h_3) of the organism.

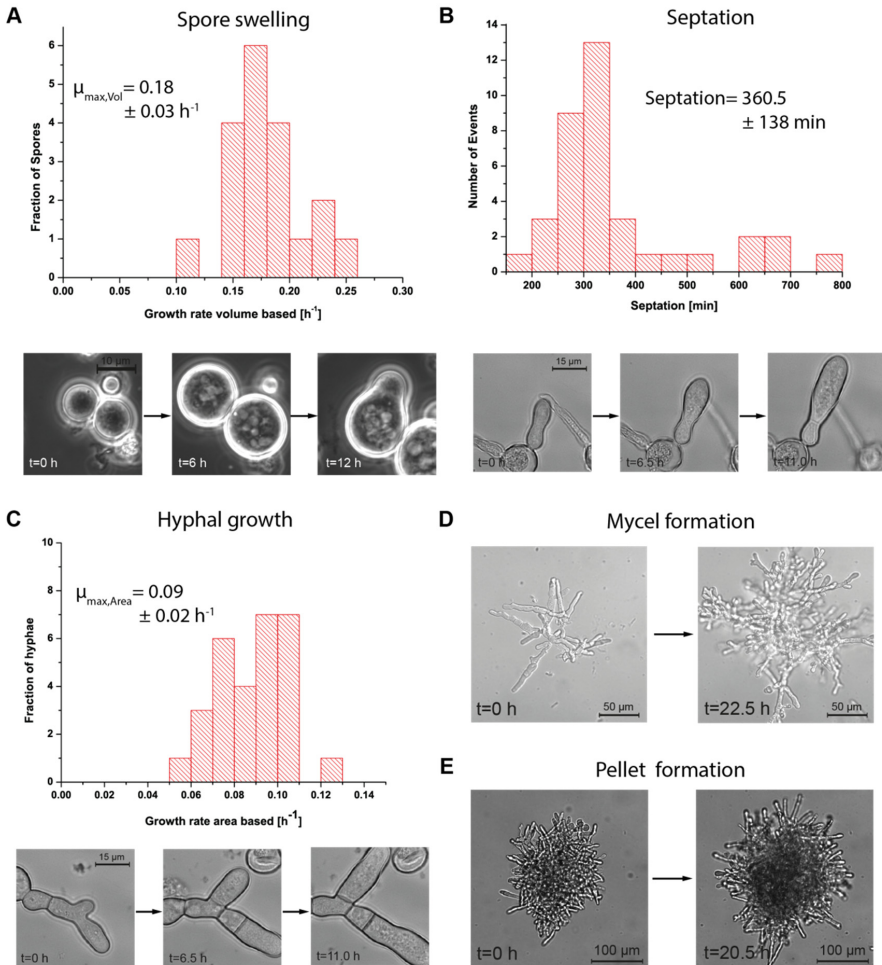


Figure 5.6: Fungal growth and morphogenesis. (A) Spore swelling, (B) septation, (C) hyphal growth, (D) mycel and (E) pellet formation.

Single-cell studies of yeast

The yeast *S. cerevisiae* is a versatile and robust cell factory for the production of various industrially important products such as ethanol [314]. Limited knowledge is available regarding growth and production heterogeneity of *S. cerevisiae* at the single-cell level. First studies revealing heterogeneity within gene expression [315] and growth [180] demonstrate the urgent need for deeper analysis. For this purpose, the CCR was optimized to match the height of approximately $3.5 \mu\text{m}$ for the trapping and cultivation of yeast cells.

As proof of principle, the growth and expression of eYFP in single *S. cerevisiae* pIE3_YFP cells expressing eYFP under control of the pGAL1-promotor was investigated. Cells were cultivated in a synthetic defined (SD) medium and eYFP

expression was induced with 2% (w/v) galactose. The SD medium consists of (per liter): 7 g yeast nitrogen base, 76 mg L-methionine, 76 mg L-histidine, 380 mg L-leucine, 1.6% (v/v) glycerine, 0.4% (v/v) DL-lactic acid. The analysis revealed significant inter- and intra-colony differences. Figure 5.7 shows two representative time-lapse series of two isogenic colonies of *S. cerevisiae* Y00000 pIE3_YFP (Kusen, unpublished). In about 50% of the colonies strong cell-to-cell heterogeneity within fluorescence protein expression was observed (Figure 5.7A), whereas the other half of the colonies showed no eYFP expression (Figure 5.7B).

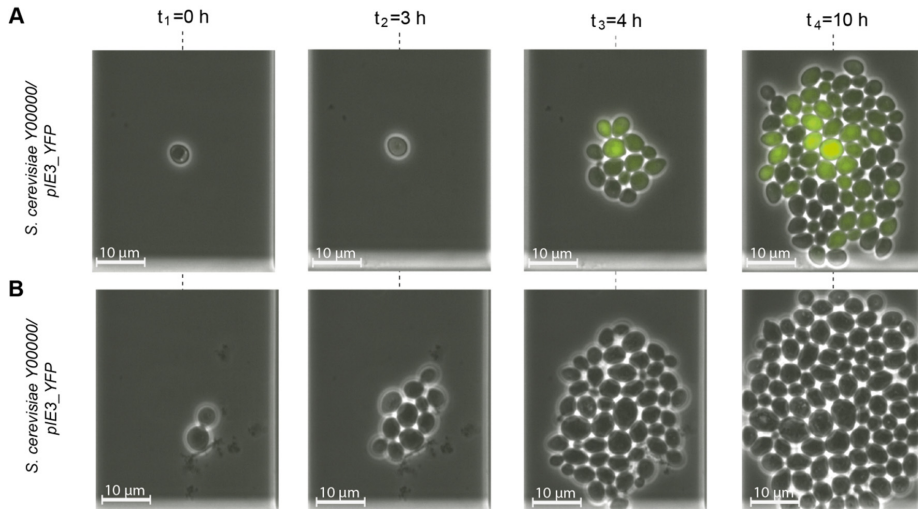


Figure 5.7: Single-cell growth of *S. cerevisiae*. (A) Time series of a yeast colony showing cell-to-cell heterogeneity within eYFP expression. (B) Time series of a yeast colony showing no eYFP expression under the same cultivation conditions as in A.

We assume that the transport and catabolism of galactose underlies strong variation and is responsible for the observed cell-to-cell heterogeneity. Further systematic studies are necessary to gain a deeper understanding.

5.2.2 Fluorescence coupled growth and production studies

Fluorescent encoded reporters can be used to investigate metabolic processes [223]. First examples, such as the investigation of stress response (Chapter 3.4), heterogeneity in phage induction (Chapter 3.1), or production of small metabolites (Chapter 3.2) were shown in this thesis. Fluorescence-based sensors are versatile tools and allow for visualization of bacterial growth and production processes even at subcellular level [177].

Inclusion bodies are commonly seen as undesirable events when microbial organisms are used to produce soluble recombinant proteins in research and industrial applications [316]. During the last years, this has changed due to a better understanding

of the inclusion body biology [317]. Microfluidics offers unique experimental proceedings to further improve the understanding of inclusion body formation during growth and production processes.

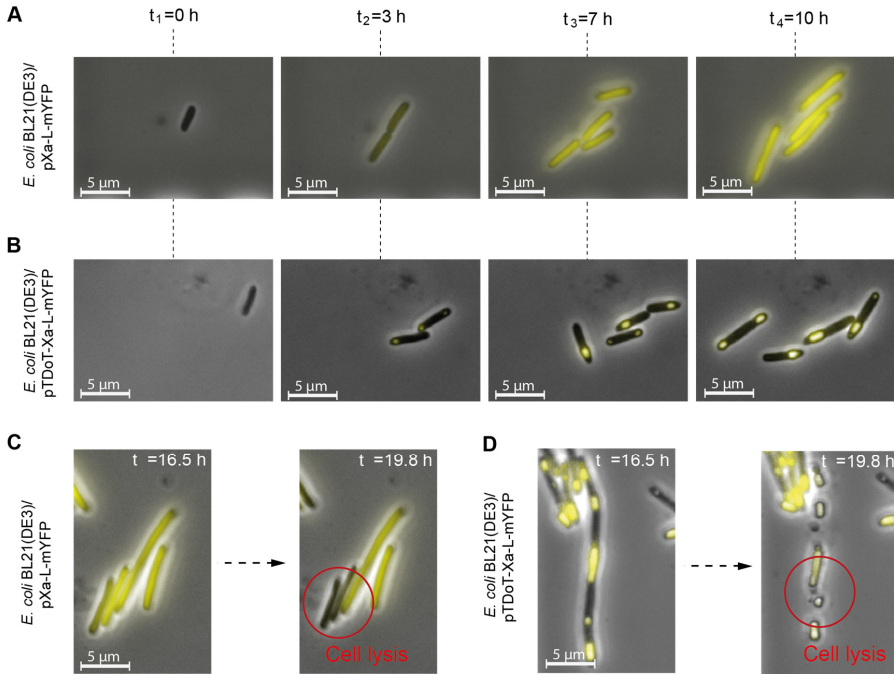


Figure 5.8: Product formation in *E. coli*. (A) Time series *E. coli* BL21(DE3)/pXa-L-mYFP showing homogenous fluorescent profiles within the cells, which indicates soluble protein formation. (B) Time series of *E. coli* BL21(DE3)/pTDoT-Xa-L-mYFP showing local fluorescent "spots" indicating inclusion body formation during growth and production process. In both cases, production was triggered by 0.5 mM IPTG. (C and D) The continuous induction leads to a decrease in growth, and even cell lysis can be observed.

We investigated the inclusion body formation of YFP-producing *E. coli* BL21(DE3). Cells were cultivated in M9 medium, supplemented with 4 g/l casamino acids (CA) and 8 g/l glycerin as carbon source. The induction was triggered by 0.5 mM IPTG directly after seeding. Figure 5.8A shows a time series of *E. coli* BL21(DE3)/pXa-L-mYFP (Diener, unpublished) producing a soluble protein. The *E. coli* BL21(DE3) strain shown in Figure 5.8B contains the pTDoT-Xa-L-mYFP plasmid (Diener, unpublished) responsible for inclusion body formation of the product. The time resolved analysis revealed inclusion body formation, located at the cell poles. In both cases growth is significantly hampered, probably due to the metabolic burden of production formation. As IPTG is continuously supplied in both cases, cells show a tendency of filamentation, probably caused by general stress response, which is rarely seen in experiments performed in conventional flasks (data not shown). Furthermore, protein overexpression even leads to cell death and finally cell lysis as pointed out in Figure 5.8C and D.

The example illustrates, that strains can be characterized regarding their product formation pattern. In future experiments, different cultivation conditions can be used to screen for optimal medium to trigger or prevent inclusion body formation. Furthermore, inclusion body formation kinetics could be investigated allowing to determine the optimal induction time of large-scale processes.

5.2.3 Co-cultivation

Co-cultivation processes are of increasing interest for bioprocess development. In combination with novel fluorescence sensors, co-cultivation or competitive growth experiments can even be used for direct strain characterization and growth performance comparison [318].

Figure 5.9 shows an example of competitive growth of *C. glutamicum* ATCC 13032 (red fluorescence) and the prophage cured *C. glutamicum* WT ATCC 13032: Δ CGP1,2,3 (yellow fluorescence). Using YFP/Crimson expression, the two strains can be discriminated and the growth behavior in the identical local environment can be investigated. Cultivation conditions were as followed: BHI preculture was used to inoculate a CGXII main culture. With growth rates of $\mu_{\max} = 0.33 \pm 0.03 \text{ h}^{-1}$ and $\mu_{\max} = 0.25 \pm 0.02 \text{ h}^{-1}$, the growth rates are significantly reduced compared to growth rates obtained from the corresponding strain without integrated fluorescence reporter. Potentially growth is influenced by the production of the fluorophore or by phototoxicity caused by the illumination during live-cell imaging. This needs to be investigated in more detail. Microfluidic experiments were performed with CGXII containing 2% (w/v) glucose und 5 μM IPTG. For further information regarding strain construction the reader is referred to [318].

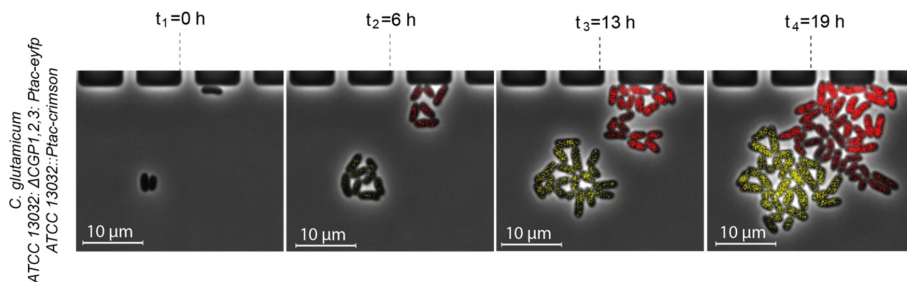


Figure 5.9: Co-cultivation of *C. glutamicum* WT. Time series showing the growth of *C. glutamicum* ATCC 13032 Δ CGP1,2,3 P_{tac} -eyfp and ATCC 13032 P_{tac} -crimson within the same cultivation chamber.

The set of experiments lays the foundation for further studies on single-cell level, for example to investigate the interactions of different bacterial strains with each other in local environments similar to the example reported by Moffitt *et al.* [115] (see Chapter 2.1).

6 Final conclusion

This chapter summarizes the achievements of the work performed within this project. Furthermore, an overall conclusion on the results is drawn. Finally, recommendations for future developments and related projects are presented.

6.1 Summary and conclusions

Microfluidic single-cell cultivation (MSCC) systems can be used to analyze and understand large-scale bioprocesses. These systems allow for innovative experiments with the potential of future impact onto bioprocess technology. In contrast to conventional technologies such as flow cytometry or agarose pad cultivation, MSCC systems provide a method for cultivation under defined environmental conditions at full spatial and temporal resolution. However, such methods were seldom applied to industrial process development yet.

In the present thesis, a detailed investigation of the application of MSCC for bioprocess development was performed. All essential fabrication steps resulting in several single-cell cultivation platforms were developed in detail. Furthermore, novel application fields were investigated.

Based on the presented results, a more detailed understanding of growth mechanisms of *C. glutamicum* was achieved (Chapter 4). Furthermore, promising application fields were presented (Chapter 5). Nevertheless, further investigations are necessary to gain a deeper understanding of *C. glutamicum* growth and production processes. This includes additional growth studies of *C. glutamicum* WT at various environmental conditions as well as selected mutant strains. For example, mutants with an interrupted or deleted PCA degradation pathway (Δ cg2621-cg2643) or deleted transport systems (Δ cg1219-cg1247) could be investigated to further understand the role of PCA metabolism and its contribution to increased growth rates.

Bacterial gene expression not only depends on specific regulatory mechanisms but also on bacterial growth [319]. MSCC allow for the cultivation at defined exponential growth rates. This enables for a deeper understanding of coupled and uncoupled growth and production processes. Additional information could be obtained by more detailed growth and production studies using fluorescence encoded metabolite sensors, as soon as the impact of metabolite sensors on cellular metabolism was further investigated [176, 320].

This work highlighted that MSCC integrated into bioprocess development is a promising tool. Especially in combination with conventional technologies, this might result in an improved understanding of production processes. A first example was shown for the detailed growth investigations of *C. glutamicum*. Ultimately, the improved knowledge should be used to scale-up the growth rate of 0.6 h^{-1} to large-scale processes. This is one of the most important steps to prove that the results obtained in single-cell cultivations provide valuable insights for bioprocess understanding and improvements.

To be able to compete with conventional methods such as flask or microtiter-based cultivation systems, microfluidic systems should be used to acquire data which is limited/impossible to obtain with conventionally used technologies. Especially for the investigation of cellular mechanisms in the early lag-phase (adaption) and late-stationary

phase (starvation and death) [239, 321], single-cell cultivation systems are promising tools. Conventional methods are limited for the analysis of these phenomena and thus MSCC could improve the understanding of these processes to a yet unknown extent.

Focus was laid on colony behavior of cells, for most of the experiments performed in the present study. Although this already permitted to get a deeper understanding of molecular mechanisms in combination with the established technologies, single-cell differences were so far often not investigated in detail. This information should be considered and analyzed in future experiments.

The impact of the trapping and cultivation method is still unknown. Filamentation of individual *C. glutamicum* (see Chapter 3.3 and 3.4) cell as well as *E. coli* (data not shown) indicate, that surface contact and or shear stress might influence physiology of cells to a yet unknown manner. Further studies are necessary to investigate the impact of the cultivation method onto cell physiology.

To perform these studies and to further integrate MSCC systems into the bioprocess development pipeline, further improvements within the microfluidic single-cell analysis workflow need to be done. The following improvements are recommended.

6.2 Recommendations

6.2.1 Platform optimization and characterization

As seen within this study, the control of the environment is of utmost importance during single-cell cultivation. Further improvements to generate defined environments and gradients would improve the applicability of the system even further. Especially the gradient generator proposed in Chapter 3.2 or integrated PDMS pumps and valves [322, 323] offers new perspectives. Promising fields are also novel materials [163] and fabrication methods [80, 164] allowing for the development of more reliable microfluidic systems, sub- μm structure fabrication, and flexibility of the device design. To enable reliable long-term cultivations as presented in Chapter 5, novel concepts in material and surface engineering need to be integrated into the microfluidic platform to prevent biofilm formation during experiments [324].

Furthermore, the “engineering aspects” of the microfluidic cultivation systems are unknown and are currently based on many assumptions. For final reactor balances and improved understanding of cellular processes, a better characterization, for example, of mass transfer rates are necessary. Figure 6.1 illustrates a schematic 2D drawing of a microchannel used in this study, consisting of a gas reservoir, the PDMS chip/membrane, a medium channel, the cell cultivation chamber/layer and an oxygen-impermeable glass substrate. Currently only limited knowledge of the key cultivation parameters is available. Following issues should therefore be investigated in more detail (Figure 6.1A):

- 1.) Gas transfer, for example of oxygen through the PDMS chip (Figure 6.1A-I) and distribution within the main channel and cultivation chamber (Figure 6.1A-II) (x and y direction)
- 2.) Nutrient exchange, waste removal and gradient formation between main channels and cultivation chambers (Figure 6.1A-III) (y direction)
- 3.) Potential leakage of media components and metabolites into the PDMS (Figure 6.1A-IV)
- 4.) Nutrient exchange and waste removal with the arrays of cultivation chambers (Figure 6.1B)
- 5.) Resulting nutrient and gas exchange and gradient formation within the growing colonies (Figure 6.1C).

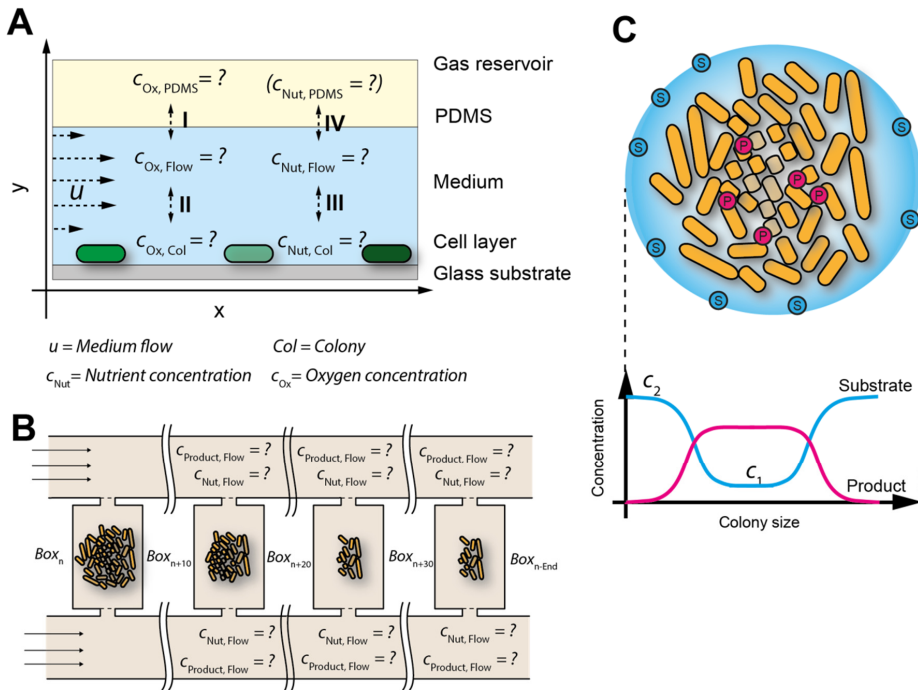


Figure 6.1: Schematic drawing of mass transport within MSCC system. (A) 2D drawing illustrating different layers for mass transport of gas and nutrients with the PDMS-glass chips. (B) Illustration of cultivation array and potential interaction between each other. (C) Illustration of a growing microcolony. Inner cells might be affected by nutrient gradients, initiating a metabolic change during cultivation.

A better characterization could be obtained by the integration of novel miniaturized sensor concepts, such as platinum sensors for the measurement of temperature [325]. Progress in novel fluorescence coupled sensors could help to get a better understanding of system parameters, for example fluorescence coupled oxygen sensors as developed by

Drepper and coworker [326] or optical sensor layers [327] could reveal potential gradients within microcolonies.

A better understanding of the mass transport within the microfluidic chip systems as well as the growing colonies is the first step towards the understanding of complex cellular processes, which are the key point for creating robust models. This offers the opportunity to improve prediction accuracy of large-scale models.

6.2.2 Cultivation parameter and analysis

Many parameters are still influencing single-cell experiments to a yet unknown manner. Especially three aspects need to be studied in more detail, to perform reproducible experiments and prevent misinterpretation of data. This includes (i) precultivation of cells, (ii) live-cell imaging parameters, and (iii) the cultivation medium:

- (i) To guarantee reproducible single-cell experiments advanced pre-cultivation protocols for microfluidic experiments need to be developed. The state of bacteria is not only determined by the present conditions, but also depends on its history [328], thus it is mandatory that the precultivation of cells used for MSCC is always performed the same. To reduce adaption time in the chip, sampling from early exponential phase is advised. As seen for *C. glutamicum* and *E. coli* in this study, cells should even be from early exponential phase ($OD_{600} = 0.1 - 0.5$) to prevent adaption of cells to early occurring environmental changes (cf. Chapter 4.2).
- (ii) Phototoxicity has long been recognized as a potential problem in live-cell imaging. Cells can be damaged by phototoxicity which results in reduced growth, morphological deformation or even death [329]. Minimal effects of phototoxicity - but sufficient to affect experimental results - have been observed for *C. glutamicum*, when imaging sampling was in the range of < 2 min or at fluorescence measurements with higher exposure time.
- (iii) In comparison to batch-cultivation systems, the outcome of an MSCC experiment is strongly determined by the initial medium composition. Therefore, quantitative growth studies should be performed using defined minimal medium compared to complex medium, which is the method of choice for most of the performed single-cell studies published.

Experimental methods and parameters should be chosen carefully [330]. Orthogonal methods should be used to validate the results. This includes either the comparison to large-scale cultivations or the use of alternative single-cell cultivation systems. Furthermore, currently different methods to determine growth rates on single-cell level are used. More detailed analysis, investigating the relationship between volumetric based growth rate and growth rate determined by cell number increase need to be performed.

6.2.3 Single-cell manipulation

Time-lapse imaging of cells is the first step towards improved understanding of cellular behavior. For future studies it is crucial to integrate active cell manipulation tools to expand the features of single-cell analysis. This includes the integration of mechanical, optical, and electrical manipulation modules. This is the basis for further investigations such as metabolite analysis of single cells, as well as to extract, separate and re-cultivate cells of interest [331, 332].

6.2.4 Automated image analysis and visualization

Currently, scientists use manual and semi-manual analysis to extract and analyze information from large amounts of microscopic image data sets. So it was done within this project. The manual approach is time consuming and subject to inter- and intra-observer variance and not applicable for large data sets anymore. Furthermore, only a fraction of the obtained information can be analyzed, hiding potential information which is not directly visible.

Image analysis has become the rate-limiting factor in realizing the full potential of dynamic cellular and molecular imaging studies. The importance of post-acquisition analysis is an emerging field and significant challenges exist in automated image-analysis (Figure 6.2). This includes accurate preprocessing of the raw image data set, segmentation, counting and tracking of cells in a large population [168]. Finally analysis and visualization is required. This is a prerequisite to analyze enough information to perform statistical analyses, instead of interpreting results from a single or few exemplary case studies which is currently still the method of choice.

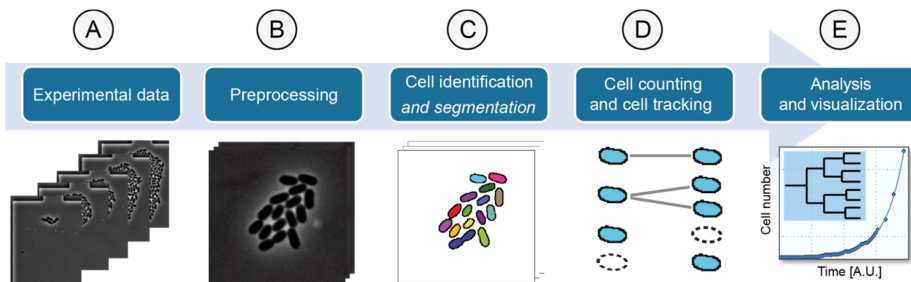


Figure 6.2: Image analysis pipeline, for the analysis of time-lapse experiments. (A) Experimental data acquisition. (B) Preprocessing of frames to remove misalignment and occurring microscopic artefacts. (C) Cell identification and segmentation of cell clusters. (D) Cell count and cell tracking of the identified objects. (E) Visualization of information (here cell number increase over time). Figure obtained and modified from S. Helfrich (Modeling and simulation group; IBG-1:Biotechnology).

6.2.5 Data management

Traditionally, experimental details such as materials, experimental parameters, observations and results are recorded in lab books. Experimentalists are able to quickly identify performed experiments and plan new ones. As the number of experiments and amount of information increases it becomes difficult to manage data and draw necessary links between performed experiments. In the worst case, experiments are unnecessarily repeated or valuable information is missed.

Ongoing parallelization of microfluidic systems and progress in the automatization within live-cell imaging, as described here, generates large image data sets. This presents additional problems because associated results cannot be written into paper-based lab-books anymore. Experimental data sets are stored on hard drives and experience confirms that they are difficult to manage and analyze.

Looking at representative experiments performed in this work, an average data amount of 40 GB of data is created. An overview of different live-cell imaging experiments and the resulting amount of data is summarized in Figure 6.3. In average, several thousands of images are taken during the time course of one experiment. The resulting data sizes are in the range of several GB (assumed image size of 3 MB (data size I)), but can exceed 100 GB when 10 MB per image is assumed (data size II). The overall generated data can easily exceed several TB per student and year. Therefore, optimal live-cell imaging parameters should to be investigated (*e.g.*, necessary positions, imaging intervals etc.), finding the best trade-off between generated data and necessary information.

Quantities of data generated per experiment

Experimental specification	Positions	Intervall	Experimental duration	Total images	Data size I	Data size II
HT live cell imaging	150	10 min	~ 15 h	~14,000	~40 GB	~140 GB
Long-term HT live cell imaging	50	10 min	> 48 h	~14,000	~40 GB	~140 GB
Fluorescence HT live cell imaging	50	15 min	< 24 h	~10,000	~30 GB	~100 GB
HR live cell imaging	1	0.025 sec	< 10 min	~2,500	~8 GB	~25 GB
HT and HR live cell imaging	50	2 min	~ 15 h	~23,000	~70 GB	~230 GB

Data size I - assumed image size of 3 MB Data size II - assumed image size of 10 MB HR= High-resolution HT= High-throughput

Figure 6.3: Quantities of data generated per experiment. Data size can vary depending on the chosen parameter such as number of positions, imaging interval and experimental duration. Furthermore image size significantly contributes to the final data size.

Successful data management requires advanced infrastructure on both, hardware and software side in future. The software should provide two kinds of features: storage management, and image analysis as described in Chapter 6.1.2. The hardware should offer adequate capacity in terms of data bandwidth, processing power and hard drive space for final storage.

The data that need to be stored and processes are manifold, ranging from raw image sequences, experimental (meta-) data, intermediate analyzed data, the processed results and final visualization. A central management solution that can deal with all types of data is advisable and indispensable for future single-cell experiments and analysis.

Alternatively, software solutions could be developed for real-time analysis of data during HT single-cell experiments (“online analytics”). This would not only reduce the amount of data generated, but would offer novel experimental features such as automated feed-back application and real-time modeling, as already demonstrated by Uhlendorf *et al.*[94].

Appendix

Appendix A

The tables presented in this Appendix contain a list of materials used for the experiments performed within this work. Additionally, a list with critical aspects, common mistakes and possible solutions for microfluidic single-cell experiments is attached.

Table A.1: Material List. This table summarizes general material, equipment and chemicals used in this work.

Name of reagent/material	Company	Catalog number
General materials		
Silicon wafer 100 mm diameter, P/BOR <100>	Si-MAT, Silicon Materials, Germany	
Photoresist SU-8 2000,5	Micro Resist Technology GmbH, Germany	
Photoresist SU-8 2010	Micro Resist Technology GmbH, Germany	
SU-8 Developer mr DEV- 600	Micro Resist Technology GmbH, Germany	
Polydimethylsiloxane (PDMS) Sylgard 184 Silicone Elastomer Kit	Dow Corning; Farnell GmbH, Germany	
Dispensing needles Precision Tips 27 GA; ID = 0.2 mm, OD = 0.42 mm	Nordson EFD Deutschland, Germany	
Glass plates D263 T eco, 30 mm x 25 mm x 0.17 mm	Schott AG, Germany	
Hole puncher AKA 5130-B-90	Harris Uni-Core	
Tubing Tygon S-54-HL, ID = 0.25 mm, OD = 0.76 mm	Saint Gobain; VWR International GmbH, Germany	
Disposable Syringes – Omnifix Spritzen BRAUN Omnifix 40 Duo, 1 mL	B. Braun Melsungen AG, Germany	552-183143
Syringes, 1mL sterile glass syringes	INNOVATIVE LABOR SYSTEME GMBH (ILS), Germany	
Chemicals		
(NH₄)₂SO₄	Carl Roth GmbH + Co. KG, Germany	
Urea	Carl Roth GmbH + Co. KG, Germany	
KH₂PO₄	Carl Roth GmbH + Co. KG, Germany	
K₂HPO₄	Carl Roth GmbH + Co. KG, Germany	

MgSO₄ x 7 H₂O	Carl Roth GmbH + Co. KG, Germany	
MOPS	Carl Roth GmbH + Co. KG, Germany	
FeSO₄ x 7 H₂O	Carl Roth GmbH + Co. KG, Germany	
MnSO₄ x H₂O	Carl Roth GmbH + Co. KG, Germany	
ZnSO₄ x 7 H₂O	Carl Roth GmbH + Co. KG, Germany	
CuSO₄	Carl Roth GmbH + Co. KG, Germany	
NiCl₂ x 6 H₂O	Carl Roth GmbH + Co. KG, Germany	
CaCl₂	Carl Roth GmbH + Co. KG, Germany	
Biotin	Carl Roth GmbH + Co. KG, Germany	
Protocatechuic acid	Carl Roth GmbH + Co. KG, Germany	
Glucose-Monohydrate	Carl Roth GmbH + Co. KG, Germany	
BHI	Becton, Dickinson	
<u>Cells</u>		
<i>Corynebacterium glutamicum</i> ATTC13032	DSMZ; Leibniz-Institut DSMZ - Deutsche Sammlung von Mikroorganismen und Zellkulturen GmbH, Germany	
<i>Escherichia coli</i> MG1655	DSMZ; Leibniz-Institut DSMZ - Deutsche Sammlung von Mikroorganismen und Zellkulturen GmbH, Germany	
<u>Equipment</u>		
Wafer Cleaner SSEC 3300	Solid State Equipment LLC	
Spin Coater SPIN150 -NPP	SPS Europe B.V.	
Mask Aligner MA-6	Karl Suess	
Hot Plate HP30A - 2	Torrey Pines Scientific	
Laboratory oven Memmert UN 200	Memmert	
Plasma Cleaner FEMTO	Diener Electronics, Germany	
neMESYS syringe pumps	Cetoni GmbH, Germany	
Magnetic stirrer CB 162	Stuart	VWR 442- 0304
Microscope Nikon Eclipse Ti	Nikon Microscopy	
Microscope incubator	Pecon GmbH, Germany	
Centrifuge minispin plus "black line"	Eppendorf	9776501
Photometer BioPhotometer plus	Eppendorf	6132000008
Shake flask shaker/incubator 3031	GFL - Gesellschaft für Labortechnik mbH, Germany	
Profilometer, Dektak 150 Stylus Profiler	Veeco	

Table A.2: Troubleshooting. This table summarizes critical aspects, common mistakes and possible solutions during experimental work.

Step	Problem	Possible reason	Solution
Wafer fabrication	Trapped air bubbles in SU-8 during soft bake	Increase of temperature to fast	Bake at 95 °C and 65 °C several times
Wafer fabrication	Disappearing and broken SU-8 structures	Not optimal fabrication procedure; mechanical stress in SU-8 structures	Optimize parameter such as baking time, exposure time
Wafer fabrication	SU-8 layers to low or high or uneven layer thickness	Problem during spin coating	Check spin-coater parameters and wafer chuck
Chip Bonding and assembly	Collapsing PLBRs	PDMS bonding parameters not optimal	Adjust power, plasma exposure time and baking time after bonding
Chip Bonding and assembly	Dirty structures and particles in the PLBRs	Chip was not properly cleaned	Apply scotch-tape for surface cleaning
Chip Bonding and assembly	Insufficient PDMS-glass bonding	Bonding parameters not optimal or insufficient cleaning	Check settings of oxygen plasma
Microfluidic Experiment	Fluid leakage	Inlet/outlet hole was not properly punched	Optimize hole punching process
Microfluidic Experiment	Many small PDMS particles during filling	Hole was not properly punched	Optimize hole punching process
Microfluidic Experiment, biological aspect	No cell growth	Solvent residue from cleaning procedure	Flush chip more extensively prior cell loading or let solvent evaporate prior bonding
Microfluidic Experiment, biological aspect	Changing growth rates	Various reasons	Check pre-culture and temperature
Microfluidic Experiment, biological aspect	Cell morphology changes during cultivation	Nutrient limitations or temperature shift	Check incubator and flow
Microfluidic Experiment, technical aspect	Drift in position during time-lapse microscopy	Temperature fluctuations	Check temperature profile prior experiments until no oscillation
Microfluidic Experiment, technical aspect	Loss of cells during cultivation	Slightly to high reactor height	Optimize reactor height
Microfluidic Experiment, technical aspect	No trapping	To low reactor height	Optimize reactor height

Appendix B

In this Appendix, supplement information to Chapter 3.2 – *Picoliter bioreactors* are given. Appendix B.1-B.3 describes additional *Material and Methods*. B.4 contains all procedures for the lab-scale cultivations.

B.1: Bacteria strains

For proof of principle growth experiments, *E. coli* BL21 and *C. glutamicum* ATCC13032 was used. For reactor comparison studies, *C. glutamicum* DM1800 was used. For combined growth and L-arginine production studies, *C. glutamicum* wild type strain was transformed with plasmid pSenLysTKP-argB(fbr), containing a feedback resistant mutant of *argB* (coding for N-acetylglutamate kinase) and a metabolite sensor cassette, enabling EYFP expression in response to enhanced intracellular L-arginine concentration [33].

B.2: Media and biological sample preparation

BHI medium (Becton-Dickinson/237500-Bacto Brain Heart Infusion) was used for *C. glutamicum* to prepare starter cultures for microfluidic experiments. *E. coli* BL 21 starter cultures were cultured in LB medium, containing 5 g yeast extract, 10 g peptone and 10 g NaCl per liter.

20 mL of sterile BHI medium (autoclaved and sterile filtered to prevent particles) were transferred into 100 mL culture flasks (Erlenmeyer shape, triple battled) and was inoculated with a single colony of *C. glutamicum* from BHI agar plates, containing no antibiotics. These cultures were incubated on an Incubator (Inforce) at 150 rpm at 30 °C 10 hours. New culture using CGXII was started and cells were resuspended in new medium and transferred to the new culture starting optical density of 0.05 for adaption to the medium overnight. This step was done, that *C. glutamicum* could adapt to the new medium. The main culture was harvested in exponential phase (OD ~ 1-4) and washed with fresh sterile filtered medium prior to inoculation of the microfluidic system. For *E. coli* the same procedure was applied, using LB- medium for preculture. *E. coli* was directly transferred to chip after the first preculture.

B.3: Microfluidic experiments

For proof of principle experiments with *E. coli* BL21 LB medium was used. The chip was flushed with Pluronic F-127 (Invitrogen) for 2 hours before culturing *E. coli*, to prevent undesired adhesion. No anti-adhesion additive was added to the medium. For microfluidic experiments with *C. glutamicum* ATCC13032 and DM 1800 CGXII medium [195] was used. The medium was adjusted to pH of 7.0 with sodium hydroxide. For artificial stationary phase CGXII medium without glucose was used. For microfluidic experiments with *C. glutamicum* the microfluidic chip was not coated before. Again, medium was not supplemented with any anti-adhesion detergence, to prevent unknown

interaction between detergent and colony growth. No active biofilm control was necessary, since experiments were finished before wall attachment and growth leads to formation of microcolonies that clog fluidic channels in average after 24-48 hours.

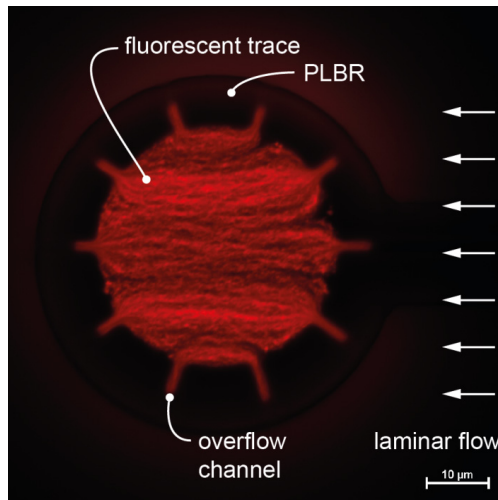


Figure B.1: Image showing the flow pattern of fluorescently labeled latex beads with 200nm diameter through a single PLBR. The PLBR chip was coated with a 0.1% Fluoronic F68 solution for 60 minutes at a total flow-rate of 700 nL/min to minimize bead adhesion to the chip material. Red fluorescent latex beads (FluoSpheres® Carboxylate-Modified Microspheres, 0.2 µm, Red Fluorescent (580/605) 2% Solids, Molecular Probes) were diluted 100 times and flushed through the microfluidic device at 10 nL/min per PLBR channel each. Image exposure time was 10 s. Fluorescent bead trajectories clearly show flow through the PLBR device.

B.4: Lab-scale cultivation

Cultivation conditions

For cultivation of *C. glutamicum* DM 1800 the defined minimal medium CGXII [195] was used containing per liter of distilled water: 20 g $(\text{NH}_4)_2\text{SO}_4$, 1 g K_2HPO_4 , 1 g KH_2PO_4 , 5 g Urea, 10 g D-glucose, 13.25 mg $\text{CaCl}_2 \cdot 2\text{H}_2\text{O}$, 0.25 g $\text{MgSO}_4 \cdot 7\text{H}_2\text{O}$, 1 mg $\text{FeSO}_4 \cdot 7\text{H}_2\text{O}$, 1 mg $\text{MnSO}_4 \cdot \text{H}_2\text{O}$, 0.02 mg $\text{NiCl}_2 \cdot 6\text{H}_2\text{O}$, 0.313 mg $\text{CuSO}_4 \cdot 5\text{H}_2\text{O}$, 1 mg $\text{ZnSO}_4 \cdot 7\text{H}_2\text{O}$. The medium was adjusted to pH of 7.0 with sodium hydroxide. The medium contained additionally 3 mL of 10% (v/v) AF 204 (Sigma) and 1 mL of a 0.2 g/L biotin stock solution per liter which were added after sterilization. Cryocultures of the two strains were stored at -80°C in CGXII medium containing 20% (v/v) glycerol.

For batch-cultivation a 1.5 L bioreactor (DASGIP AG, Jülich) with a working volume of 1 L was prepared and inoculated directly with 2 mL of cryoculture. To increase reproducibility no pre-cultivation was performed. All cultivations were carried out at constant air flow (1 vvm) and 30°C . The pH was maintained at 7.0 by adding 4 M NaOH and 4 M HCl, respectively. Aerobic process conditions (dissolved oxygen > 30%) were ensured via stirrer speed control (200-1200 rpm). During cultivation dissolved oxygen (Visiferm DO 225, Hamilton), pH (405-DPAS-SC-K80/225, Mettler Toledo) and exhaust

gas concentrations of carbon dioxide and oxygen (GA4, DASGIP AG Jülich) were measured online.

Offline-Analysis

Cell number and size were monitored offline via coulter counter equipped with a 45 μm capillary (CASY® 1 Modell TT, Roche Diagnostics). For analysis a cell suspension volume of 2 mL was sucked into a 5 mL plastic syringe and dropped to withdrawal the dead volume of the sample port. After that 1 mL was sucked into a fresh 2 mL plastic syringe. The cell suspension was diluted with isotonic dilution liquid (CASY®ton, Roche Diagnostics) into the detection range of the coulter counter and measured as triplicates.

Appendix C

The presented method in this chapter was established in the second year of this project and describe a rapid filling procedure for the cultivation chambers presented in Chapter 3.3. The final implementation was performed in close cooperation with Christopher Probst (Microscale bioengineering group; IBG-1: Biotechnology).

C.1: Single-cell inoculation

We found that by injecting a small air bubble into the main channels drastically improves the amount of trapped cells in the growth sites. A similar approach was suggested by He *et al.* [333] for the trapping of embryonic body cells, but was not characterized in detail. Figure C.1 describes the air-assisted cell loading procedure. Figure C.1-A illustrates the flow profile prior to the injection of the air bubble and during cultivation. Following, the air bubble is injected through the main channel and hindered to pass the smaller sub channels (Figure C.1-B). The temporal blockage of several sub channels forces the flow through the growth sites and hence leading to a spontaneous confinement of cells (Figure C.1-C). Applying a sufficient high pressure on the liquid leads to diffusion of the air bubble through the PDMS surface until it is completely vanished. During dissipation of the air-bubble, the parallelized MGC arrays are filled successively.

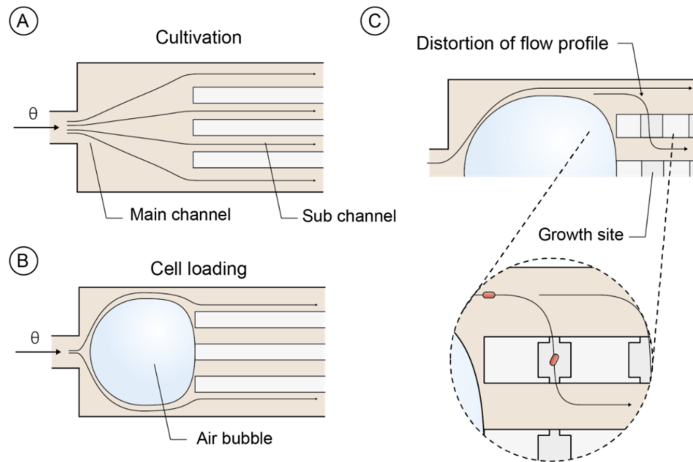


Figure C.1: Illustration of air bubble cell loading for single-cell analysis of isogenic bacterial microcolonies in a high-throughput manner. (A) Flow profile before air bubble injection and during cultivation. (B) Air bubble is injected into the main channel and hindered to pass the sub channels. This leads to a change in the flow pattern. (C) Temporal blockage of multiple sub channels forces the flow through the MGCs, leading to spontaneous confinement of cells.

Air bubble injection and removal

First, the necessary diffusion time of the air-bubble was characterized for different pressure levels, namely 200, 300, 400 and 500 mbar (Figure C.2). Figure C.2 shows a time-lapse image series of an air bubble being injected and removed by a constantly applied pressure (p) of 300 mbar. The air bubble is prevented by the capillary force induced pressure (p_c) of the sub channels to be pushed through. For pressure higher than 500 mbar, the air bubble is pushed through the sub channels and no filling of the growth areas is obtained.

It can be seen from Figure C.2-B that a pressure of more than 200 mbar is needed to remove the air bubble. Increasing the pressure above 200 mbar revealed a constant reduction of the air bubble area over time. Repeated experiments ($N=3$) at different pressure levels revealed a reduction of the necessary time to remove the air bubble with 100 seconds at 300 mbar, 60 seconds at 400 mbar and 50 seconds at 500 mbar. Further, the initial area of the air bubble was smaller with an increased pressure.

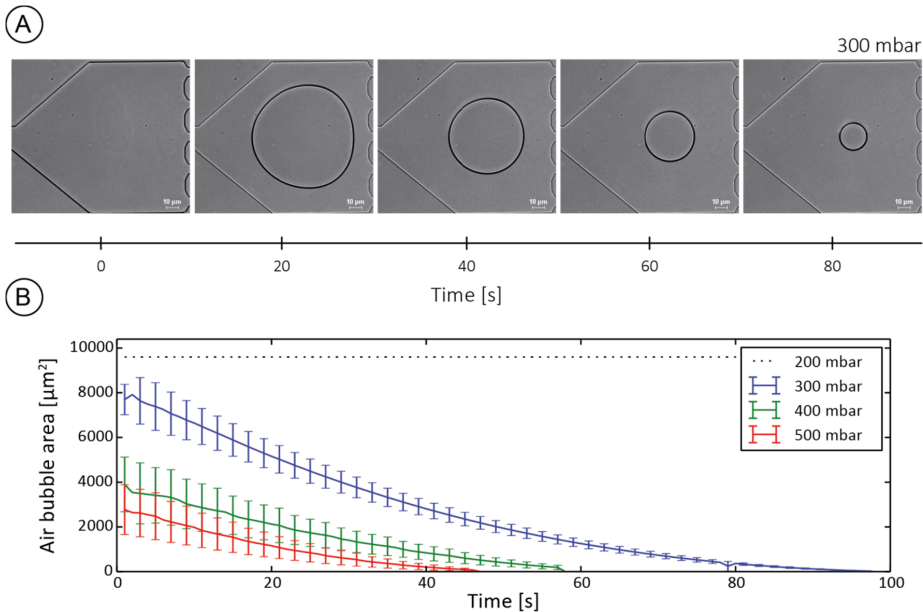


Figure C.2: Characterization of air bubble injection and removal in the microfluidic main channel. (A) Time-lapse images of air bubble injection and removal at 300 mbar. (B) Time needed for complete removal of air bubble, using pressure levels from 200 mbar to 500 mbar.

Characterization of air bubble assisted cell loading

The flow within the growth sites was further characterized during the air bubble assisted cell loading. Fluorescence labeled particles were used to visualize the flow before and after the injection of the air bubble. Figure C.3-A shows the flow profile before the

air bubble is injected into the main channel. The flow profile is equally distributed leading to the same flow rate within each of the sub channels. After the air bubble is injected (Figure C.3-B) the partial blockage of the sub channels leads to different flow profiles. At the illustrated time point, the flow rate in sub channel 3 is smaller than in sub channels 1, 2, 4 and 5. This forces the flow temporally through the growth sites in between the sub channels 2-4.

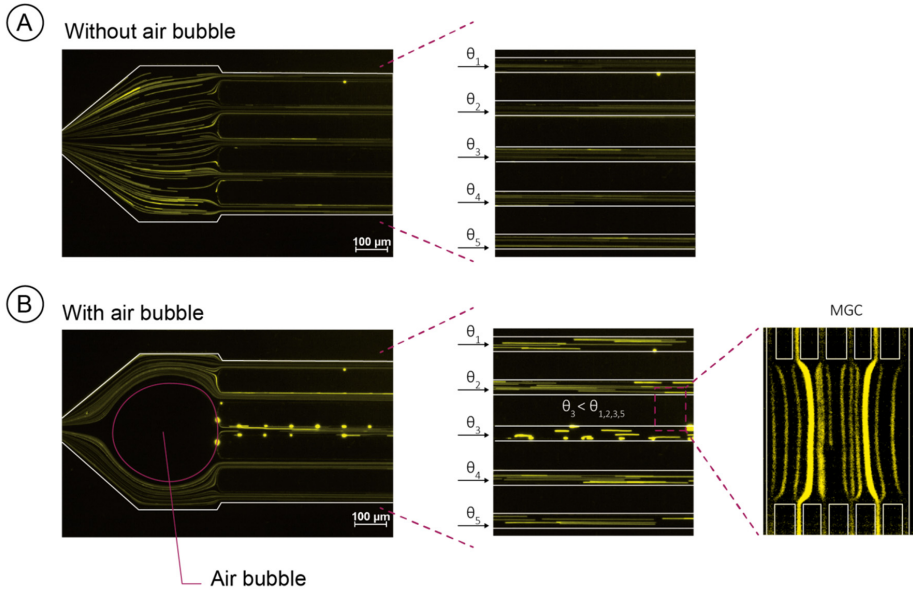


Figure C.3: Characterization of the flow profile before and during cell loading. (A) Flow profile before the injection of the air-bubble. (B) Flow profile after injection of air bubble. The right side visualizes the different flow speeds for this particular time point and the flow profile within the MGC.

C.2: CFD simulations

The data presented in Appendix C.2 contain supplement information regarding the characterization and application of the cultivation chambers described in Chapter 3.3.

Model geometry and mesh

The model geometry of the MGC is generated in COMSOL as 3D model (Figure C.4). For the given geometry a structured hexahedron mesh is generated in COMSOL.

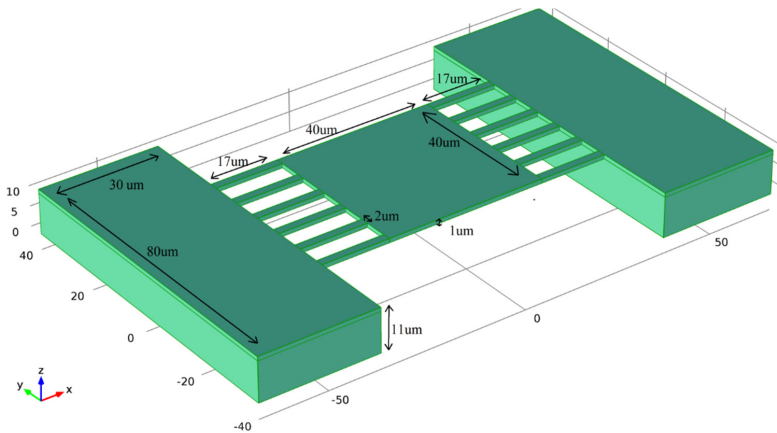


Figure C.4: COMSOL model geometry of the MGC used for the flow profile simulations as well as glucose distribution and metabolite production within this study.

Mathematical equations and definitions

Flowing fluid

The incompressible stationary flow was modeled by the Navier-Stokes equation (Equation C.1 and C.2).

$$\rho(\vec{u} \cdot \nabla)\vec{u} = \nabla \cdot [-pI + \mu(\nabla \vec{u} + (\nabla \vec{u})^T)] \quad (C.1)$$

$$\nabla \cdot \vec{u} = 0 \quad (C.2)$$

With \vec{u} : velocity, p : pressure, $\eta = 0.0012 \text{ Pa s}$: dynamic viscosity of 4% water-glucose solution; $\rho = 1016.5 \text{ kg m}^{-3}$: fluid density of 4% water-glucose solution. The velocity on the inlet was given with 0.002 ms^{-1} which corresponds to a volumetric flow rate of 40 nL min^{-1} .

Glucose mass transport

The transport of glucose (dc/dt) was represented by the time depended convection-diffusion equation (Equation C3).

$$\frac{\partial c}{\partial t} = -\vec{u} \cdot \nabla c + \nabla \cdot (D \nabla c) \quad (C.3)$$

with c : molecule concentration of glucose, $D = 0.67 \cdot 10^{-9} m^2 s^{-1}$: diffusion coefficient of glucose, u : velocity field given by the solved Navier Stokes equation.

Equation C.3 was defined for the outer and inner channels in the geometry for the glucose transport. The glucose inflow is equivalent to the inlet of the stationary flow. The starting concentration of glucose was defined as 2444 mol m^{-3} , which corresponds to the solution concentration of 44 g/l .

Uptake rate glucose

Next to the mass transport in the MGC the uptake and the product and by-product formation is modeled. As an example, the simulation was performed for a MGC loaded with 400 cells which a uniformly distributed.

To date no reliable single-cell data are available. The following estimations are made for *C. glutamicum* based on data obtained from bulk measurements.

Assumption I	1 cell has an uptake rate of:	81 nMol/(mgDW·min)
Assumption II	1 g/l BTM equals at least:	$4 \cdot 10^9$ cells
→	Uptake rate per cell	$3.375E-16 \text{ mol} \cdot \text{sec}^{-1}$
→	Uptake rate per 400 cells	$1.35E-13 \text{ mol} \cdot \text{sec}^{-1}$
→	Related to the volume of the chamber: uptake rate corresponds to	$84.4 \text{ mol}/(\text{sec} \cdot \text{m}^3)$

The uptake rate for glucose was modeled as reaction in the convection-diffusion equation for the glucose transport as follows:

$$\frac{\partial c}{\partial t} = -\vec{u} \cdot \nabla c + D \cdot \Delta c + R_{gluc} \quad (C.4)$$

$$\frac{\partial c}{\partial t} = -\vec{u} \cdot \nabla c + D \cdot \Delta c - 84.4 \left[\frac{\text{mol}}{\text{m}^3 \cdot \text{s}} \right] \quad (C.5)$$

Product and by-product production and mass transport

For *C. glutamicum* the following is assumed:

One cell has a production rate of secreted products and by-products of $0.5 \cdot R_{gluc}$. For the modeling of the production and the transport in MGC, Equation C.6 is used:

$$\frac{\partial c}{\partial t} = -\vec{u} \cdot \nabla c_2 + D \cdot \Delta c + R_{Product} \quad (C.6)$$

$$\frac{\partial c}{\partial t} = -\vec{u} \cdot \nabla c_2 + D \cdot \Delta c - 0.5 \cdot 84.4 \left[\frac{mol}{m^3 \cdot s} \right] \quad (C.7)$$

with c_2 : molecule concentration of secreted metabolites, D: diffusion coefficient of metabolites (here for acetate as representative) $= 1.5 \cdot 10^{-9} m^2 s^{-1}$, U = velocity field given by the solved Navier-Stokes equation. For the modeling of the metabolite transport outside of the MGC the same equation without the reaction term is defined.

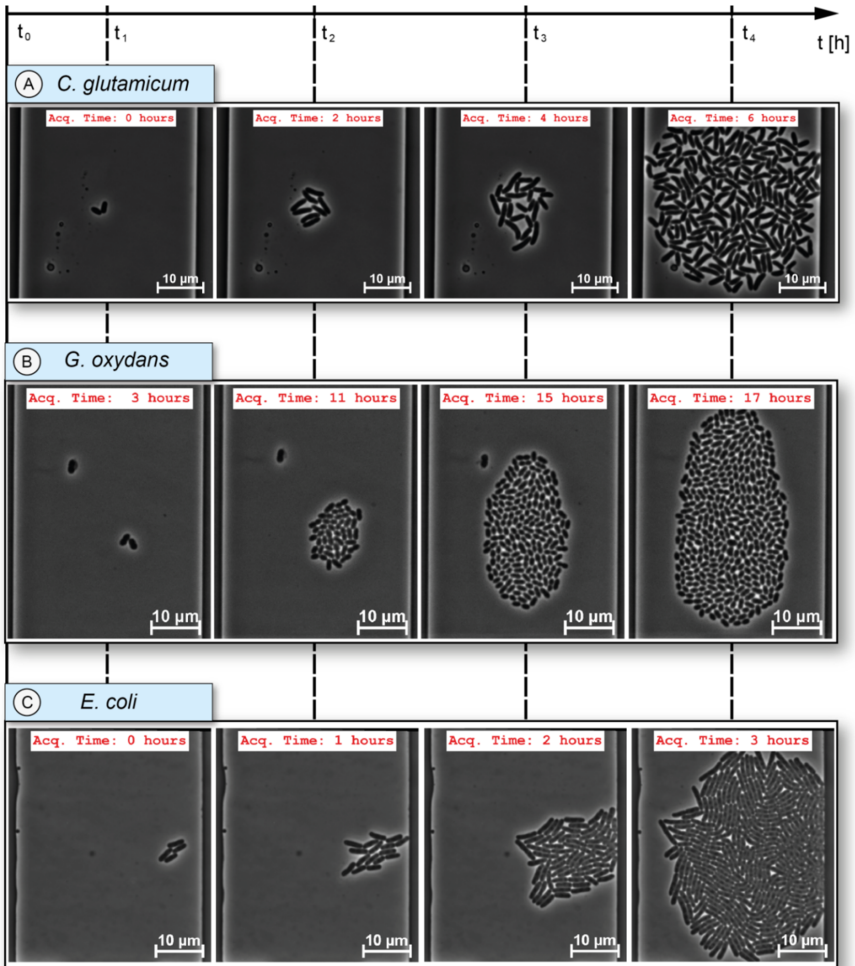


Figure C.5: Time-lapse experiments of different organisms in MGCs. Microcolony growth can be followed over time, until chambers are filled. (A) *C. glutamicum* colony. (B) *G. oxydans* colony. (C) *E. coli* MG 1655 colony. All cells were grown in complex medium.

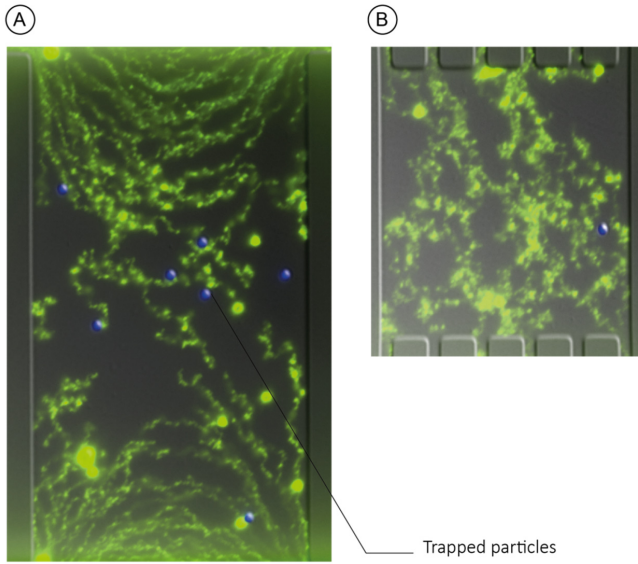


Figure C.6: Flow profile of monolayer cultivation systems (A) Open MGC. Flow tracer studies visualize convective flow at the upper and lower boarder of the chambers, leading to potential loss of cells during cultivation. (B) Flow profile of the MGC showing mainly diffusive behavior of particles within the chamber.

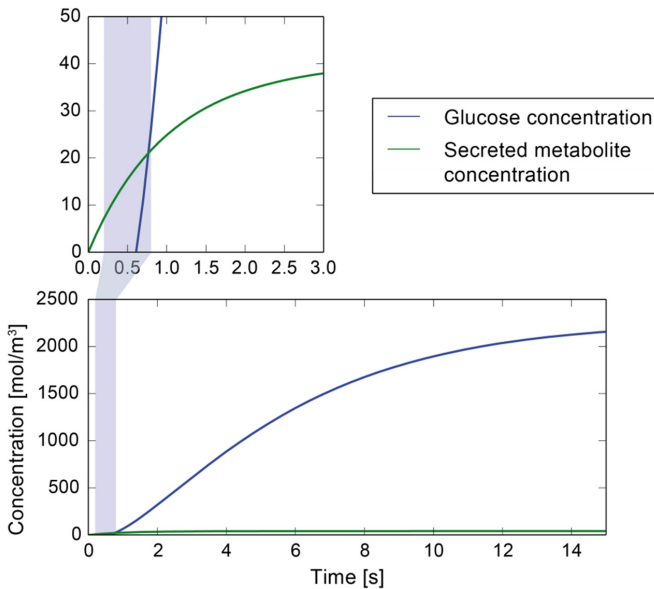


Figure C.7: Simulated steady state cultivation conditions for a colony of 400 cells. Secreted metabolites are continuously removed, leading to low metabolite concentration ($< 50 \text{ mol/m}^3$) compared to the substrate concentration. For the chosen simulation parameters see Appendix C.1.

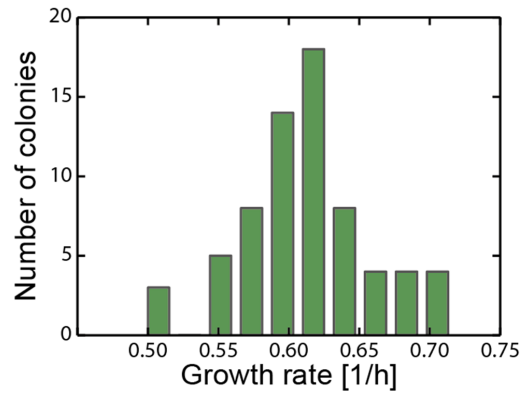


Figure C.8: Growth rate histogram for the cultivation of *C. glutamicum* under standard cultivation conditions.

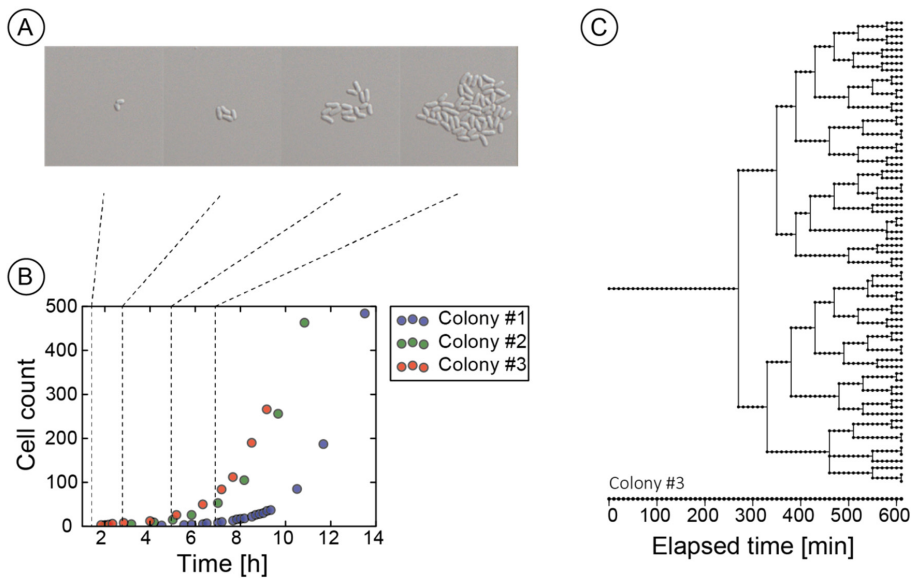


Figure C.9: Lineage tree of a *C. glutamicum* under standard cultivation conditions. In this case the mother cells shows a significant increased lag-phase compared to typical colonies obtained within the experiments performed in this work.

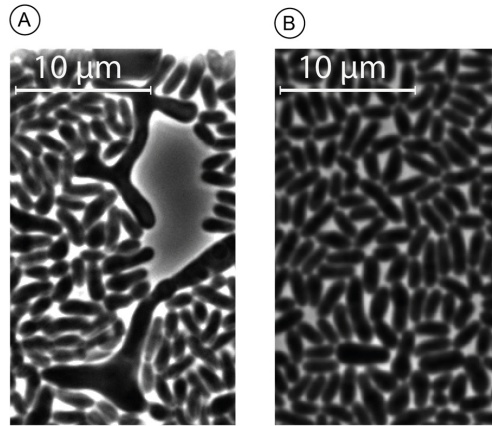


Figure C.10: Rare cellular events of *C. glutamicum* cultivated under standard conditions (A) Branched structures of *C. glutamicum* WT (B) *C. glutamicum* with deformed cell shape.

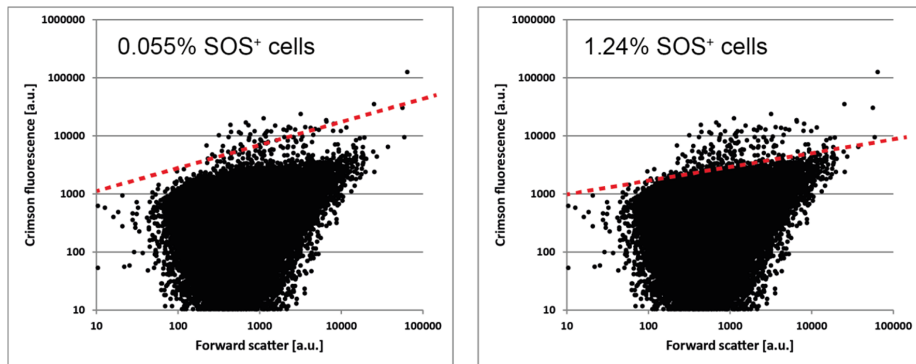


Figure C.11: FACS scatter plot of the strain *C. glutamicum*/pJC1- P_{recA} -*e2-crimson*. A total of 100.00 cells were analyzed for their size characteristics (forward scatter) and their fluorescent properties. Even under non-inducing conditions, small fractions of cells exhibited an increased reporter signal. (left) Gating of cells with approximately 15 times the mean value. (right) Gating of cells with approximately 5 times the mean fluorescence value.

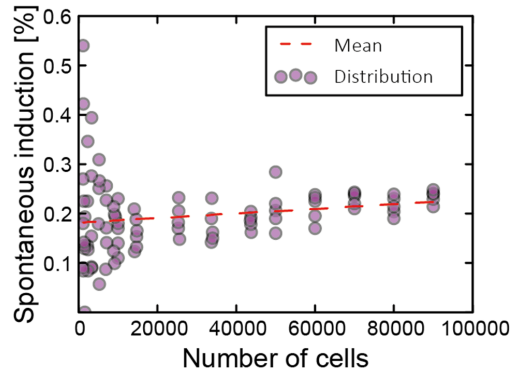


Figure C.12: Frequency of spontaneous induced cell depending on the number of analyzed cells during FACS measurements.

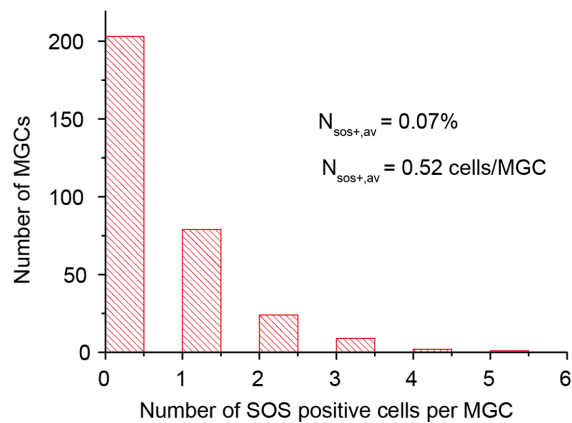


Figure C.13: Frequency of spontaneous induced cells, when cells with an 15-fold increased reporter signal were counted as SOS-positive.

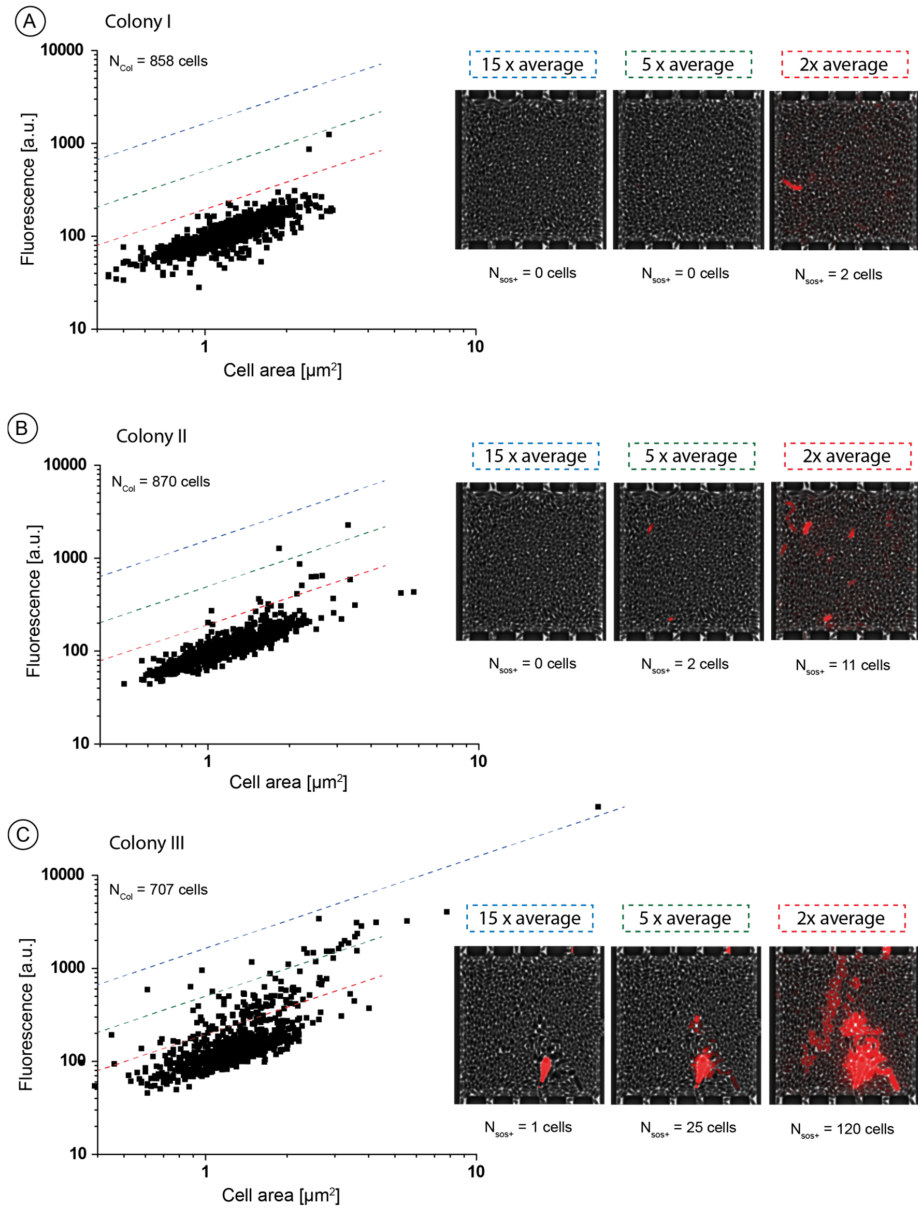


Figure C.14: Frequency of spontaneous induced cell depending colony quantification method. Here, cells with an 2 (red line), 5 (green line) and 15-fold (blue line) increased reporter signal were counted as SOS-positive

Appendix D

The presented data in this Appendix supplement the data described in Chapter 3.4 and contain additional growth results of *C. glutamicum*..

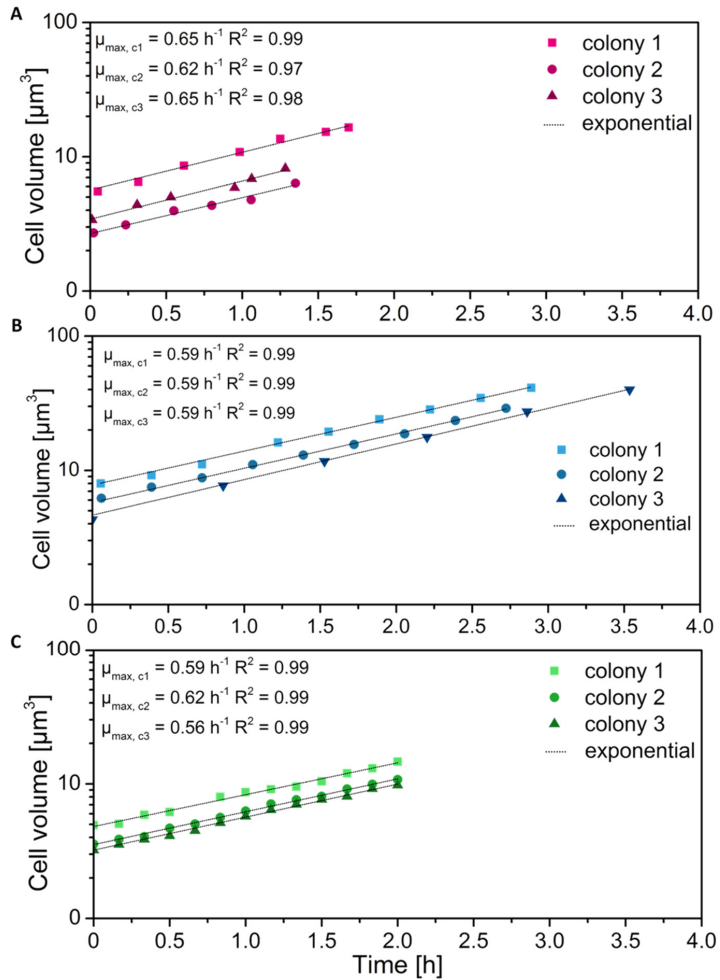


Figure D.1: Growth of *C. glutamicum* wild type in (A) nDEP, (B), MGC and (C) agarose pads.

Appendix E

The presented data in this Appendix supplement the study described in Chapter 4.1. E.1 contains additional information to the model used in the study. E.2-E.7 contain the raw data of growth experiments performed at different cultivation scales.

E.1: Unstructured model of batch growth

To model the negative effect of a by-product on batch-growth an unstructured model is formulated using well-known Monod-Kinetics [334]:

$$\dot{X} = r_X$$

$$\dot{S} = r_S$$

$$\dot{P} = r_P$$

with

$$r_X = \mu(S, P) \cdot X, \quad r_S = -\left(\frac{\mu(S, I)}{Y_{X/S}} + \pi_P\right) \cdot X, \quad r_P = -\left(\frac{\mu(P)}{Y_{X/P}} - \pi_P\right) \cdot X$$

and

$$\mu(S, P) = \mu(S, I) + \mu(P)$$

$$\mu(P) = \mu_{\max, P} \cdot \frac{P}{K_P + P}$$

$$\mu(S, I) = \mu_{\max, S} \cdot \frac{S}{K_S + S} \cdot \frac{k_I}{k_I + P}$$

Here S denotes the primary substrate that is converted to biomass X and the by-product P with a constant rate π_P . The by-product is allowed to be coutilized in parallel and hence the resulting specific growth rate $\mu(S, P)$ is a sum of the substrate specific growth rates $\mu(P)$ and $\mu(S, I)$. The latter is further modulated by a multiplicative term representing a non-competitive inhibition by P .

The model parameters $\mu_{\max, S}$ and $\mu_{\max, P}$ denote the “true” maximum growth rates on the primary substrate and by-product, respectively (cf. Eq. (4.2)). The respective half-

saturation constants, yield coefficients and the inhibition constant are denoted as K_S , K_P , $Y_{X/S}$, $Y_{X/P}$ and k_I , respectively.

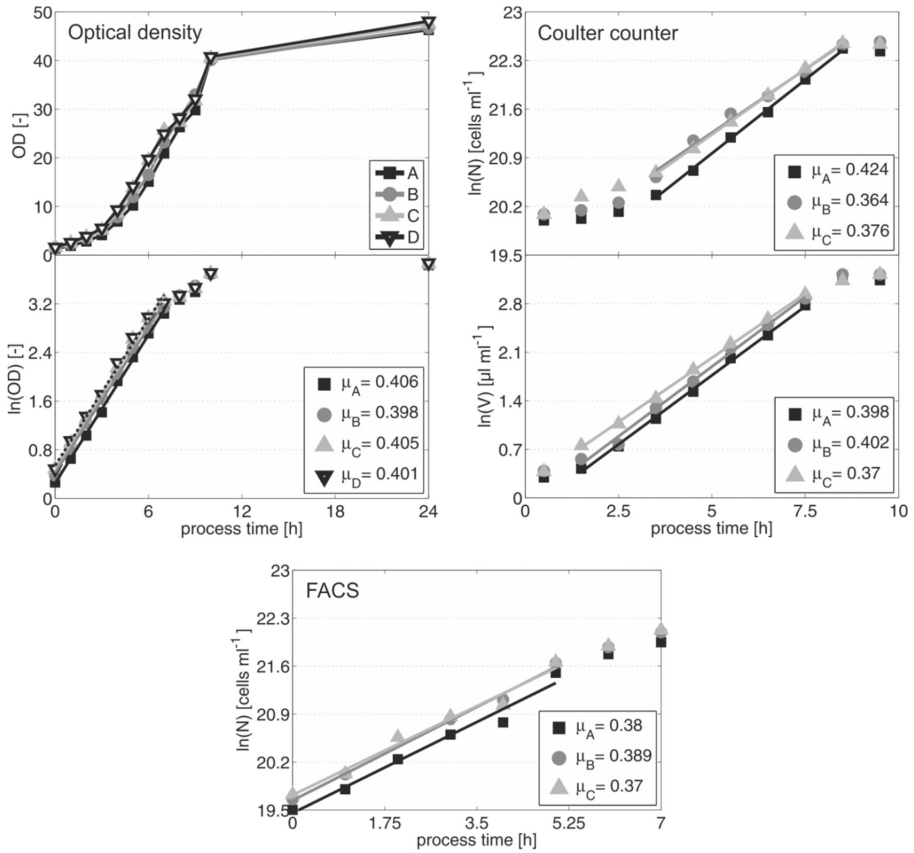


Figure E.1: Growth of *C. glutamicum* wild type in bioreactor batch-cultivations on CGXII glucose medium. Maximum growth rates were determined based on optical density, cell number and cell volume via Coulter counter and cell number via FACS.

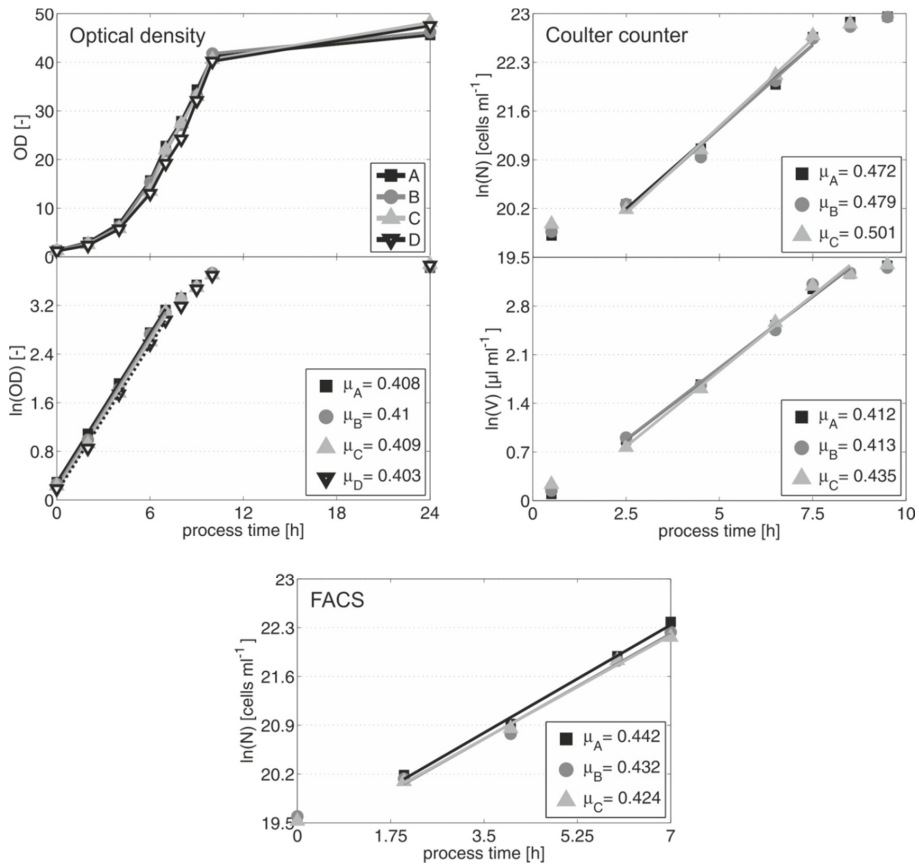


Figure E.2: Growth of *C. glutamicum* wild type in shake flasks on CGXII glucose medium. Maximum growth rates were determined based on optical density, cell number and cell volume via Coulter counter and cell number via FACS.

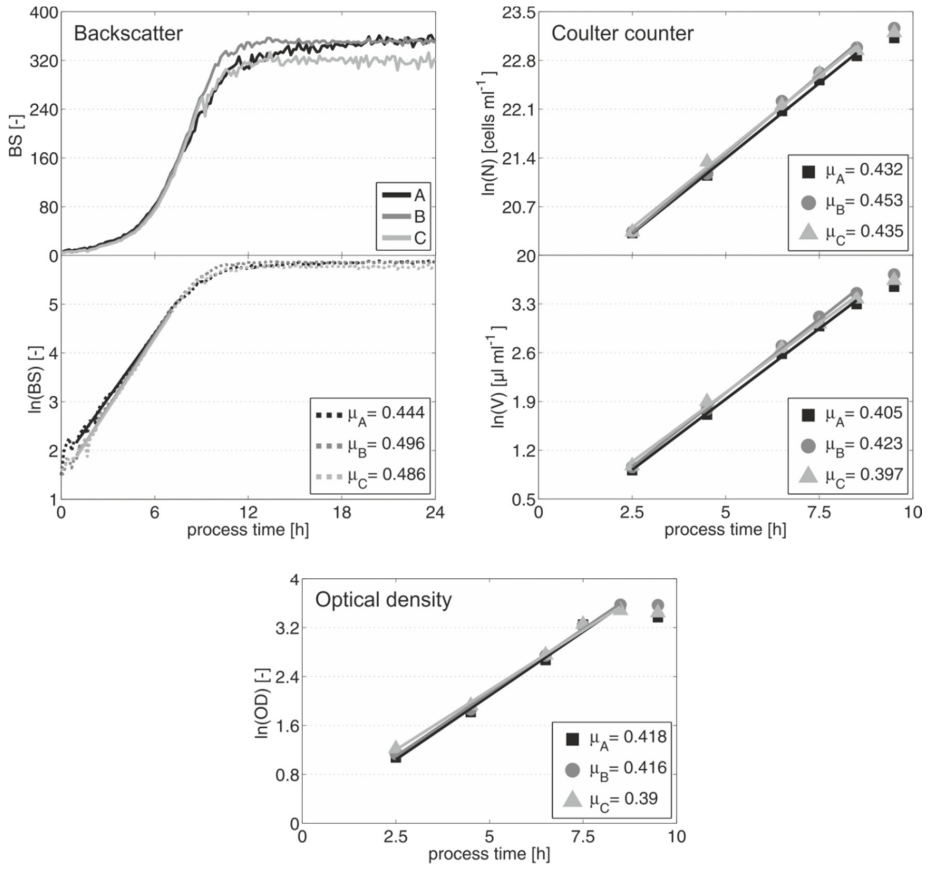


Figure E.3: Growth of *C. glutamicum* wild type in microtiter plates on CGXII glucose medium. Maximum growth rates were determined based on backscatter, cell number and cell volume via Coulter counter and optical density.

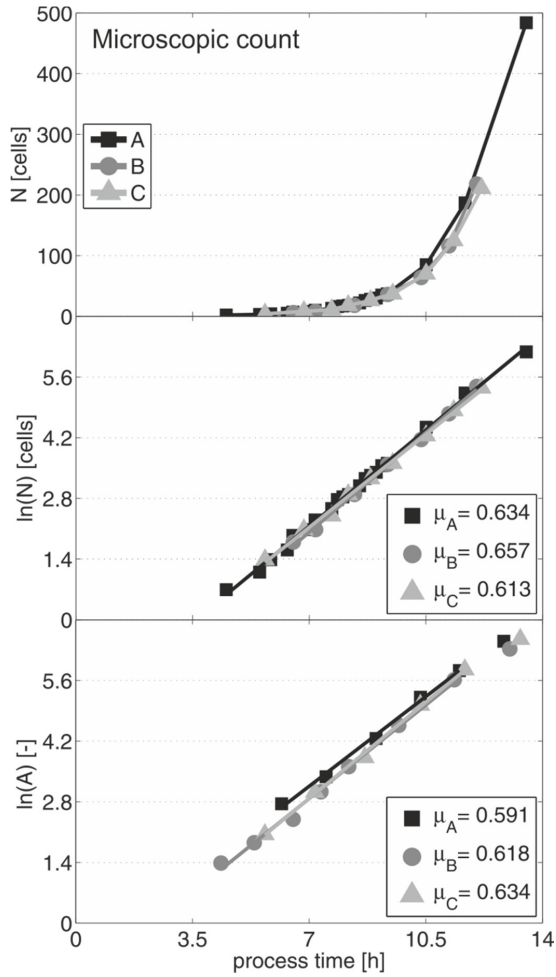


Figure E.4: Growth of *C. glutamicum* wild type under PLBR conditions on CGXII glucose medium. Maximum growth rates were determined based on cell number and cell size via microscopic count.

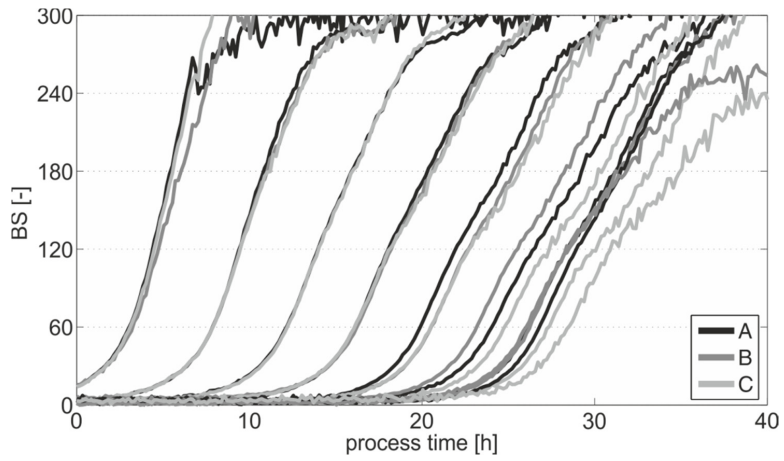


Figure E.5: Growth of *C. glutamicum* wild type in microtiter plates on CGXII glucose medium applying different inoculum concentrations. Log-dilution series were generated from three reference cultures and grown in parallel.

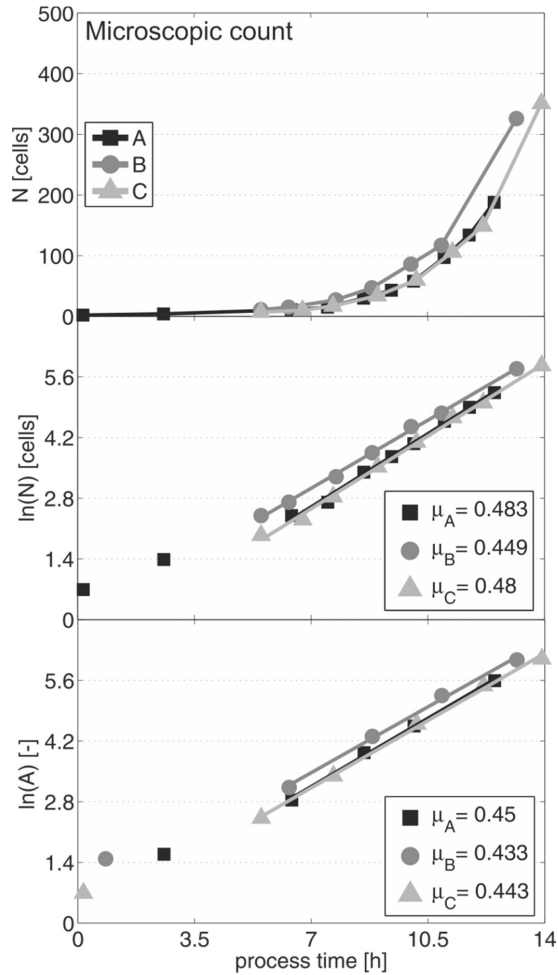


Figure E.6: Growth of *C. glutamicum* wild type under PLBR conditions on cell-free supernatant from shaking flask cultivation. Maximum growth rates were determined based on cell number and cell size via microscopic count.

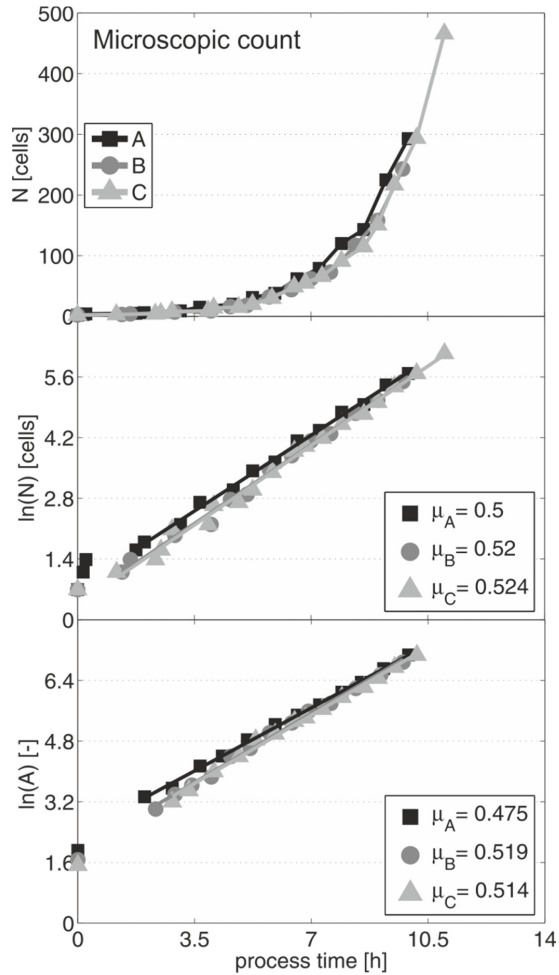


Figure E.7: Growth of *C. glutamicum* wild type under PLBR conditions on CGXII glucose medium supplemented with 5 mM acetate. Maximum growth rates were determined based on cell number and cell size via microscopic count.

Appendix F

The presented data in this Appendix supplement the study described in Chapter 4.2. F.1-F.4 contain additional information of the performed transcriptome analysis, additional growth data and results of the untargeted metabolome analysis.

Table F.1: Significantly up or down-regulated genes between the first and second growth phase of *C. glutamicum* during bioreactor batch cultivations in CGXII glucose medium.

Gene	Annotation	M-value	p-value
cg0201	<i>iolB</i> , enzyme involved in inositol metabolism	1.04	0.00
cg1765	predicted transcriptional regulator	1.06	0.00
cg1761	<i>nifS2</i> , cysteine desulfhydrase / selenocysteine lyase	1.07	0.00
cg3321	ABC-type transport system, involved in lipoprotein release, ATPase component	1.09	0.00
cg2560	<i>aceA</i> , isocitrate lyase	1.12	0.03
cg0337	<i>whcA</i> , negative role in SigH-mediated (oxidative) stress response	1.13	0.03
cg1090	<i>ggtB</i> , probable gamma-glutamyltranspeptidase precursor PR	1.14	0.08
cg1762	<i>sufC</i> , iron-regulated ABC transporter ATPase subunit	1.16	0.00
cg1764	<i>sufB</i> , component of an uncharacterized iron-regulated ABC-type transporter	1.20	0.00
cg3048	<i>pta</i> , phosphate acetyltransferase	1.21	0.02
cg3011	<i>groEL</i> , chaperonin groEL	1.31	0.00
cg0834	bacterial extracellular solute-binding protein, fa	1.32	0.00
cg0197	<i>iolC</i> , myo-Inositol catabolism, carbohydrate kinase	1.35	0.01
cg0346	<i>fadE</i> , glutaryl-CoA dehydrogenase	1.46	0.00
cg2137	<i>gluB</i> , glutamate secreted binding protein	1.47	0.05
cg1091	hypothetical protein cg1091	1.53	0.00
cg1411	ABC-type sugar (aldose) transport system, ATPase component	1.56	0.00
cg2628	<i>pcaI</i> , 3-oxoadipate enol-lactone hydrolase/4-carboxymuconolactonedecarboxylase	1.60	0.00
cg0444	<i>ramB</i> , transcriptional regulator, involved in acetate metabolism	1.66	0.04
cg3195	flavin-containing monooxygenase (FMO)	1.69	0.05
cg2181	ABC-type peptide transport system, secreted component	1.72	0.05
cg2184	ATPase component of peptide ABC-type transport system, contains duplicated ATPase domains	1.75	0.03
cg0953	Na ⁺ /proline, Na ⁺ /panthothenate symporter or related permease	1.86	0.03
cg2610	ABC-type dipeptide/oligopeptide/nickel transport system, secreted component	1.86	0.00

... Table F.1: Continued.

Gene	Annotation	M-value	p-value
cg3216	<i>gntP</i> , gluconate permease	1.93	0.01
cg2629	<i>pcaB1</i> , 3-carboxy-cis,cis-muconate cycloisomerase	1.93	0.00
cg0344	<i>fabG1</i> , 3-oxoacyl-(acyl-carrier protein) reductase	1.93	0.00
cg2623	<i>scoA</i> , probable FESUCCINYL-CoA:3-ketoacid-coenzyme A transferase subunit	1.96	0.01
cg3022	acetyl-CoA acetyltransferase	1.96	0.00
cg1226	<i>pobB</i> , 4-hydroxybenzoate 3-monooxygenase	2.24	0.00
cg2630	<i>pcaG</i> , protocatechuate dioxygenase alpha subunit	2.88	0.00
cg3107	<i>adhA</i> , Zn-dependent alcohol dehydrogenase	3.01	0.02
cg2631	<i>pcaH</i> , protocatechuate dioxygenase beta subunit	3.12	0.00
cg2636	<i>catA1</i> , catechol 1,2-dioxygenase	4.46	0.01
cg3213	putative secreted protein	-1.01	0.01
cg1484	putative secreted protein	-1.03	0.00
cg0317	<i>arsR2</i> , arsenate/arsenite regulatory protein	-1.04	0.00
cg1256	<i>dapD</i> , tetrahydrodipicolinate succinylase	-1.05	0.01
cg0933	DNA or RNA helicase of superfamily II	-1.09	0.01
cg1218	ADP-ribose pyrophosphatase	-1.13	0.03
cg1279	putative secreted protein	-1.13	0.04
cg2880	HIT family hydrolase	-1.18	0.00
cg1514	secreted protein	-1.22	0.00
cg1343	<i>narH</i> , probable respiratory nitrate reductase oxidoreduct	-1.23	0.00
cg1551	<i>uspA1</i> , universal stress protein UspA and related nucleotide-binding proteins	-1.30	0.01
cg1341	<i>narI</i> , respiratory nitrate reductase 2 gamma chain	-1.46	0.00
cg2211	hypothetical protein cg2211	-1.53	0.00
cg3082	bacterial regulatory proteins, ArsR family	-1.60	0.00
cg1342	<i>narJ</i> , nitrate reductase delta chain	-1.64	0.00
cg0078	hypothetical protein cg0078	-2.27	0.01
cg3286	putative secreted protein	-3.44	0.02

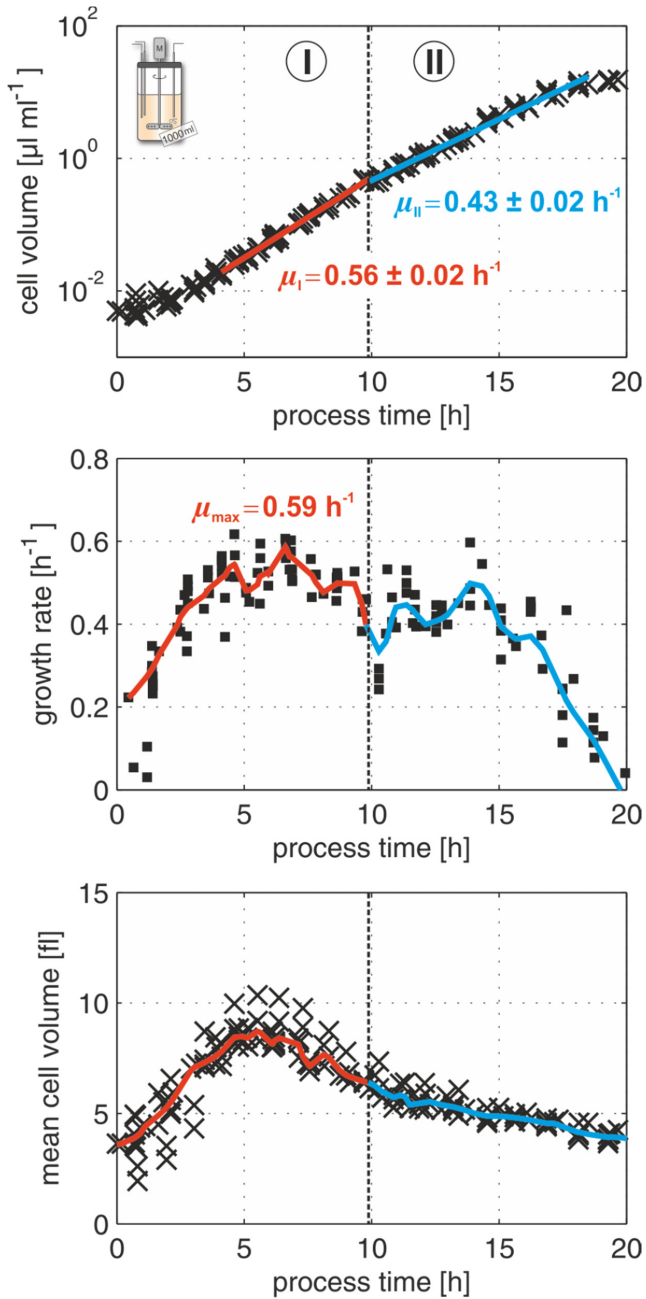


Figure F.1: Time dependent changes in the overall cell volume, the specific growth rate (based on cell volume measurements) and the mean single-cell volume of *C. glutamicum* during batch cultivation in 1 l bioreactors on CGXII glucose medium.

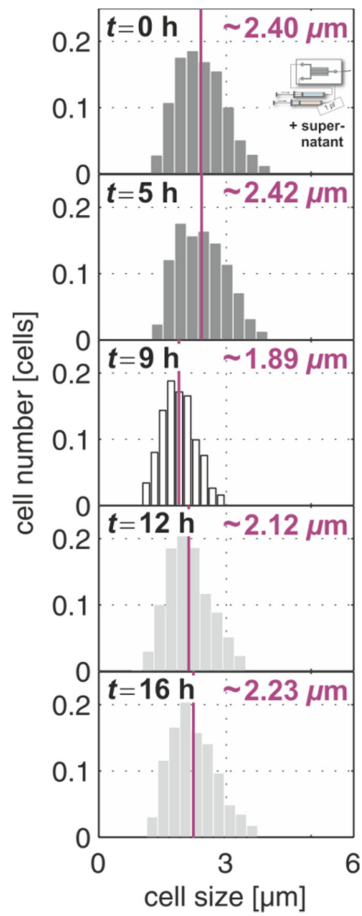


Figure F.2: Cell size distributions of *C. glutamicum* during MSCC on culture supernatants from bioreactor batch experiments in CGXII glucose medium (cf. Figure 4.6).

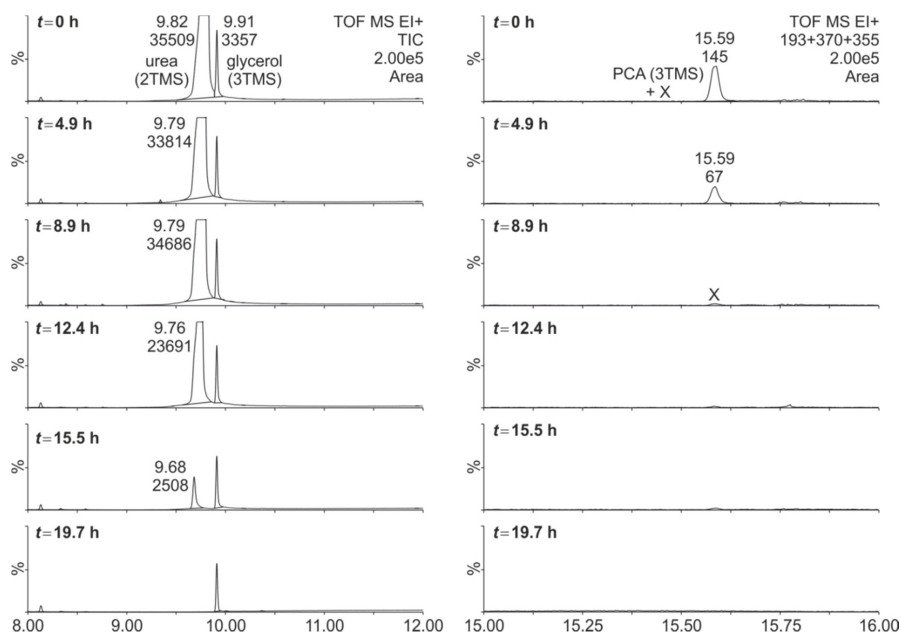


Figure F.3: Selected chromatograms from untargeted metabolome screening of culture supernatant samples from batch cultivation of *C. glutamicum* in CGXII glucose medium. While the amount of urea continuously decreased along the cultivation (left), the iron-chelator PCA was already absent at the switch to the second growth phase (right).

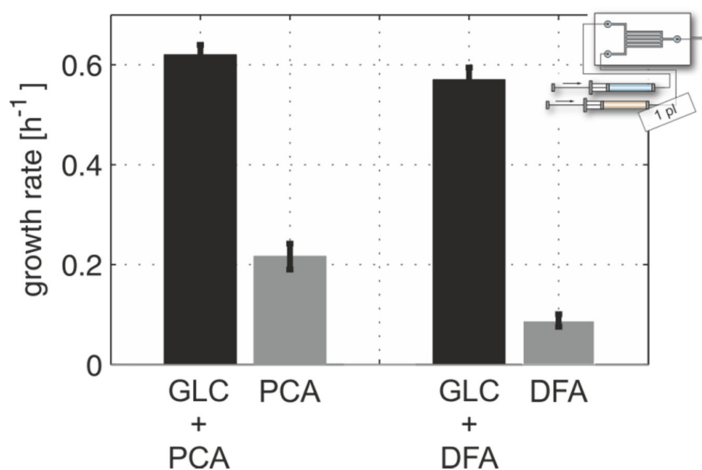


Figure F.4: Impact of the availability of different iron chelator on growth of *C. glutamicum*. MSCC experiments were performed on CGXII medium with either PCA or deferoxamine (DFA), each in combination with or without glucose.

Appendix G

The presented data in this Appendix supplements the data of the study described in Chapter 4.3. G.1-G.2 contains additional growth results and a literature overview of reported growth rates at various C-sources.

Table G.1: Maximum colony growth rates at different growth conditions. N_{Colony} denotes the numbers of evaluated colonies. Mean values and standard deviations were estimated from the respective replicates.

C-source	+ MOPS; + PCA		- MOPS; + PCA		+ MOPS; + DFA	
	$\mu_{\text{max}}[\text{h}^{-1}]$	N_{Colony}	$\mu_{\text{max}}[\text{h}^{-1}]$	N_{Colony}	$\mu_{\text{max}}[\text{h}^{-1}]$	N_{Colony}
Glucose	0.59±0.03	60	0.66±0.03	40	0.50±0.04	10
Gluconate	0.57±0.01	10	0.60±0.03	15	0.52±0.02	10
Fructose	0.24±0.05	10	0.51±0.02	10	0.30±0.03	10
Acetate	0.45±0.02	10	0.49±0.02	10	0.40±0.03	10
Pyruvate	0.38±0.02	15	0.38±0.03	10	0.22±0.01	10
Lactate	0.17±0.02	10	0.25±0.02	10	0.19±0.01	10
Citrate	0.49±0.01	10	0.56±0.02	10	0.43±0.03	10
Succinate	0.24±0.04	10	0.28±0.03	10	0.08±0.02	10
Malate	0.17±0.01	10	0.24±0.02	15	0.13±0.02	5
*	0.21±0.03	20	0.27±0.04	5	0.09±0.02	5

*No main C-source

Table G.2: Reported growth rates of *C. glutamicum* at various C-sources.

C-source	Maximum growth rate $\mu_{\text{max}} [\text{h}^{-1}]$
Glucose	0.34 [335]; 0.32 [272]; 0.38 [274]; 0.38 [336]; 0.33 [299]; 0.36 [337]; 0.37 [338]; 0.44 [302]; 0.43 [339]; 0.41 [301]; 0.35 [340]
Gluconate	0.46 [339]
Fructose	0.38 [335]
Pyruvate	0.28 [340]
Lactate	0.25 [301]
Acetate	0.28 [272]; 0.28 [274]; 0.28 [336]; 0.29 [301]; 0.3 [340]
Citrate	0.32 [299]; 0.2 [298]; 0.32 [301]; 0.12 [340]
Succinate	no growth [302]
Malate	no growth [302]

References

1. Verma, A.S., Agrahari, S., *et al.*, **2011**, *Biotechnology in the realm of history*, Journal of Pharmacy and Bioallied Sciences **3**(3): 321-323.
2. Berg, P. and Mertz, J.E., **2010**, *Personal reflections on the origins and emergence of recombinant DNA technology*, Genetics, **184**(1): 9-17.
3. Buchholz, K. and Collins, J., **2013**, *The roots - a short history of industrial microbiology and biotechnology*, Applied Microbiology and Biotechnology, **97**(9): 3747-3762.
4. Du, J., Shao, Z., *et al.*, **2011**, *Engineering microbial factories for synthesis of value-added products*, Journal of Industrial Microbiology & Biotechnology, **38**(8): 873-890.
5. Festel, G., Detzel, C., *et al.*, **2012**, *Industrial biotechnology – markets and industry structure*, Journal of Commercial Biotechnology, **18**(1).
6. Becker, J. and Wittmann, C., **2012**, *Bio-based production of chemicals, materials and fuels - Corynebacterium glutamicum as versatile cell factory*, Current Opinion in Biotechnology, **23**(4): 631-640.
7. Chen, G.Q., **2012**, *New challenges and opportunities for industrial biotechnology*, Microbial Cell Factories, **11**(1): 111.
8. Dellomonaco, C., Fava, F., *et al.*, **2010**, *The path to next generation biofuels: Successes and challenges in the era of synthetic biology*, Microbial Cell Factories, **9**(1): 3.
9. Erickson, B., Nelson, J.E., *et al.*, **2012**, *Perspective on opportunities in industrial biotechnology in renewable chemicals*, Biotechnology Journal, **7**(2): 176-185.
10. Doig, S., Baganz, F., *et al.*, **2006**, *High throughput screening and process optimisation*, in *Basic Biotechnology*, C. Ratledge and B. Kristiansen, Editors. Cambridge: Cambridge University Press.
11. Villadsen, J., Nielsen, J., *et al.*, **2011**, *Bioreaction engineering principles*. Springer US.
12. Rohe, P., Venkanna, D., *et al.*, **2012**, *An automated workflow for enhancing microbial bioprocess optimization on a novel microbioreactor platform*, Microbial Cell Factories, **11**(1): 144.
13. Lara, A.R., Galindo, E., *et al.*, **2006**, *Living with heterogeneities in bioreactors*, Molecular Biotechnology, **34**(3): 355-381.
14. Bylund, F., Collet, E., *et al.*, **1998**, *Substrate gradient formation in the large-scale bioreactor lowers cell yield and increases by-product formation*, Bioprocess Engineering, **18**(3): 171-180.
15. Takors, R., **2012**, *Scale-up of microbial processes: Impacts, tools and open questions*, Journal of Biotechnology, **160**(1-2): 3-9.
16. Noorman, H., **2011**, *An industrial perspective on bioreactor scale-down: What we can learn from combined large-scale bioprocess and model fluid studies*, Biotechnology Journal, **6**(8): 934-943.
17. Carlquist, M., Fernandes, R.L., *et al.*, **2012**, *Physiological heterogeneities in microbial populations and implications for physical stress tolerance*, Microbial Cell Factories, **11**: 94.
18. Enfors, S.O., Jahic, M., *et al.*, **2001**, *Physiological responses to mixing in large scale bioreactors*, Journal of Biotechnology, **85**(2): 175-185.
19. Huang, S., **2009**, *Non-genetic heterogeneity of cells in development: more than just noise*, Development, **136**(23): 3853-3862.
20. Schmid, A., Kortmann, H., *et al.*, **2010**, *Chemical and biological single cell analysis*, Current Opinion in Biotechnology, **21**(1): 12-20.
21. Yin, H.B. and Marshall, D., **2012**, *Microfluidics for single cell analysis*, Current Opinion in Biotechnology, **23**(1): 110-119.

22. Grünberger, A., Wiechert, W., *et al.*, **2014**, *Single-cell microfluidics: Opportunity for bioprocess development*, *Current Opinion in Biotechnology*, **29** 15-23.
23. Eggeling, L. and Bott, M., **2005**, *Handbook of Corynebacterium glutamicum*. Inc., Boca Raton, FL: Academic Press.
24. Ferrer-Miralles, N. and Villaverde, A., **2013**, *Bacterial cell factories for recombinant protein production: Expanding the catalogue*, *Microbial Cell Factories*, **12**(1): 113.
25. Çelik, E. and Çalik, P., **2012**, *Production of recombinant proteins by yeast cells*, *Biotechnology Advances*, **30**(5): 1108-1118.
26. Locke, J.C.W., Young, J.W., *et al.*, **2011**, *Stochastic pulse regulation in bacterial stress response*, *Science*, **334**(6054): 366-369.
27. Brehm-Stecher, B.F. and Johnson, E.A., **2004**, *Single-cell microbiology: Tools, technologies, and applications*, *Microbiology and Molecular Biology Reviews*, **68**(3): 538-559.
28. Prindle, A., Selimkhanov, J., *et al.*, **2012**, *Genetic circuits in Salmonella typhimurium*, *ACS Synthetic Biology*, **1**(10): 458-464.
29. Fritzsche, F.S.O., Dusny, C., *et al.*, **2012**, *Single-cell analysis in biotechnology, systems biology, and biocatalysis*, *Annual Review of Chemical and Biomolecular Engineering*, **3**(1): 129-155.
30. Avery, S.V., **2006**, *Microbial cell individuality and the underlying sources of heterogeneity*, *Nat. Rev. Microbiol.*, **4**(8): 577-587.
31. Watson, J.V., **1991**, *Introduction to flow cytometry*. Cambridge: Cambridge University Press.
32. Shapiro, H.M., **1995**, *Practical flow cytometry*. New York: Wiley-Liss.
33. Binder, S., Schendzielorz, G., *et al.*, **2012**, *A high-throughput approach to identify genomic variants of bacterial metabolite producers at the single-cell level*, *Genome Biology*, **13**(5): R40.
34. Binder, S., Siedler, S., *et al.*, **2013**, *Recombineering in Corynebacterium glutamicum combined with optical nanosensors: a general strategy for fast producer strain generation*, *Nucleic Acids Research*, **41**(12): 6360-6369.
35. Fulwyler, M.J., **1965**, *Electronic separation of biological cells by volume*, *Science*, **150**(3698): 910-911.
36. Tzur, A., Moore, J.K., *et al.*, **2011**, *Optimizing optical flow cytometry for cell volume-based sorting and analysis*, *Plos One*, **6**(1): e16053.
37. Erlebach, C.E., Illmer, P., *et al.*, **2000**, *Changes of cell size distribution during the batch culture of Arthrobacter strain Pl/1-95*, *Antonie Van Leeuwenhoek International Journal of General and Molecular Microbiology*, **77**(4): 329-335.
38. Hewitt, C.J., Nebe-Von Caron, G., *et al.*, **1999**, *Use of multi-staining flow cytometry to characterise the physiological state of Escherichia coli W3110 in high cell density fed-batch cultures*, *Biotechnology and Bioengineering*, **63**(6): 705-711.
39. Rieseberg, M., Kasper, C., *et al.*, **2001**, *Flow cytometry in biotechnology*, *Applied Microbiology and Biotechnology*, **56**(3-4): 350-360.
40. Neumeyer, A., Hubschmann, T., *et al.*, **2013**, *Monitoring of population dynamics of Corynebacterium glutamicum by multiparameter flow cytometry*, *Microbial Biotechnology*, **6**(2): 157-167.
41. Abu-Absi, N.R., Zamamiri, A., *et al.*, **2003**, *Automated flow cytometry for acquisition of time-dependent population data*, *Cytometry Part A*, **51A**(2): 87-96.
42. Broger, T., Odermatt, R.P., *et al.*, **2011**, *Real-time on-line flow cytometry for bioprocess monitoring*, *Journal of Biotechnology*, **154**(4): 240-247.
43. Mullassery, D., Horton, C.A., *et al.*, **2008**, *Single live-cell imaging for systems biology*, *Essays in Biochemistry: Systems Biology*, **45**: 121-133.
44. Antony, P.M.A., Trefois, C., *et al.*, **2013**, *Light microscopy applications in systems biology: Opportunities and challenges*, *Cell Communication and Signaling*, **11**(1): 24.

45. Spiegelhalter, C., Tosch, V., *et al.*, **2010**, *From dynamic live cell imaging to 3D ultrastructure: novel integrated methods for high pressure freezing and correlative light-electron microscopy*, Plos One, **5**(2): e9014.
46. Sung, M.H. and McNally, J.G., **2011**, *Live cell imaging and systems biology*, Wiley Interdisciplinary Reviews-Systems Biology and Medicine, **3**(2): 167-182.
47. Gahlmann, A. and Moerner, W.E., **2014**, *Exploring bacterial cell biology with single-molecule tracking and super-resolution imaging*, Nature Reviews Microbiology, **12**(1): 9-22.
48. Walden, M. and Elf, J., **2011**, *Studying transcriptional interactions in single cells at sufficient resolution*, Current Opinion in Biotechnology, **22**(1): 81-86.
49. Streets, A.M. and Huang, Y., **2014**, *Microfluidics for biological measurements with single-molecule resolution*, Current Opinion in Biotechnology, **25**: 69-77.
50. Barber, M.A., **1908**, *The rate of multiplication of Bacillus coli at different temperatures*, Journal of Infectious Diseases, **5**(4): 379-400.
51. Hort, E.C., **1920**, *The cultivation of aerobic bacteria from single cells*, Journal of Hygiene, **18**(4): 361-368.
52. Kelly, C.D. and Rahn, O., **1932**, *The growth rate of individual bacterial cells*, Journal of Bacteriology, **23**(2): 147-153.
53. Orskov, J., **1922**, *Method for the isolation of bacteria in pure culture from single cells and procedure for the direct tracing of bacterial growth on a solid medium*, Journal of Bacteriology, **7**(6): 537-549.
54. Bretz, H.W., **1962**, *Simple method for estimating slide culture survival*, Journal of Bacteriology, **84**(5): 1115-1116.
55. Young, J.W., Locke, J.C.W., *et al.*, **2012**, *Measuring single-cell gene expression dynamics in bacteria using fluorescence time-lapse microscopy*, Nature Protocols, **7**(1): 80-88.
56. Bean, J.M., Siggia, E.D., *et al.*, **2006**, *Coherence and timing of cell cycle start examined at single-cell resolution*, Molecular Cell, **21**(1): 3-14.
57. Kaufmann, B.B., Yang, Q., *et al.*, **2007**, *Heritable stochastic switching revealed by single-cell genealogy*, Plos Biology, **5**(9): 1973-1980.
58. Long, Z., Nugent, E., *et al.*, **2013**, *Microfluidic chemostat for measuring single cell dynamics in bacteria*, Lab on a Chip, **13**(5): 947-954.
59. Beebe, D.J., Mensing, G.A., *et al.*, **2002**, *Physics and applications of microfluidics in biology*, Annual Review of Biomedical Engineering, **4**: 261-286.
60. Berthier, J. and Silberzan, P., **2010**, *Microfluidics for biotechnology* Boston, Mass.: Artech House.
61. Eriksson, E., Scrimgeour, J., *et al.*, **2007**, *Optical manipulation and microfluidics for studies of single cell dynamics*, Journal of Optics A: Pure and Applied Optics, **9**(8): S113-S121.
62. Umehara, S., Wakamoto, Y., *et al.*, **2003**, *On-chip single-cell microcultivation assay for monitoring environmental effects on isolated cells*, Biochemical and Biophysical Research Communications, **305**(3): 534-540.
63. Evander, M., Johansson, L., *et al.*, **2007**, *Noninvasive acoustic cell trapping in a microfluidic perfusion system for online bioassays*, Analytical Chemistry, **79**(7): 2984-2991.
64. Koschwanetz, J.H., Carlson, R.H., *et al.*, **2007**, *Easily fabricated magnetic traps for single-cell applications*, Review of Scientific Instruments, **78**(4): 044301.
65. Fritzsche, F.S.O., Rosenthal, K., *et al.*, **2013**, *Picoliter nDEP traps enable time-resolved contactless single bacterial cell analysis in controlled microenvironments*, Lab on a Chip, **13**(3): 397-408.
66. Kortmann, H., Chasanis, P., *et al.*, **2009**, *The Envirostat - a new bioreactor concept*, Lab on a Chip, **9**(4): 576-585.

67. Tanyeri, M., Ranka, M., *et al.*, **2011**, *A microfluidic-based hydrodynamic trap: Design and implementation*, *Lab on a Chip*, **11**(10): 1786-1794.
68. Johann, R.M., **2006**, *Cell trapping in microfluidic chips*, *Analytical and Bioanalytical Chemistry*, **385**(3): 408-412.
69. Nilsson, J., Evander, M., *et al.*, **2009**, *Review of cell and particle trapping in microfluidic systems*, *Analytica Chimica Acta*, **649**(2): 141-157.
70. Su, X.J., Theberge, A.B., *et al.*, **2013**, *Effect of microculture on cell metabolism and biochemistry: Do cells get stressed in microchannels?*, *Analytical Chemistry*, **85**(3): 1562-1570.
71. Jakiela, S., Kaminski, T.S., *et al.*, **2013**, *Bacterial growth and adaptation in microdroplet chemostats*, *Angewandte Chemie-International Edition*, **52**(34): 8908-8911.
72. Lagus, T.P. and Edd, J.F., **2013**, *A review of the theory, methods and recent applications of high-throughput single-cell droplet microfluidics*, *Journal of Physics D-Applied Physics*, **46**(11).
73. Dusny, C., Fritsch, F.S.O., *et al.*, **2012**, *Isolated microbial single cells and resulting micropopulations are growing faster in controlled environments*, *Applied and Environmental Microbiology*, **78**(19): 7132-7136.
74. Boedicker, J.Q., Vincent, M.E., *et al.*, **2009**, *Microfluidic confinement of single cells of bacteria in small volumes initiates high-density behavior of quorum sensing and growth and reveals its variability*, *Angewandte Chemie-International Edition*, **48**(32): 5908-5911.
75. Hofmann, T.W., Anselmann, S.H., *et al.*, **2012**, *Applying microdroplets as sensors for label-free detection of chemical reactions*, *Lab on a Chip*, **12**(5): 916-922.
76. Probst, C., Grünberger, A., *et al.*, **2013**, *Polydimethylsiloxane (PDMS) sub-micron traps for single-cell analysis of bacteria*, *Micromachines*, **4**(4): 357-369.
77. Rowat, A.C., Bird, J.C., *et al.*, **2009**, *Tracking lineages of single cells in lines using a microfluidic device*, *Proceedings of the National Academy of Sciences of the United States of America*, **106**(43): 18149-18154.
78. Wessel, A.K., Hmelo, L., *et al.*, **2013**, *Going local: technologies for exploring bacterial microenvironments*, *Nature Reviews Microbiology*, **11**(5): 337-348.
79. Xia, Y.N. and Whitesides, G.M., **1998**, *Soft lithography*, *Angewandte Chemie-International Edition*, **37**(5): 551-575.
80. Moolman, M.C., Huang, Z.X., *et al.*, **2013**, *Electron beam fabrication of a microfluidic device for studying submicron-scale bacteria*, *Journal of Nanobiotechnology*, **11**(1): 12.
81. Love, K.R., Bagh, S., *et al.*, **2013**, *Microtools for single-cell analysis in biopharmaceutical development and manufacturing*, *Trends in Biotechnology*, **31**(5): 16-22.
82. Avesar, J., Ben Arye, T., *et al.*, **2014**, *Frontier microfluidic techniques for short and long-term single cell analysis*, *Lab on a Chip*. DOI: 10.1039/C4LC00013G.
83. Gan, M.Z., Su, J., *et al.*, **2011**, *A scalable microfluidic chip for bacterial suspension culture*, *Lab on a Chip*, **11**(23): 4087-4092.
84. Groisman, A., Lobo, C., *et al.*, **2005**, *A microfluidic chemostat for experiments with bacterial and yeast cells*, *Nature Methods*, **2**(9): 685-689.
85. Balagadde, F.K., You, L.C., *et al.*, **2005**, *Long-term monitoring of bacteria undergoing programmed population control in a microchemostat*, *Science*, **309**(5731): 137-140.
86. Luo, X.J., Shen, K.Y., *et al.*, **2010**, *An automatic microturbidostat for bacterial culture at constant density*, *Biomedical Microdevices*, **12**(3): 499-503.
87. Dai, J., Yoon, S.H., *et al.*, **2013**, *Charting microbial phenotypes in multiplex nanoliter batch bioreactors*, *Analytical Chemistry*, **85**(12): 5892-5899.
88. Sun, P., Liu, Y., *et al.*, **2011**, *High-throughput microfluidic system for long-term bacterial colony monitoring and antibiotic testing in zero-flow environments*, *Biosensors & Bioelectronics*, **26**(5): 1993-1999.

89. Mohan, R., Mukherjee, A., *et al.*, **2013**, *A multiplexed microfluidic platform for rapid antibiotic susceptibility testing*, *Biosensors & Bioelectronics*, **49**: 118-125.
90. Park, J., Wu, J.Z., *et al.*, **2013**, *Microchemostat array with small-volume fraction replenishment for steady-state microbial culture*, *Lab on a Chip*, **13**(21): 4217-4224.
91. Taylor, R.J., Falconnet, D., *et al.*, **2009**, *Dynamic analysis of MAPK signaling using a high-throughput microfluidic single-cell imaging platform*, *Proceedings of the National Academy of Sciences of the United States of America*, **106**(10): 3758-3763.
92. Falconnet, D., Niemisto, A., *et al.*, **2011**, *High-throughput tracking of single yeast cells in a microfluidic imaging matrix*, *Lab on a Chip*, **11**(3): 466-473.
93. Cookson, S., Ostroff, N., *et al.*, **2006**, *Monitoring dynamics of single-cell gene expression over multiple cell cycles*, *Molecular Systems Biology*, **1**: 2005.0024.
94. Uhlendorf, J., Miermont, A., *et al.*, **2012**, *Long-term model predictive control of gene expression at the population and single-cell levels*, *Proceedings of the National Academy of Sciences of the United States of America*, **109**(35): 14271-14276.
95. Mather, W., Mondragon-Palomino, O., *et al.*, **2010**, *Streaming instability in growing cell populations*, *Physical Review Letters*, **104**(20): 208101.
96. Volfson, D., Cookson, S., *et al.*, **2008**, *Biomechanical ordering of dense cell populations*, *Proceedings of the National Academy of Sciences of the United States of America*, **105**(40): 15346-15351.
97. Ullman, G., Wallden, M., *et al.*, **2013**, *High-throughput gene expression analysis at the level of single proteins using a microfluidic turbidostat and automated cell tracking*, *Philosophical Transactions of the Royal Society B: Biological Sciences*, **368**(1611): 20120025.
98. Grünberger, A., van Ooyen, J., *et al.*, **2013**, *Beyond growth rate 0.6: *Corynebacterium glutamicum* cultivated in highly diluted environments*, *Biotechnology and Bioengineering*, **110**(1): 220-228.
99. Paliwal, S., Iglesias, P.A., *et al.*, **2007**, *MAPK-mediated bimodal gene expression and adaptive gradient sensing in yeast*, *Nature*, **446**(7131): 46-51.
100. Wang, L., Liu, J.J., *et al.*, **2011**, *Growth propagation of yeast in linear arrays of microfluidic chambers over many generations*, *Biomicrofluidics*, **5**(4): 044118.
101. Lee, S.S., Avalos Vizcarra, I., *et al.*, **2012**, *Whole lifespan microscopic observation of budding yeast aging through a microfluidic dissection platform*, *Proceedings of the National Academy of Sciences of the United States of America*, **109**(13): 4916-4920.
102. Xie, Z.W., Zhang, Y., *et al.*, **2012**, *Molecular phenotyping of aging in single yeast cells using a novel microfluidic device*, *Aging Cell*, **11**(4): 599-606.
103. Ricicova, M., Hamidi, M., *et al.*, **2013**, *Dissecting genealogy and cell cycle as sources of cell-to-cell variability in MAPK signaling using high-throughput lineage tracking*, *Proceedings of the National Academy of Sciences of the United States of America*, **110**(28): 11403-11408.
104. Dénervaud, N., Becker, J., *et al.*, **2013**, *A chemostat array enables the spatio-temporal analysis of the yeast proteome*, *Proceedings of the National Academy of Sciences*, **110**(39): 15842-15847.
105. Cho, H.J., Jonsson, H., *et al.*, **2007**, *Self-organization in high-density bacterial colonies: Efficient crowd control*, *Plos Biology*, **5**(11): 2614-2623.
106. Stricker, J., Cookson, S., *et al.*, **2008**, *A fast, robust and tunable synthetic gene oscillator*, *Nature*, **456**(7221): 516-519.
107. Danino, T., Mondragon-Palomino, O., *et al.*, **2010**, *A synchronized quorum of genetic clocks*, *Nature*, **463**(7279): 326-330.
108. Connell, J.L., Wessel, A.K., *et al.*, **2010**, *Probing prokaryotic social behaviors with bacterial "Lobster traps"*, *Mbio*, **1**(4): e00202-10.

109. Aldridge, B.B., Fernandez-Suarez, M., *et al.*, **2012**, *Asymmetry and aging of mycobacterial cells lead to variable growth and antibiotic susceptibility*, *Science*, **335**(6064): 100-104.
110. Probst, C., Grünberger, A., *et al.*, **2013**, *Microfluidic growth chambers with optical tweezers for full spatial single-cell control and analysis of evolving microbes*, *Journal of Microbiological Methods*, **95**(3): 470-476.
111. Mannik, J., Driessen, R., *et al.*, **2009**, *Bacterial growth and motility in sub-micron constrictions*, *Proceedings of the National Academy of Sciences of the United States of America*, **106**(35): 14861-14866.
112. Balaban, N.Q., Merrin, J., *et al.*, **2004**, *Bacterial persistence as a phenotypic switch*, *Science*, **305**(5690): 1622-1625.
113. Tan, W.H. and Takeuchi, S., **2008**, *Dynamic microarray system with gentle retrieval mechanism for cell-encapsulating hydrogel beads*, *Lab on a Chip*, **8**(2): 259-266.
114. Wang, P., Robert, L., *et al.*, **2010**, *Robust growth of escherichia coli*, *Current Biology*, **20**(12): 1099-1103.
115. Moffitt, J.R., Lee, J.B., *et al.*, **2012**, *The single-cell chemostat: An agarose-based, microfluidic device for high-throughput, single-cell studies of bacteria and bacterial communities*, *Lab on a Chip*, **12**(8): 1487-1494.
116. Norman, T.M., Lord, N.D., *et al.*, **2013**, *Memory and modularity in cell-fate decision making*, *Nature*, **503**(7477): 481-486.
117. Schendzielorz, G., Dippong, M., *et al.*, **2013**, *Taking control over control: Use of product sensing in single cells to remove flux control at key enzymes in biosynthesis pathways*, *ACS Synthetic Biology*, **3**(1): 21-29.
118. Teng, S.W., Mukherji, S., *et al.*, **2013**, *Robust circadian oscillations in growing cyanobacteria require transcriptional feedback*, *Science*, **340**(6133): 737-740.
119. Pelletier, J., Halvorsen, K., *et al.*, **2012**, *Physical manipulation of the Escherichia coli chromosome reveals its soft nature*, *Proceedings of the National Academy of Sciences of the United States of America*, **109**(40): E2649-E2656.
120. Caspi, Y., **2014**, *Deformation of filamentous Escherichia coli cells in a microfluidic device: a new technique to study cell mechanics*, *Plos One*, **9**(1): e83775.
121. Youngren, B., Nielsen, H.J., *et al.*, **2014**, *The multifork Escherichia coli chromosome is a self-duplicating and self-segregating thermodynamic ring polymer*, *Genes & Development*, **28**(1): 71-84.
122. Wakamoto, Y., Grosberg, A.Y., *et al.*, **2012**, *Optimal lineage principle for age-structured populations*, *Evolution*, **66**(1): 115-134.
123. Fehrmann, S., Paoletti, C., *et al.*, **2013**, *Aging yeast cells undergo a sharp entry into senescence unrelated to the loss of mitochondrial membrane potential*, *Cell Reports*, **5**(6): 1589-1599.
124. Fisher, J.K., Bourniquel, A., *et al.*, **2013**, *Four-dimensional imaging of E. coli nucleoid organization and dynamics in living cells*, *Cell*, **153**(4): 882-895.
125. Lu, Y., Gao, J., *et al.*, **2013**, *Single cell antimicrobial susceptibility testing by confined microchannels and electrokinetic loading*, *Analytical Chemistry*, **85**(8): 3971-3976.
126. Banaeiyan, A.A., Ahmadpour, D., *et al.*, **2013**, *Hydrodynamic cell trapping for high throughput single-cell applications*, *Micromachines*, **4**(4): 414-430.
127. Di Carlo, D., Wu, L.Y., *et al.*, **2006**, *Dynamic single cell culture array*, *Lab on a Chip*, **6**(11): 1445-1449.
128. Ryley, J. and Pereira-Smith, O.M., **2006**, *Microfluidics device for single cell gene expression analysis in Saccharomyces cerevisiae*, *Yeast*, **23**(14-15): 1065-1073.
129. Rosa, P., Tenreiro, S., *et al.*, **2012**, *High-throughput study of alpha-synuclein expression in yeast using microfluidics for control of local cellular microenvironment*, *Biomicrofluidics*, **6**(1): 014109.

130. Zhang, Y., Luo, C.X., *et al.*, **2012**, *Single cell analysis of yeast replicative aging using a new generation of microfluidic device*, Plos One, **7**(11): e48275.
131. Lee, P.J., Helman, N.C., *et al.*, **2008**, *A microfluidic system for dynamic yeast cell imaging*, Biotechniques, **44**(1): 91-95.
132. Kim, M.C., Isenberg, B.C., *et al.*, **2011**, *Programmed trapping of individual bacteria using micrometre-size sieves*, Lab on a Chip, **11**(6): 1089-1095.
133. Zhu, Z., Frey, O., *et al.*, **2012**, *Microfluidic single-cell cultivation chip with controllable immobilization and selective release of yeast cells*, Lab on a Chip, **12**(5): 906-915.
134. Guo, P., Hall, E.W., *et al.*, **2012**, *Microfluidic capture and release of bacteria in a conical nanopore array*, Lab on a Chip, **12**(3): 558-561.
135. Stratz, S., Eyer, K., *et al.*, **2013**, *Towards quantitative analysis of single E. coli lysates*. in *17th International Conference on Miniaturized Systems for Chemistry and Life Sciences*. Freiburg, Germany.
136. Vasdekis, A.E., **2013**, *Single microbe trap and release in sub-microfluidics*, Rsc Advances, **3**(18): 6343-6346.
137. Charvin, G., Cross, F.R., *et al.*, **2008**, *A microfluidic device for temporally controlled gene expression and long-term fluorescent imaging in unperturbed dividing yeast cells*, Plos One, **3**(1): e1468.
138. Ducret, A., Maisonneuve, E., *et al.*, **2009**, *A microscope automated fluidic system to study bacterial processes in real time*, Plos One, **4**(9): e7282.
139. Golchin, S.A., Stratford, J., *et al.*, **2012**, *A microfluidic system for long-term time-lapse microscopy studies of mycobacteria*, Tuberculosis, **92**(6): 489-496.
140. Choi, J., Jung, Y.G., *et al.*, **2013**, *Rapid antibiotic susceptibility testing by tracking single cell growth in a microfluidic agarose channel system*, Lab on a Chip, **13**(2): 280-287.
141. Wakamoto, Y., Dhar, N., *et al.*, **2013**, *Dynamic persistence of antibiotic-stressed mycobacteria*, Science, **339**(6115): 91-95.
142. Nghe, P., Boulineau, S., *et al.*, **2013**, *Microfabricated polyacrylamide devices for the controlled culture of growing cells and developing organisms*, Plos One, **8**(9): e75537.
143. Li, B., Qiu, Y., *et al.*, **2014**, *Gradient microfluidics enables rapid bacterial growth inhibition testing*, Analytical Chemistry. DOI: 10.1021/ac5001306.
144. Lidstrom, M.E. and Konopka, M.C., **2010**, *The role of physiological heterogeneity in microbial population behavior*, Nature Chemical Biology, **6**(10): 705-712.
145. Müller, S., Harms, H., *et al.*, **2010**, *Origin and analysis of microbial population heterogeneity in bioprocesses*, Current Opinion in Biotechnology, **21**(1): 100-113.
146. Delvigne, F. and Goffin, P., **2014**, *Microbial heterogeneity affects bioprocess robustness: dynamic single-cell analysis contributes to understanding of microbial populations*, Biotechnology Journal, **9**(1): 61-72.
147. Fernandes, R.L., Nierychlo, M., *et al.*, **2011**, *Experimental methods and modeling techniques for description of cell population heterogeneity*, Biotechnology Advances, **29**(6): 575-599.
148. Fernandes, P., Carvalho, F., *et al.*, **2011**, *Miniaturization in biotechnology: speeding up the development of bioprocesses*, Recent Patents on Biotechnology, **5**(3): 160-173.
149. Marques, M.P.C. and Fernandes, P., **2011**, *Microfluidic devices: useful tools for bioprocess intensification*, Molecules, **16**(10): 8368-8401.
150. Tracy, B.P., Gaida, S.M., *et al.*, **2010**, *Flow cytometry for bacteria: Enabling metabolic engineering, synthetic biology and the elucidation of complex phenotypes*, Current Opinion in Biotechnology, **21**(1): 85-99.
151. Diaz, M., Herrero, M., *et al.*, **2010**, *Application of flow cytometry to industrial microbial bioprocesses*, Biochemical Engineering Journal, **48**(3): 385-407.
152. Schneider, T., Kreutz, J., *et al.*, **2013**, *The potential impact of droplet microfluidics in biology*, Analytical Chemistry, **85**(7): 3476-3482.

153. Klepárník, K. and Foret, F., **2013**, *Recent advances in the development of single cell analysis - A review*, *Analytica Chimica Acta*, **800**: 12-21.
154. Okumus, B., Yildiz, S., *et al.*, **2014**, *Fluidic and microfluidic tools for quantitative systems biology*, *Current Opinion in Biotechnology*, **25**: 30-38.
155. Lecault, V., White, A.K., *et al.*, **2012**, *Microfluidic single cell analysis: From promise to practice*, *Current Opinion in Chemical Biology*, **16**(3-4): 381-390.
156. Jin, B.J., Ko, E.A., *et al.*, **2013**, *Microfluidics platform for single-shot dose-response analysis of chloride channel-modulating compounds*, *Lab on a Chip*, **13**(19): 3862-3867.
157. Mu, X., Zheng, W.F., *et al.*, **2013**, *Microfluidics for manipulating cells*, *Small*, **9**(1): 9-21.
158. Unthan, S., Grünberger, A., *et al.*, **2014**, *Beyond growth rate 0.6: What drives *Corynebacterium glutamicum* to higher growth rates in defined medium*, *Biotechnology and Bioengineering*, **111**(2): 359-371.
159. Muzzey, D. and van Oudenaarden, A., **2009**, *Quantitative time-lapse fluorescence microscopy in single cells*, *Annual Review of Cell and Developmental Biology*, **25**(1): 301-327.
160. Bakstad, D., Adamson, A., *et al.*, **2012**, *Quantitative measurement of single cell dynamics*, *Current Opinion in Biotechnology*, **23**(1): 103-109.
161. Okumoto, S., Jones, A., *et al.*, **2012**, *Quantitative imaging with fluorescent biosensors*, *Annual Review of Plant Biology*, **63**: 663-706.
162. Müller, K. and Weber, W., **2013**, *Optogenetic tools for mammalian systems*, *Molecular Biosystems*, **9**(4): 596-608.
163. Ren, K., Chen, Y., *et al.*, **2014**, *New materials for microfluidics in biology*, *Current Opinion in Biotechnology*, **25**: 78-85.
164. Connell, J.L., Ritschdorff, E.T., *et al.*, **2013**, *3D printing of microscopic bacterial communities*, *Proceedings of the National Academy of Sciences*, **110**(46): 18380-18385.
165. Kim, M.C., Lam, R.H.W., *et al.*, **2013**, *Mathematical analysis of oxygen transfer through polydimethylsiloxane membrane between double layers of cell culture channel and gas chamber in microfluidic oxygenator*, *Microfluidics and Nanofluidics*, **15**(3): 285-296.
166. Coutu, D.L. and Schroeder, T., **2013**, *Probing cellular processes by long-term live imaging - historic problems and current solutions*, *Journal of Cell Science*, **126**(17): 3805-3815.
167. Nienhaus, K. and Ulrich Nienhaus, G., **2014**, *Fluorescent proteins for live-cell imaging with super-resolution*, *Chemical Society Reviews*, **43**(4): 1088-1106.
168. van Teeffelen, S., Shaevitz, J.W., *et al.*, **2012**, *Image analysis in fluorescence microscopy: Bacterial dynamics as a case study*, *BioEssays*, **34**(5): 427-436.
169. Grünberger, A., Paczia, N., *et al.*, **2012**, *A disposable picolitre bioreactor for cultivation and investigation of industrially relevant bacteria on the single cell level*, *Lab on a Chip*, **12**(11): 2060-2068.
170. Rubakhin, S.S., Lanni, E.J., *et al.*, **2013**, *Progress toward single cell metabolomics*, *Current Opinion in Biotechnology*, **24**(1): 95-104.
171. Trouillon, R., Passarelli, M.K., *et al.*, **2012**, *Chemical analysis of single cells*, *Analytical Chemistry*, **85**(2): 522-542.
172. Heinemann, M. and Zenobi, R., **2011**, *Single cell metabolomics*, *Current Opinion in Biotechnology*, **22**(1): 26-31.
173. Lin, Y., Trouillon, R., *et al.*, **2011**, *Chemical analysis of single cells*, *Analytical Chemistry*, **83**(12): 4369-4392.
174. Fornera, S., Kuhn, P., *et al.*, **2012**, *Sequential immobilization of enzymes in microfluidic channels for cascade reactions*, *Chempluschem*, **77**(2): 98-101.
175. Wiedenmann, J., Oswald, F., *et al.*, **2009**, *Fluorescent proteins for live cell imaging: Opportunities, limitations, and challenges*, *IUBMB Life*, **61**(11): 1029-1042.
176. Schallmey, M., Frunzke, J., *et al.*, **2014**, *Looking for the pick of the bunch: High-throughput screening of producing microorganisms with biosensors*, *Current Opinion in Biotechnology*, **26**: 148-154.

177. Mustafi, N., Grünberger, A., *et al.*, **2012**, *The development and application of a single-cell biosensor for the detection of l-methionine and branched-chain amino acids*, *Metabolic Engineering*, **14**(4): 449-457.
178. Mustafi, N., Grünberger, A., *et al.*, **2014**, *Application of a genetically encoded biosensor for live cell imaging of L-valine production in pyruvate dehydrogenase complex-deficient *Corynebacterium glutamicum* strains.*, *Plos One*, **9**(1): e85731.
179. Huang, Y., Cai, D., *et al.*, **2011**, *Micro- and nanotechnologies for study of cell secretion*, *Analytical Chemistry*, **83**(12): 4393-4406.
180. Kortmann, H., Kurth, F., *et al.*, **2009**, *Towards real time analysis of protein secretion from single cells*, *Lab on a Chip*, **9**(21): 3047-3049.
181. Love, K.R., Panagiotou, V., *et al.*, **2010**, *Integrated single-cell analysis shows *Pichia pastoris* secretes protein stochastically*, *Biotechnology and Bioengineering*, **106**(2): 319-325.
182. Jeon, N.L., Dertinger, S.K.W., *et al.*, **2000**, *Generation of solution and surface gradients using microfluidic systems*, *Langmuir*, **16**(22): 8311-8316.
183. Ahmed, T., Shimizu, T.S., *et al.*, **2010**, *Microfluidics for bacterial chemotaxis*, *Integrative Biology*, **2**(11-12): 604-629.
184. Chung, B.G. and Choo, J., **2010**, *Microfluidic gradient platforms for controlling cellular behavior*, *Electrophoresis* **31**(18): 3014-3027.
185. Keenan, T.M. and Folch, A., **2008**, *Biomolecular gradients in cell culture systems*, *Lab on a Chip*, **8**(1): 34-57.
186. Kensy, F., Zang, E., *et al.*, **2009**, *Validation of a high-throughput fermentation system based on online monitoring of biomass and fluorescence in continuously shaken microtiter plates*, *Microbial Cell Factories*, **8**(1): 31.
187. Araci, I.E. and Brisk, P., **2014**, *Recent developments in microfluidic large scale integration*, *Current Opinion in Biotechnology*, **25**: 60-68.
188. Kobel, S.A., Burri, O., *et al.*, **2012**, *Automated analysis of single stem cells in microfluidic traps*, *Lab on a Chip*, **12**(16): 2843-2849.
189. Park, S., Wolanin, P.M., *et al.*, **2003**, *Influence of topology on bacterial social interaction*, *Proceedings of the National Academy of Sciences of the United States of America*, **100**(24): 13910-13915.
190. Wei, P., Wong, W.W., *et al.*, **2012**, *Bacterial virulence proteins as tools to rewire kinase pathways in yeast and immune cells*, *Nature*, **488**(7411): 384-388.
191. Boedicker, J.Q., Li, L., *et al.*, **2008**, *Detecting bacteria and determining their susceptibility to antibiotics by stochastic confinement in nanoliter droplets using plug-based microfluidics*, *Lab on a Chip*, **8**(8): 1265-1272.
192. Keymer, J.E., Galajda, P., *et al.*, **2008**, *Computation of mutual fitness by competing bacteria*, *Proceedings of the National Academy of Sciences of the United States of America*, **105**(51): 20269-20273.
193. Keymer, J.E., Galajda, P., *et al.*, **2006**, *Bacterial metapopulations in nanofabricated landscapes*, *Proceedings of the National Academy of Sciences of the United States of America*, **103**(46): 17290-17295.
194. Huber, R., Ritter, D., *et al.*, **2009**, *Robo-Lector - a novel platform for automated high-throughput cultivations in microtiter plates with high information content*, *Microbial Cell Factories*, **8**: 41.
195. Keilhauer, C., Eggeling, L., *et al.*, **1993**, *Isoleucine synthesis in *Corynebacterium glutamicum*: Molecular analysis of the *ilvB-ilvN-ilvC* operon*, *Journal of Bacteriology*, **175**(17): 5595-5603.
196. Frunzke, J., Bramkamp, M., *et al.*, **2008**, *Population heterogeneity in *Corynebacterium glutamicum* ATCC 13032 caused by prophage CGP3*, *Journal of Bacteriology*, **190**(14): 5111-5119.

197. Di Carlo, D. and Lee, L.P., **2006**, *Dynamic single-cell analysis for quantitative biology*, Analytical Chemistry, **78**(23): 7918-7925.
198. Dubnau, D. and Losick, R., **2006**, *Bistability in bacteria*, Molecular Microbiology, **61**(3): 564-572.
199. Smits, W.K., Kuipers, O.P., *et al.*, **2006**, *Phenotypic variation in bacteria: The role of feedback regulation*, Nature Reviews Microbiology, **4**(4): 259-271.
200. Veening, J.W., Smits, W.K., *et al.*, **2008**, *Bistability, epigenetics, and bet-hedging in bacteria*, Annual Review of Microbiology, **62**: 193-210.
201. Lidstrom, M.E. and Meldrum, D.R., **2003**, *Life-on-a-chip*, Nature Reviews Microbiology, **1**(2): 158-164.
202. Blot, M., Papadopoulos, D., *et al.*, **1999**, *Genomic evolution during a 10,000-generation experiment with bacteria*, Proceedings of the National Academy of Sciences of the United States of America, **96**(7): 3807-3812.
203. Huh, D. and Paulsson, J., **2011**, *Non-genetic heterogeneity from stochastic partitioning at cell division*, Nature Genetics, **43**(2): 95-100.
204. Prindle, A., Samayoa, P., *et al.*, **2012**, *A sensing array of radically coupled genetic 'biopixels'*, Nature, **481**(7379): 39-44.
205. Davey, H.M. and Kell, D.B., **1996**, *Flow cytometry and cell sorting of heterogeneous microbial populations: the importance of single-cell analyses*, Microbiological Reviews, **60**(4): 641-696.
206. El-Ali, J., Sorger, P.K., *et al.*, **2006**, *Cells on chips*, Nature, **442**(7101): 403-411.
207. Lee, K.S., Boccazzi, P., *et al.*, **2011**, *Microfluidic chemostat and turbidostat with flow rate, oxygen, and temperature control for dynamic continuous culture*, Lab on a Chip, **11**(10): 1730-1739.
208. Studier, F.W., Daegelen, P., *et al.*, **2009**, *Understanding the differences between genome sequences of Escherichia coli B strains REL606 and BL21(DE3) and comparison of the E. coli B and K-12 genomes*, Journal of Molecular Biology, **394**(4): 653-680.
209. Burkovski, A., **2008**, *Corynebacteria: Genomics and molecular biology*. Norfolk UK: Caister Academic Press.
210. Zanzotto, A., Szita, N., *et al.*, **2004**, *Membrane-aerated microbioreactor for high-throughput bioprocessing*, Biotechnology and Bioengineering, **87**(2): 243-254.
211. van Ooyen, J., Emer, D., *et al.*, **2011**, *Citrate synthase in Corynebacterium glutamicum is encoded by two gltA transcripts which are controlled by RamA, RamB, and GlxR*, Journal of Biotechnology, **154**(2-3): 140-148.
212. Bäumchen, C., Knoll, A., *et al.*, **2007**, *Effect of elevated dissolved carbon dioxide concentrations on growth of Corynebacterium glutamicum on D-glucose and L-lactate*, Journal of Biotechnology, **128**(4): 868-874.
213. Müller, S. and Nebe-von-Caron, G., **2010**, *Functional single-cell analyses: Flow cytometry and cell sorting of microbial populations and communities*, FEMS Microbiology Reviews, **34**(4): 554-587.
214. Donnenberg, A.D. and Donnenberg, V.S., **2007**, *Rare-event analysis in flow cytometry*, Clinics in Laboratory Medicine, **27**(3): 627-652.
215. Hedley, B.D. and Keeney, M., **2013**, *Technical issues: Flow cytometry and rare event analysis*, International Journal of Laboratory Hematology, **35**(3): 344-350.
216. Keren, I., Kaldalu, N., *et al.*, **2004**, *Persister cells and tolerance to antimicrobials*, FEMS Microbiology Letters, **230**(1): 13-18.
217. Korch, S.B., Henderson, T.A., *et al.*, **2003**, *Characterization of the hipA7 allele of Escherichia coli and evidence that high persistence is governed by (p)ppGpp synthesis*, Molecular Microbiology, **50**(4): 1199-1213.
218. Chen, Y.C., Li, P., *et al.*, **2014**, *Rare cell isolation and analysis in microfluidics*, Lab on a Chip, **14**(4): 626-645.

219. Weaver, W.M., Tseng, P., et al., **2014**, *Advances in high-throughput single-cell microtechnologies*, Current Opinion in Biotechnology, **25**: 114-123.
220. Jaqaman, K., Loerke, D., et al., **2008**, *Robust single-particle tracking in live-cell time-lapse sequences*, Nature Methods, **5**(8): 695-702.
221. Li, K., Miller, E.D., et al., **2008**, *Cell population tracking and lineage construction with spatiotemporal context*, Medical Image Analysis, **12**(5): 546-566.
222. Pratt, E.D., Huang, C., et al., **2011**, *Rare cell capture in microfluidic devices*, Chemical Engineering Science, **66**(7): 1508-1522.
223. Elowitz, M.B., Levine, A.J., et al., **2002**, *Stochastic gene expression in a single cell*, Science, **297**(5584): 1183-1186.
224. Tarnok, A., **2011**, *Which is which and who is who? Pinpointing complex and rare cells*, Cytometry Part A, **79A**(8): 589-590.
225. Nesvera, J. and Patek, M., **2011**, *Tools for genetic manipulations in Corynebacterium glutamicum and their applications*, Applied Microbiology and Biotechnology, **90**(5): 1641-1654.
226. Varela, C., Rittmann, D., et al., **2012**, *MmpL genes are associated with mycolic acid metabolism in mycobacteria and corynebacteria*, Chemistry & Biology, **19**(4): 498-506.
227. Nanda, A.M., Heyer, A., et al., **2014**, *Analysis of SOS-induced spontaneous prophage induction in Corynebacterium glutamicum at the single-cell level*, Journal of Bacteriology, **196**(1): 180-188.
228. Natarajan, A. and Srienc, F., **2000**, *Glucose uptake rates of single E. coli cells grown in glucose-limited chemostat cultures*, Journal of Microbiological Methods, **42**(1): 87-96.
229. Paczia, N., Nilgen, A., et al., **2012**, *Extensive exometabolome analysis reveals extended overflow metabolism in various microorganisms*, Microbial Cell Factories, **11**(1): 122.
230. Young, K.D., **2006**, *The selective value of bacterial shape*, Microbiology and Molecular Biology Reviews, **70**(3): 660-703.
231. Bennett, B.D., Yuan, J., et al., **2008**, *Absolute quantitation of intracellular metabolite concentrations by an isotope ratio-based approach*, Nature Protocols, **3**(8): 1299-1311.
232. Ogino, H., Teramoto, H., et al., **2008**, *DivS, a novel SOS-inducible cell-division suppressor in Corynebacterium glutamicum*, Molecular Microbiology, **67**(3): 597-608.
233. Sliusarenko, O., Heinritz, J., et al., **2011**, *High-throughput, subpixel precision analysis of bacterial morphogenesis and intracellular spatio-temporal dynamics*, Molecular Microbiology, **80**(3): 612-627.
234. Youssef, S., Gude, S., et al., **2011**, *Automated tracking in live-cell time-lapse movies*, Integrative Biology, **3**(11): 1095-1101.
235. Dawson, C.C., Intapa, C., et al., **2011**, *"Persisters": Survival at the cellular level*, Plos Pathogens, **7**(7): e1002121.
236. Fritz, G., Megerle, J.A., et al., **2014**, *Single cell kinetics of phenotypic switching in the arabinose utilization system of E. coli*, Plos One, **9**(2): e89532.
237. Acar, M., Mettetal, J.T., et al., **2008**, *Stochastic switching as a survival strategy in fluctuating environments*, Nature Genetics, **40**(4): 471-475.
238. Aguirre, J.S., Monis, A., et al., **2014**, *Improvement in the lag phase estimation of individual cells that have survived mild heat treatment*, International Journal of Food Science & Technology, **49**(3): 884-894.
239. Bridson, E.Y. and Gould, G.W., **2000**, *Quantal microbiology*, Letters in Applied Microbiology, **30**(2): 95-98.
240. Dhar, N. and McKinney, J.D., **2007**, *Microbial phenotypic heterogeneity and antibiotic tolerance*, Current Opinion in Microbiology, **10**(1): 30-38.
241. Lewis, K., **2007**, *Persister cells, dormancy and infectious disease*, Nature Reviews Microbiology, **5**(1): 48-56.
242. Wood, T.K., Knabel, S.J., et al., **2013**, *Bacterial persister cell formation and dormancy*, Applied and Environmental Microbiology, **79**(23): 7116-7121.

243. Kalinowski, J., Bathe, B., *et al.*, **2003**, *The complete Corynebacterium glutamicum ATCC 13032 genome sequence and its impact on the production of L-aspartate-derived amino acids and vitamins*, Journal of Biotechnology, **104**(1-3): 5-25.
244. Schnelle, T., Hagedorn, R., *et al.*, **1993**, *Three-dimensional electric field traps for manipulation of cells: Calculation and experimental verification*, Biochimica et Biophysica Acta, **1157**(2): 127-140.
245. Kinoshita, S., Udaka, S., *et al.*, **2004**, *Studies on the amino acid fermentation - Part I. Production of L-glutamic acid by various microorganisms*, Journal of General and Applied Microbiology, **50**(6): 331-343.
246. Mentz, A., Neshat, A., *et al.*, **2013**, *Comprehensive discovery and characterization of small RNAs in Corynebacterium glutamicum ATCC 13032*, BMC Genomics, **14**(1): 714.
247. Woldringh, C.L., Huls, P.G., *et al.*, **1993**, *Volume growth of daughter and parent cells during the cell cycle of Saccharomyces cerevisiae a/alpha as determined by image cytometry*, Journal of Bacteriology, **175**(10): 3174-3181.
248. Niven, G.W., Morton, J.S., *et al.*, **2008**, *Influence of Environmental Stress on Distributions of Times to First Division in Escherichia coli Populations, as Determined by Digital-Image Analysis of Individual Cells*, Applied and Environmental Microbiology, **74**(12): 3757-3763.
249. Schaechter, M., Williamson, J.P., *et al.*, **1962**, *Growth, Cell and Nuclear Divisions in some Bacteria*, Journal of General Microbiology, **29**(3): 421-434.
250. Letek, M., Fiuza, M., *et al.*, **2008**, *Cell growth and cell division in the rod-shaped actinomycete Corynebacterium glutamicum*, Antonie Van Leeuwenhoek, **94**(1): 99-109.
251. Thanky, N.R., Young, D.B., *et al.*, **2007**, *Unusual features of the cell cycle in mycobacteria: polar-restricted growth and the snapping-model of cell division*, Tuberculosis, **87**(3): 231-236.
252. Dunlop, E.H. and Ye, S.J., **1990**, *Micromixing in fermentors: metabolic changes in Saccharomyces cerevisiae and their relationship to fluid turbulence*, Biotechnology and Bioengineering, **36**(8): 854-864.
253. Cuny, C., Lesbats, M., *et al.*, **2007**, *Induction of a global stress response during the first step of Escherichia coli plate growth*, Applied and Environmental Microbiology, **73**(3): 885-889.
254. Donato, S.S., Chu, V., *et al.*, **2013**, *Metabolic viability of Escherichia coli trapped by dielectrophoresis in microfluidics*, Electrophoresis, **34**(4): 575-582.
255. Justice, S.S., Hunstad, D.A., *et al.*, **2008**, *Morphological plasticity as a bacterial survival strategy*, Nature Reviews Microbiology, **6**(2): 162-168.
256. Donovan, C., Schauss, A., *et al.*, **2013**, *Chromosome segregation impacts on cell growth and division site selection in Corynebacterium glutamicum*, Plos One, **8**(2): e55078.
257. Khanna, S. and Srivastava, A.K., **2005**, *Statistical media optimization studies for growth and PHB production by Ralstonia eutropha*, Process Biochemistry, **40**(6): 2173-2182.
258. Mandenius, C.F. and Brundin, A., **2008**, *Bioprocess optimization using design-of-experiments methodology*, Biotechnology Progress, **24**(6): 1191-1203.
259. Fong, S.S. and Palsson, B.O., **2004**, *Metabolic gene-deletion strains of Escherichia coli evolve to computationally predicted growth phenotypes*, Nature Genetics, **36**(10): 1056-1058.
260. Wiechert, W. and Noack, S., **2011**, *Mechanistic pathway modeling for industrial biotechnology: challenging but worthwhile*, Current Opinion in Biotechnology, **22**(5): 604-610.
261. Feist, A.M., Zielinski, D.C., *et al.*, **2010**, *Model-driven evaluation of the production potential for growth-coupled products of Escherichia coli*, Metabolic Engineering, **12**(3): 173-186.
262. San, K.Y., Bennett, G.N., *et al.*, **1994**, *Strategies in high-level expression of recombinant protein in Escherichia coli*, Annals of the New York Academy of Sciences, **721**: 257-267.

263. Zhang, Y.H.P., **2010**, *Production of biocommodities and bioelectricity by cell-free synthetic enzymatic pathway biotransformations: Challenges and opportunities*, *Biotechnology and Bioengineering*, **105**(4): 663-677.
264. Luli, G.W. and Strohl, W.R., **1990**, *Comparison of growth, acetate production, and acetate inhibition of Escherichia coli strains in batch and fed-batch fermentations*, *Applied and Environmental Microbiology*, **56**(4): 1004-1011.
265. Suresh, S., Srivastava, V.C., *et al.*, **2009**, *Critical analysis of engineering aspects of shaken flask bioreactors*, *Critical Reviews in Biotechnology*, **29**(4): 255-278.
266. Guillouet, S. and Engasser, J.M., **1996**, *Kinetics of volume variation of Corynebacterium glutamicum following saline osmotic upshifts*, *Biotechnology Letters*, **18**(2): 145-148.
267. Petelenz-Kurdziel, E., Eriksson, E., *et al.*, **2011**, *Quantification of cell volume changes upon hyperosmotic stress in Saccharomyces cerevisiae*, *Integrative Biology*, **3**(11): 1120-1126.
268. Volkmer, B. and Heinemann, M., **2011**, *Condition-dependent cell volume and concentration of Escherichia coli to facilitate data conversion for systems biology modeling*, *Plos One*, **6**(7): e23126.
269. Litsanov, B., Kabus, A., *et al.*, **2012**, *Efficient aerobic succinate production from glucose in minimal medium with Corynebacterium glutamicum*, *Microbial Biotechnology*, **5**(1): 116-128.
270. Sisignano, M., Morbitzer, D., *et al.*, **2010**, *A 2-oxoacid dehydrogenase complex of Haloferax volcanii is essential for growth on isoleucine but not on other branched-chain amino acids*, *Microbiology*, **156**(2): 521-529.
271. Han, S.O., Inui, M., *et al.*, **2008**, *Effect of carbon source availability and growth phase on expression of Corynebacterium glutamicum genes involved in the tricarboxylic acid cycle and glyoxylate bypass*, *Microbiology*, **154**(10): 3073-3083.
272. Wendisch, V.F., De Graaf, A.A., *et al.*, **2000**, *Quantitative determination of metabolic fluxes during cointilization of two carbon sources: Comparative analyses with corynebacterium glutamicum during growth on acetate and/or glucose*, *Journal of Bacteriology*, **182**(11): 3088-3096.
273. Shin, H.S., Kim, Y.J., *et al.*, **2011**, *Autoinduction of a genetic locus encoding putative acyltransferase in Corynebacterium glutamicum*, *Biotechnology Letters*, **33**(1): 97-102.
274. Arndt, A., Auchter, M., *et al.*, **2008**, *Ethanol catabolism in Corynebacterium glutamicum*, *Journal of Molecular Microbiology and Biotechnology*, **15**(4): 222-233.
275. Kramer, R., Lambert, C., *et al.*, **1990**, *Uptake of glutamate in Corynebacterium glutamicum: 1. Kinetic-properties and regulation by internal pH and potassium*, *European Journal of Biochemistry*, **194**(3): 929-935.
276. Wendisch, V.F., Bott, M., *et al.*, **2006**, *Emerging Corynebacterium glutamicum systems biology*, *Journal of Biotechnology*, **124**(1): 74-92.
277. Cremer, J., Treptow, C., *et al.*, **1988**, *Regulation of enzymes of lysine biosynthesis in Corynebacterium glutamicum*, *Journal of General Microbiology*, **134**: 3221-3229.
278. Kind, S., Jeong, W.K., *et al.*, **2010**, *Systems-wide metabolic pathway engineering in Corynebacterium glutamicum for bio-based production of diaminopentane*, *Metabolic Engineering*, **12**(4): 341-351.
279. Liebl, W., Klamer, R., *et al.*, **1989**, *Requirement of chelating compounds for the growth of Corynebacterium glutamicum in synthetic media*, *Applied Microbiology and Biotechnology*, **32**(2): 205-210.
280. Moker, N., Brocker, M., *et al.*, **2004**, *Deletion of the genes encoding the MtrA-MtrB two-component system of Corynebacterium glutamicum has a strong influence on cell morphology, antibiotics susceptibility and expression of genes involved in osmoprotection*, *Molecular Microbiology*, **54**(2): 420-438.

281. Brazma, A., Hingamp, P., *et al.*, **2001**, *Minimum information about a microarray experiment (MIAME) - toward standards for microarray data*, *Nature Genetics*, **29**(4): 365-371.
282. Polen, T. and Wendisch, V.F., **2004**, *Genomewide expression analysis in amino acid-producing bacteria using DNA microarrays*, *Applied Biochemistry and Biotechnology*, **118**(1-3): 215-232.
283. Von der Osten, C.H., Giannetti, C., *et al.*, **1989**, *Design of a defined medium for growth of Corynebacterium glutamicum in which citrate facilitates iron uptake*, *Biotechnology Letters*, **11**(1): 11-16.
284. Haussmann, U. and Poetsch, A., **2012**, *Global proteome survey of protocatechuate- and glucose-grown Corynebacterium glutamicum reveals multiple physiological differences*, *Journal of Proteomics*, **75**(9): 2649-2659.
285. Merkens, H., Beckers, G., *et al.*, **2005**, *Vanillate metabolism in Corynebacterium glutamicum*, *Current Microbiology*, **51**(1): 59-65.
286. Shen, X.H., Zhou, N.Y., *et al.*, **2012**, *Degradation and assimilation of aromatic compounds by Corynebacterium glutamicum: another potential for applications for this bacterium?*, *Applied Microbiology and Biotechnology*, **95**(1): 77-89.
287. Brinkrolf, K., Brune, I., *et al.*, **2006**, *Transcriptional regulation of catabolic pathways for aromatic compounds in Corynebacterium glutamicum*, *Genetics and Molecular Research*, **5**(4): 773-789.
288. Fontecave, M. and Ollagnier-De-Choudens, S., **2008**, *Iron-sulfur cluster biosynthesis in bacteria: Mechanisms of cluster assembly and transfer*, *Archives of Biochemistry and Biophysics*, **474**(2): 226-237.
289. Wennerhold, J. and Bott, M., **2006**, *The DtxR regulon of Corynebacterium glutamicum*, *Journal of Bacteriology*, **188**(8): 2907-2918.
290. Yao, Z.Z., Davis, R.M., *et al.*, **2012**, *Regulation of cell size in response to nutrient availability by fatty acid biosynthesis in Escherichia coli*, *Proceedings of the National Academy of Sciences of the United States of America*, **109**(38): E2561-E2568.
291. Woo, H.M., Noack, S., *et al.*, **2010**, *Link between phosphate starvation and glycogen metabolism in Corynebacterium glutamicum, revealed by metabolomics*, *Applied and Environmental Microbiology*, **76**(20): 6910-6919.
292. Schellenberger, J., Que, R., *et al.*, **2011**, *Quantitative prediction of cellular metabolism with constraint-based models: the COBRA Toolbox v2.0*, *Nature Protocols*, **6**(9): 1290-1307.
293. van Ooyen, J., Noack, S., *et al.*, **2012**, *Improved L-lysine production with Corynebacterium glutamicum and systemic insight into citrate synthase flux and activity*, *Biotechnology and Bioengineering*, **109**(8): 2070-2081.
294. Noack, S., Nöh, K., *et al.*, **2011**, *Stationary versus non-stationary C-13-MFA: A comparison using a consistent dataset*, *Journal of Biotechnology*, **154**(2-3): 179-190.
295. Tillack, J., Paczia, N., *et al.*, **2012**, *Error propagation analysis for quantitative intracellular metabolomics*, *Metabolites*, **2**(4): 1012-1030.
296. Martin, C., Galbe, M., *et al.*, **2002**, *Comparison of the fermentability of enzymatic hydrolyzates of sugarcane bagasse pretreated by steam explosion using different impregnating agents*, *Applied Biochemistry and Biotechnology*, **98**: 699-716.
297. Megason, S.G. and Fraser, S.E., **2007**, *Imaging in systems biology*, *Cell*, **130**(5): 784-795.
298. Brocker, M., Schaffer, S., *et al.*, **2009**, *Citrate utilization by Corynebacterium glutamicum is controlled by the CitAB two-component system through positive regulation of the citrate transport genes citH and tctCBA*, *Journal of Bacteriology*, **191**(12): 3869-3880.
299. Polen, T., Schluesener, D., *et al.*, **2007**, *Characterization of citrate utilization in Corynebacterium glutamicum by transcriptome and proteome analysis*, *FEMS Microbiology Letters*, **273**(1): 109-119.

300. Koch, D.J., Ruckert, C., *et al.*, **2005**, *The transcriptional regulator SsuR activates expression of the Corynebacterium glutamicum sulphonate utilization genes in the absence of sulphate*, *Molecular Microbiology*, **58**(2): 480-494.
301. Rittmann, D., Schaffer, S., *et al.*, **2003**, *Fructose-1,6-bisphosphatase from Corynebacterium glutamicum: Expression and deletion of the fbp gene and biochemical characterization of the enzyme*, *Archives of Microbiology*, **180**(4): 285-292.
302. Youn, J.W., Jolkver, E., *et al.*, **2008**, *Identification and characterization of the dicarboxylate uptake system DccT in Corynebacterium glutamicum*, *Journal of Bacteriology*, **190**(19): 6458-6466.
303. Youn, J.W., Jolkver, E., *et al.*, **2009**, *Characterization of the dicarboxylate transporter DctA in Corynebacterium glutamicum*, *Journal of Bacteriology*, **191**(17): 5480-5488.
304. Chien, A.C., Hill, N.S., *et al.*, **2012**, *Cell size control in bacteria*, *Current Biology*, **22**(9): R340-R349.
305. Robert, L., Hoffmann, M., *et al.*, **2014**, *Division in Escherichia coli is triggered by a size-sensing rather than a timing mechanism*, *BMC Biology*, **12**(1): 17.
306. Katzke, N., Arvani, S., *et al.*, **2010**, *A novel T7 RNA polymerase dependent expression system for high-level protein production in the phototrophic bacterium Rhodospirillum rubrum*, *Protein Expression and Purification*, **69**(2): 137-146.
307. Grünberger, A., Probst, C., *et al.*, **2011**, *Single-cell trapping and analysis of prokaryotic production strains in sub- μ m fluidic structures*. in *15th International Conference on Miniaturized Systems for Chemistry and Life Science*. Seattle.
308. Wösten, H.A.B., van Veluw, G.J., *et al.*, **2013**, *Heterogeneity in the mycelium: implications for the use of fungi as cell factories*, *Biotechnology Letters*, **35**(8): 1155-1164.
309. Wucherpfennig, T., Kiep, K.A., *et al.*, **2010**, *Morphology and rheology in filamentous cultivations*, *Advances in Applied Microbiology*, **72**: 89-136.
310. Spohr, A., Dam-Mikkelsen, C., *et al.*, **1998**, *On-line study of fungal morphology during submerged growth in a small flow-through cell*, *Biotechnology and Bioengineering*, **58**(5): 541-553.
311. Held, M., Lee, A.P., *et al.*, **2010**, *Microfluidics structures for probing the dynamic behaviour of filamentous fungi*, *Microelectronic Engineering*, **87**(5-8): 786-789.
312. Demming, S., Sommer, B., *et al.*, **2011**, *Disposable parallel poly(dimethylsiloxane) microreactor with integrated readout grid for germination screening of Aspergillus ochraceus*, *Biomicrofluidics*, **5**(1): 014104.
313. Grünberger, A., Schmitz, K., *et al.*, **2013**, *Simple microfluidics for complex organisms: a microfluidic chip system for growth and morphogenesis studies of filamentous fungi*. in *17th International Conference on Miniaturized Systems for Chemistry and Life Science*. Freiburg.
314. Nielsen, J., Larsson, C., *et al.*, **2013**, *Metabolic engineering of yeast for production of fuels and chemicals*, *Current Opinion in Biotechnology*, **24**(3): 398-404.
315. Mano, Y., Kobayashi, T.J., *et al.*, **2013**, *Single cell visualization of yeast gene expression shows correlation of epigenetic switching between multiple heterochromatic regions through multiple generations*, *Plos Biology*, **11**(7): e1001601.
316. Georgiou, G. and Valax, P., **1996**, *Expression of correctly folded proteins in Escherichia coli*, *Current Opinion in Biotechnology*, **7**(2): 190-197.
317. Garcia-Fruitos, E., **2010**, *Inclusion bodies: a new concept*, *Microbial Cell Factories*, **9**(1): 80.
318. Baumgart, M., Unthan, S., *et al.*, **2013**, *Construction of a prophage-free variant of Corynebacterium glutamicum ATCC 13032 for use as a platform strain for basic research and industrial biotechnology*, *Applied and Environmental Microbiology*, **79**(19): 6006-6015.

319. Klumpp, S., Zhang, Z.G., *et al.*, **2009**, *Growth rate-dependent global effects on gene expression in bacteria*, *Cell*, **139**(7): 1366-1375.
320. Goers, L., Kyllilis, N., *et al.*, **2013**, *Chapter 5 - engineering microbial biosensors*, in *Methods in Microbiology*, H. Colin and W. Anil, Editors. Academic Press. 119-156.
321. Bren, A., Hart, Y., *et al.*, **2013**, *The last generation of bacterial growth in limiting nutrient*, *BMC Systems Biology*, **7**: 27.
322. Melin, J. and Quake, S.R., **2007**, *Microfluidic large-scale integration: the evolution of design rules for biological automation*, *Annual Review of Biophysics and Biomolecular Structure*, **36**: 213-231.
323. Thorsen, T., Maerkl, S.J., *et al.*, **2002**, *Microfluidic large-scale integration*, *Science*, **298**(5593): 580-584.
324. Gu, H. and Ren, D., **2014**, *Materials and surface engineering to control bacterial adhesion and biofilm formation: A review of recent advances*, *Frontiers of Chemical Science and Engineering*, **8**(1): 20-33.
325. Wu, J.B., Cao, W.B., *et al.*, **2009**, *Polydimethylsiloxane microfluidic chip with integrated microheater and thermal sensor*, *Biomicrofluidics*, **3**(1): 012005.
326. Drepper, T., Huber, R., *et al.*, **2010**, *Flavin mononucleotide-based fluorescent reporter proteins outperform green fluorescent protein-like proteins as quantitative in vivo real-time reporters*, *Applied and Environmental Microbiology*, **76**(17): 5990-5994.
327. Ungerböck, B., Charwat, V., *et al.*, **2013**, *Microfluidic oxygen imaging using integrated optical sensor layers and a color camera*, *Lab on a Chip*, **13**(8): 1593-1601.
328. Casadesus, J. and D'ari, R., **2002**, *Memory in bacteria and phage*, *Bioessays*, **24**(6): 512-518.
329. Tarnok, A., **2013**, *Visualization can be harmful for live cells*, *Cytometry Part A*, **83A**(6): 521-522.
330. Sung, M.-H., **2013**, *A checklist for successful quantitative live cell imaging in systems biology*, *Cells*, **2**(2): 284-293.
331. Yi, C.Q., Li, C.W., *et al.*, **2006**, *Microfluidics technology for manipulation and analysis of biological cells*, *Analytica Chimica Acta*, **560**(1-2): 1-23.
332. Yun, H., Kim, K., *et al.*, **2013**, *Cell manipulation in microfluidics*, *Biofabrication*, **5**(2): 022001.
333. He, X., Kimura, H., *et al.*, **2013**, *A high-throughput device for patterned differentiation of embryoid bodies*, *Journal of Robotics and Mechatronics*, **25**(4): 623-630.
334. Monod, J., **1949**, *The growth of bacterial cultures*, *Annual Review of Microbiology*, **3**: 371-394.
335. Georgi, T., **2006**, *Regulation der Zuckerverwertung in Corynebacterium glutamicum*, PhD-Thesis, HHU Düsseldorf
336. Gerstmeir, R., Wendisch, V.F., *et al.*, **2003**, *Acetate metabolism and its regulation in Corynebacterium glutamicum*, *Journal of Biotechnology*, **104**(1-3): 99-122.
337. Krause, F.S., Henrich, A., *et al.*, **2010**, *Increased glucose utilization in Corynebacterium glutamicum by use of maltose, and its application for the improvement of L-valine productivity*, *Applied and Environmental Microbiology*, **76**(1): 370-374.
338. Lindner, S.N., Seibold, G.M., *et al.*, **2011**, *Phosphotransferase system-independent glucose utilization in Corynebacterium glutamicum by inositol permeases and glucokinases*, *Applied and Environmental Microbiology*, **77**(11): 3571-3581.
339. Frunzke, J., Engels, V., *et al.*, **2008**, *Co-ordinated regulation of gluconate catabolism and glucose uptake in Corynebacterium glutamicum by two functionally equivalent transcriptional regulators, GntR1 and GntR2*, *Molecular Microbiology*, **67**(2): 305-322.
340. Netzer, R., Krause, M., *et al.*, **2004**, *Roles of pyruvate kinase and malic enzyme in Corynebacterium glutamicum for growth on carbon sources requiring gluconeogenesis*, *Archives of Microbiology*, **182**(5): 354-363.

Publications

The thesis is based on the following original publications.

Peer-reviewed journal articles:

- I A. Grünberger, N. Paczia, C. Probst, G. Schendzielorz, L. Eggeling, W. Wiechert and D. Kohlheyer, *A disposable picoliter bioreactor for cultivation and investigation of industrially relevant bacteria on single cell level*, **Lab on a Chip** **2012**, 12, p.2060-2068, [DOI:10.1039/C2LC40156H](https://doi.org/10.1039/C2LC40156H)
- II A. Grünberger, J. van Ooyen, N. Paczia, P. Rohe, G. Schendzielorz, L. Eggeling, W. Wiechert, D. Kohlheyer, S. Noack, *Beyond growth rate 0.6: C.glutamicum cultivated in highly diluted environment*, **Biotechnology and Bioengineering** **2013**, 110(1), p. 220-228, [DOI: 10.1002/bit.24616](https://doi.org/10.1002/bit.24616)
- III A. Grünberger, C. Probst, A. Heyer, J. Frunzke, W. Wiechert and D. Kohlheyer, *Microfluidic Picoliter Bioreactor for Microbial Single Cell Analysis: Fabrication, System Setup and Operation*, **Journal of Visualized Experiments** **2013**, (82), e50560, [DOI:10.3791/50560](https://doi.org/10.3791/50560)
- IV S. Unthan[§], A. Grünberger[§], J. van Ooyen, J. Gätgens, J. Heinrich, N. Paczia, W. Wiechert, D. Kohlheyer, S. Noack, *Beyond Growth Rate 0.6: What drives Corynebacterium glutamicum to higher growth rates in defined medium*, **Biotechnology and Bioengineering** **2014**, 111, p. 459-371, [DOI: 10.1002/bit.25103](https://doi.org/10.1002/bit.25103)
- V A. Grünberger, W. Wiechert and D. Kohlheyer, *Single-Cell Microfluidics: Opportunity for Bioprocess Development*, **Current Opinion in Biotechnology** **2014**, 29, p. 15-23

[§] Authors contributed equally to the respective publication

(Peer-reviewed) conference proceedings:

- I A. Grünberger, K. Schmitz, C. Probst, S. Noack, W. Wiechert and D. Kohlheyer, *Simple microfluidics for complex organisms: A microfluidic chip system for growth and morphogenesis studies of filamentous fungi*, **Proceedings of the 17th International Conference on Miniaturized Systems for Chemistry and Life Science**, 27th-31th October 2013, Freiburg, Germany, ISBN 978-0-9798064-6-9, [→ Link](#)
- II A. Grünberger, C. Probst, S. Helfrich, W. Wiechert, K. Nöh and D. Kohlheyer, *-Industrial Biotechnology meets Microfluidics – Disposable high-throughput single cell analysis device for industrially relevant bacterial strains*, **Proc. of 3rd European Conference on Microfluidics**, 03th-05th December 2012, Heidelberg, Germany
- III A. Grünberger, S. Helfrich, C. Probst, W. Wiechert, K. Nöh and D. Kohlheyer, *High-Throughput lineage tree investigations of bacteria microcolonies using arrays of monolayer growth chambers*, **Proceedings of the 16th International Conference on Miniaturized Systems for Chemistry and Life Science**, 28th October – 01st November 2012, Okinawa, Japan, ISBN 978-0-9798064-5-2, [→ Link](#)
- IV A. Grünberger, C. Probst, W. Wiechert and D. Kohlheyer, *Femtoliter Growth Channels: Bacteria Long-Term Growth Patterns Analysis on Single Cell Level*, **Chemie Ingenieur Technik** **2012**, 84(8), p.1407-1407, [DOI: 10.1002/cite.201250343](https://doi.org/10.1002/cite.201250343)

-
- V A. Grünberger, C. Probst, W. Wiechert and D. Kohlheyer, *High-Throughput Growth Rate Determination of Bacteria Microcolonies on Single Cell Level*, **Chemie Ingenieur Technik**, **2012**, 84(8), p.1336-1337, [DOI: 10.1002/cite.201250342](https://doi.org/10.1002/cite.201250342)
- VI A. Grünberger, C. Probst, S. Binder, R. Ziaee, L. Eggeling, W. Wiechert and D. Kohlheyer, *Single Cell Trapping and Analysis for Prokaryotic Production Strains in Sub- μ m Fluidic Structures*, **Proceedings of the 15th International Conference on Miniaturized Systems for Chemistry and Life Science**, 02th-06th October 2011, Seattle, WA, USA, ISBN 987-0-9798064-4-5, [→ Link](#)

In addition some unpublished data are presented

Associated publications during this thesis, that are NOT included within this thesis:

- K.E. Scholz, D. Okrob, B. Kopka, A. Grünberger, M. Pohl, K.E. Jaeger and U. Krauss, Synthesis of chiral cyanohydrins with recombinant *Escherichia coli* cells in a micro-aqueous reaction system, **Applied and Environmental Microbiology** **2012**, 78 (14), p. 5025-5027, [DOI: 10.1128/AEM.00582-12](https://doi.org/10.1128/AEM.00582-12)
- N. Mustafi, A. Grünberger, D. Kohlheyer, M. Bott and J. Frunzke, *The development and application of a single-cell biosensor for the detection of L-methionine and branched-chain amino acids*, **Metabolic Engineering** **2012**, 14(4), p. 449-457, [DOI: 10.1016/j.ymben.2012.02.002](https://doi.org/10.1016/j.ymben.2012.02.002)
- M. Baumgart, S. Unthan, C. Rückert, J. Sivalingam, A. Grünberger, J. Kalinowski, M. Bott, S. Noack and J. Frunzke, *Construction of a prophage-free variant of *Corynebacterium glutamicum* ATCC 13032 - a platform strain for basic research and industrial biotechnology*, **Applied and Environmental Microbiology** **2013**, 79 (19), p. 6006-6015, [DOI:10.1128/AEM.01634-13](https://doi.org/10.1128/AEM.01634-13)
- K. Hoffmann, A. Grünberger, F. Lausberg, M. Bott and L. Eggeling, *Imbalances in sulfur assimilation and synthesis of sulfur-containing amino acids: Visualization at the single-cell level*, **Applied and Environmental Microbiology** **2013**, 79(21), p. 6730-6736, [DOI: 10.1128/AEM.01804-13](https://doi.org/10.1128/AEM.01804-13)
- C. Probst, A. Grünberger, W. Wiechert and D. Kohlheyer, *Microfluidic growth chambers with optical tweezers for full spatial single-cell control and analysis of evolving microbes*, **Journal of Microbiological Methods** **2013**, 95(3), p. 470-476, [DOI:10.1016/j.mimet.2013.09.002](https://doi.org/10.1016/j.mimet.2013.09.002)
- C. Probst, A. Grünberger, W. Wiechert and D. Kohlheyer, *PDMS sub-micron traps for single-cell analysis of bacteria*, **Micromachines** **2013**, 4(4), p. 357-369, [DOI:10.3390/mi4040357](https://doi.org/10.3390/mi4040357)
- G. Schendzielorz, M. Dippong, A. Grünberger, D. Kohlheyer, A. Yoshida, S. Binder, C. Nishiyama, M. Nishiyama, M. Bott and L. Eggeling *Taking control over control: Use of product sensing in single cells to remove flux control at key enzymes in biosynthesis pathways*, **ACS Synthetic Biology** **2014**, 3(1), p. 21-29 [DOI:10.1021/sb400059v](https://doi.org/10.1021/sb400059v)
- M. Nanda, A. Heyer, C. Krämer, A. Grünberger, D. Kohlheyer and J. Frunzke, *SOS-induced spontaneous prophage induction in *Corynebacterium glutamicum* - An analysis at the single-cell level*, **Journal of Bacteriology** **2013**, 196 (1), p. 180-188, [DOI:10.1128/JB.01018-13](https://doi.org/10.1128/JB.01018-13)
- N. Mustafi[§], A. Grünberger[§], S. Helfrich, K. Nöh, B. Blombach, D. Kohlheyer and J. Frunzke, *Application of a genetically encoded biosensor for live cell imaging of L-valine production in pyruvate dehydrogenase complex-deficient *Corynebacterium glutamicum* strains*, **PLOS ONE** **2014**, 9:e85731, [DOI:10.1371/journal.pone.0085731](https://doi.org/10.1371/journal.pone.0085731)
- D. Binder[§], A. Grünberger[§], A. Loeschcke, C. Probst, C. Bier, J. Pietruszka, W. Wiechert, D. Kohlheyer, K.E. Jaeger and T. Drepper, *Light-responsive control of bacterial gene expression: Precise triggering of the lac promoter activity using photocaged IPTG*, **Integrative Biology**, 2014, submitted

Band / Volume 101

Modification and characterization of potential bioelectronic interfaces

K. Greben (2015), 76 pp

ISBN: 978-3-95806-028-9

Band / Volume 102

Extending the precision and efficiency of the all-electron full-potential linearized augmented plane-wave density-functional theory method

G. Michalíček (2015), 195 pp

ISBN: 978-3-95806-031-9

Band / Volume 103

Metabolic engineering of *Escherichia coli* for the production of plant phenylpropanoid derived compounds

P. V. van Summeren-Wesenhagen (2015), V, 92 pp

ISBN: 978-3-95806-039-5

Band / Volume 104

Spin-reorientation transition in epitaxial $\text{Ni}_x\text{Pd}_{1-x}$ films on Cu(001): a microscopic analysis

D. Gottlob (2015), x, 134 pp

ISBN: 978-3-95806-049-4

Band / Volume 105

Resonant Magnetic Scattering Studies using Synchrotron Radiation and Laser-Generated Extreme Ultraviolet Light

C. M. Weier (2015), vii, 143 pp

ISBN: 978-3-95806-052-4

Band / Volume 106

Neutron Scattering

Lectures of the JCNS Laboratory Course held at Forschungszentrum Jülich and at the Heinz-Maier-Leibnitz Zentrum Garching

edited by Th. Brückel, D. Richter, G. Roth, A. Wischnewski and R. Zorn (2015), ca 300 pp

ISBN: 978-3-95806-055-5

Band / Volume 107

Neutron Scattering

Experimental Manuals of the JCNS Laboratory Course held at

Forschungszentrum Jülich and at the Heinz-Maier-Leibnitz Zentrum Garching

edited by Th. Brückel, D. Richter, G. Roth, A. Wischnewski and R. Zorn (2015), ca 150 pp

ISBN: 978-3-95806-056-2

Band / Volume 108

STM-based quantum transport through molecular wires

N. Fournier (2015), ix, 295 pp

ISBN: 978-3-95806-059-3

Band / Volume 109

Study on the electroforming and resistive switching behaviour of nickel oxide thin films for non-volatile memory applications

R. Weng (2015), xxi, 159 pp

ISBN: 978-3-95806-062-3

Band / Volume 110

Microswimmers – From Single Particle Motion to Collective Behaviour

Lecture Notes of the DFG SPP Summer School 2015

edited by G. Gompper, C. Bechinger, S. Herminghaus, R. E. Isele-Holder, U.B. Kaupp, H. Löwen, H. Stark, R. G. Winkler (2015)

ISBN: 978-3-95806-083-8

Band / Volume 111

Long range order in 3D nanoparticle assemblies

E. Josten (2015), 238 pp

ISBN: 978-3-95806-087-6

Band / Volume 112

Silicon nanowire structures for neuronal cell interfacing

S. Pud (2015), 153 pp

ISBN: 978-3-95806-089-0

Band / Volume 113

**Memristive Phenomena -
From Fundamental Physics to Neuromorphic Computing**

Lecture Notes of the 47th IFF Spring School 2016

22 February – 04 March 2016, Jülich, Germany

ed. by R. Waser and M. Wuttig (2016), ca 1000 pp

ISBN: 978-3-95806-091-3

Band / Volume 114

**Single-Cell Analysis of Microbial Production Strains
in Microfluidic Bioreactors**

A. M. Grünberger (2015), XIX, 225 pp

ISBN: 978-3-95806-092-0

**Schlüsseltechnologien /
Key Technologies
Band / Volume 114
ISBN 978-3-95806-092-0**

